Characterisation of urban and remote atmospheres using comprehensive two dimensional gas chromatography

Rachel Ellen Dunmore

Doctor of Philosophy

University of York

Chemistry

September, 2015

Dedication

To all the people who made this possible.

You know who you are.

"An education isn't how much you have committed to memory, or even how much you know. It's being able to differentiate between what you know and what you don't."

Anatole France

Abstract

Volatile organic compounds (VOCs) are key precursors to ozone and particulate matter, two of the most important air pollutants. Air quality interventions have successfully reduced the release of short chain VOCs in urban areas. The increased use of diesel vehicles has created an increase in the direct emission of longer chain VOCs. However, these compounds are not considered as part of air quality strategies and there are few atmospheric measurements of them to date.

This thesis details continuous measurements of VOCs in London, a developed megacity, using comprehensive two dimensional gas chromatography. Analysis of this large suite of VOC measurements have shown that the higher carbon number species emitted from diesel vehicles can dominate gas phase reactive carbon in cities with a significant diesel fleet. Comparison of these real-world observations with emissions inventories has highlighted that there is a significant under prediction of the emissions of higher carbon number species. This presents a considerable policy challenge; the focus must now switch to VOCs released from diesel as this vehicle type is increasingly replacing gasoline world-wide.

Further analysis of the London data has provided evidence of both anthropogenic and biogenic emission sources. The measurement of the higher carbon number species has allowed for OH reactivity to be more accurately modelled. Detailed analysis of the ethanol observations provided direct evidence that the use of bio-ethanol blended gasoline in the UK is having an impact on the composition of the atmosphere.

The combination of heart-cut and comprehensive two dimensional gas chromatography into a single instrument has made the measurement of both small and large chain VOCs possible. This instrument compares well to existing instrumentation and when deployed to a rural location (Bachok, Malaysia) provided hourly time-resolved measurements of C_5-C_{13} VOCs.

Contents

List of Figures

List of Tables

Acknowledgements

Firstly, I would like to thank NERC for funding my PhD.

Secondly, to my supervisors Dr Jacqui Hamilton and Dr James Lee, thank you for putting your faith in me and pushing me through my comfort zone. You are both an inspiration to me and I hope to accomplish even half as much as you have.

A big thank you must go to Dr Richard Lidster and Dr Jimmy Hopkins. Your knowledge and time were priceless and much appreciated.

To the whole Atmospheric Chemistry group at York, thanks to everyone for all your help and support. The many amazing nights out and laughs were a major part of why I didn't lose my mind. Special mention to Kelly....I feel your pain now and you're right, never again!

Many thanks go to the people of the ClearfLo campaign; Lisa, Dan, Nicky, James, Bill, Dave and many others too numerous to mention. Thank you for all the useful discussions and good times during field work. Thanks to the Bachok IOF people, specifically Iq and Dave for taking care of me when I was ill and making sure the instrument didn't die. Brian Bandy....what can I say....it was interesting working with you, you're a great bloke and I especially enjoyed playing pool with you.

Particular thanks go to my family for all your love and support. Mam, Dad, Alex, Grandma Pat, Lee and the Dunmores, you have given me the courage to strive to the highest possible level. To those no longer here, I hope I have made you proud.

Last, and definitely not least, my husband. Chris, you put up with my craziness and believed in me; even when I had given up hope. Your support meant the world, I love you.

Declaration

The research described in this thesis is original work, which I undertook at the University of York during 2011-2015. Except where stated, all of the work contained within this thesis represents the original contribution of the author. Some parts of this thesis have been published in journals; where items were published jointly with collaborators, the author of this thesis is responsible for the material presented here. For each published item the primary author is the first listed author. Publications are listed at the beginning of the chapter to which they relate.

Chapter 1

The role of volatile organic compounds in urban air quality

1.1 Air quality

The negative impacts of poor air quality have long been studied, from the 1100's in Egypt, to 13th Century London,[1] and through the London and Los Angeles Smog episodes of the 1950's[2] to the present day. These events have motivated the funding of research into atmospheric science and from this, policy regulations can be put into place to improve future air quality. Studies of urban areas have increased dramatically over the past two decades, where poor air quality is often associated with the high emissions due to large populations.

Residents in urban areas can be significantly affected by the health problems associated with poor air quality. Ozone (O_3) and particulate matter (PM) are two of the most important pollutants, with exposure causing an estimated 17,400 and 458,000 premature deaths in Europe respectively in 2011.[3] There has been a small decrease in the observed trend in the direct emission of PM, however no discernible trend has been observed for O_3 in Europe.[3] Another pollutant of interest is nitrogen dioxide (NO_2) which although it has shown a decreasing trend in the past decade, the increased use of diesel-powered vehicles has resulted in an increase in direct emissions into the atmosphere.[3] New techniques have allowed for an estimate to be made of the mortality expected from long-term exposure to NO_2, with an approximate 5,879 premature deaths in London for the year 2010.[4]

Megacities are classified as urban areas with a population of more than 10 million. Figure 1.1 shows the evolution of urban land use and the growth of urban areas into megacities, from only 10 cities in 1990 to 28 in 2014 and a projected 40 by 2030.[5] There is also growth in the overall percentage of the World that is classified as urban, as well as an increase in larger cities in general; cities with a population of 5-10 million and 1-5 million are predicted to increase from 21 in 1990 to 63 in 2030 and 239 to 558 respectively.[5] Megacities present many challenges for air quality, not simply as a source of local air pollution but also by contributing to transboundary pollution which can lead to increases in global concentrations.[6,7] Human activities within these cities emit primary PM as well as nitrogen oxides (NO_x, the sum of nitrogen monoxide (NO) and NO_2) and volatile organic compounds (VOCs) as primary pollutants, which can then react in the atmosphere to create secondary pollutants, such as O_3, secondary organic aerosol and secondary inorganic aerosol (SOA and SIA, different types of particulate matter).

Comparing pollution concentrations in different megacities can provide information about possible sources and how effective individual countries are at controlling emissions.

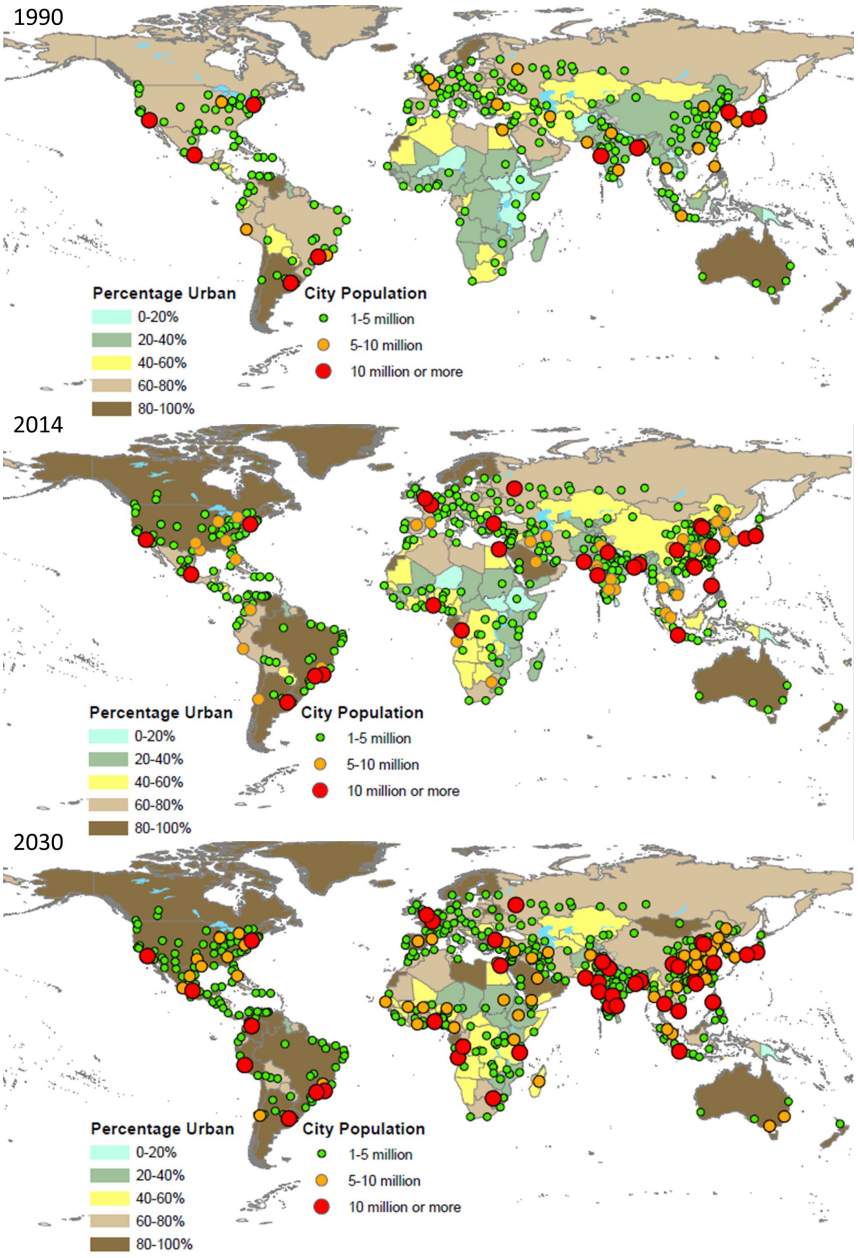

Figure 1.1: Percentage of urban land use and city population for 1990 (top), 2014 (middle) and predicted for 2030 (bottom). Data maps taken from the United Nations, Department for Economic and Social Affairs, http://esa.un.org/unpd/wup/Maps/CityDistribution/CityPopulation/CityPop.aspx

Studies have shown that it is possible to pinpoint emission sources through the statistical analysis of ambient air pollution concentrations.[8] The UN estimates that over 600 million people in urban areas worldwide are exposed to potentially harmful levels of air pollution, mainly from traffic emissions.[9] This is supported by Parrish *et al.*, (2009), who found that emissions from gasoline-fuelled vehicles dominate in megacities, indicating that vehicular emission controls are an important policy to put in place.[8] This is particularly important for urban areas where vehicle emissions usually dominate the concentrations of NO_x,

carbon monoxide (CO) and VOCs. A new area for concern is the rapid growth in the use of diesel-powered vehicles in Europe which could potentially change the composition of emissions in urban areas. The ramifications of this change are discussed in detail in Chapter 2.

1.1.1 Health effects of air pollution

The health effects of both short- and long-term exposure to air pollution have been studied extensively over the past three decades (see the World Health Organisation (WHO), "Review of evidence on health aspects of air pollution" report, (REVIHAAP) and references within).[10] By definition, an air pollutant is a compound that could have an adverse effect on either humans, animals, vegetation or materials.[11] Exposure could be from inhalation, ingestion or dermal contact (although this is only a minor route).[11]

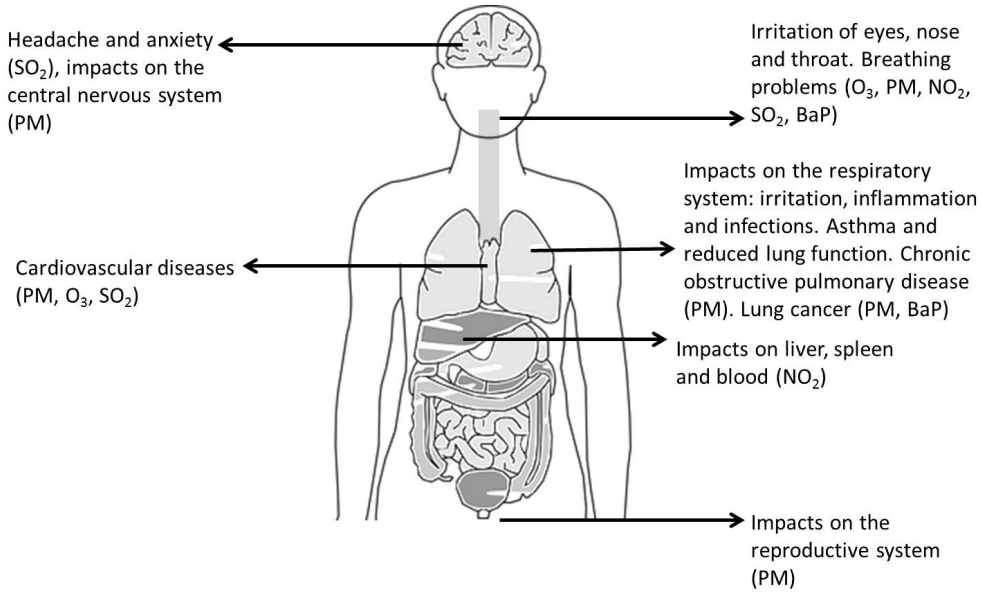

Figure 1.2: Summary of the key health effects associated with exposure to the major pollutants: benzo(a)pyrene (BaP), NO_2, O_3, PM and sulphur dioxide (SO_2).$^{(modified from\ 12,13\ )}$

Health effects from exposure to air pollution can range in severity and affect different bodily systems and/or organs as shown in Figure 1.2. This figure shows the main health effects associated with specific pollutants. These effects could be anything from minor respiratory symptoms to cardiovascular diseases, culminating in increased morbidity and premature mortality.[11] The EU has implemented exposure guidelines, levels above which the pollutant would adversely affect human health. However, many EU countries are exceeding these guidelines.[10] This is of particular importance as the REVIHAAP report

reviewed a significant number of recent publications that suggest exposure to pollution at levels significantly lower than the 2005 guidelines can still adversely affect human health.[10]

The direct emission of VOCs and PM, and the production of O_3, SOA and SIA, can affect health in different ways and to varying degrees. This is dependent on multiple factors; the specific type of pollutant and its concentration, duration of exposure, any other pollutants present and the individuals susceptibility to any particular ailments (*i.e.* pre-existing medical conditions).[11] These effects are particularly relevant for megacities due to the high population densities present there.

Some VOCs are classified as carcinogenic, likely to adversely affect health just from their direct emission, such as benzene and polycyclic aromatic hydrocarbons (PAHs).[3] The WHO have estimated that an exposure to benzene concentrations of only 1.7 μg m^{-3} over a person's lifetime could cause a cancer risk to up to 10 out of every one million people exposed.[14] This is quite a small value considering the regulated annual average of benzene for the EU is 5 μg m^{-3}.[15] Also of note are the interactions between different VOCs. The VOCs themselves may not be harmful, but the combination of two or more in a pollutant mixture such as the emission of vehicle exhaust, could cause an adverse health effect.[14] The health effects associated with exposure to VOCs range from respiratory symptoms to neurological conditions such as headaches, nausea and depression.[14,16,17] However, the effect of VOCs on health is not limited to direct emission, the secondary pollutants formed through reactions of VOCs in the atmosphere (*i.e.* O_3 and SOA) can also lead to adverse health effects.

Ozone is an important, and highly toxic, component of photochemical smog.[18] Exposure to O_3 can cause a variety of adverse health effects, such as reductions in lung function and other respiratory conditions.[18] This is exacerbated in people with pre-existing medical conditions such as asthma.[19] The WHO 2005 guideline for a mean 8 hour exposure to O_3 is 100 μg m^{-3}, although it is likely that exposure below this threshold will also cause adverse health effects. Bell *et al.*, (2007) analysed the results of nearly 40 studies and found that a short-term exposure to O_3 can cause a statistically increased mortality, particularly from either cardiovascular or respiratory illnesses.[20] Long-term exposure to O_3 can also have effects on health.[19] Recent studies have postulated that exposure to levels of O_3 from the year 2000, could potentially have caused 0.20 – 0.47 million premature deaths globally for the year.[21,22]

PM has been linked to a variety of adverse human health effects. These include, but

are not limited to, premature mortality and morbidity, pulmonary disease and respiratory illnesses, specifically asthma. Long-term exposure to PM has been found to dominate the health burden of the population.[19,23] No lower limit has been found at which the exposure to PM will not cause health impairment and as such it is dangerous when people are exposed to even relatively small amounts.[18] The size of particles (discussed in detail in Section 1.2.3) is particularly important to consider when determining to what extent health will be affected. Small particles can reach the gas-exchange region of the lungs and very small particles have been found to be able to pass through to other organs in the body therefore causing more damage.[18,24–26] Additionally, there is increasing evidence of effects on cardiorespiratory health and the central nervous system through exposure to ultrafine particles.[10,19,26]

1.1.2 Climate effects of air pollution

Drivers of climate change are anthropogenic species and processes that can alter the Earth's energy budget. The strengths of these drivers to change the energy flux is quantified as radiative forcing in units of Watts per square metre (W m^{-2}).[27] The contribution of the emissions of various species to radiative forcing is shown in the well-know Intergovernmental Panel on Climate Change (IPCC) graph in Figure 1.3. This is the latest version from the fifth IPCC Assessment Report (AR5) which shows the contributions of, not only emissions, but also the atmospheric drivers which result from those emissions.[28]

A positive radiative forcing value indicates warming of the Earth's surface, with negative values showing the opposite (surface cooling). Estimates of radiative forcing are based on either in-situ and/or remote observations, properties of greenhouse gases and aerosols, and calculations from numerical models that are used to represent the observed processes. Figure 1.3 shows that the total anthropogenic radiative forcing for 2011 relative to 1750 is positive (2.29 W m^{-2}), leading to an uptake of energy by the climate system. This value is 43% higher than that reported in the previous IPCC report, (AR4, total anthropogenic radiative forcing for the year 2005 relative to 1750, 1.6 W m^{-2}). It is likely this large increase is due to the combination of the continued growth in the concentrations of most greenhouse gases and improved estimates of the radiative forcing from aerosols, which indicated a weaker net cooling effect than previous reports (*i.e.* a negative radiative forcing).[28]

The relationship between climate and O_3 has been well studied over the past couple of

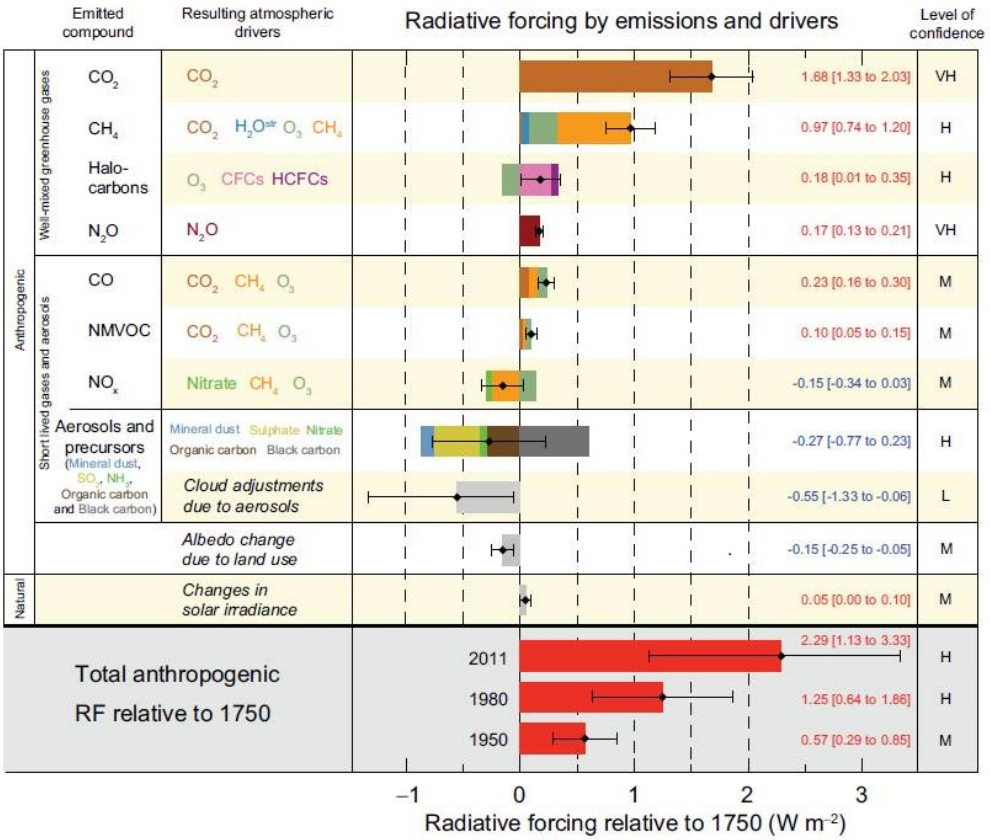

Figure 1.3: Radiative forcing estimates for 2011 relative to 1750 and aggregated uncertainties for the main drivers of climate change. Values are global average radiative forcing, partitioned according to emitted compounds or processes that result in a combination of drivers. Best estimates of net radiative forcing are shown with black diamonds with corresponding uncertainty intervals; the numerical values are provided on the right of the figure, together with the confidence level in the net forcing (VH - very high, H - high, M - medium, L - low and VL - very low). Albedo forcing due to black carbon on snow and ice is included in the black carbon aerosol bar. Small forcings due to contrails (0.05 W m^{-2}, including contrail induced cirrus), and HFCs, PFCs, and SF_6 (total 0.03 W m^{-2}) are not shown. Concentration-based radiative forcings for gases can be obtained by summing the like-coloured bars. Volcanic forcing is not included as its episodic nature makes it difficult to compare to other forcing mechanisms. Total anthropogenic radiative forcing is provided for three different years relative to 1750.[28]

decades. O_3 is a radiatively active greenhouse gas with current radiative forcing estimates for 2011 of +0.35 W m^{-2} for total O_3.[19] The majority of the radiative forcing from O_3 can be attributed to increases in the emission of O_3 precursor species, such as NO_x, CO, non-methane VOCS (NMVOCs) and methane (CH_4). Methane, while an important precursor of O_3, is also a strong greenhouse gas in its own right (it has a higher radiative forcing value than O_3, seen in Figure 1.3) and will be discussed in more detail later. The remaining O_3 precursor species have a variety of indirect effects on climate which are not limited to their influence on O_3 production.[19] For example, methane, NMVOCs and CO

can be oxidised to carbon dioxide (CO_2) which has an additional warming effect although this is relatively small, in the order of +0.02 to +0.09 W m^{-2}.[28,29]

Methane is one of the most important greenhouse gases, it has a radiative forcing value of $+0.5 \pm 0.05$ W m^{-2} which makes up approximately 28% of the total radiative forcing from non-CO_2 constituents in 2010.[30] It is a powerful infra-red absorber, making it a more efficient greenhouse gas than CO_2 (28 times more efficient over a century time-scale).[31] The atmospheric lifetime of methane is approximately 10 years,[31–33] so its potential effects on climate are substantial.

Both anthropogenic and biogenic source NMVOCs can contribute to climate warming, although through different pathways. Anthropogenic NMVOCs affect both O_3 production and increases in the lifetime of methane. A number of studies have shown the correlation between increased NMVOC and CO concentrations and the increased radiative forcings from O_3 and methane.[29,34–38] Biogenic VOCs (BVOCs) are particularly important in remote forested regions where there are typically low NO_x but high VOC concentrations. Oxidation of these BVOCs produces peroxy radicals, but the lack of sufficient NO_x leads to inhibited O_3 formation.[39] BVOCs can then further decrease the O_3 concentrations though direct VOC + O_3 reactions. This, combined with the removal of oxidant species during VOC oxidation, reduces the oxidising capacity of the atmosphere.[40] This increases the lifetime of methane, as its main sink (the OH radical) is removed from the atmosphere through reactions with the BVOCs,[41,42] thus increasing the warming that occurs. Additionally, BVOCs can contribute to aerosol formation as some of their oxidation products can undergo gas-to-particle partitioning to form SOA.[43] This both directly affects the Earth's radiation budget through the scattering of solar radiation by aerosols and indirectly from the formation of cloud condensation nuclei (CCN).[44,45]

The relationship between climate and aerosols is less understood and more complex, as they have both warming and cooling effects.[18] Aerosols can affect climate directly through aerosol-radiation effects and indirectly via aerosol-cloud effects.[19] The former is from aerosol particles either absorbing or scattering radiation which can warm the atmosphere and cool the Earth's surface respectively. The latter is based on the capability of particles to act as CCN. These are usually particles with diameters larger than 50-100 nm that are activated in rising air masses to form cloud droplets. If there is a sufficient concentration of cloud droplets, there is a higher cloud albedo, causing back scattering of solar radiation, reduced precipitation, and a longer lifetime of the clouds. This is a cooling

climate driver where the Earth's surface is shaded from solar radiation.[46] It is estimated that the cooling exceeds the warming effects from aerosols. However there is quite a high level of uncertainty, indicated by the large error bars in Figure 1.3, about the overall effect of aerosols on climate.[28]

1.1.3 Air quality and climate change

Air quality and climate change are usually considered as separate issues for many areas of science and policy. However, they are highly connected and linked through (1) emissions to the atmosphere, (2) atmospheric properties, processes and chemistry, and (3) mitigation strategies.[19] There are many common sources that emit both climate change driving forcers and air quality pollutants. Once these pollutants have been emitted into the atmosphere, they have a variety of atmospheric properties, which can influence whether they have a direct or indirect effect on radiative forcing. Their lifetime in the atmosphere and the atmospheric chemical processes they are involved in can also influence their effect on human health and the ecosystem. Current mitigation strategies can potentially both improve air quality and mitigate climate change, termed win-win. However, some so called win-lose or trade-off strategies only provide benefits to one area and exacerbate the situation in another.[19] This is shown in Figure 1.4, where for example, the increased use of diesel cars to reduce CO_2 emissions (a climate change benefit) resulted in an increased emission of NO_x and PM (a detriment to air quality).

There is still a significant amount of work to be done to fill knowledge gaps, despite the recognition that there are strong links between climate change and air pollution. This needs to be in both scientific and political communities through the coordination of future mitigation and/or adaptation strategies. These strategies must be put into the broader context of the big picture, that the atmosphere is a limited resource. Thus future policies can be implemented with fewer unforeseen, potentially negative, consequences arising. However, there are challenges to this process. Specifically what feedback effects do climate policies have on air quality and vice versa.

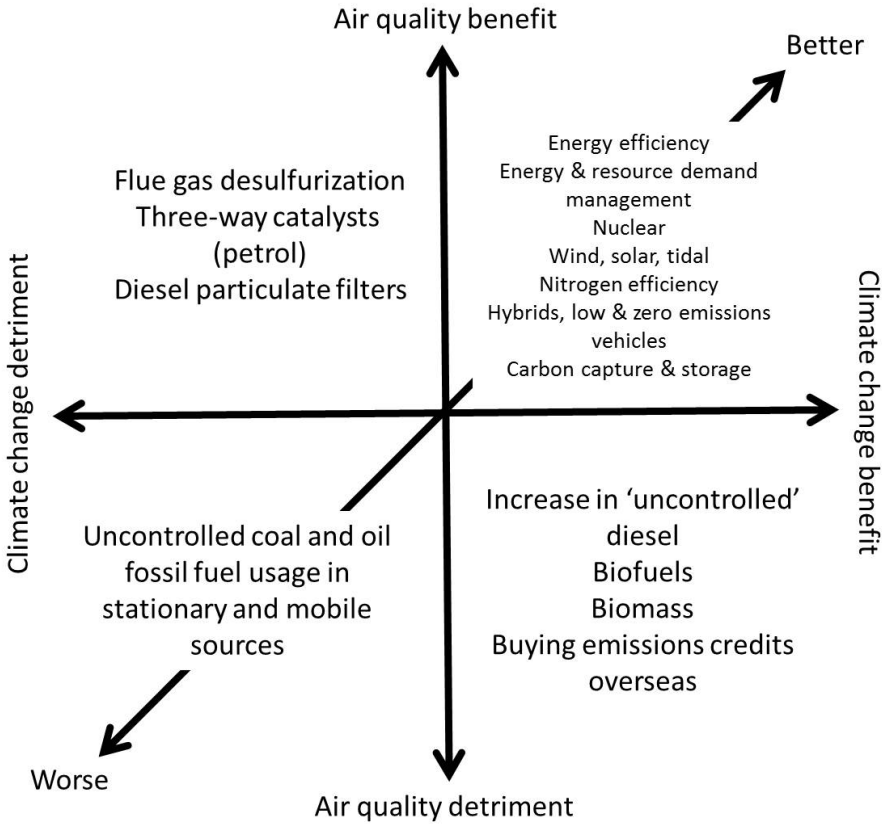

Figure 1.4: Trade-offs from policies and technologies to tackle climate change and air quality [19,47–49]

1.2 Volatile organic compounds

The focus of this thesis will be on one specific type of pollutant, VOCs, and the effects they have on PM and O_3 concentrations. It is important to measure VOCs as they play a key role in the atmosphere through reactions that determine concentrations of other important atmospheric species, such as PM and O_3.[50] VOC is a term used to describe a very large group of vapour-phase organic compounds, excluding CO and CO_2 but including hydrocarbons, oxygenated, halogenated and other hetero atomic compounds,[39] which play a central role in atmospheric chemistry; and have both natural and anthropogenic sources. VOCs can be primary and/or secondary pollutants, and react in the atmosphere at rates which can vary by orders of magnitudes.[51]

As a large group of compounds with differing volatilities, VOCs can be broadly grouped based on their effective saturation concentrations (C*, in μg m^{-3}), an empirical expression of volatility. This can be calculated using Equation 1.1 where; C_i^{vap} (μg m^{-3}) is the concentration of the species i in the vapor phase, C_{OA} (μg m^{-3}) is the total organic aerosol concentration, C_i^{aer} (μg m^{-3}) is the mass concentration of species i in the condensed phase,

R is the gas constant, T (K) is the temperature, M_i (g mol^{-1}) is the molecular weight of the species i, $\zeta_i^{'}$ is the molarity-based activity coefficent (assumed to be 1) and $P_{L,i}^{o}$ (Torr) is the saturation vapor pressure of pure species i at temperature T.[52,53] As the saturation concentrations decrease, the volatility also drops and the individual VOC species is more likely to partition from the gas phase into the particulate phase as shown in the lower panel of Figure 1.5 for the reaction of O_3 with α-pinene, where the white and green bars represent species in the gas and particle phases respectively.[53]

$$C_i^* = \frac{C_i^{vap}.C_{OA}}{C_i^{aer}} = \frac{M_i.10^6.\zeta_i^{'}.P_{L,i}^{o}}{760.R.T} \tag{1.1}$$

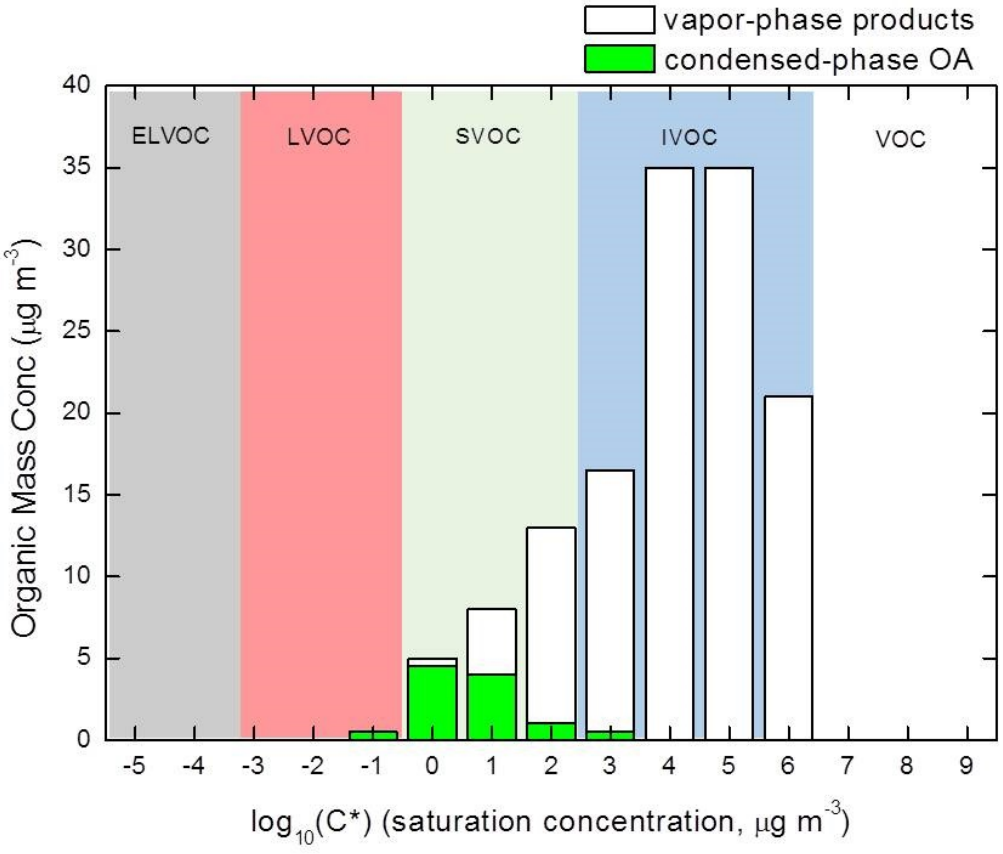

Figure 1.5: Gas-to-particle partitioning diagram of products from the reaction of O_3 and α-pinene. One dimensional volatility basis set product distribution, for each $\log_{10}$C* bin. Partitioning is shown for approximately 10 μg m^{-3} of SOA, obtained from the oxidation of 100 μg m^{-3} of α-pinene, with condensed-phase OA in green and vapor-phase products in white.$^{(modified from\ 53)}$

VOC - Volatile organic compounds (C* of $> 10^6$ μg m^{-3}, white shaded region in Figure 1.5). These compounds exist in the gas phase under ambient conditions.

IVOC - Intermediate volatility organic compounds (C* of 10^3 to 10^6 μg m^{-3}, light blue

shaded region in Figure 1.5), exist almost entirely in the gas phase under ambient conditions, only a small portion of the organic mass is highlighted as being in the particle phase in Figure 1.5.[53,54]

SVOC - Semi-volatile organic compounds (C^* of 1 to 10^3 μg m^{-3}, light green shaded region in Figure 1.5), can exist in both the gas and particle phases at ambient conditions.[53,54]

LVOC - Low volatility organic compounds (C^* of 10^{-2} to 1 μg m^{-3}, light red shaded region in Figure 1.5), exist predominantly in the particle phase with some small gas-phase fractions.[53,54]

ELVOC - Extremely low volatility organic compounds (C^* of $< 10^{-3}$ μg m^{-3}, gray shaded region in Figure 1.5), resides almost entirely in the particle phase at ambient conditions.[53,54]

1.2.1 Emission sources of volatile organic compounds

VOCs are released into the atmosphere from both natural emission from the Earth's vegetation (termed biogenic emission) and as a result of human activities (anthropogenic emission). By definition, anthropogenic VOCs are either directly emitted to the atmosphere or produced during combustion.[55] The dominant sources of these VOCs in urban areas is from the use of fossil fuels in the transport sector and industrial processes.[55] Biogenic VOCs (BVOCs) are species that are directly emitted to the atmosphere from the Earth's surface. These can generally be categorised into emissions from terrestrial vegetation, soils and the ocean.[56,57] However, the line between anthropogenic and biogenic sources of VOCs is not straightforward. Many VOCs can be produced or emitted from both sources. Although the emission from anthropogenic sources is particularly important in urban areas and megacities, biogenic emissions of VOCs worldwide are approximately ten times larger, by mass, than anthropogenic emissions.[58–60]

Concentrations of VOCs do not continue to increase with time so there must be one or more removal processes or sinks. The most important of these sinks is through gas phase chemical oxidation primarily with the hydroxyl ($^{\bullet}$OH) radical, but also with O_3 and nitrate ($NO_3^{\bullet}$) and halogen radicals.[61,62] Some of the gas phase VOCs can also absorb sunlight and be photolysed. These oxidised compounds can then be removed by dry or wet deposition to the Earth's surface through absorption to vegetation[58,63] or in rain,[64,65] respectively and either through adsorption onto the surface, absorption into aerosols or

partitioning into aerosols.[66] This will be discussed in more detail in Section 1.2.2.

1.2.1.1 Anthropogenic sources

There are many different and varied anthropogenic sources of VOCs. The three main global sources of anthropogenic VOCs are use of fossil fuels, industrial processes and biofuel combustion. VOC emissions from the use of fossil fuel in vehicles is the most important global anthropogenic source of VOCs.[55] Emissions from industrial applications such as manufacturing, residential heating and cooking are small in comparison to fossil fuel use but can be important in some regions. For example, in China where approximately 30% of total Chinese anthropogenic VOC emissions, for the year 2000, were from the substantial use of coal and biofuels in residential cooking.[67] Fugitive emission of VOCs through evaporation can also occur during the distribution and storage of fuel, typically from ships, road tankers and fuel stations. Evaporative emissions from fuel stations are particularly important on local and regional scales, not just from concerns about O_3 formation but also adverse health effects. There can be substantial emissions of toxic and carcinogenic species, such as benzene.[55]

Industrial process emissions are largely from solvent use in paints, adhesives and inks *etc.*, where the solvent evaporates after use. This can lead to much higher emissions during warm seasons.[68] Other important industrial uses are the manufacture of pharmaceuticals, metal surface cleaning, extraction of oil seeds and printing. However, many industries have had to reduce emissions due to policy interventions. This has lead to companies either recycling the VOCs emitted or thermally destroying them.[55]

The primary energy source in developing countries is the combustion of biomass. The emissions are overwhelming from the residential sector through heating and cooking. More recently, there has been a large influx of emissions from the combustion of biofuels in the transport sector. Largely from, mainly Brazil but also other countries, the use of pure ethanol and blended ethanol and gasoline as vehicle fuels.[55] This will be discussed in more detail in Chapter 4, Section 4.2.

1.2.1.2 Biogenic sources

BVOCs are predominantly emitted from the foliage of terrestrial vegetation. This encompasses both natural vegetation (trees, shrubs, grasses, ferns and mosses) and anthropogenically induced vegetation such as crops and urban landscapes. There are other

minor sources from ocean and soil emissions that can contribute to the global concentrations of BVOCs.[57] Although many thousands of species can be emitted,[68,69] those emitted in the largest concentrations are isoprene, monoterpenes, sesquiterpenes and a selection of oxygenated VOCs (OVOCs), specifically methanol, acetone, ethanol and acetaldehyde.[19,56,57,70]

1.2.2 Chemistry of volatile organic compounds

The degradation reactions of VOCs have been well documented. These reactions are particularly important due to the generation of numerous secondary pollutants, specifically O_3 and SOA. VOCs emitted into the troposphere, react with radical species (such as the $^{\bullet}OH$ and hydroperoxyl ($HO_2^{\bullet}$) radicals) and sunlight then, in the presence of NO_x, form O_3, a simplified reaction scheme is shown in Figure 1.6. A key part of this scheme is the catalytic cycling of radicals which allow for a sustained concentration of the $^{\bullet}OH$ radical during the day. This helps the propagation of further reactions.[39]

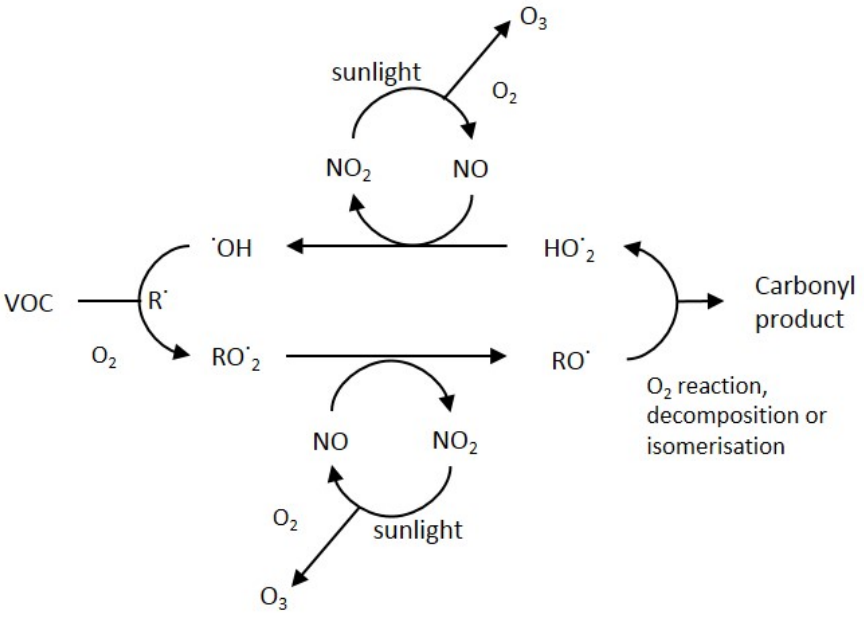

Figure 1.6: Simplified reaction cycle through which VOCs form O_3[71]

The chemistry of VOCs is extremely complex as there are many hundreds of emitted species that possess a variety of physico-chemical properties due to differences in their structure and functional group.[72] The degradation mechanism of each individual VOC is essentially unique.[72] A further complication to understanding VOC chemistry, is that when VOCs are oxidised in the atmosphere it is possible for thousands of partially oxidised

intermediate organic products to be generated. These possess a wide variety of properties which influence their potential to form O_3 and SOA. The intermediate species can also undergo secondary reactions to produce O_3 thus further increasing the complexity. It is vital to have intensive measurement studies on VOC emissions, so that the intermediate oxidised species produced during atmospheric reactions, such as the alkyl peroxy ($RO_2^{\bullet}$) and alkoxy ($RO^{\bullet}$) radicals (shown in Figure 1.6), can be modelled as they cannot usually be measured due to their very short lifetimes in the atmosphere. These intermediate species are the route to form increased amounts of O_3.

1.2.2.1 Reaction of volatile organic compounds with radicals

The most important daytime radical is the $^{\bullet}OH$ radical, as it is usually the first and rate determining step in the removal of many trace species (Figure 1.7).[73] The $^{\bullet}OH$ radical reacts with a large number of pollutants, forming oxidised species that can be more easily removed from the atmosphere, leading to it been termed the "atmospheric detergent".[73–75]

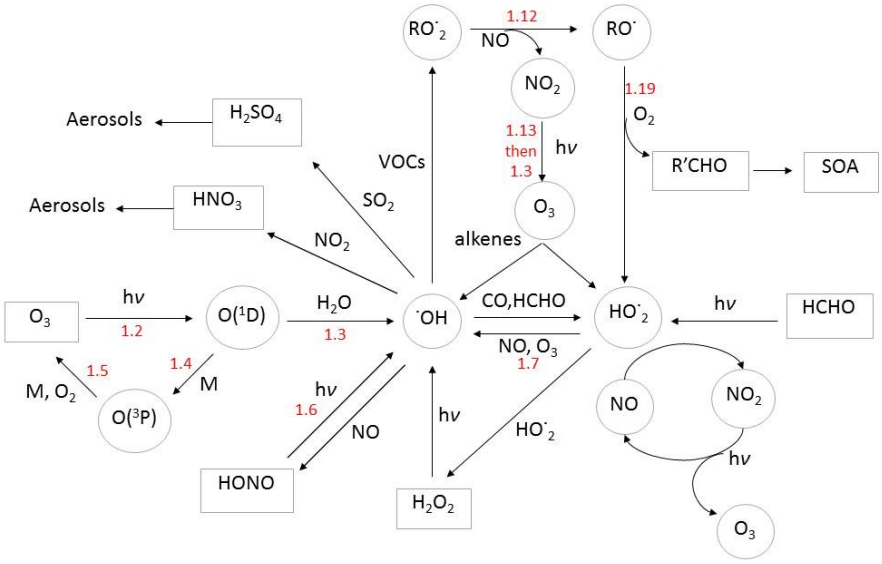

Figure 1.7: A simple schematic diagram through which the reactions of OH and HO_2 radicals are shown to produce secondary pollutants such as O_3, PM and SOA.[76] Numbers in red correspond to equations included in the body of text.

The main source of the $^{\bullet}OH$ radical is through the photolysis of O_3 to form electronically excited $O(^1D)$, (Equation 1.2), which then reacts with water vapour (H_2O) to form two $^{\bullet}OH$ radicals, (Equation 1.3). Only 10% of the $O(^1D)$ actually forms the $^{\bullet}OH$ radical; while the other 90% relaxes to form $O(^3P)$ which reforms O_3 (Equations 1.4 and 1.5).[77]

$$O_3 + h\nu \longrightarrow O(^1D) + O_2 \qquad (\lambda \leq 320\,\text{nm}) \tag{1.2}$$

$$O(^1D) + H_2O \longrightarrow 2\ {}^{\bullet}OH \tag{1.3}$$

$$O(^1D) + M \longrightarrow O(^3P) + M \qquad \text{where M} = N_2 \text{ or } O_2 \tag{1.4}$$

$$O(^3P) + O_2 + M \longrightarrow O_3 + M \qquad \text{where M} = \text{air molecules} \tag{1.5}$$

However, in urban areas that are heavily polluted, there are other mechanisms that become available for the formation of the $^{\bullet}$OH radical. This is mainly through the photolysis of nitrous acid (HONO, Equation 1.6). In areas with high concentrations of NO, reactions with $HO_2^{\bullet}$ radicals can also generate significant concentrations of $^{\bullet}$OH radicals, Equation 1.7.

$$HONO + h\nu \xrightarrow{\lambda<400nm} {}^{\bullet}OH + NO \tag{1.6}$$

$$HO_2^{\bullet} + NO \longrightarrow {}^{\bullet}OH + NO_2 \tag{1.7}$$

During the daytime, $^{\bullet}$OH radicals can initiate the degradation of many atmospheric trace gases, particularly VOCs,[78,79] with the $^{\bullet}$OH radical budget in the atmosphere being controlled by the concentrations of O_3, water, sunlight, VOCs, CO and NO_x.[79] As the $^{\bullet}$OH radical source is mainly photochemical, during the night, the $NO_3^{\bullet}$ radical (formed through the reaction of NO_2 and O_3 in Equation 1.8) takes over as the most important reactive oxidant in the troposphere; even though it is less reactive.[80] The $NO_3^{\bullet}$ radical is not as important as the $^{\bullet}$OH radical during the day, due to it being rapidly photolysed to NO_2 and O_3 in the presence of solar radiation (Equations 1.9 and 1.5).[73,80] The reaction of VOCs with O_3 is also important both day and night, particularly with unsaturated compounds through addition across the double bond.[81]

$$NO_2 + O_3 \longrightarrow NO_3^{\bullet} + O_2 \tag{1.8}$$

$$NO_3^{\bullet} + h\nu \longrightarrow NO_2 + O(^3P) \tag{1.9}$$

The reactions of VOCs with the $^{\bullet}OH$ radical is the key removal mechanism for the majority of VOCs in urban atmospheres. This cycle is also responsible for the production of tropospheric O_3, in the presence of NO_x. Generally, the reaction of $^{\bullet}OH$ radicals with organic species such as VOCs is *via* hydrogen atom abstraction to form water and an alkyl radical ($R^{\bullet}$), shown in Equation 1.10. The alkyl radical can then react with molecular oxygen (O_2) to form alkyl peroxy radicals ($RO_2^{\bullet}$, Equation 1.11), the subsequent reaction of these with NO forms an alkoxy radical ($RO^{\bullet}$) and NO_2, Equation 1.12.

$$RH + {}^{\bullet}OH \longrightarrow R^{\bullet} + H_2O \tag{1.10}$$

$$R^{\bullet} + O_2 \xrightarrow{M} RO_2^{\bullet} \tag{1.11}$$

$$NO + RO_2^{\bullet} \longrightarrow RO^{\bullet} + NO_2 \tag{1.12}$$

$$NO + RO_2^{\bullet} \longrightarrow RONO_2 + M \tag{1.13}$$

The NO_2 produced in Equation 1.12 photo-dissociates to form $O(^3P)$ in Equation 1.14 which can form a molecule of O_3 *via* Equation 1.5.

$$NO_2 + hv \longrightarrow NO + O(^3P) \tag{1.14}$$

The $RO_2^{\bullet}$ radical resulting from Equation 1.11 can also react with $HO_2^{\bullet}$, other $RO_2^{\bullet}$ radicals and NO_2 to form a series of products, detailed below in Equations 1.15-1.20. The products from Equation 1.20 are peroxyacyl nitrates (PAN).[82]

$$RO_2^{\bullet} + HO_2^{\bullet} \longrightarrow ROOH \tag{1.15}$$

$$RO_2^{\bullet} + HO_2^{\bullet} \longrightarrow R{=}O + H_2O + O_2 \tag{1.16}$$

$$RO_2^{\bullet} + HO_2^{\bullet} \longrightarrow RO + OH + O_2 \tag{1.17}$$

$$RO_2^{\bullet} + HO_2^{\bullet} \longrightarrow ROH + O_3 \tag{1.18}$$

$$RO_2^{\bullet} + R'O_2^{\bullet} \longrightarrow \text{products} \tag{1.19}$$

$$RO_2^{\bullet} + NO_2 \rightleftharpoons RO_2NO_2(PAN) \tag{1.20}$$

The $RO^{\bullet}$ radical, formed through Equation 1.12 can react with a number of different species, depending on the structure of the R hydrocarbon chain. The reaction of $RO^{\bullet}$ radicals with O_2 is one of the most important (Equation 1.21), particularly if the R chain is an alkane. From this reaction a carbonyl compound (R=O) and a $HO_2^{\bullet}$ radical is formed. The $HO_2^{\bullet}$ radical can then react *via* Equation 1.7 to re-form an $^{\bullet}OH$ radical. The NO_2 from this reaction will dissociate and eventually form O_3 (Equations 1.14 and 1.5). This completes a catalytic cycle, as the $^{\bullet}OH$ radical is regenerated, as seen previously in Figure 1.6. An oxidised product and two molecules of O_3 are also formed.

$$RO^{\bullet} + O_2 \longrightarrow R'CHO + HO_2^{\bullet} \tag{1.21}$$

As discussed previously, the lifetime of many species in the atmosphere are governed by the concentration of the $^{\bullet}OH$ radical. The lifetime of VOCs is slightly more complex, usually the reaction with the $^{\bullet}OH$ radical dominates however this is dependent on the individual VOC. The reactions with O_3 and/or the $NO_3^{\bullet}$ radical can dominate due to higher concentrations of them in comparison to the $^{\bullet}OH$ radical. Lifetimes of VOCs can vary from several months for some alkanes to just a few hours or less for alkenes and even minutes or seconds for very reactive species such as sesquiterpenes. The lifetime of VOCs with respect to the $^{\bullet}OH$ radical can be calculated by Equation 1.22; where τ is the lifetime, which is the time it takes for the concentration of compound i to fall to $\frac{1}{e}$ of its initial concentration, k_{VOC_i} is the rate constant of compound i and $[^{\bullet}OH]$ is the concentration of the hydroxyl radical.

$$\tau = \frac{1}{k_{VOC_i} \cdot [^{\bullet}OH]} \tag{1.22}$$

When conducting studies of VOCs and their reaction with the $^{\bullet}$OH radical, another important consideration is $^{\bullet}$OH reactivity, *k'*. This is the product of multiplying the bimolecular rate coefficient for the species *X* when reacting with the $^{\bullet}$OH radical with its associated concentration.[83] This is shown in Equation 1.23, where [X] is the concentration and $k_{X,OH}$ is the bimolecular rate coefficient for the species *X* when reacting with the $^{\bullet}$OH radical. Total $^{\bullet}$OH reactivity (k_{OH}), the inverse of the lifetime of the $^{\bullet}$OH radical, can be calculated by summing the reactivity of all the chemical species under study, shown in Equation 1.24 and discussed in more detail in Chapter 3.[78,83] All these factors are important when studying the chemistry of urban areas as studies have shown that VOC concentrations can be the limiting factor for O_3 production, (discussed in detail in the next section).[84]

$$k_X = k_{X,OH} \cdot [X] \tag{1.23}$$

$$k_{OH} = \sum_{i=1}^{n} k_{X,OH} \cdot [X]_i \tag{1.24}$$

1.2.3 Formation of ozone

O_3 can pose a significant threat to health, ecosystems, climate and materials on local, regional and global scales.[3] As such, it is important to fully understand why, despite controls in place to decrease concentrations of precursor air pollutants, this has not happened to the degree expected.[85]

There is no direct emission source of O_3 in the atmosphere, rather it is formed through a chain of photochemical reactions of the precursor gases NO_x, VOCs and CO, discussed previously. The reductions of these precursor gases does not appear to have resulted in the expected decrease in ambient O_3 concentrations in Europe.[3] For example, 2012 EU emissions relative to 2003 were decreased by 30%, 32%, 28% and 15% for NO_x, CO, NMVOCs and CH_4 respectively, while O_3 did not show any clear trend.[3] O_3 formation is extremely complex, further compounded by the huge number of VOCs involved. This can have an impact on how regulations for emission reductions are constructed as there are numerous sources of VOCs and their oxidation pathways are complex.

The meteorology of the area where measurements are taken should also being taken into account when considering O_3 formation. The most frequently examined relationship

is the correlation between O_3 formation and atmospheric temperature.[86,87] It has been shown that the relationship between the daily O_3 concentration and temperature is non linear, where O_3 concentration appears to show no dependence on temperatures below 20-25 °C, but is strongly dependent on temperatures above 30 °C.[88–92] Historically, the major O_3 pollution episodes have been shown to correlate with slow-moving, high-pressure weather systems combined with high concentrations of VOCs. This effect is increased when these meteorological conditions occur during summer, as this is the time with the greatest amount of sunlight thus photochemical reactions are at a maximum.[93,94] Another important factor associated with the meteorology is that the conditions can determine whether O_3 precursor species, such as VOCs and NO_x, are either contained in the local region or transported to other regions thus likely affecting the air quality in surrounding areas.

Haagen-Smit and Fox (1954) first plotted a graph (Figure 1.8) which shows how concentrations of O_3 relate to mixtures of VOCs and NO_x in the region under investigation.[2] This is called an isopleth graph, showing the effect of reducing VOC and NO_x levels on O_3 concentrations and is an empirical representation of the VOC-NO_x-O_3 relationship.[51] The location of a particular point on the O_3 isopleth graph is defined as the ratio of VOC and NO_x at that point. This is important to consider in the VOC-NO_x-O_3 relationship and shows the major effects of reducing VOC and/or NO_x concentrations on corresponding O_3 concentrations.[2]

Kleinman (1994) proposed an addition to the original isopleth graphs by schematically showing how the O_3 production rate can be limited by either VOCs or NO_x through the use of a Empirical Kinetic Modelling Approach (EKMA) diagram, shown in Figure 1.9.[95,96] This shows two species limited, opposing regimes and a transitional region (the diagonal ridge from the lower left to upper right corner in Figure 1.9), where O_3 is equally sensitive to VOCs and NO_x; but is relatively insensitive compared to the limited regimes. The transitional ridge corresponds to a VOC/NO_x ratio of approximately 8:1. This ratio is dependent on individual region factors such as the oxidative chemistry of that area, initial concentrations of pollutants and available oxidants *etc.* There are two very useful regions to consider on this graph which show the chemistry of either relatively unpolluted rural/suburban or polluted urban regions. The right of the transitional ridge is characteristic of a rural/suburban region which is usually NO_x limited. This is shown by the fact that a reduction in peak O_3 concentration is achieved by lowering NO_x con-

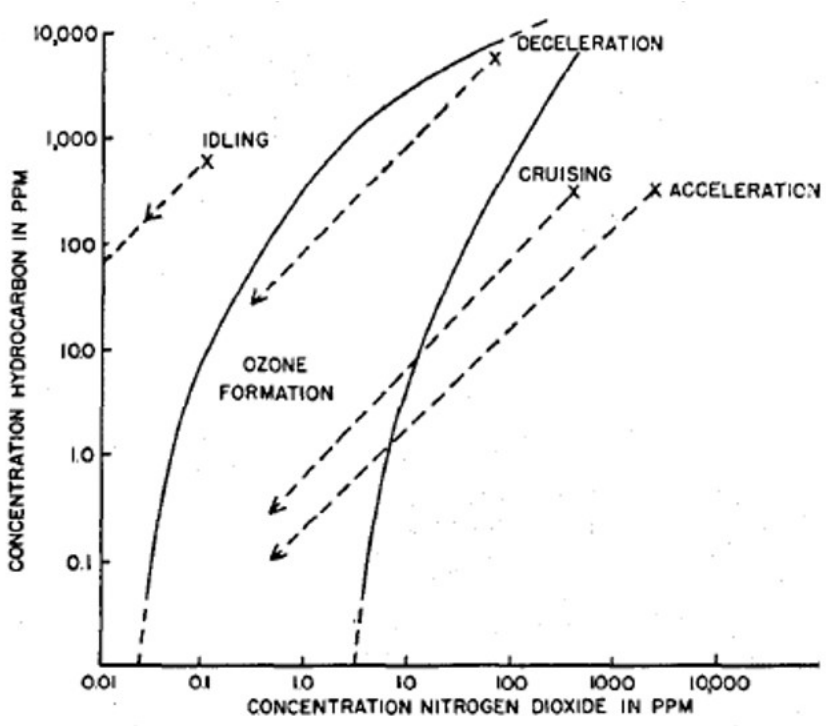

Figure 1.8: Photochemical ozone formation as a function of the concentrations of VOCs and NO_x from vehicle exhaust emissions under different driving conditions.[2]

centrations, resulting in a high VOC/NO_x ratio and is relatively insensitive to changes in VOC concentrations. The left of the transitional ridge is systematic of a polluted area that is VOC limited. This shows the opposite scenario, where reducing VOC concentrations results in lower peak ambient O_3 concentration and thus has a low VOC/NO_x ratio.

The VOC-NO_x-O_3 relationship should be taken into account when implementing policies specifically for O_3 reduction. Depending on the region under scrutiny, the specific VOC/NO_x ratios of that area can be used to customise emission controls.[51] However it is not this simple. The effects of other emission reductions need to be considered with respect to the effects they would have on secondary pollutants. These in themselves can be harmful and have multiple further reactions in the atmosphere. An added complexity is the role of biogenic emissions. Depending on the area of study, reductions in the anthropogenic emissions of VOCs may not produce a correlated reduction in O_3 concentrations if there are significant biogenic sources. This shows how regulations need to take into account all the effects of reducing certain pollutants and a reliable evaluation of the contributions from anthropogenic and biogenic VOC sources.[51]

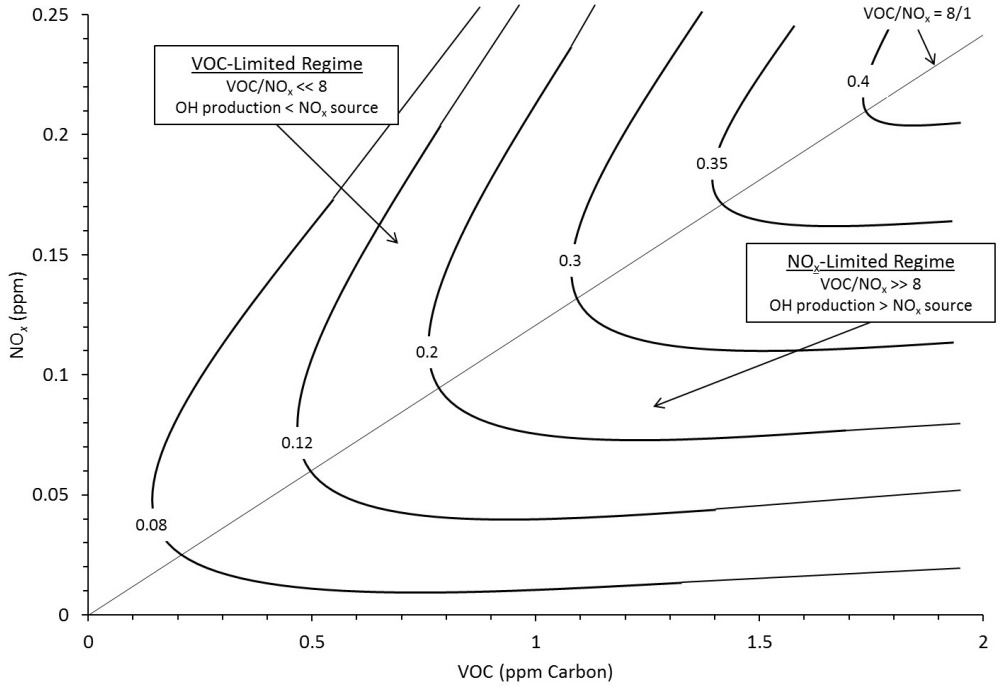

Figure 1.9: Typical EKMA diagram showing isopleths of 1-hr maximum ozone concentrations (in parts per million by volume (ppm)) calculated as a function of initial VOC and NO_x concentrations and the regions of the diagram that are characterized by VOC limitation or NO_x limitation. "OH production" refers to the rate of OH photochemical production and "NO_x source" refers to the rate at which NO_x is emitted into the boundary layer.[95,96]

1.2.4 Particulate matter in urban areas

Aerosols are defined as the suspension of fine liquid or solid particles in a gas. Aerosols have a variety of sizes and chemical composition. PM has both natural, (*i.e.* dust, pollen and sea-spray) and anthropogenic sources, (such as transportation and industry) and two main sinks, wet and dry deposition. Traffic-related emissions are estimated to contribute to over 50% of total PM concentrations in urban areas.[9] Particles have a number of properties that should be taken into account when trying to understand the roles they play in atmospheric processes, these are number, concentration, size, mass, chemical composition, and aerodynamic and optical properties.

There are two main size ranges measured for air quality; PM_{10}, coarse particles which encapsulates particles with diameters of 10 μm or less, and $PM_{2.5}$, fine particles whose diameters are equal to or less than 2.5 μm (shown in Figure 1.10). The sources of coarse particles are usually mechanical processes, such as grinding, wind and wear. For fine particles, the main source is the gas-to-particle partitioning of low-volatility vapours, with urban areas dominated by combustion emissions.

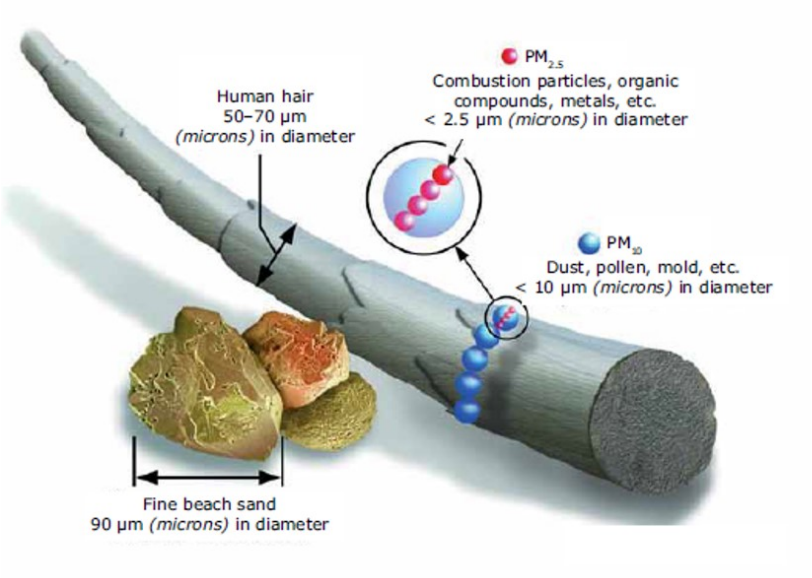

Figure 1.10: Illustration of the size of PM_{10} and $PM_{2.5}$ particles in comparison to a human hair and a grain of sand.[97,98]

Organic aerosols (OA) are particularly important, as they can account for between 20-90% of submicron particulate mass and can be either primary or secondary.[99] Primary organic aerosol (POA) is directly emitted into the atmosphere from sources such as biomass burning and fossil fuel consumption. SOA is produced through the oxidation of precursor VOCs to form lower volatility species that have the ability to partition into the aerosol phase (discussed previously in Section 1.2). There has been a slow decline in the direct emission of PM from 2006 to 2012, however emissions in rural and urban backgrounds remained consistent. Even with this decline, exposure limits were exceeded in over 50% of EU countries in 2012.[3] The evolution of both POA and SOA are not fully understood and as such future research must be carried out on PM, with special emphasis on OA, to determine the sources of PM.

1.3 Measurements of volatile organic compounds

When analysing atmospheric VOCs, there are many techniques to choose from. The method of choice is dependent on many factors, including the choice of measurement sites and whether the analysis will be done *in-situ i.e.* in the field or off-line where samples are brought back and analysed in the lab. When making observations in the field there are certain criteria which must be met; portability, power consumption, gases required, consumables and the fact that the environment in the field is not always suitable for

sensitive instrumentation, such as mass spectrometers.

1.3.1 Gas chromatography

One of the most common methods of in situ analysis is thermal desorption-gas chromatography coupled to either a flame ionisation detector or a mass spectrometer (TD-GC-FID/MS).[100] Thermal desorption is a versatile, sample introduction technique which is used to extract analytes of interest from complex samples such as air. The GC column and oven temperature programme are selected to provide the required selectivity and resolution of compound peaks. The FID is a detector that gives a response proportional to the number of carbon atoms in the individual species.[101] It is widely used due to its fast acquisition rate, broad sensitivities and the fact that it doesn't produce a signal for inorganic compounds such as CO and CO_2.[102] Compound identification is established through comparison of GC column retention times with previous standard injections. When using a MS it is possible to identify unknown compounds, as some structural information is provided.

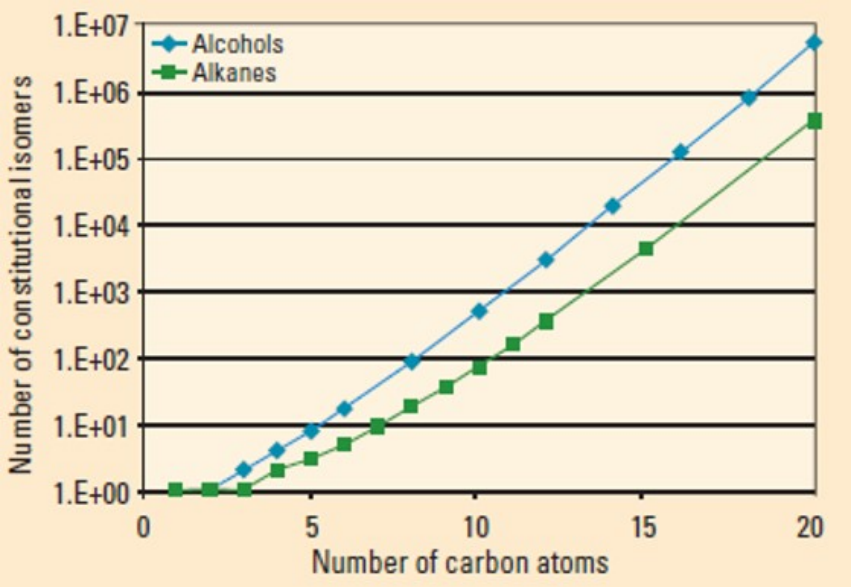

Figure 1.11: Number of unique isomers possible as a function of the number of carbon atoms in the molecule for alkanes and alcohols.[103]

There are challenges to these methods, specifically that there are hundreds, if not thousands, of individual VOCs in the atmosphere.[103] The situation is further complicated due to the presence of structural isomers, shown in Figure 1.11 where the number of isomers exponentially increases as the number of carbon atoms increase.[103] Many of these

VOCs are not seen in conventional GC methods due to the limited separation power. Even through the use of long, extremely narrow bore columns, the vast amount of species present in an atmospheric sample are too large to be accurately separated.[104]

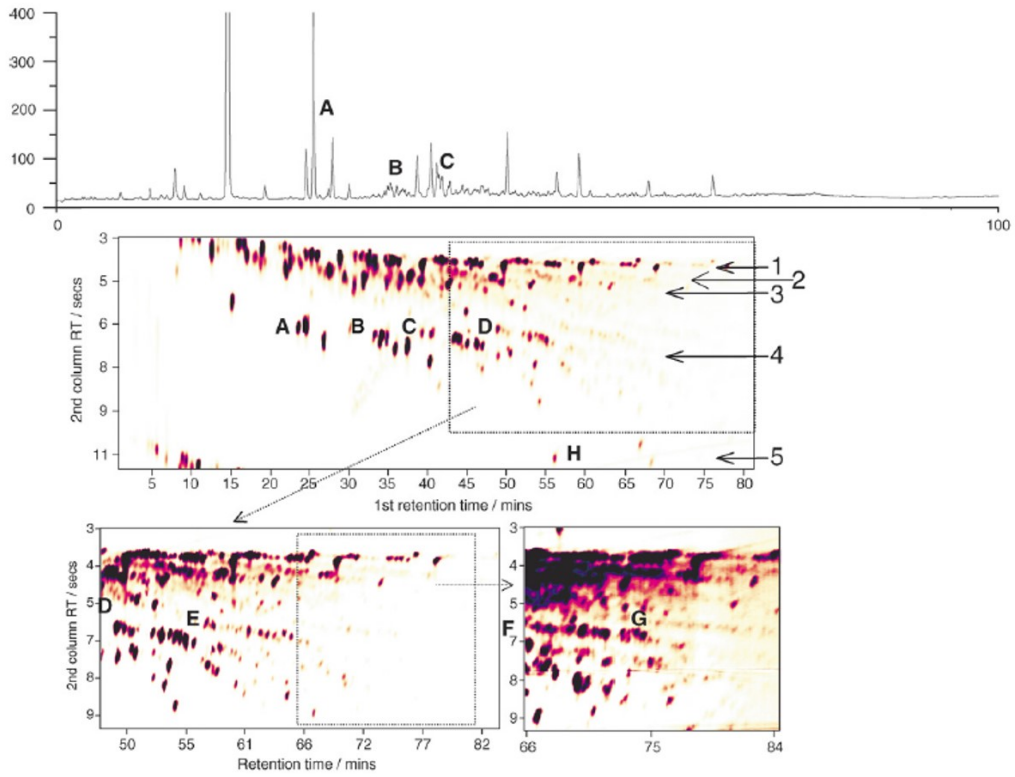

Figure 1.12: Analysis of a Leeds urban air sample, with comparison of a single column (upper) and GC×GC (lower) separation. Successively extracted chromatograms are shown to illustrate the complexity found at higher boiling points. The GC×GC chromatogram has been labelled at the start of individual C_n substituted monoaromatic bands that run from right to left: A = C_2, B = C_3, C = C_4, D = C_5, E = C_6, F = C_7, G = C_8, and H = naphthalene. The chemical bands have also been assigned: 1 = aliphatic, 2 = olefins, 3 = oxygenates, 4 = monoaromatics and 5 = polyaromatics.[105]

A possible solution to this was first introduced by Giddings in 1987, who proposed the use of a multidimensional chromatographic separation (MDGC, discussed in more detail in Chapter 5). This involves the use of heart-cutting, where a fraction of the eluent from the first column was sampled then injected onto a second column with a different selectivity.[106] However, for the analysis of unknown species, this technique proved ineffective as only a fraction of the original sample was separated in two dimensions. For a full analysis, the entire sample must be subjected to a multidimensional separation.[107] Figure 1.12 shows a comparison of the same sample analysed using a conventional GC method and a relatively new method, termed comprehensive two-dimensional gas chromatography (GC×GC, discussed in more detail in the following section) where the sample

is fully separated in two dimensions.[105] This shows that the number of species identified in a multidimensional separation (lower panels) greatly exceeds those found in the 1D GC method (upper panel).

1.3.2 Comprehensive two-dimensional gas chromatography

Comprehensive two-dimensional gas chromatography (GC×GC), first introduced in 1991 by Liu and Phillips,[108] is where two columns of different selectivities are combined in series using a modulator (shown in Figure 1.13). The modulator works by fractionating effluent flow from the primary column and injecting, at rapid and regular time intervals, onto the secondary column, where a fast separation, usually <10 seconds, is completed before the modulator begins injecting the next sample of eluent. This greatly increases the separation and resolution power over conventional separations and helps provide a comprehensive analysis of complex samples.[109] The analysis of complex mixtures, such as urban air samples, using GC×GC increases the number of VOC species identified when compared to single column GC.[110]

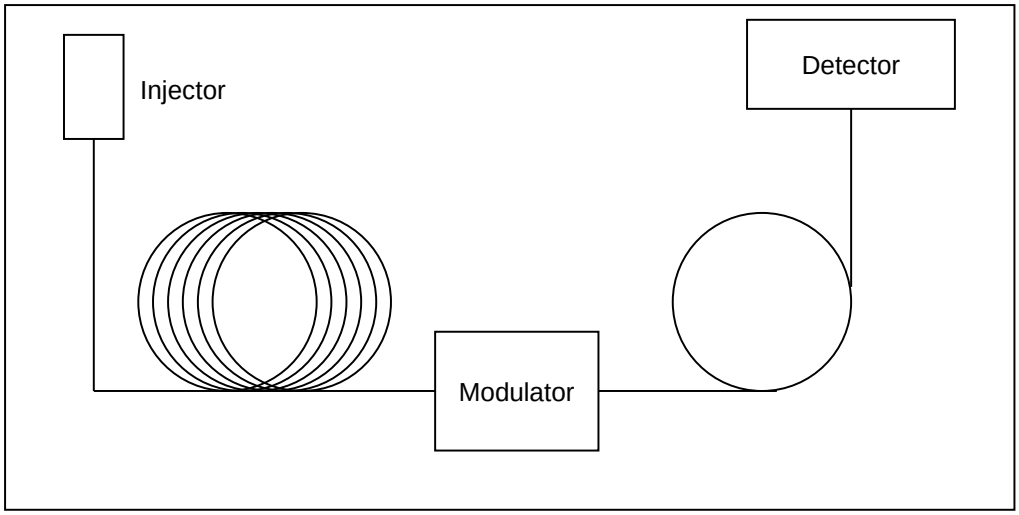

Figure 1.13: Typical GC×GC schematic showing the position of the modulation interface

The modulating interface is positioned between the primary and secondary columns, also known as dimensions, allowing for analytes to be separated using two different molecular properties, usually volatility, chirality and/or polarity. For modulation to be effective, the modulation period should occur at frequent and consistent times throughout the entire analysis.[107] Murphy *et al.*, (1998) determined that each analyte should be sampled in the second dimension at less three to four times to preserve the primary column separation.[111]

1.3.2.1 Peak capacity

Peak capacity, n, was defined by Giddings in 1967, as the maximum number of peaks that can theoretically be resolved in the available retention space.[112,113] It is used as a measure of how effective the chromatographic separation is. The column can be separated into a series of identical segments, or theoretical plates (N) which are related to the peak capacity (n_c) of that column through Equation 1.25. The theory behind this equation assumes that the peaks resolved on the column will separate evenly across the chromatogram. In reality, however, the situation is more complex. Peaks do not separate out equally and even systems with a high peak capacity still see co-elution, where 2 or more compounds occupy the same retention time on the column and cannot be separated. Thus, the actual peak capacity of the column is lower than the theoretical calculation.[114]

$$n_c \approx 1 + N^{\frac{1}{2}} \tag{1.25}$$

For GC×GC systems, the maximum theoretical peak capacity (n_{tot}) is approximately equal to the product of the peak capacities of the two columns (n_{c1} and n_{c2}), Equation 1.26.[106,113] The actual peak capacity will be slightly lower than that calculated due to some correlation between the retention on the different dimensions (discussed in more detail in the next section). However, the peak capacity of GC×GC systems greatly exceed those of conventional 1D or heart-cut (discussed in more detail in Chapter 5, Section 5.1.1) GC systems, even when using 2 columns that have only moderate peak capacities. For example, if the peak capacities of the primary and secondary columns are 50 and 20 respectively, the peak capacity of the system will be ≈ 1000.[114] This is well beyond the values that can be obtained using only one column. Dalluge *et al* (2002) showed that if the system is optimised, peak capacities into the tens of thousands can be achieved.[115]

$$n_{tot} \approx n_{c1} \times n_{c2} \tag{1.26}$$

1.3.2.2 Orthogonality

Creating an orthogonal system is an important aspect of using GC×GC. The separations from the two columns must be independent of each other,[106,113] allowing for maximum use of the available separation space. Typically this is done by using two columns that separate based on different criteria that do not correlate with each other (*i.e.* the combination of a boiling point and polarity separation).[116,117] The timing of the two separations aids this

process. Usually, the separation from the primary column is quite long and the separation is based on volatility, with the GC oven temperature increased at a known rate throughout the entire run. On the other hand, the separation in the second dimension is very fast, mostly in the order of only a few seconds. This means that the separation from the second column should be isothermal and, by properly tuning the two columns, the species in each modulation pulse should have the same or similar boiling points.[114] Therefore, any separation in the second dimension is only due to differences in either chirality or polarity.[117]

1.3.2.3 Data visualisation

The raw data produced by GC×GC can be hard to visualise as the detector output is in the form of a continuous one dimensional chromatogram that consists of a series of short second dimension separations, produced during modulation. One way to de-convolute this, is by using 3D imaging software to display the data as a contour or surface plot. This is where the retention times from the primary and secondary columns are the x and y axis respectively, and compound intensity is the coloured contour (or z-axis); an example of which can be seen in Figure 1.14.[116] The two retention times provided through separation by GC×GC can be used, dependent on the choice of columns, to give information about compound volatility, chirality and/or polarity. However, even with this advantage, an identification cannot be easily made unless the compound has been previously analysed. There is another way to infer compound identity which will be discussed in the next section.

1.3.2.4 Ordered chromatograms

As discussed previously, there are many thousands of VOCs that could potentially be separated and resolved when analysing complex mixtures using GC×GC.[103] This can make data analysis a time consuming and challenging prospect. However, a useful feature of using GC×GC, is the production of ordered chromatograms where species with similar functionalities (*i.e.* alkanes, alkenes and aromatics) form bands across the separation space.[104,118] This is shown in plot (a) of Figure 1.15, where the structured features of the chromatogram allows for a basic group type analysis to be made. The regions of the chromatogram that corresponds to the aliphatics, monoaromatics and polyaromatics are identified by the arrows 1, 2 and 3 respectively.[105] Another common feature is also shown

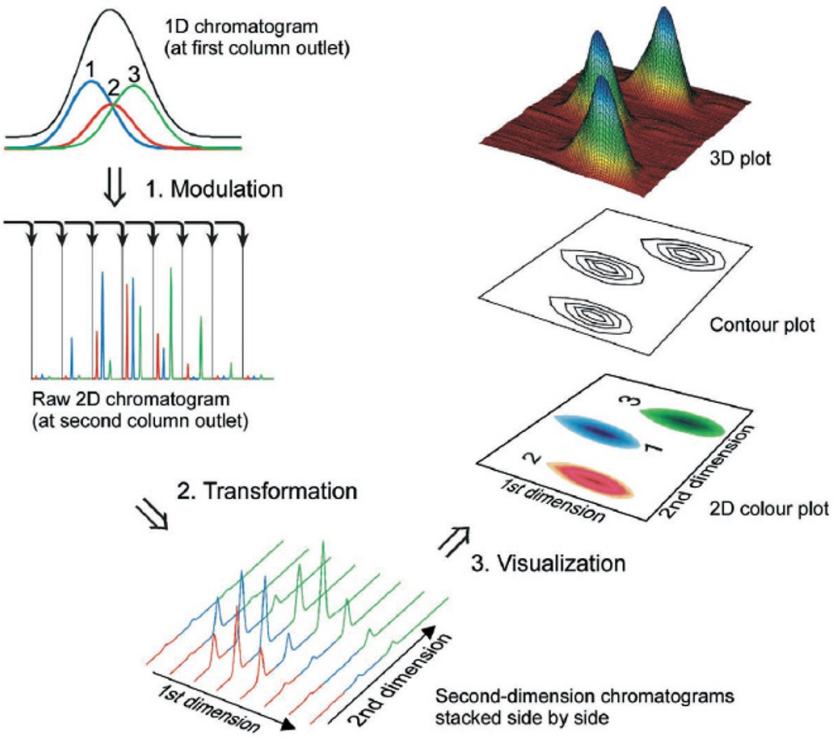

Figure 1.14: Visualisation of how a GC×GC chromatogram is produced.[116]

in Figure 1.15, plot (b) specifically. This is a "roof-tile" structure, where each tile shows an isobaric group of monoaromatics that have C_4, C_5, C_6, and C_7 substitution. These features can be used to help identify unknown species by providing information about functionality, volatility and/or carbon number.

1.3.3 Modulators

A key component of GC×GC is the modulator. This fractionates the primary column effluent into smaller portions that are then further separated on the secondary column. The modulator must concentrate each fraction and introduce it to the secondary column as a narrow band in order to secure the maximum resolution possible in the secondary separation.[114] There are three main types of modulators that can be used; thermal, cryogenic and valve based. A schematic of the basic set-up of the three modulator designs are shown in Figure 1.16. These will be discussed in further detail in the following sections.

1.3.3.1 Thermal modulators

Thermal modulators are usually the most frequently used type of modulator. These were designed so that analytes of interest are physically retained onto and then desorbed from

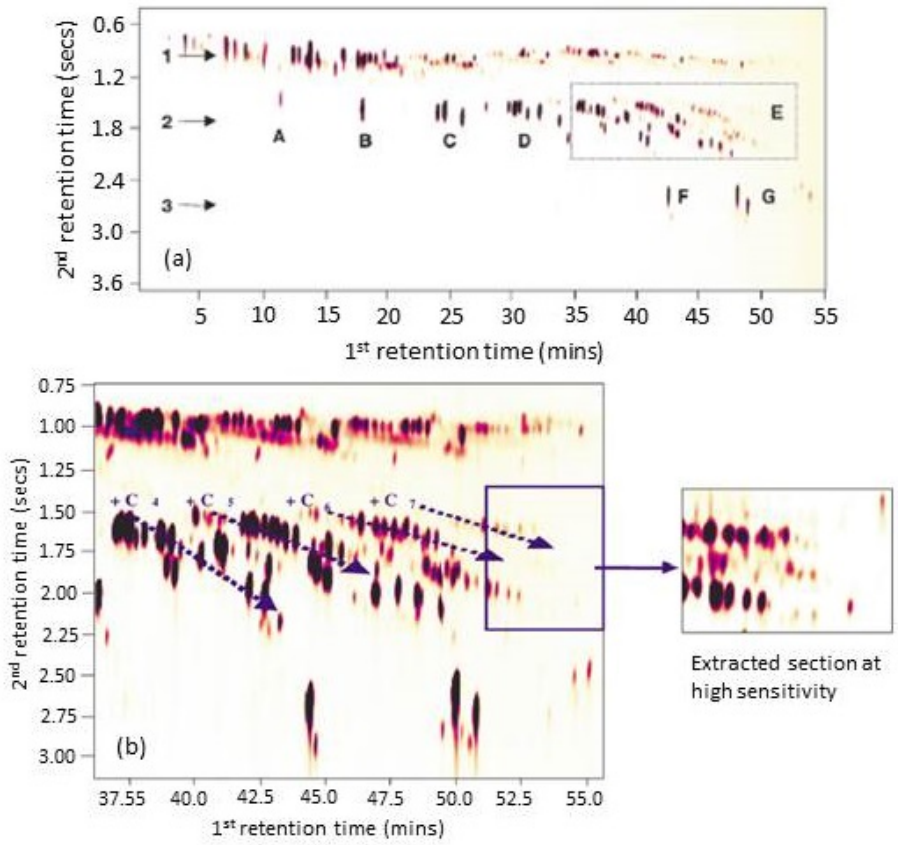

Figure 1.15: Valve modulated GC×GC analysis of leaded gasoline. Plot (a) shows three bands of compounds: 1) aliphatic, 2) monoaromatic and 3) polyaromatic bands and A benzene, B toluene, C xylenes, D C_3 substituted monoaromatics, E higher monoaromatics, F naphthalene (with adjacent benzothiophene) and G methyl naphthalenes. Plot (b) shows an expanded section of the GC×GC chromatogram, with the C_4-C_7 substituted monoaromatic groups highlighted.[105]

a thick film of stationary phase.[119] This was achieved through changing the temperature applied to the stationary phase.[119] The original design by Liu and Phillips in 1991, had a piece of capillary tubing that was coated with thin layers of metal (usually gold or aluminium), resistively heated using pulses of electronic current.[108,114] The desorbed analytes could then be passed through the secondary column by the carrier gas. Although good results were seen using thermal modulators,[120–125] this design proved to be unreliable.[119] The application of the metal layer was not always uniform, resulting in local regions of overheating and causing a temperature gradient in the modulator.[114] These were eventually replaced with modulators using mechanical movements in two different ways. The first was based on a rotating mechanical heater called a 'sweeper'. The second was based on cryogenic cooling and will discussed in the next section.

The 'sweeper' design by Phillips and Ledford in 1996 is shown in the top panel (a) of

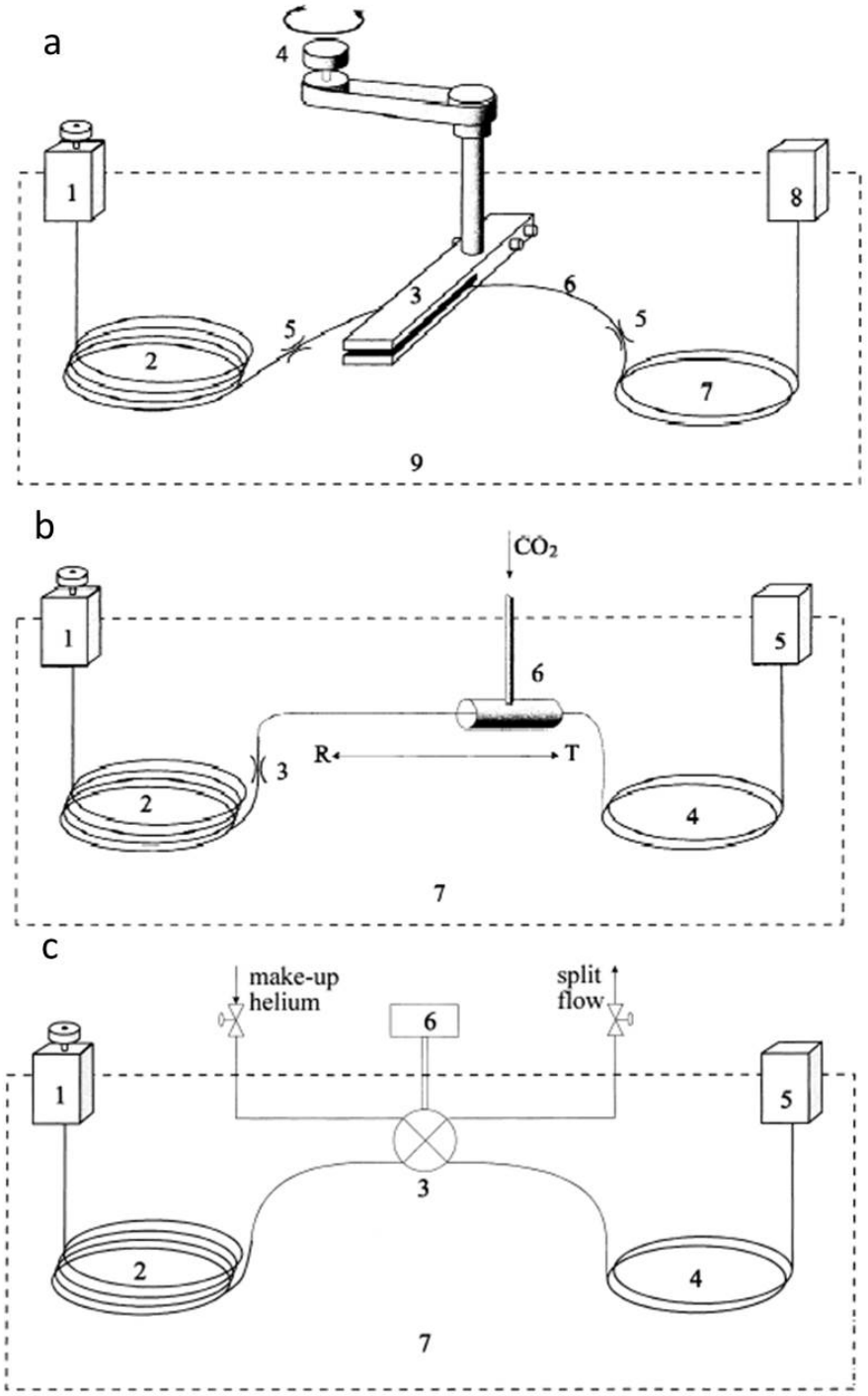

Figure 1.16: Schematics of GC×GC setups with various modulators, (a) thermal (b) cryogenic and (c) valve. Numbers in (a) correspond to: 1 - injector, 2 - first dimension column, 3 - slotted heater, 4 - stepper motor to turn the slotted heater, 5 - micro press fit column connections, 6 - thick film modulator capillary, 7 - second dimension column, 8 - detector, 9 - GC oven. Numbers in (b) correspond to: 1 - injector, 2 - first dimension column, 3 - column connector, 4 - second dimension column, 5 - detector, 6 - moving cryogenic trap, 7 - GC oven. Numbers in (c) correspond to: 1 - injector, 2 - first dimension column, 3 - diaphragm valve, 4 - second dimension column, 5 - detector, 6 - valve controller, 7 - GC oven.[119]

Figure 1.16.[126] This design has been fully described in Phillips *et al* (1999).[127] Briefly, this design has a separate heating element, the 'sweeper' (part 3 and 4 in panel a of Figure 1.16), which moves over the modulator capillary (part 6) to provide local heating. Importantly, this method of heating is able to provide a stable and controllable temperature.[119] The commercial version of this thermal modulator has proved to be quite satisfactory in several laboratories.[127–129] However, this design was not without its disadvantages, the main one being that in order for the retained analytes to be desorbed, a temperature difference of nearly 100 °C must be applied. This reduces the maximum temperature of both the oven and the primary column.[119]

1.3.3.2 Cryogenic modulators

The second type of mechanical modulators are based on the use of cryogens, such as liquid CO_2 or nitrogen (N_2), as cooling agents to trap analytes of interest.[114] The use of this type of modulator was spearheaded by Marriott and Kinghorn (1997) for the analysis of essential oils,[130] and extended to atmospheric samples in 2000 by Lewis *et al.*[84] These modulators are designed so that, usually the second dimension column, is threaded through a small chamber or trap that is cooled using a cryogen, shown in the middle panel (b) of Figure 1.16. This trap is moved back and forth along the column to achieve modulation. Eluent from the primary column is condensed as it enters the trap while it is being cooled. This condensed material forms a small plug. At this point in the modulation sequence, the trap position is moved. This causes the cooled section of column to be heated by the temperature of the oven. Thus the plug of analyte material is released due to it being rapidly heated, vaporised and propelled down the secondary column by the carrier gas.[114]

For the analysis of more difficult or low concentration samples, this type of modualtor is preferred. The rapid and reproducible thermal cycling to trap and release analytes produces sharpened peaks and a high sensitivity.[102] This sensitivity is enhanced due to the combination of conservation of all sample material between the two columns and peak compression in the second column.[131] However the use of cryogenic modulators is not without disadvantages. They typically have a limited retention of high volatility species and difficultly in removing water from humid samples.[131] Also, cryogenic modulators have reduced portability and the use of liquid N_2 results in a large consumable budget.[132] This is important when performing in-situ analysis of the atmosphere.

1.3.3.3 Valve modulators

The third type of modulator, and most important for this thesis, is valve based. Valve modulators have some significant advantages over those based on thermal and cryogenic processes, particularly for the analysis of atmospheric samples.[114,133] Typically, valve modulators can be used independent of temperature and if housed within the GC oven, analytes are transferred between the two dimensions at an ambient oven temperature. For use in atmospheric analysis, this is particularly important as there can be compounds that have high volatility and/or polarity. As mentioned in the previous section, cryogenic modulators have difficulty trapping high volatility analytes something that is not seen when using valve modulators. Also, there is no large use of cryogens, making valve modulators an ideal choice for field studies. The only drawback to the use of valve modulators is the venting of some sample to waste, seen in early designs.[114,133] However this has been addressed using total transfer flow modulators.

Valve based modulators transfer fractions of primary column eluent onto the secondary column using a switching valve. Typically, valve modulators have two different valve positions that correspond to a sampling and injection period. In the sampling position, the primary column eluent enters the valve and in some later designs is collected in a sample loop. The valve then switches to the injection position where the eluent is transferred onto the secondary column. At this point in early designs, any eluent leaving the primary column was vented to waste. Usually the modulator is in the sampling and injection positions for 80% and 20% of the total modulation time, respectively.

Bruckner *et al* (1998) introduced the first valve-based GC×GC modulator. This was a multi-port diaphragm valve housed within the GC oven.[134] A second valve modulator was designed by Seeley *et al* in 2000, using a six-port diaphragm valve with sample loop that was housed in a secondary oven.[135] This design was based on differential flow, where the secondary column had a much higher carrier gas flow rate than the primary column, (usually about 20 times higher) to rapidly flush eluent down the secondary column. This ensured maximum analyte transference but also reduced any band broadening effects by minimising the thickness of the transferred plug.[135] Both of these designs were quite successful, however, approximately 20% of the primary column eluent was vented to waste and the separations were not considered to be truly comprehensive.[114]

New developments were made through the introduction of a total transfer flow modulator by Bueno and Seeley in 2004.[136] This design provided a full transfer of material

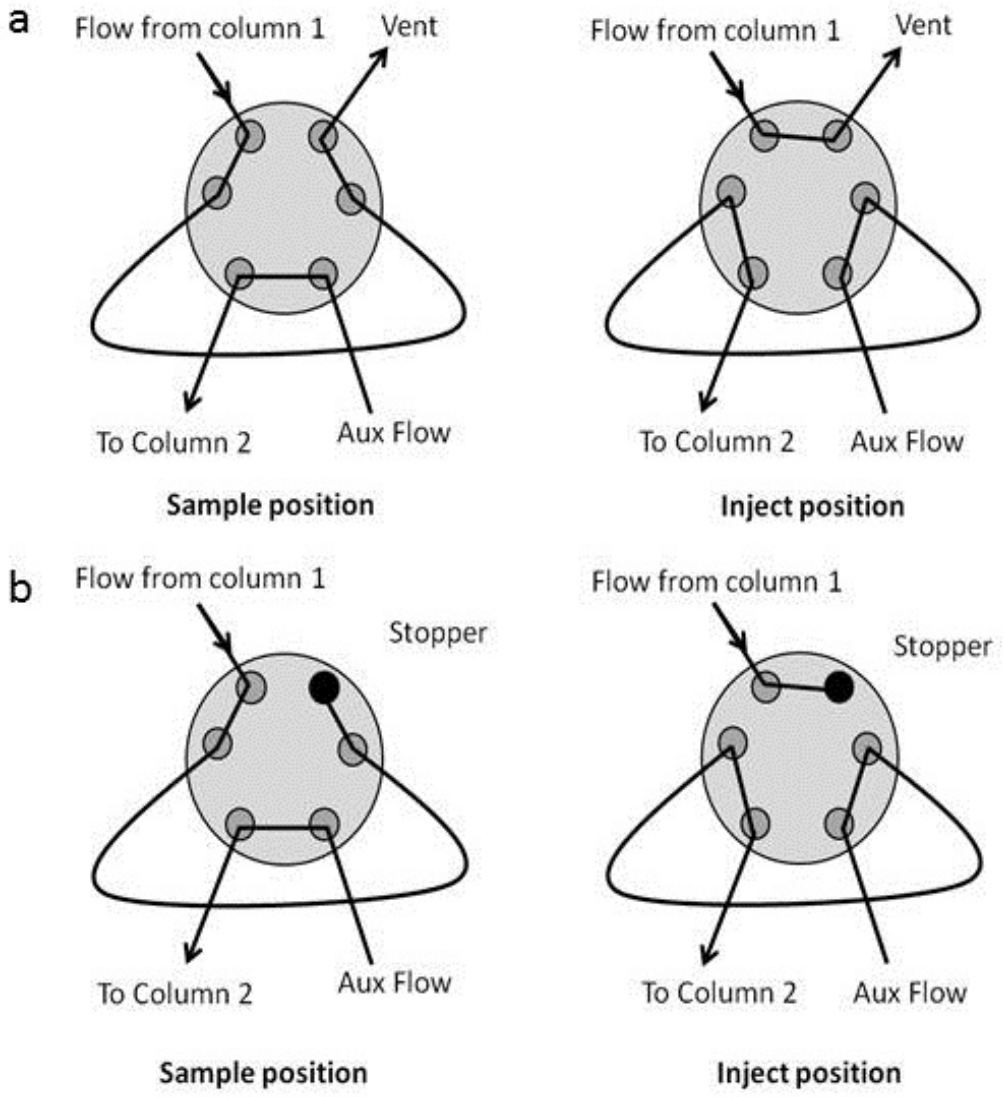

Figure 1.17: Schematics of GC×GC valve modulators using open flow (a, upper panel) and stopped flow (b, lower panel) [131]

between both columns using a fluidic switching device. This idea was developed further by Mohler *et al* who, using the Seeley diaphragm valve and a stopper, also prevented the venting of primary column eluent. [137] The stopper is placed in the vent position of the differential flow modulator design. A comparison of the set up of differential (a, upper panel) and total transfer (b, lower panel) flow modulators is shown in Figure 1.17. A successful modulation using a total transfer flow modulator was achieved through sample compression within the sample loop. [131] When the valve is actuated, the contents of the sample loop are injected under a higher pressure onto the secondary column. Lidster *et al* further developed this into a rugged, single piece modulator that was ideally suited for long term field use. [131] By modifying the GC to internally house the modulator with con-

nections between the valve and columns inside the oven, and introducing an independent heating block, the temperature range of the modulator was increased. This meant that the valve could be heated to prevent any sample desorption and also could withstand any temperature changes produced by high temperatures from the GC oven.[131]

1.4 Thesis outline

This thesis will present work carried out during the Clean Air for London project and the development of a single instrument to measure a wider range of VOCs than are typically observed.

Chapter 2 presents the results of the ClearfLo project, specifically the impact of diesel-related emissions and the subsequent effects on OH reactivity, O_3 formation and SOA production. This chapter aims to provide a wider characterisation of the VOC loading of London's atmosphere through the combination of two GC instruments which can quantify individual VOCs from C_1-C_{12}. Additionally, from the GC×GC instrument, a grouping quantification can provide further information about the total observed VOC loading. From this analysis, the contribution of different VOC emission sources to VOC mixing ratio, OH reactivity, potential O_3 formation and SOA production can be estimated. This could provide information for policy makers to help reduce air pollution by targeting specific high impact emission source.

Chapter 3 details further analysis of the large suite of VOCs measured during the ClearfLo campaign. A measurement of OH reactivity was also made during the campaign. The contributions of various functional groups of VOCs to a modelled reactivity are compared to the actual observation in an attempt to fill the 'missing' reactivity seen in previous studies. This chapter aims to identify which specific individual or grouped VOC species are important in terms of VOC mixing ratio, OH reactivity and potential O_3 formation. The influence of different air mass trajectories and ages could show whether London's atmosphere is influenced by local or long-range transported emissions. Two main emission types, anthropogenic and biogenic sources, are discussed with the former shown to be more influential during the winter campaign. In terms of OH reactivity, the contributions of a standard, extended and an extended plus additional species VOC sets of measurements to a modelled reactivity are compared to the actual measurement. From this it may be possible to determine which species are very important for OH reactivity,

some of which may not be routinely measured (*i.e.* included in the extended or extended plus additional species groups rather than the standard set).

Chapter 4 discusses the analysis of the extensive suite of OVOC measurements made during the ClearfLo campaign, with attempts made to identify potential sources. A detailed investigation is carried out on the impacts of present biofuel use in the UK, specifically the inclusion of ethanol in gasoline. This chapter aims to provide a measurement of a large group of OVOC species, more than is usually measured, particularly in an urban area. The second half of this chapter will investigate how the inclusion of ethanol in biofuel in the UK has affected the balance of emitted OVOCs into London's atmosphere. Modelling of both the observations and emission inventory estimates will be compared to determine if the inventories are accurate. As these inventory estimates are used routinely in models where actual observations are not available, this comparison can make an assessment on whether it is likely that the impact of using biofuels is been under/overestimated.

Chapter 5 shows the development of a combined heart-cut and GC×GC instrument (GC-GC×GC-2FID) to measure a wider range of VOCs. A comparison of this instrument with a well-reported GC instrument is discussed. This instrument was also deployed to Malaysia to characterise a remote atmosphere, heavily influenced by biogenic emissions of VOCs. Although the original GC×GC instrument that will be described in Chapter 2 (the results of which are discussed in Chapters 2, 3 and 4) could quantify a very wide range of VOC species, if only one instrument was to be used this range was not complete. This chapter aims to show how the development of a new GC-GC×GC-2FID instrument has not only extended the carbon range of VOC species that can be quantified, but also allowed for isoprene (a particularly important compound in tropical regions) to be analysed.

Chapter 6 summarises the main findings from this thesis and provides a discussion of future work.

Chapter 2

Diesel-related hydrocarbons can dominate gas phase reactive carbon in megacities

The majority of this chapter has been published in the article of the same name: Rachel E. Dunmore, James R. Hopkins, Richard T. Lidster, James D. Lee, Mathew J. Evans, Andrew R. Rickard, Alastair C. Lewis and Jacqueline F. Hamilton. *Atmospheric Chemistry and Physics*, **15**, 9983-9996, 2015.

2.1 Introduction

With an increasing proportion of the world's population living in cities, rising from only 3% in the 1800s to over 47% by the end of the 20th Century,[1] the impact of urban air pollution has become a significant factor in global health.[85] The costs of air pollution are high even in those locations that have seen considerable improvements in air quality over the past decades;[51] in the UK exposure to PM alone is estimated to reduce life expectancy on average by around 7-8 months, with a cost to society estimated at up to £20 billion per year.[138]

Primary urban air pollution emissions are dominated by PM, NO_x, CO and VOCs. Many of these species can react in the atmosphere to create secondary pollutants, such as O_3, OVOCs, PANs and condensed materials in the form of SOA, which add to the overall PM load.[82,139,140]

Air quality in London has been controlled and monitored for over 60 years, making it in theory one of the better understood atmospheres of the world's megacities. Current measurements in London focus on assessing national compliance with legally prescribed air quality standards, and this includes the hydrocarbons 1,3-butadiene and benzene. However, compliance measurements in themselves are insufficient to fully describe the chemical and physical processes occurring in the urban atmosphere,[7] and a particular weakness lies in speciating the many different classes of carbon compounds in urban air.

The past two decades have seen declining concentrations of most smaller hydrocarbons in European and US cities, a result of tighter regulation of sources such as vehicle exhaust, evaporation and solvents,[141,142] better control of natural gas leakage and an overall switch from gasoline to diesel powered vehicles, shown in Figure 2.1. Current national emissions estimates suggest that the bulk of organic emissions to air are associated with smaller hydrocarbons, and this has driven policy, regulation and observation strategies for compliance. Figure 2.2 shows Government-estimated emissions for the UK (left) and United States (right), categorised into the dominant emission sources.

The speciated emissions inventory supplied in a report from Passant (2002)[144] provides data on a large range of individual non-methane hydrocarbons (NMHCs) and their specific emission sources. From this comprehensive speciation profile, it is possible to apply the most recent UK National Atmospheric Emissions Inventory (NAEI) from 2012 and calculate scaling factors that can applied to each source category (the UK NAEI data is available at http://naei.defra.gov.uk/ data/data-selector, and was last accessed on 30/01/2014).

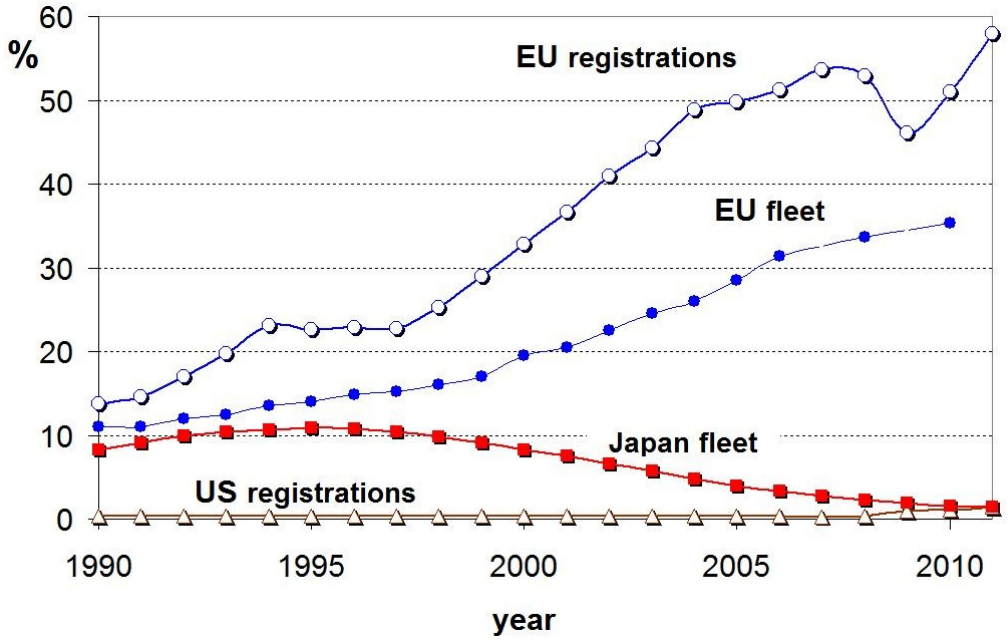

Figure 2.1: Annual percentages of either new diesel car registrations or entire diesel car fleet compositions for the EU, US and Japan over the last two decades.[143]

The speciated proportion profiles of the individual NMHCs emitted from given sources should not change significantly, however the total emission from a source will as a result of changes in activity levels and the impact of regulations/abatement. The US has no equivalent NAEI speciated emission inventory. The SPECIATE database (U.S. Environmental Protection Agency (EPA)) provides detailed species profiles for a larger range of emission sources (the US EPA SPECIATE data is available at http://cfpub.epa.gov/si/speciate/, and was last accessed on 20/02/2014). In order to compare directly to the UK NAEI from Passant, the SPECIATE emission profiles are used to calculate scaling factors as above. All VOC sources have been included in the inventory calculation with the exception of the Forests source category, due to the lack of chemical speciation (given as isoprene+BVOC). There is a small anthropogenic emission source of terpenoids in the inventory from fuel sources and wood product manufacture categories.

It is clear that based on current emission inventories, gaseous organic emissions from diesel appear to represent a negligible fraction of reactive carbon released into the atmosphere. The global demand for diesel fuel is expected to increase by 75% between 2010 and 2040 and by 2020 it is expected to overtake gasoline as the number one transport fuel used worldwide.[145] The environmental impacts of this change are evaluated in part based on the national emission inventories that underpin Figure 2.2.

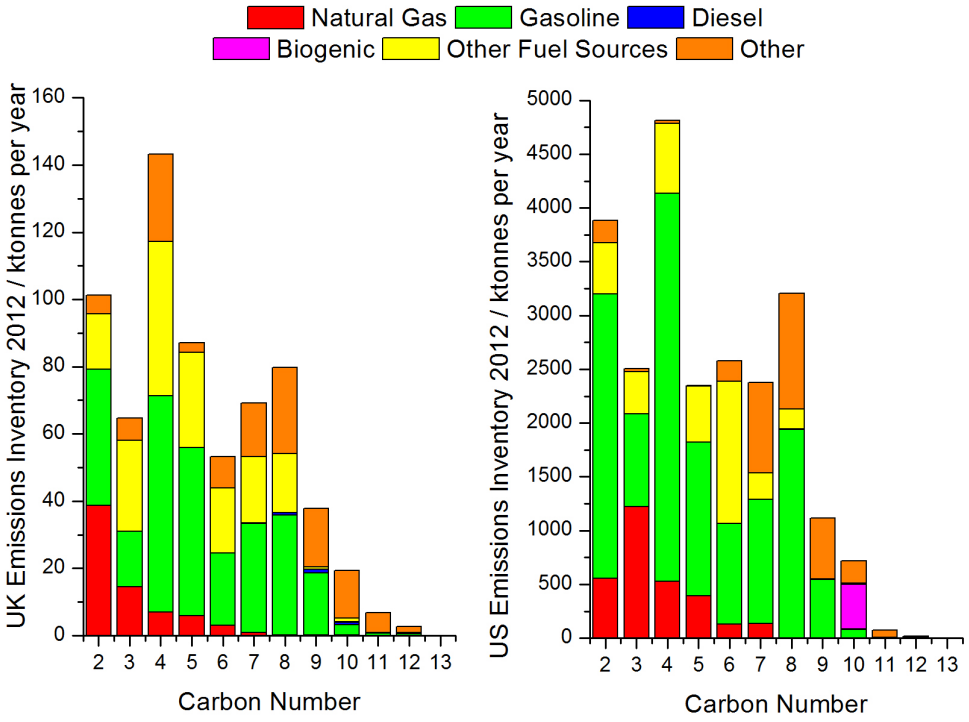

Figure 2.2: Total mass by carbon number and functionality from UK 2012 (left) and US 2011 (right) emission inventories. The carbon number and functionality of emissions have been estimated by applying the speciated inventory of emission sources of Passant (2002)[144] to the most recent estimates of non-methane hydrocarbon source apportionment for each country.

The efficiency with which O_3 and SOA can be formed from diesel or gasoline emissions is dependent on the mass of available organic carbon, and the reactivity and volatility of that material.[53,146,147] To quantify this requires individual speciation of VOCs in order that each property can be properly estimated. The key urban sources of organic compounds include combustion products, unburnt fuels and evaporative emissions of fuels and solvents, all of which are highly complex, often propagating the original complexity of fossil fuels into the air. Whilst each VOC has a unique set of reaction mechanisms, in general terms, as the carbon number increases, the relative complexity of reactions and yields of SOA and O_3 also increase.[105] The organic mixture in air is complicated further by the presence of secondary oxygenated products. This requires a combined approach to investigate VOC composition, such as using two different gas chromatography systems.

Several recent field studies have investigated the relative importance of gasoline, diesel and biogenic emissions in generating SOA.[148–155] These have been carried out predominately in the US, particularly in California, where current diesel usage is rather low by global standards. The US diesel fleet is dominated by heavy-duty vehicles, leading to a difference in the source strength of diesel and gasoline engines between weekdays and

the weekend. In contrast, this trend is not observed in London (see Section 2.5.4.1 and Figure 2.16), which has a different vehicle fleet composition, with 60% diesel fuel use, and a large number of diesel buses operating at similar times to domestic vehicles. It is also important to consider that London and Los Angeles (arguably the world's most well studied city for air pollution) have significant differences in terms of urban geography, population density, commuting patterns, amount of green space/trees and upwind sources (expanded in Section 2.5.4 and Table 2.4). Specifically, the high population density in central London, and the fact that many vehicle journeys both begin and end in central London (rather than radial vehicle commuting); resulting in central London's atmosphere experiencing both cold and warm start vehicle emissions. Also worth noting is that there is no large upwind source of BVOCs in London, rather the natural emissions are distributed homogeneously across the city. Figure 2.3 shows the annual sum of isoprene (left map) and total monoterpenes (right map) flux emissions for Great Britain in 1998.

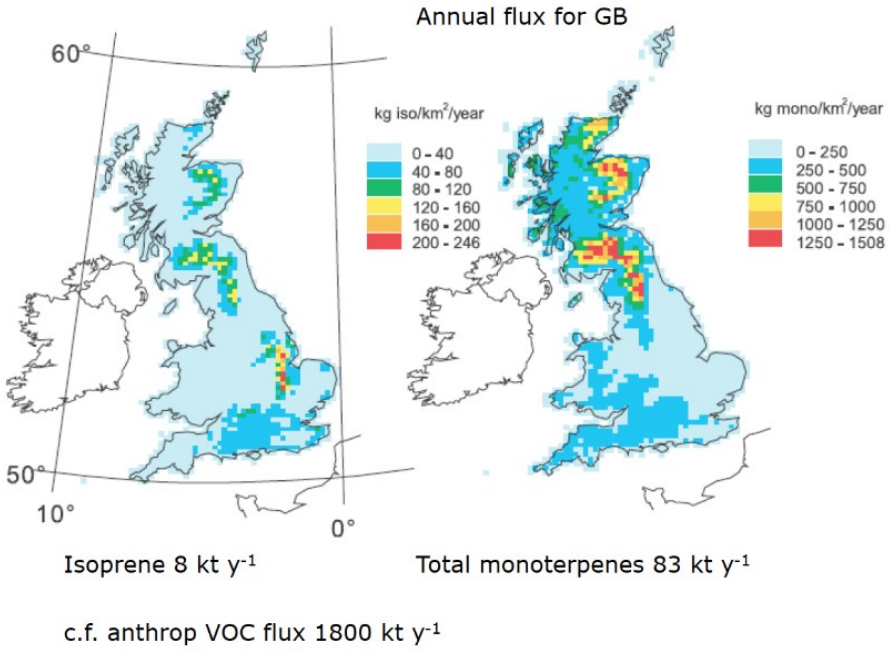

Figure 2.3: Isoprene and monoterpene annual flux for Great Britain in 1998.[156]

This work uses high resolution VOC measurements to investigate the abundance and trends of diesel related hydrocarbons in the atmosphere at a typical urban background site in London. Comparison to the emissions inventories, highlights a severe underestimate in the impact of gaseous VOC emissions from diesel on urban air quality that is likely replicated across Europe and other cities globally where diesel vehicle use is high.

2.1.1 Air quality in London

London is the largest conurbation in the UK (and one of the largest cities in Europe) with a population of roughly 8-12 million and is one of a growing number of megacities in the world. Situated in the south east of England, London has a predominantly maritime/oceanic climate that is typical of west coast, mid-latitude countries. These climates generally have very narrow annual temperature ranges, with warm summers and cool winters, and evenly dispersed precipitation thorough-out the year likely due to prevailing south westerly winds from the Atlantic Ocean.

The word 'Smog' was originally coined by Harold Antoine Des Voeux, a member of the Coal Smoke Abatement Society, in 1905 to describe the mixture of smoke and fog that was attributed to emissions from the burning of coal and other raw materials in London.[157] The London Smog events of the 19th and 20th Centuries culminated in the premature deaths of many thousands of people in all age groups, however those above 45 years of age and suffering from pre-existing heart or respiratory conditions accounted for over 80% of casualties. The Great Smog of 1952, attributed with causing 4000 excess deaths, was a major factor in the increased focus on tackling poor air quality.[85] However, despite the improvements that have been made through legislature and policy; the European air quality limits are still been breached, especially those regarding NO_2 and PM.[158,159] This is likely due to the increased use of road traffic which, in conjunction with the availability of cleaner energy, caused a shift in the balance of pollutants. Recent studies have found that road traffic in and around London is a major contributor to emissions of primary pollutants, such as; PM, NO_x, CO and VOCs.[7]

2.2 Clean Air for London campaign

The National Environment Research Council (NERC) funded Clean air for London campaign (ClearfLo) consisted of a consortium of institutes whose aim was to establish a network of air pollution monitoring sites to investigate boundary layer pollution concurrent with meteorological measurements across London. From this, measurements of the meteorology, gaseous composition and particulate loading of London's atmosphere were made, at both street and elevated level sites; as well as, kerbside, rural and urban background locations. These observations can then be combined with modelling to improve the prediction capability of existing air quality models.[159]

2.2.1 Campaign sites

Figure 2.4 shows the measurement sites chosen during the ClearfLo campaign. The three rural sites (Detling, Chilbolton and Harwell) are all ground-level and were chosen to represent the down and up wind regions surrounding London. Detling is east of London and should have a slightly more polluted atmosphere than is typical of a rural area as it is situated down-wind of the prevailing London outflow. Chilbolton and Harwell are situated up-wind of London's prevailing winds to the west and as such, should have relativity unpolluted air. The four central London sites (all within 4 km of Hyde Park) are all urban but of different classifications. North Kensington is an urban background site and will be discussed in more detail in the next section. Marylebone Road is situated kerbside; as such it should experience major pollution from fresh emissions. The BT tower and King's College sites are both elevated and should provide insights into boundary layer characteristics and street canyon effects respectively.

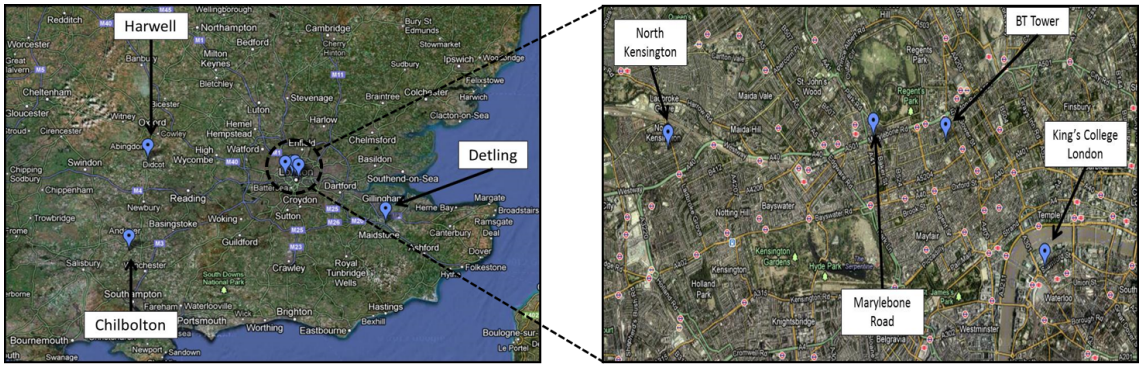

Figure 2.4: Location of all ClearfLo sites, chosen for both long-term and intensive measurements; four in central London and three in the surrounding country. These are a combination of urban kerbside, urban background and rural and are at a variety of height levels

2.2.2 Intensive operating periods

As part of the ClearfLo campaign, intensive operating periods (IOPs) allowed for more detailed observations to be made. Two 5-week IOPs were conducted in January/February and July/August 2012 at the North Kensington site (see Figure 2.5) based at Sion Manning School. To the east and south; the site is bounded by trees and hedges, separated from quite high density housing and development (all sides), Ladbroke Grove, a main transport street approximately 0.17 km away (highlighted by a yellow dashed line) and Meanwhile Gardens approximately 0.74 km away (green circle). To the west are the main school buildings and beyond those (approximately 0.17 km away) is the Carmelite Monastery

Gardens and further away at approximately 0.98 km is Little Wormwood Scrubs (green circles). To the south, approximately 0.41 km away, is Westway, a large transport street with 6-lanes of traffic and two London Underground stations (yellow dashed line and circles, respectively). To the north, highlighted by red circles, is the Kensington Gas Works (0.87 km away) and the North Pole Depot (1.27 km). For more information about this site, refer to Bigi and Harrison (2012).[160]

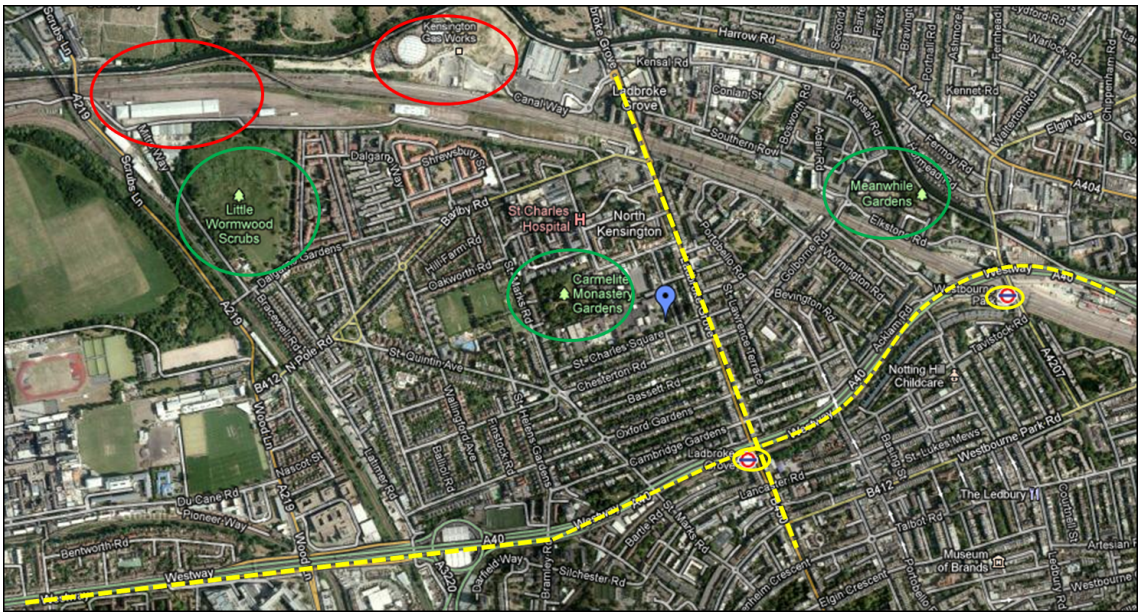

Figure 2.5: Location of the North Kensington site with possible VOC emission sources highlighted. Red circles-Kensington Gas Works and the North Pole Depot, Green circles-Little Wormwood Scrubs, Carmelite Monastery Gardens and Meanwhile Gardens, Yellow circles and dashed lines-2 tube stations, Ladbroke Grove and Westway

2.3 Experimental

2.3.1 Gas chromatography measurements

Two GC instruments were used during the ClearfLo campaign, a dual channel (DC)-GC-FID and a GC×GC-FID. Outside air was sampled from a manifold at 4 m from the ground through a condensation finger in an ethylene glycol bath held at -30 °C, to remove any moisture from the sample.

The DC-GC-FID was operated by the National Centre for Atmospheric Science (NCAS) Facility for Ground Atmospheric Measurements (FGAM) with detailed instrument set up and calibration described in Hopkins *et al.* (2003).[161] In brief, the system has three GC columns that operate in parallel, where after sampling and desorption the flow is split

50:50 to; an aluminium oxide (Al_2O_3) Porous Layer Open Tubular (PLOT, 50 m, 0.53 mm id) for NHMCs analysis; and two, in series, LOWOX columns (10 m, 0.53 mm id) for OVOC analysis.

The GC×GC-FID comprised of a Markes TT24-7 TD unit with an air server attachment (Markes International, Llantrisant, UK) and an Agilent 7890 GC (Agilent Technologies, Wilmington, DE, USA) equipped with a splitless injector and an FID operating at 200 Hz. The TD unit sampled at a rate of 100 mL min^{-1} for 55 min, giving a total sample volume of 5.5 L. The trap temperature was set to -10 °C, held for 3 min, then on injection heated at 100 °C min^{-1} to 200 °C to ensure all analytes of interest were desorbed.

The GC×GC-FID system first dimension column was a BPX-5 (25 m x 0.15 mm, 0.4 μm df), at 50 psi; combined with a second dimension column of a BP-20 (5 m x 0.25 mm, 0.25 μm df), at 23 psi (SGE, Australia). Column pressures were controlled using the Agilent 7890 EPC. The total transfer flow valve modulator incorporated a 6-port, 2-way diaphragm valve (Valco Instruments, Houston, TX, USA), with actuation achieved using a solenoid valve, controlled by software written 'in house'. The modulator was held at 120 °C throughout the run and had a modulation period of 5 s, with 4.7 s sample and 0.3 s injection times. The chromatographic and modulation configuration of the GC×GC-FID system is detailed in Lidster *et al.* (2011).[131] During the injection of sample, liquid CO_2 was sprayed onto the first 2 cm portion at the head of the first dimension column for 60 s to re-focus the sample, discussed in more detail in Chapter 5.

An oven temperature programme was developed which optimised separation and resolution of compounds of interest. The initial oven temperature was 30 °C, held for 1 min, ramped at 2.5 °C min^{-1} to 130 °C, held for 1 min then ramped at 10 °C min^{-1} to 200 °C, and held for 1 min; giving a total run time of 50 minutes. This, combined with the TD run time, gave a total analysis time of 55 minutes.

During the summer campaign, some parameters had to be changed. Ambient temperatures were higher in comparison to the winter, meaning the oven temperature programme had to be altered to allow the oven to reach its minimum temperature. The initial oven temperature was changed to 35 °C held for 2 min and the final temperature of 200 °C was held for 2 min. All other oven parameters were kept the same. Due to a sensitivity drop, the TD sampling rate was increased to 200 mL min^{-1} for 55 min, to give a total sample volume of 11 L.

2.3.1.1 Calibrations and uncertainties

Calibrations were performed at regular intervals on both instruments using a gas standard (NPL30, National Physical Laboratory, Teddington, UK) containing 30 ozone precursor species (C_2-C_8) at 3-5 ppb levels. For the higher carbon number hydrocarbons measured on the GC×GC, a separate NPL standard was used which contained 24 species from C_5-C_{11} (including a range of aromatics). The species contained in the two standards are shown in Table 2.1 with their associated mixing ratios and uncertainties. However many of the higher hydrocarbon measurements from the GC×GC-FID were ultimately based on calibrations from liquid standards introduced by splitless injection (full details in the next section). Instrument zeros, including testing of sample lines and water removal stages, were made using high purity N_2, with further purification using an Aeronex Gatekeeper catalyst (Sigma Aldrich Company Ltd., Poole, UK).

Measurement uncertainties are described in Hopkins *et al.*, (2003)[161] and Lidster *et al.*, (2012),[131] however they are broadly dominated by the gravimetric uncertainty associated with gas standard preparation, typically 5%. Run to run reproducibility was better than 1% for light C_2-C_7 hydrocarbons (when >1 ppb) and better than 5% for higher hydrocarbons. The uncertainty for the carbon class measurements reported in this chapter are estimated at 6% for C_2-C_7 and 5-11% for C_8-C_{13} (depending on the specific compound).

2.3.1.2 Liquid injections

For those compounds not included in gas standard mixtures, a response factor (RF) was calculated from liquid injections, to allow compound concentrations to be quantified (Equation 2.1). The GC×GC compounds quantified using a response factor are flagged in Table 2.2 using a superscript e. Please see Hopkins *et al* (2011) for details on the quantification of specific compounds measured using the DC-GC.[162] The RF was determined as the response of a compound (i) with respect to a reference compound (ref), where $R_{ref,st}$ and $R_{i,st}$ are the responses of the reference and i compounds in the standard (or in this case from liquid mixtures, st) respectively, and $C_{ref,st}$ and $C_{i,st}$ are the corresponding concentrations.[163] The response factor can then be used in a second equation to quantify the concentrations of the compounds in air samples. This is shown in Equation 2.2, where X_{ref} and X_i are the concentrations of the reference and i compounds in air samples, and PA_{ref} and PA_i are the peak areas of the reference and i compounds respectively. For the grouped compounds (discussed in more detail later in this chapter, see Figure 2.12

Table 2.1: Contents of the two NPL standards, along with measured mixing ratios and associated uncertainties

NPL 30 Standard			
Species	**Mixing ratio ± uncertainty (ppbv)**	**Species**	**Mixing ratio ± uncertainty (ppbv)**
Ethane	4.12 ± 0.08	Pentane, 2-methyl-	3.97 ± 0.08
Ethene	4.08 ± 0.08	*n*-Hexane	3.97 ± 0.08
Propane	4.07 ± 0.08	Isoprene	3.97 ± 0.08
Propene	4.02 ± 0.08	*n*-Heptane	3.92 ± 0.08
Propane, 2-methyl-	4.09 ± 0.08	Benzene	3.99 ± 0.08
n-Butane	3.97 ± 0.08	Pentane, 2,2,4-trimethyl-	4.00 ± 0.08
Ethyne	4.07 ± 0.08	*n*-Octane	3.96 ± 0.08
Butene, *trans*-2-	3.97 ± 0.08	Toluene	3.94 ± 0.08
1-Butene	3.90 ± 0.08	Benzene, ethyl-	3.90 ± 0.08
Butene, *cis*-2-	3.91 ± 0.08	*m*-Xylene	3.90 ± 0.08
Butane, 2-methyl-	3.96 ± 0.08	*p*-Xylene	3.85 ± 0.08
n-Pentane	4.02 ± 0.08	*o*-Xylene	4.02 ± 0.08
1,3-butadiene	4.02 ± 0.08	Benzene, 1,3,5-trimethyl-	4.01 ± 0.08
Pentene, *trans*-2-	3.83 ± 0.08	Benzene, 1,2,4-trimethyl-	4.17 ± 0.08
1-Pentene	3.90 ± 0.08	Benzene, 1,2,3-trimethyl-	3.91 ± 0.08
NPL Heavy Standard			
Species	**Mixing ratio ± uncertainty (ppbv)**	**Species**	**Mixing ratio ± uncertainty (ppbv)**
n-Pentane	4.84 ± 0.24	*o*-Xylene	4.97 ± 0.25
Pentane, 2-methyl-	5.04 ± 0.25	Benzene, 1,3,5-trimethyl-	5.04 ± 0.35
n-Hexane	4.95 ± 0.25	Benzene, 1,2,4-trimethyl-	5.34 ± 0.27
Hexane, 3-methyl-	5.02 ± 0.25	Benzene, 1,2,3-trimethyl-	4.80 ± 0.24
n-Heptane	4.99 ± 0.25	*n*-Nonane	4.20 ± 0.42
Benzene	4.98 ± 0.25	Benzene, iso-propyl-	4.93 ± 0.35
Pentane, 2,2,4-trimethyl-	4.95 ± 0.25	Benzene, propyl-	4.97 ± 0.35
n-Octane	5.00 ± 0.25	Toluene, 3-ethyl-	4.98 ± 0.35
Toluene	4.97 ± 0.25	Toluene, 4-ethyl-	4.93 ± 0.35
Benzene, ethyl-	4.97 ± 0.25	Toluene, 2-ethyl-	4.99 ± 0.35
m-Xylene	5.03 ± 0.25	*n*-Decane	5.00 ± 0.50
p-Xylene	4.96 ± 0.25	*n*-Undecane	4.99 ± 0.50

and Table 2.3), the *n*-alkane response has been used for quantification as FID response is assumed to be linear with carbon number.[164]

$$RF_{i \cdot ref} = \frac{R_{ref,st} \times C_{i,st}}{R_{i,st} \times C_{ref,st}} \tag{2.1}$$

$$[X_i] = \frac{\left(\frac{PA_i}{PA_{ref}}\right) \times [X_{ref}]}{RF_{i \cdot ref}} \tag{2.2}$$

Liquid injections were carried out using the same parameters as described in Section 2.3, except that the sample was injected in liquid form without the use of the TD unit. Injections were made using a Agilent Technologies autosampler set at 250 °C, operating in split mode with a split ratio of 100:1 and an injection volume of 1 μL.

A 'template' standard mixture of compounds were prepared at 100 ppb containing; straight-chained *n*-alkanes from C_5-C_{12}, a cyclic alkane and four aromatics, shown in the upper panel (a) of Figure 2.6. Sample mixtures were made using the same 'template' standard mixture, along with two 'unknown' compounds per mixture which have dissimilar boiling points; and injected to provide identification of each individual compound. Figure 2.6, middle panel (b), shows two 'unknown' compounds, 2-Pentanone and α-Pinene which have boiling points of 103 °C and 155 °C , respectively. Once the compounds were initially identified, a second set of solutions were prepared of groups of compounds with similar retention times, where each compound was at a different concentration (lower panel (c) of Figure 2.6). For all solutions, the 'template' standard mixture was included, with its composition maintained to provide a baseline for identification and for use in quantification *via* response factors, discussed previously. The ordered chromatograms that are produced when using GC×GC allow for easier identification as 'patterns' can be distinguished from groups of compounds. The groups of compounds from the liquid samples could then be compared to ambient samples to identify unknown species.

2.3.2 Supporting measurements

Measurements of NO_x were made using a single channel, chemiluminesence instrument (Air Quality Design Inc., USA), which has a wide linear range (1 ppt to 500 ppb).[165] Ozone measurements were made using an UV Absorption TEI 49C and 49i (Thermo Scientific) with a limit of detection of 1 ppb.

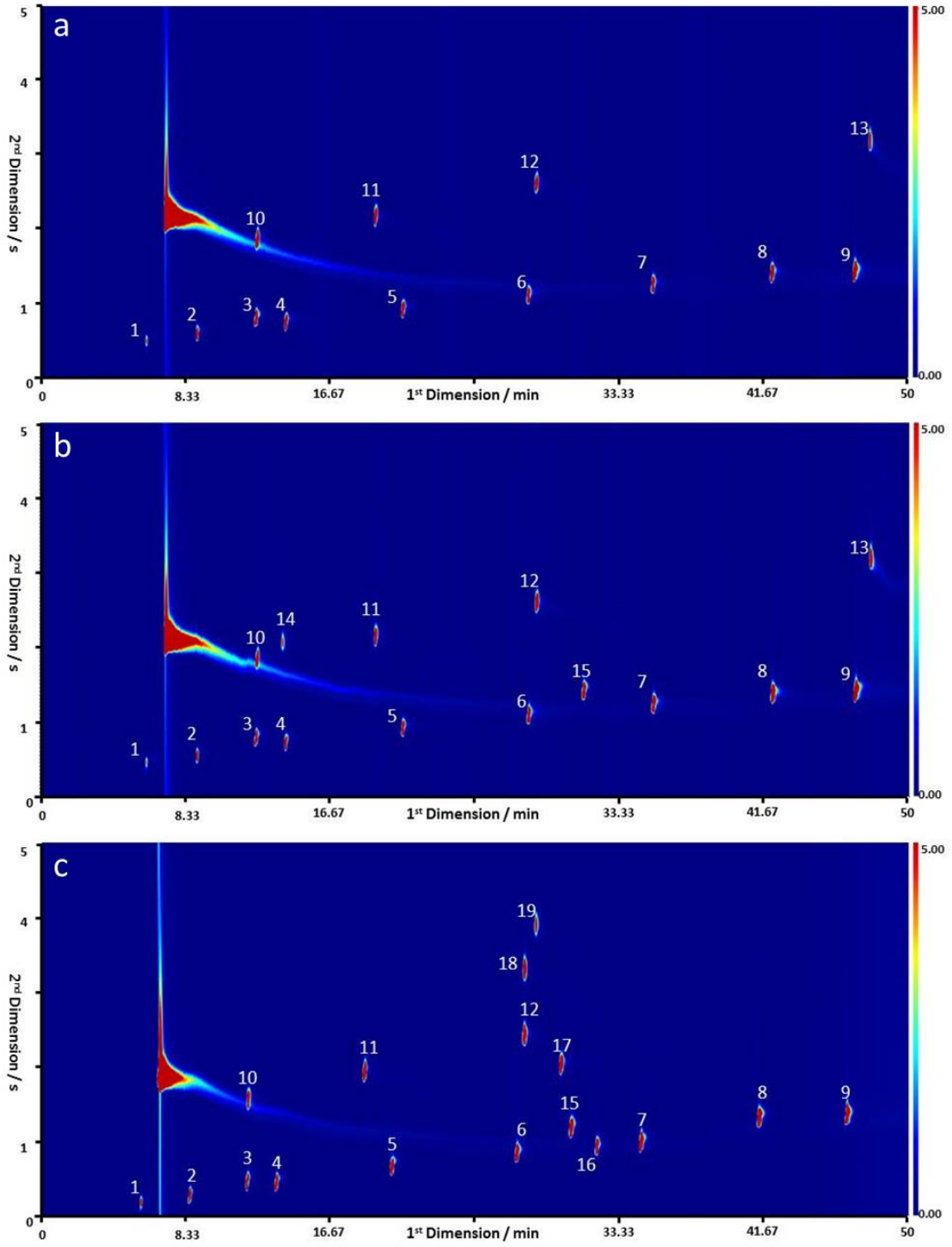

Figure 2.6: GC×GC plots of the three different types of liquid injections. Upper panel (a) shows the 'template' standard mixture of compounds all at 100 ppbv: 1 - *n*-Pentane, 2 - *n*-Hexane, 3 - Cyclohexane, 4 - *n*-Heptane, 5 - *n*-Octane, 6 - *n*-Nonane, 7 - *n*-Decane, 8 - *n*-Undecane, 9 - *n*-Dodecane, 10 - Benzene, 11 - Toluene, 12 - *o*-Xylene, 13 - Naphthalene. Middle panel (b) shows the 'template' standard mixture plus two 'unknown' compounds of different boiling points all at 100 ppbv: 14 - 2-Pentanone, 15 - α-Pinene. Lower panel (c) shows the 'template' standard mixture (without 13, naphthalene, all at 100 ppbv) plus a group of 'unknown' compounds of similar boiling points with different concentrations: 15 - α-Pinene (100 ppbv), 16 - 2-methyl-Nonane (50 ppbv), 17 - 4-*iso*-propyl-Toluene (70 ppbv), 18 - Styrene (100 ppbv), 19 - Cyclohexanone (50 ppbv).

2.4 Meteorology observations

The meteorological observations made during the winter and summer ClearfLo campaigns are shown in Figures 2.7-2.9. The meteorological measurements shown in Figures 2.7 and 2.8 were obtained by the University of Leeds using a Davis Vantage Pro 2 met station. For information regarding the operation of this instrument please refer to https://www.weathershop.co.uk/shop/brands/davis-instruments/vantage-pro/davis-envoy-iss-weather-station.

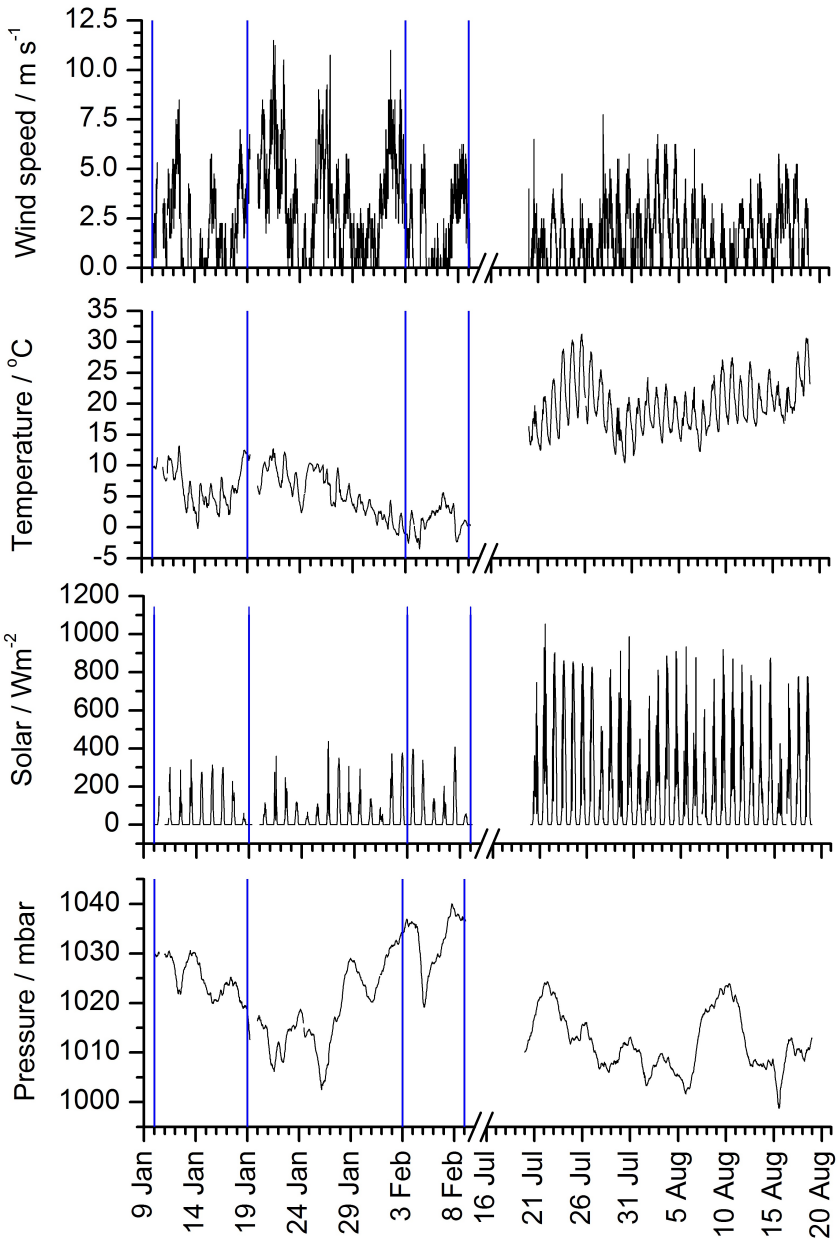

Figure 2.7: Meteorological measurements of wind speed, temperature, solar radiation and pressure from the winter and summer campaigns

Figure 2.7 shows the winter and summer measurements of wind speed, temperature, solar radiation and pressure. The highlighted sections in the winter correspond to two stagnant, relatively high pressure periods that will discussed later in Section 2.5.3.1. During these periods, the wind speed was typically quite low, while the pressure was high. The wind speed was more variable and had a larger overall range in winter, compared to the summer. The pressure observed also has a more variable winter profile. Not surprisingly, the temperature and solar radiation are higher during the summer campaign. There is also an observable summer correlation between the two as they increase and decrease at approximately the same time each day, something which is not seen to the same degree in winter.

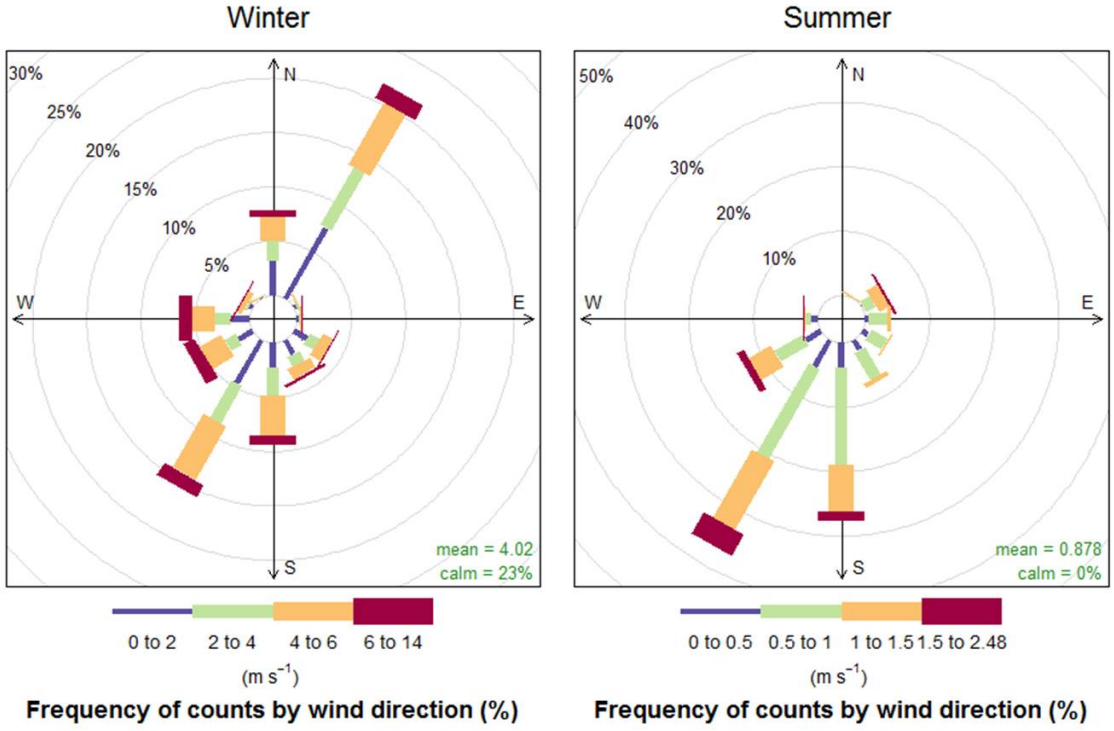

Figure 2.8: Campaign averaged wind rose plots for the winter (left) and summer (right) campaigns. These plots show how wind direction and speed vary over the entire campaign. Wind direction is averaged into 30 ° segments and wind speed is shown by the 'paddles'. Please note the vastly different scales for the different coloured segments representing the wind speed. This figure was constructed using the OpenAir project for R.[166–168]

Figure 2.8 shows the winter (left) and summer (right) campaign averaged relationship between wind direction and speed. These are windRose plots created using the OpenAir project for the R statistical package. This displays wind direction in 30 ° segments. Wind speed is shown by the 'paddles', where speed in m s^{-2} is given by the different coloured segments and percent frequency in each wind direction is represented by the length of each

'paddle'. The percent is shown by the radiating circles. This also shows that the winter has a larger range of observed wind speed. Although, there does seem to be more frequent and higher wind speeds from the north east and south west, there is still wind seen from all directions. In summer, however, there appears to be little to no wind from the north, while wind from the south west at high speeds dominates.

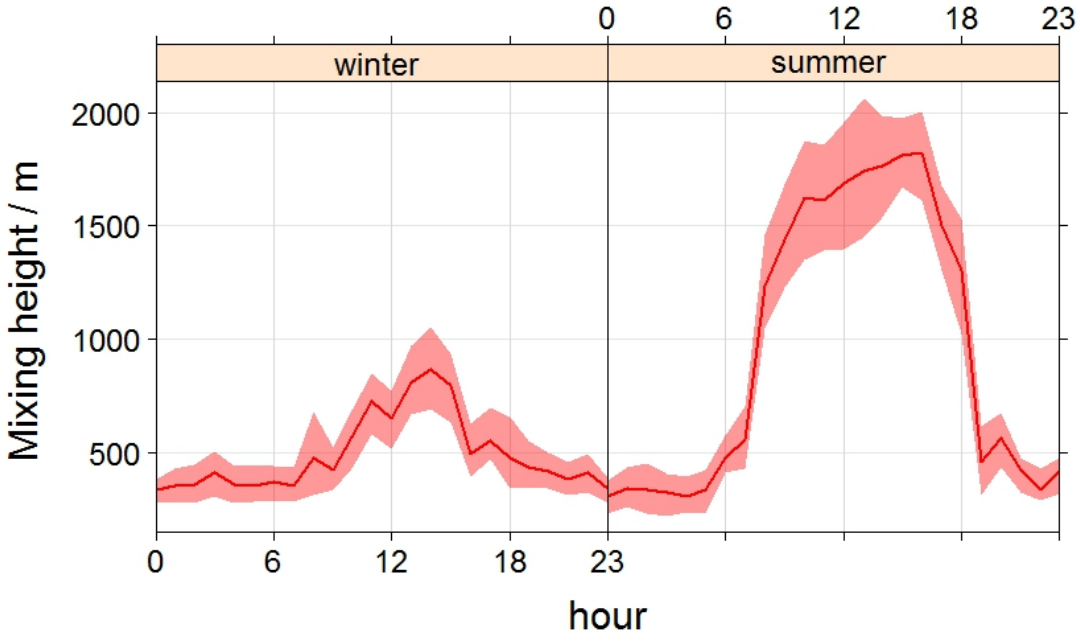

Figure 2.9: Diurnal profiles of mixing layer height in winter (left-hand side) and summer (right-hand side). Winter and summer are plotted on the same y- axes to show seasonal differences. This figure was constructed using the OpenAir project for R where the solid line represents the mean daily concentration and the shaded regions shows the 95% confidence intervals surrounding the mean.[166–168]

Figure 2.9 shows the campaign average diurnal profiles of the mixing heights during the winter and summer campaigns. The measurement of mixing layer height was conducted by the University of Reading using a Doppler lidar. Please see Barlow *et al.*, (2015) for details.[169] The summer diurnal shows a profile that appears to be strongly linked with that of the solar radiation (third panel of Figure 2.7), with an approximate midday maxima and overnight minimum. The mixing height appears to stabilise after ≈ 20:00 and stays at ≈ 200-300 m overnight until it starts to rise at ≈ 05:00. A similar, but smaller scale, profile is seen in winter although the timings of maxima and minimum are slightly different.

2.5 Observations of hydrocarbons in urban air

The two GC instruments individually quantified 78 VOCs (36 aliphatics, 19 monoaromatics, 21 oxygenated and 2 halogenated), as well as many hundreds more included in a lumped carbon number assessment from 2667 samples (1352 winter and 1315 summer). The DC-GC instrument measured volatile VOCs, C_1-C_7 hydrocarbons and a selection of OVOCs, with effective saturation concentrations ranging from 3×10^7 to 1.4×10^{12} μg m^{-3}. The saturation concentrations were calculated[52] with compound vapour pressures determined from the UManSysProp website (http://umansysprop.seaes.manchester.ac.uk/) at 298.15 K with the Nannoolal vapour pressure and boiling point extrapolation methods.[170,171] The GC×GC-FID instrument measured the less volatile VOC fraction (effective saturation concentration range of 1.8×10^6 to 2.4×10^9 μg m^{-3}), with hydrocarbons from C_6 to C_{13}, plus a large group of OVOCs (from C_3 onwards). There was some overlap in species measured by both instruments, with good agreement seen (*e.g.* Figure 2.10: benzene R^2 0.92, slope 1.070 ± 0.013 and *n*-hexane R^2 0.91, slope 0.966 ± 0.012).

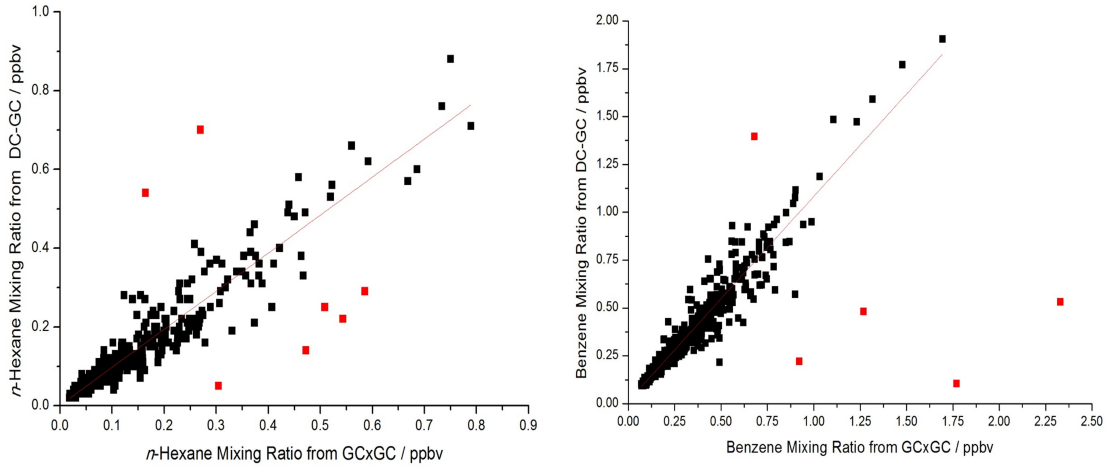

Figure 2.10: Example correlations of the GC×GC-FID (x-axis) and the DC-GC-FID (y-axis) instruments for *n*-hexane (left) and benzene (right). Points shown in red have been removed from the correlation as outliers at SD ± 1 σ.

The C_2-C_6 volatility range contains both primary hydrocarbon emissions, with isomers quantified individually, along with several oxygenated compounds. Between C_6 to C_{13}, a wide range of hydrocarbon and OVOC species, including the *n*-alkanes, α-pinene, limonene, monoaromatics with up to 3 substituents and naphthalene were quantified individually (see Figure 2.11 and Table 2.2). Figure 2.11 is a typical GC×GC-FID plot, where the retention times from column 1 (separation based on volatility) and column 2

(separation based on polarity) are the x and y axis respectively, and compound intensity is the coloured contour. Two simplified bands of compounds can be seen; an aromatic band that is well separated from the aliphatic band, however, these are just general features and some oxygenated and other hetero atom containing species are present: both within and outside these lines. Figure 2.11b and 2.11c are expanded sections of Figure 2.11a to improve visualisation.

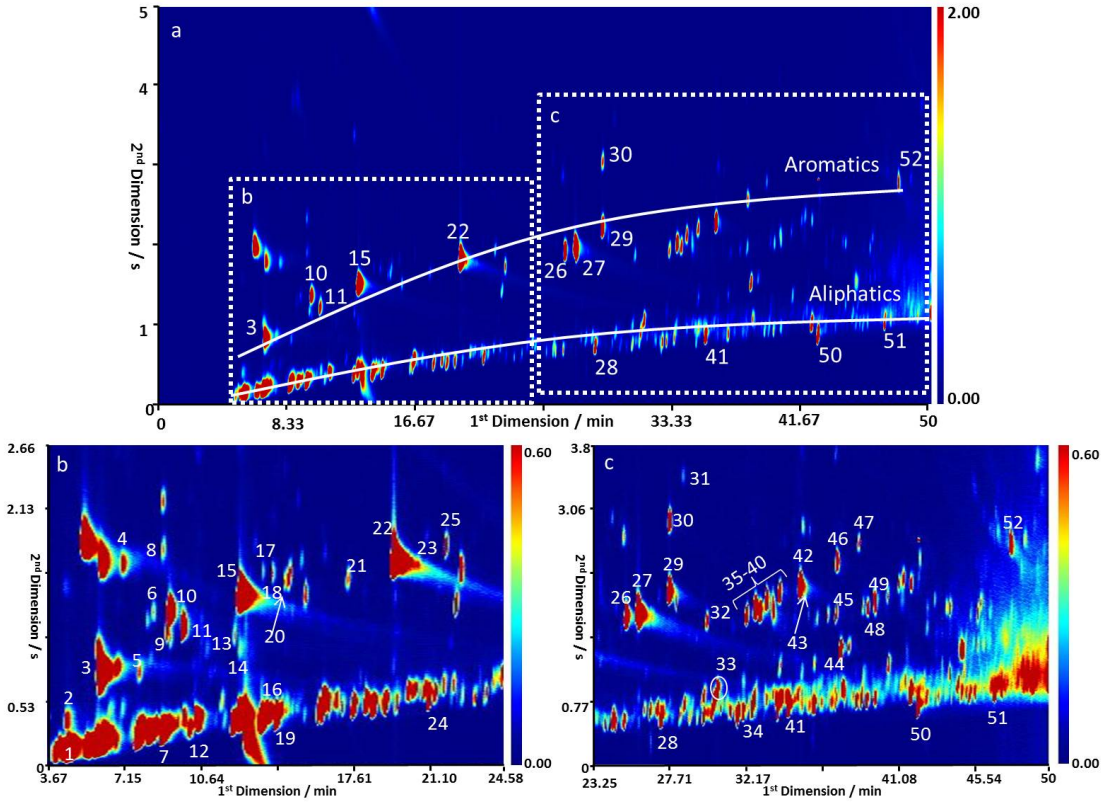

Figure 2.11: A typical GC×GC-FID plot from 2012-02-07 at 08:32, showing two separate bands of compounds, aromatic and aliphatics. Box b and c show zoomed in sections of the original plot. Labelled peaks for sections a, b and c are given in Table 2.2, Peak Identity column.

Table 2.2 shows the mean and median mixing ratios, standard deviation, limit of detection (LOD), measurement instrument and identification in GC×GC plot (numbers shown Figure 2.11), if applicable, for each individually identified compound from the winter and summer campaigns. For both instruments, the LOD was calculated at S/N=3. In the GC×GC chromatogram, this was accomplished using the largest modulated peak for each compound in either a gas standard or liquid run. For most compounds, the LOD is calculated to be less than 10 pptv, making these measurements highly sensitive.

Table 2.2: Individually identified VOC mixing ratios, grouped by functionality, ordered by carbon number. [a]N/a indicates compounds that were not measured during the winter campaign, [b]values in bold are higher during the summer campaign, [c]<LOD indicates values that are below the detection limit of the specified instrument, calculated at S/N = 3, [d]peak identity corresponds to the labelled peaks in Figure 2.11, [e]compounds measured using the GC×GC instrument where quantification was through the use of response factors as detailed in Section 2.3.1.2, [f]SD ± 1 σ .

	Winter[a]			Summer[b]					
	Mean	Median	SD[f]	Mean	Median	SD[f]	LOD[c]	Measured	Peak
Compound	**/ pptv**	**/ pptv**	**/ pptv**	**/ pptv**	**/ pptv**	**/ pptv**	**/ pptv**	**Using**	**Identity[d]**
Saturated									
Methane	2.24×10^6	2.18×10^6	3.45×10^5	1.83×10^6	1.81×10^6	1.44×10^5	100	DC-GC	-
Ethane	11,074	7,324	13,503	4,287	3,007	5,201	9	DC-GC	-
Propane	4,250	2,944	4,207	1,703	1,253	1,514	3	DC-GC	-
n-Butane	2,317	1,617	2,513	1,366	972	1,166	1	DC-GC	-
iso-Butane	1,359	916	1,424	686	473	624	1	DC-GC	-
n-Pentane	394	292	342	340	236	289	1	DC-GC	-
iso-Pentane	833	574	825	751	540	647	1	DC-GC	-
Cyclopentane	106	55	208	106	59	312	1	DC-GC	-
n-Hexane	122	85	112	91	60	82	1	DC-GC	7
Pentane, 2+3-methyl-	337	249	351	256	189	218	1	DC-GC	1
n-Heptane	89	62	99	66	49	57	1	DC-GC	16
Butane, 2,2,3-trimethyl-[e]	111	78	107	71	55	50	1	GC×GC	12
n-Octane	32	22	101	21	16	18	2	DC-GC	24
Pentane, 2,2,4-trimethyl-	42	34	30	23	17	19	2	DC-GC	19
n-Nonane	526	380	481	128	102	99	3	GC×GC	28
n-Decane	398	328	339	132	87	138	2	GC×GC	41
Nonane, 2-methyl-[e]	50	35	49	43	28	44	4	GC×GC	34
n-Undecane	397	288	364	165	125	123	1	GC×GC	50
n-Dodecane[e]	374	321	279	273	207	244	1	GC×GC	51
Unsaturated									
Ethene	1,703	1,340	1,477	638	508	402	7	DC-GC	-
Acetylene	1,214	947	915	374	289	247	3	DC-GC	-
Propene	425	275	465	199	163	124	3	DC-GC	-
Propadiene	16	12	14	6	4	4	3	DC-GC	-
Propyne		N/a		44	37	16	3	DC-GC	-
Butene, *trans*-2-	43	29	44	20	16	14	1	DC-GC	-
1-Butene	75	53	68	61	53	31	1	DC-GC	-
iso-Butene	105	75	97	53	44	33	1	DC-GC	-
Butene, *cis*-2-	28	19	30	14	11	11	1	DC-GC	-
1,2-Butadiene		N/a		143	67	885	1	DC-GC	-
1,3-Butadiene	53	39	47	32	26	19	1	DC-GC	-
Pentene, *trans*-2-	48	29	152	26	21	24	1	DC-GC	-
1-Pentene	37	27	75	25	21	18	1	DC-GC	-
Isoprene	28	19	31	**117**	**88**	111	1	DC-GC	2
Styrene[e]	34	17	54	33	19	34	8	GC×GC	30
α-Pinene[e]	14	11	10	**94**	**77**	79	1	GC×GC	33
Limonene[e]	4	2	7	**49**	**30**	52	3	GC×GC	44
Aromatics									
Benzene	356	293	236	147	117	93	2	DC-GC	15
Toluene	635	452	658	481	347	427	2	DC-GC	22
Benzene, ethyl-	140	99	118	81	61	70	3	DC-GC	26

Table 2.2: continued. [a]N/a indicates compounds that were not measured during the winter campaign, [b]values in bold are higher during the summer campaign, [c]<LOD indicates values that are below the detection limit of the specified instrument, calculated at S/N = 3, [d]peak identity corresponds to the labelled peaks in Figure 2.11, [e]compounds measured using the GC×GC instrument where quantification was through the use of response factors as detailed in Section 2.3.1.2, [f]SD ± 1 σ.

	Winter[a]			Summer[b]					
	Mean	Median	SD[f]	Mean	Median	SD[f]	LOD[c]	Measured	Peak
Compound	**/ pptv**	**/ pptv**	**/ pptv**	**/ pptv**	**/ pptv**	**/ pptv**	**/ pptv**	**Using**	**Identity[d]**
Aromatics continued									
m- and *p*-Xylene	185	128	181	113	81	104	3	DC-GC	27
o-Xylene	156	106	157	70	48	67	3	DC-GC	29
Benzene, *iso*-propyl-	27	21	22		<LOD		3	GC×GC	32
Benzene, propyl-	90	53	108	12	7	13	4	GC×GC	35
Toluene, 3-ethyl-	139	84	160	17	8	26	6	GC×GC	36
Toluene, 4-ethyl-	98	52	125	12	4	19	1	GC×GC	37
Benzene, 1,3,5-trimethyl-	93	64	90	12	7	16	5	GC×GC	38
Toluene, 2-ethyl-	65	41	71	8	3	12	6	GC×GC	39
Benzene, 1,2,4-trimethyl-	195	120	224	27	15	42	1	GC×GC	42
Toluene, 4-*iso*-propyl-[e]	10	6	11	**35**	**24**	32	3	GC×GC	45
Benzene, 1,2,3-trimethyl-	66	42	76	7	3	10	1	GC×GC	46
Indan[e]	11	8	9		<LOD		4	GC×GC	47
Benzene, *tert*-butyl-[e]	7	4	7	10	3	14	1	GC×GC	43
Benzene, 1,3-diethyl-[e]	6	3	6	7	4	9	2	GC×GC	48
Benzene, 1,4-diethyl-[e]	5	3	7	3	2	3	1	GC×GC	49
Naphthalene[e]	36	25	35	35	26	29	3	GC×GC	52
Oxygenates									
Acetaldehyde	2,256	1,703	1,680	**4,301**	**3,261**	3,207	1	DC-GC	-
Propanal, 2-methyl-[e]		<LOD		**48**	**32**	43	6	GC×GC	5
Butanal[e]	9	5	15	**13**	**8**	13	1	GC×GC	11
Butanal, 3-methyl-[e]		<LOD		**28**	**19**	27	6	GC×GC	13
Butanal, 2-methyl-[e]		<LOD		**21**	**12**	22	8	GC×GC	14
Methacrolein[e]		<LOD		**24**	**15**	24	1	GC×GC	6
Pentanal[e]		<LOD		**23**	**15**	21	8	GC×GC	18
Hexanal[e]	9	6	10	**19**	**11**	19	3	GC×GC	25
Benzaldehyde[e]	24	16	25	13	9	12	1	GC×GC	40
Methanol	1,246	962	1,605	**3,376**	**2,462**	2,580	40	DC-GC	-
Ethanol	5,005	3,514	4,557	4,978	3,506	4,229	9	DC-GC	-
Propanol	370	209	699	252	183	195	10	DC-GC	-
Butanol	1,157	748	1,538	484	376	488	20	DC-GC	-
Acetone	1,076	896	565	**2,405**	**2,114**	1,093	9	DC-GC	3
Butanone[e]	29	25	22	**64**	**44**	54	2	GC×GC	10
Ketone, methyl-vinyl-[e]		<LOD		**33**	**22**	32	4	GC×GC	8
Pentanone, 2-[e]		<LOD		**29**	**19**	28	1	GC×GC	17
Pentanone, 4-methyl-2-[e]	36	10	57	**51**	**33**	48	1	GC×GC	21
Hexanone, 2-[e]		<LOD		**38**	**27**	33	3	GC×GC	23
Cyclohexanone[e]		<LOD		**17**	**11**	18	9	GC×GC	31
Acetate, ethyl-[e]	45	34	40	46	30	44	2	GC×GC	9
Halogenated									
Methane, dichloro[e]	29	18	31	**35**	**25**	29	2	GC×GC	4
Trichloroethylene[e]		<LOD		**10**	**7**	8	5	GC×GC	20

2.5.1 Grouping of unresolved complex mixtures

Even though over 70 compounds have been identified and quantified, this is only a small portion of the total VOC loading. The number of possible structural isomers increases exponentially with carbon number and beyond around C_9 it becomes impossible to accurately identify the structure of every hydrocarbon present in air.[172] Using the retention behaviour of each compound on chromatographic columns it is however possible to assign individual species to particular chemical classes and functionalities. In previous studies using GC-FID, the larger hydrocarbon fraction, where diesel VOC emissions are predominately found, is part of an unresolved complex mixture (UCM). One method used to estimate the relative amounts of VOCs in this region is to identify the *n*-alkane (which is often observed as a well defined peak above a raised baseline) and then integrate the area above the blank baseline between two consecutive linear alkanes (using an FID) or to use the alkyl *m/z* 57 fragment ion to represent primary IVOC.[173] In reality, this gives an estimate of the total or alkyl containing IVOC within this volatility range and will not only include the hydrocarbon fraction with a specific carbon number but other compounds as well (*i.e.* lower carbon number aromatics, OVOCs). This chapter details the improved resolution of VOCs using GC×GC to allow for a more stringent grouping of the UCM by carbon number and functionality, rather than by volatility alone.

Higher carbon number aliphatic compounds (C_6-C_{13}, predominantly alkanes with some alkenes and cycloalkanes), C_4 substituted monoaromatics and C_{10} monoterpenes have been grouped together and the combined class abundance estimated using a response ratio to the corresponding straight-chained *n*-alkane, 1,3-diethyl benzene and α-pinene respectively. The group boundaries are shown in Figure 2.12, where for example, box 7 corresponds to the C_{12} aliphatic group and encompasses alkanes, cyclic alkanes and alkenes. Only the material within the box is integrated within this retention window. This is a clear improvement over the 1D case, as there are a considerable number of peaks, with a higher 2^{nd} dimension retention time, such as the two peaks labelled as # and $ in Figure 2.12 that would co-elute with the C_{12} aliphatic group, if the entire retention window was co-sampled (*i.e.* aromatics, oxygenates and other hetero species). The number of individual isomer peaks that could be isolated in each grouping rises from 9 for the C_6 group to 40 for C_{10} (Figure 2.19, black squares). A full table of the number of included isomers and concentrations of the grouped species is provided in Table 2.3.

Unfortunately, the separation of the linear alkanes, branched alkanes, cyclic aliphatic

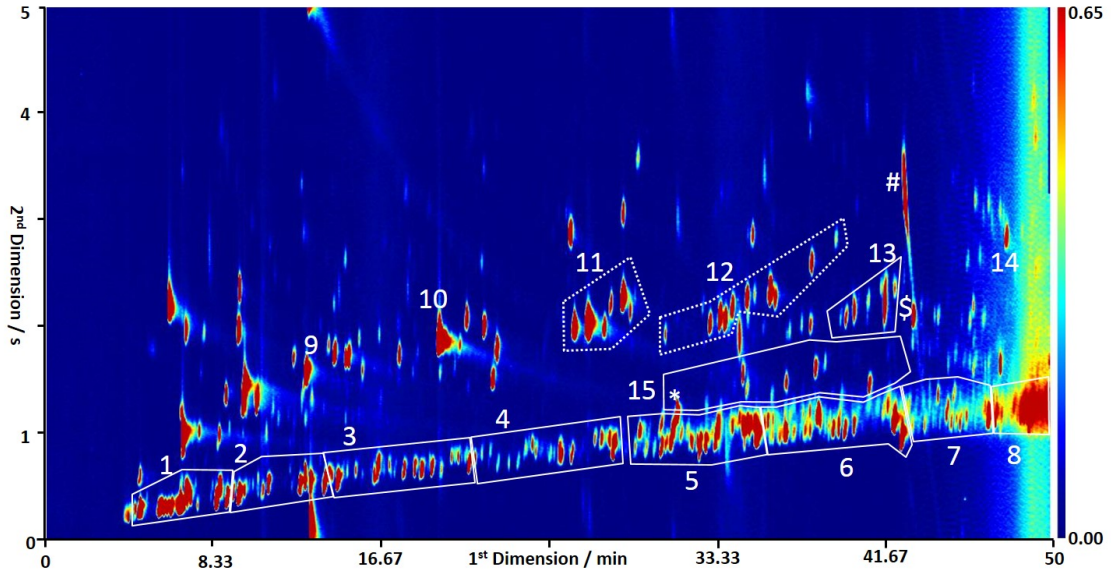

Figure 2.12: Typical GC×GC-FID chromatogram from 2012-07-25, demonstrating the grouping of compounds. Labelled peaks and groups are identified as follows, with the dashed and solid lines indicating compounds that were identified individually and as a group respectively; (1-8) aliphatic groups from C_6 to C_{13}, (9) benzene, (10) toluene, (11) C_2 substituted monoaromatics, (12) C_3 substituted monoaromatics, (13) C_4 substituted monoaromatics, (14) naphthalene, and (15) C_{10} monoterpenes with * corresponding to α-pinene which is the start of that group. The remaining compounds, not enclosed in a box contain hetero-atoms, primarily oxygenates. The grouping of compounds was accomplished using the lasso technique in Zoex GC image software (Zoex, USA). This technique allows the software to calculate the area of all peaks included in the lasso.

and alkenes on the GC×GC chromatogram is not sufficient at higher carbon numbers to allow them to be more fully resolved. This is a direct consequence of the use of the cryogen free and field deployable valve modulator, which when used in total transfer mode, where the flow in the first column slows during the modulation pulse, imposes restrictions on the column dimensions and internal diameters that can be used.[131] Also, given the temperature constraints on this instrument, it is likely that the GC×GC not only misses a fraction of the C_{13} aliphatic group but that it may also be under-reporting the number of isomers in the higher carbon number groups. This would explain why the number of isomers decreases after C_{11} aliphatics, rather than increases as would be expected. The aliphatic groups have diurnal behaviour (discussed in the Section 2.5.3) that indicate a dominant traffic related source. Fuel composition measurements suggest there is unlikely to be significant quantities of alkenes from traffic related sources; gasoline contains around 3-4 wtC% of alkenes, and diesel contains negligible quantities.[148]

Table 2.3: Grouped VOC mixing ratio and the number of isomers in each group. [a]The number of isomers correspond to the groupings shown in the GC×GC-FID plot shown in Figure 2.12, [b]cumulative mixing ratio of each specified compound group not including those given individually in Table 2.2 (*i.e.* the C_7 aliphatics do not include *n*-Heptane and 2,2,3-trimethyl butane), [c]values in bold are higher during summer campaigns., [d]SD ± 1 σ

	Number	Winter[b]			Summer[b,c]		
	of	Mean	Median	SD[d]	Mean	Median	SD[d]
Groups	Isomers[a]	/ pptv	/ pptv	/ pptv	/ pptv	/ pptv	/ pptv
C_6 Aliphatics	9	502	434	256	304	234	250
C_7 Aliphatics	10	586	379	617	127	93	132
C_8 Aliphatics	25	602	427	572	107	78	106
C_9 Aliphatics	28	214	143	220	79	49	98
C_{10} Aliphatics	40	283	176	340	95	61	147
C_{11} Aliphatics	41	459	320	452	137	89	209
C_{12} Aliphatics	37	591	363	696	163	111	244
C_{13} Aliphatics	30	937	654	914	187	117	170
C_4 substituted monoaromatics	16	210	102	298	33	14	57
C_{10} Monoterpenes	25	13	7	17	**51**	**34**	48

2.5.2 Seasonal behaviour

Figure 2.13 shows two typical GC×GC-FID plots from the winter (upper) and summer (lower) ClearfLo campaigns. The winter campaign (Figure 2.13, upper) shows the expected higher number and concentrations of aliphatic species given the combination of increased fuel consumption and a reduced boundary layer thus lowering the volume into which the species are emitted. In summer, there is an increase in the presence of monoterpenes and isoprene (shown between the two bands of compounds and along the aromatic band in particular); which would be expected due to an increase in emissions from biogenic sources as ambient temperatures and sunlight are higher.[174] Also note the presence of some highly retained compounds which could possibly be alcohols or acids (shown by the "streaky" nature of the contours and highlighted in Figure 2.13 lower panel by white arrows; however these have not been conclusively identified) and more oxygenated species present at higher concentrations during the summer, likely as a result of increased photochemistry.

2.5.3 Diurnal behaviour

The average diurnal behaviour of a selection of VOCs, O_3 and NO_x, are shown in Figure 2.14. VOCs with an anthropogenic source (*e.g.* ethane, toluene, C_4 substituted monoaromatics and C_{13} aliphatics) have higher mixing ratios in winter, consistent with reduced rates of photochemical removal in the northern European winter and a lower

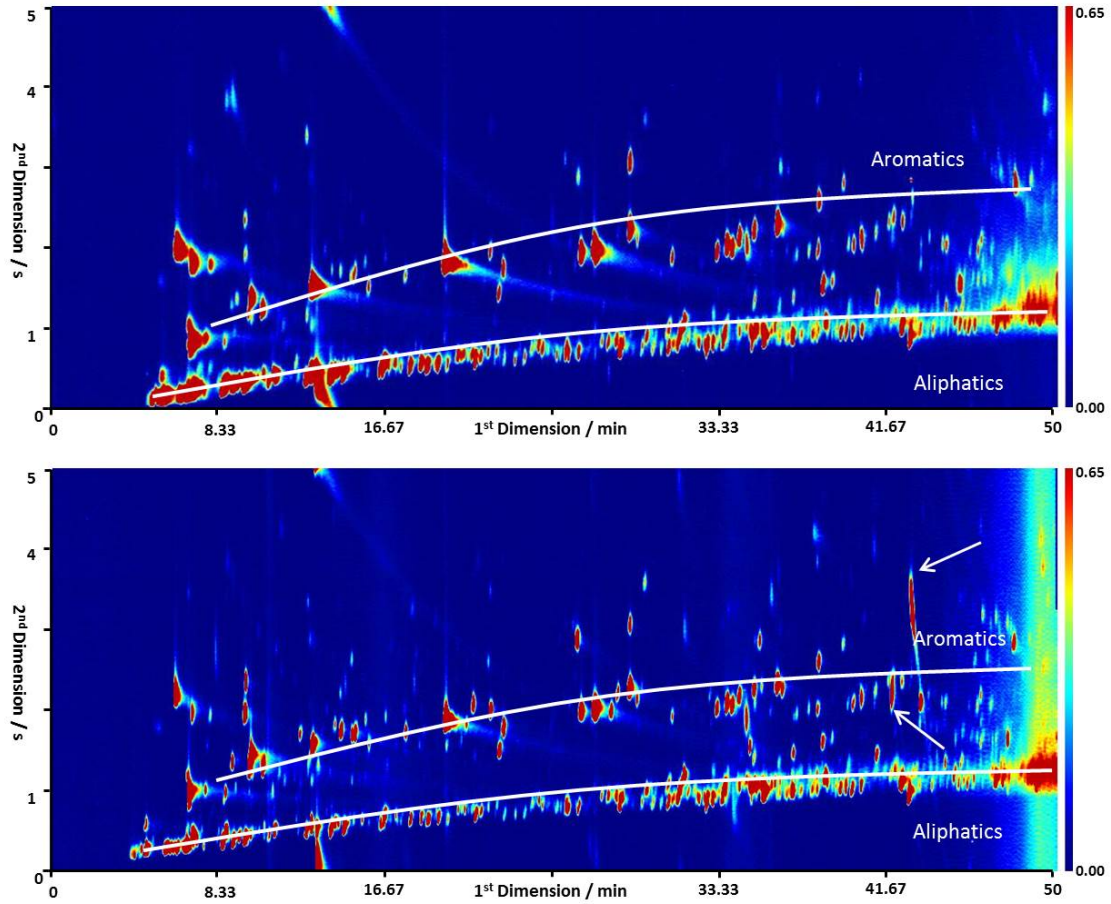

Figure 2.13: Typical GC×GC-FID plot from the winter (upper; 2012-02-07 at 08:32) and summer (lower; 2012-07-25 at 08:32) ClearfLo campaigns.

boundary layer height. Toluene and NO_x are strong indicators of traffic related emissions, and both have diurnal profiles with rush hour peaks, commonly observed in urban areas.[8,174,175] The profiles of the higher carbon classes, C_4 substituted monoaromatics and C_{13} aliphatics, show similar traffic-related profiles, strongly indicative that this is their major source. Those species with a dominant biogenic source (*e.g.* isoprene and α-pinene) are higher in summer, due to increased emission. The winter profiles of isoprene and α-pinene show possible anthropogenic sources, likely traffic and cleaning products respectively.

2.5.3.1 Impact of local meteorology in winter

Ethane generally shows a different behaviour than other VOCs, characteristic of a persistent fugitive release, in this case from the natural gas network,[174,176] and is also impacted by changing boundary layer height (see Figure 2.9). In the original winter diurnal profile of ethane (includes all data points, seen in Figure 2.14, blue profile), a pattern is seen

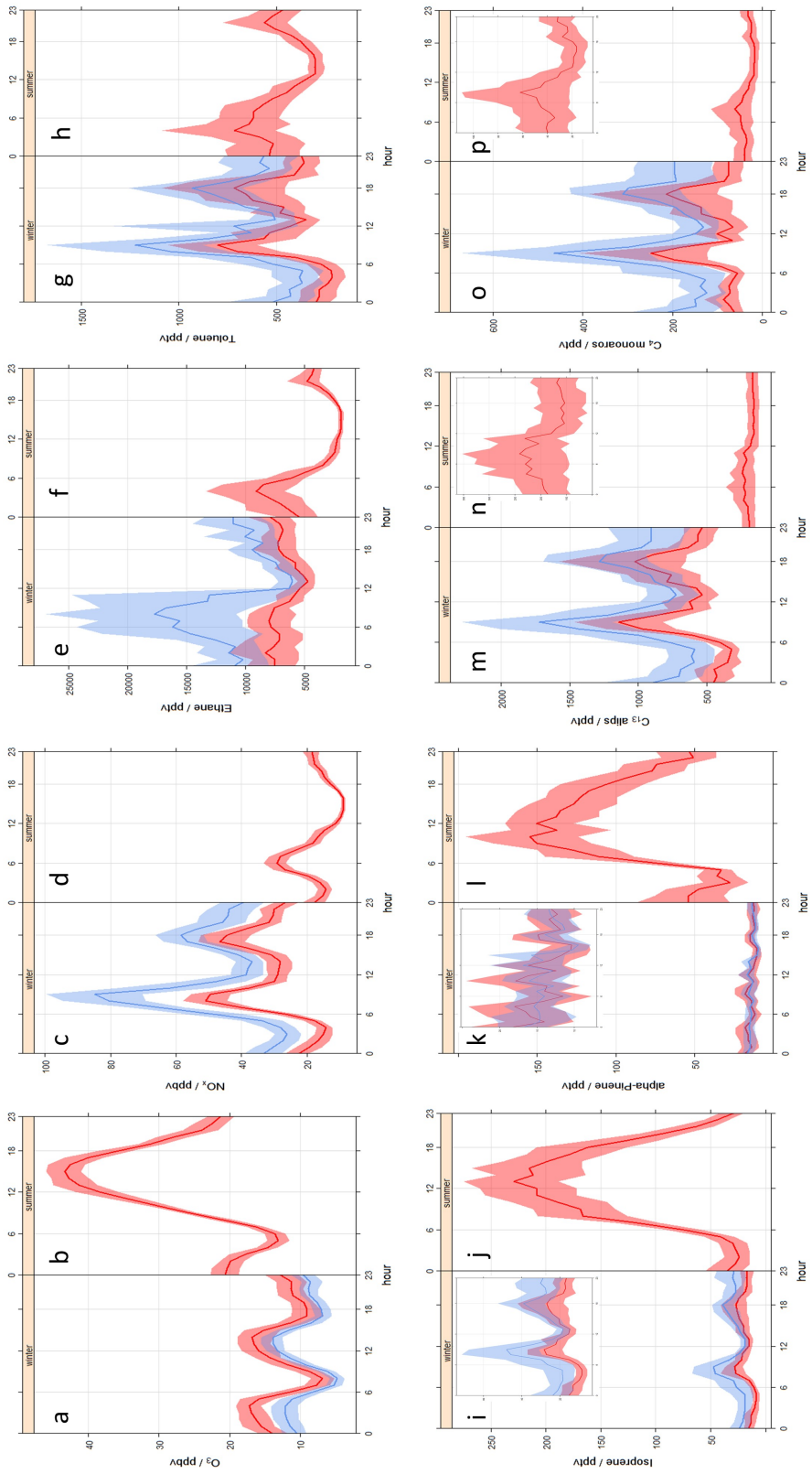

Figure 2.14: Diurnal profiles of selected urban pollutants in winter (left-hand side of each plot) and summer (right-hand side of each plot). Winter and summer are plotted on the same y- axes to show seasonal differences, with insets allowing the profile to be easily seen. a and b; ozone ($n = 2915$, 1520 and 2880; winter blue, winter red and summer, respectively), c and d; nitrogen oxides ($n = 2915$, 1520 and 2880), e and f; ethane ($n = 660$, 353 and 681), g and h; toluene ($n = 660$, 353 and 680), i and j; isoprene ($n = 660$, 353 and 681), k and l; α-pinene ($n = 691$, 390 and 634), m and n: C_{13} aliphatics ($n = 692$, 390 and 632), o and p; C_4 substituted monoaromatics ($n = 692$, 390 and 563). This figure was constructed using the OpenAir project for R where the solid line represents the mean daily concentration and the shaded regions shows the 95% confidence intervals surrounding the mean.[166–168]

which appears to show a large increase in the early morning hours. This is likely due to two stagnant, high pressure periods experienced at the start and end of the campaign where data profiles were driven by meteorological conditions (10/01/2012-18/01/2012 and 03/02/2012-08/02/2012). The dispersion of VOCs would be low given decreased wind speeds, and as such the ethane concentration would appear to rise.

In order to see the most accurate profile of ethane, the data points corresponding to the two stagnant periods were removed and a new diurnal profile constructed (shown in Figure 2.14, red profile). This profile shows the typical diurnal profile expected given an almost constant source and slow removal processes. The dip seen in both profiles of ethane at approximately 12 noon correlates to a rise in the boundary layer. A boundary layer decrease in the afternoon is also seen to have an effect on the profiles of ethane with a small rise at approximately 15:00 (see Figure 2.9). There is no difference seen in the two profiles of the other individual VOCs and grouped species, except for a larger range in the unconstrained profiles, likely due to the higher concentrations seen during the two stagnant, high pressure periods and their shorter lifetimes in the atmosphere compared to ethane.

2.5.4 Comparison between London and Los Angeles

Similar compounds were measured during the 2010 California Research at the Nexus of Air Quality and Climate Change (CALNEX) campaign in Bakersfield, California.[177] Table 2.4 shows the differences between London and Los Angeles in terms of population density, green space and diesel fuel use to highlight the very different urban geography and traffic make up in the two cities. A smaller sub set of data is also included for North Kensington, where this study was carried out and Bakersfield, CA, the site of the CALNEX project.

Table 2.4: Comparison of London, North Kensington, LA and Bakersfield

	Area (km^2)	Number of Inhabitants	Pop. density (inhab. km^{-2})	Cars per household	Percent public green space	Percent diesel use	Average Temp. (°C) Winter	Average Temp. (°C) Summer	Average hrs sunlight Winter	Average hrs sunlight Summer
London	1572[a]	7,825,200[a]	4978[a]	0.8[f]	38.4[a]	57[g]	3[i]	18.9[i]	2.2[k]	5.9[k]
NK	12.13[b]	158,700[c,d]	13,087[c,d]	0.6[f]		56[c,g]				
LA	10510[a]	9,818,605[a]	934[a]	1.9[3]	6.7[a]	13[h]	13.8[j]	21.4[j]	6.6[l]	11.1[l]
Bakersfield	244.77[b]	357,603[3]	1461[d]			33[h]				

References

[a]World Cities Cultural Report, 2013. [b]Calculated from Number of Inhabitants and Population density. [c]Values for Kensington and Chelsea. [d]Census, July 2012. [e]US Census Bureau. [f]UK Office of National Statistics. [g]Department of Energy and Climate Change Statistics. [h]Gentner *et al.*, (2012)[148]

[i]metoffice.gov.uk, mean daily temperature. [j]los-angeles.climatemps.com/temperatures.php [k]metoffice.gov.uk, mean daily hours of sunshine.

[l]los-angeles.climatemps.com/sunlight.php

This comparison is particularly important when considering the sources of BVOCs. In

California, where many of the previous studies have taken place, the cities are surrounded by high BVOC emitting regions *i.e.* Blodgett Forest, Angeles National Park, Sequoia National Park and Los Padres National Park. Los Angeles itself only has around 6.7% public greenery. In contrast, London has an estimated 38% public green space and is the greenest city of its size in the World. The emission maps shown in Figure 2.3 show that current emission models do not predict a significant downwind source of BVOC to London. Therefore in summer in London, the majority of BVOCs measured are likely to be from relatively local sources.

2.5.4.1 Weekday *vs.* weekend

Previous measurements of VOCs in Bakersfield showed a lower toluene/benzene ratio (t/b) at the weekend (t/b = 1.7) compared to weekdays (t/b = 2.4).[149] This was used as an indicator of reduced photochemistry at the weekend as a result of changes in diesel emissions due to reductions in heavy-duty vehicles. Using this same approach, the winter campaign ratio has been calculated for weekends (red, t/b = 2.6) and weekdays (black, t/b = 2.2) as shown in Figure 2.15. The t/b ratios found in Bakersfield are also shown in this figure with dashed lines. Figure 2.15 shows the opposite of the Bakersfield study, with a higher t/b ratio at the weekend. However, it should be noted that the correlation between the two species is poorer during the weekdays (R^2 = 0.73, *c.f.* weekend R^2 = 0.93).

Also, no discernible differences were found between the behaviour of gasoline (2,2,4-trimethyl pentane and toluene) and diesel tracers (dodecane, C_{13} aliphatics) as shown in Figure 2.16, with average diurnal profiles at the weekends shown in blue and weekdays in red. In general there are lower concentrations during the evening rush hour (16:00-19:00) of all VOCs and NO_x at the weekend, with an increase later in the evening (19:00-00:00), reflecting the increase in night-time social activities during the weekends. However, the highest mixing ratios of most VOCs were observed on Saturday 14/01/2012, as a result of low wind speeds and a low boundary layer depth. The traffic make up in London is different to US cities, with a high degree of diesel powered buses and cars. Thus the influence of reduced heavy-duty truck traffic is not observed in the ratio of diesel to gasoline VOCs.

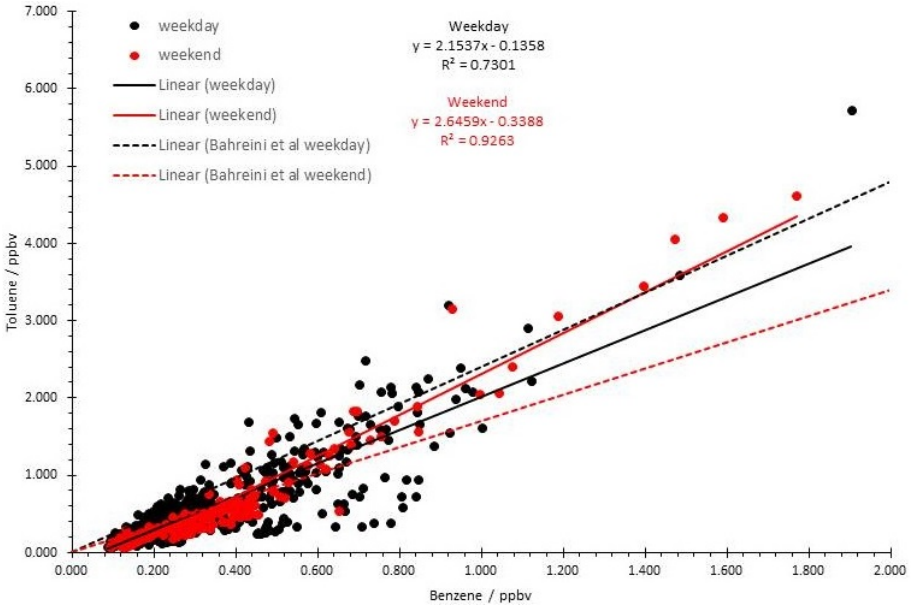

Figure 2.15: Correlations of toluene and benzene measured during the winter campaign, weekday (black) and weekend (red). Fitting of the data is shown with the solid lines, the equations and R^2 values of the linear lines of best fit are provided. The dashed lines show the fitting of weekday and weekend toluene/benzene correlations from Bahreini *et al* (2012).[149]

2.5.5 Reactivity and mass calculations of grouped compounds

The relative emission source contributions of compounds to the total hydrocarbon mixing ratio, mass concentration and primary hydrocarbon $^{\bullet}$OH radical reactivity, have been calculated by carbon number, and split according to emission source (shown in Figure 2.17). For each sample, the mass concentration (μg m^{-3}) and primary hydrocarbon $^{\bullet}$OH radical reactivity (s^{-1}) were calculated and a seasonal median calculated using the mixing ratios of the individual components and the summation of all further unidentified species within the ten class groups, not including the OVOCs. OH reactivity is defined as the total psuedo first order rate coefficient for loss of OH when reacting with VOCs in the atmosphere. This is important in urban atmospheres that are VOC limited, such as London, as the reaction of VOCs with the OH radical is the driving force for the formation of O_3 and other secondary pollutants.

The Passant (2002) speciated emissions inventory[144] was used to determine the main emission sources for each compound. For C_2 to C_5, the main source was either natural gas usage or leakage, followed by road transport use. From C_6 onwards, the main emission source was classified as road transport or other fuel usage categories (*i.e.* filling of petrol stations). To determine the percentage contributions from diesel or gasoline fuel usage,

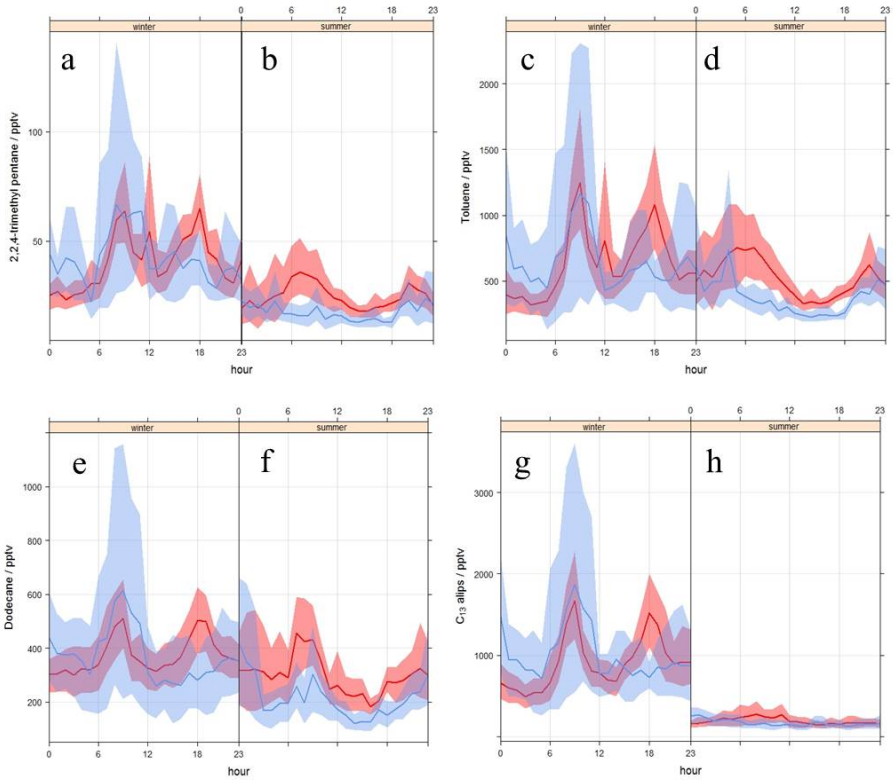

Figure 2.16: Diurnal profiles of typically traffic source related compounds showing weekday (red) and weekend (blue) profiles. Petrol compounds are 2,2,4-trimethyl pentane (a and b) and toluene (c and d), and diesel compounds are dodecane (e and f) and C_{13} aliphatics (g and h).

the detailed fuel characterisation of Gentner *et al.*, 2012[148] was used with a value of 60% diesel use in the UK.[178]

The following equation was used to calculate the primary hydrocarbon $^{\bullet}$OH radical reactivity, using observed meteorological data. Due to a lack of information on rate constant temperature dependence below 298 K for most species, the 298 K OH rate constants were used from Atkinson and Arey, (2003) for all individually identified species.[82]

$$s^{-1} = \left([\mathrm{VOC}]\,(\mathrm{ppb}) \times 10^{-9} \times [\mathrm{M}]\right) \times k_{OH}\,(298\ \mathrm{K}) \tag{2.3}$$

Where

$$[\mathrm{M}] = \left(\frac{\mathrm{Pressure\,(mbar)} \times 10^{-4}}{(8 \cdot 314 \times (273 \cdot 15 + \mathrm{temperature\,(^{\circ}C)}))}\right) \times 6 \cdot 022E + 23 \tag{2.4}$$

In order to calculate the primary hydrocarbon $^{\bullet}$OH radical reactivity of diesel emissions, rate constants need to be estimated as each individual species is not uniquely identified and because the rate constants (and subsequent chemistry) are unmeasured in the

majority of cases for hydrocarbons larger than C_8. The nearest straight-chain alkane rate constant [82] is applied to all carbon in that aliphatic grouping. This will lead to a conservative estimate of reactivity since cycloalkanes and alkenes would be expected to react faster (*i.e.* the k_{OH} for the reaction of *n*-dodecane is 1.32 $\times$ 10^{-11} cm^3 $molecule^{-1}$ s^{-1}, compared to that of 1-dodecene which is 5.03 $\times$ 10^{-11} cm^3 $molecule^{-1}$ s^{-1}). For the C_4 substituted monoaromatic and C_{10} monoterpene groups, the rate constants of 1,3 diethyl benzene and α-pinene respectively were used.

For each aliphatic group, the appropriate C number *n*-alkane k_{OH} rate constant was used to calculate the primary $^{\bullet}OH$ radical reactivity. Each group is likely to contain branched alkanes, cycloalkanes and alkenes in addition to the *n*-alkane. The measured rate constants of branched alkanes with the $^{\bullet}OH$ radical are usually similar or slower than the linear alkane, depending on the location and degree of branching. There are very few measurements of OH rate constants for cycloalkanes, but generally they react faster than the equivalent linear alkane. Alkenes react around an order of magnitude faster with the $^{\bullet}OH$ radical than alkanes, and the rate increases further with increasing degrees of unsaturation.

Rate constants were calculated, to investigate the potential bias of using the *n*-alkane, for 354 C_{12} alkane isomers (298 K) using the H atom abstraction structure activity relationship defined in Ziemann *et. al.,* (2012) .[179] The average rate constant was found to be 1.15 $\times$ 10^{-11} cm^3 $molecule^{-1}$ s^{-1} which, when compared to the measured rate constant for *n*-dodecane (1.32 ($\pm$ 0.26) $\times$ 10^{-11} cm^3 $molecule^{-1}$ s^{-1}), is within the error limits for this measurement.[180] A selection of the calculated rate constants are shown in Table 2.5, along with some alkenes to highlight the range of reactivities of the C_{12} species.

For the C_{10} terpenoid group the use of α-pinene rate constant (5.23 $\times$ 10^{-11} cm^3 $molecule^{-1}$ s^{-1}) produces a conservative underestimate of the $^{\bullet}OH$ radical reactivity for this group, as it is one of the slowest reacting species, e.g. when compared to limonene (1.64 $\times$ 10^{-10} cm^3 $molecule^{-1}$ s^{-1}).[82] If a rate constant half way between α-pinene and limonene (1.08 $\times$ 10^{-10} cm^3 $molecule^{-1}$ s^{-1}) was used, this would increase the contribution of the C_{10} terpenoid group to primary $^{\bullet}OH$ radical reactivity from 0.0093 s^{-1} to 0.0192 s^{-1} and 0.0416 s^{-1} to 0.0861 s^{-1} in winter and summer respectively.

Figure 2.17 shows the winter (left) and summer (right) contributions of the main four emission sources (natural gas, gasoline, diesel and biogenic sources) to median hydrocarbon mixing ratios (upper panel), mass concentration (middle panel) and primary hydrocarbon

Table 2.5: Room Temperature Rate Constants for the Gas-Phase Reactions of OH Radicals with C_{12} Aliphatic Compounds[82,179–182].

		$10^{12} \times k_{OH}$[a] (cm^3 molecules^{-1} s^{-1})	
Species	**Structure**	**Measured**[b]	**Calculated**[c]
Alkanes (linear, branched, cyclic)			
n-dodecane		13.2[d]	13.9
2-methylundecane		-	13.9
2,2-dimethyldecane	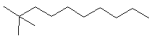	-	10.3
3,3,4-trimethylnonane	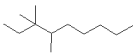	-	8.79
6-ethyl-3-methylnonane	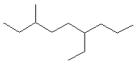	-	14.9
2,2,3,3,4,4-hexamethylhexane		-	2.49
cyclododecane		-	17.0
Alkenes/dienes			
1-dodecene	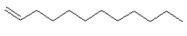	50.3±1.3[e]	47.1
trans-5-dodecene	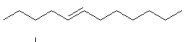	-	71.1
2,9-dimethyl-1,9-decadiene	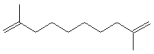	-	77.8
2,4-dimethyl-2,4-decadiene	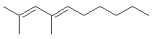	-	176

[a]All data measured/calculated at atmospheric pressure.

[b]298 K data taken from Atkinson (2003)[180] unless otherwise stated; estimated uncertainty of ± 20 % unless otherwise stated.

[c]Calculated using the hydroxyl radical H-atom abstraction and OH addition structure activity relationships given in Ziemann and Atkinson (2012)[179] and Kwok and Atkinson (1995)[181] respectively; calculated rate constants for alkanes and alkenes within a factor of 2 of those measured.

[d]Atkinson and Arey (2003)[82]

[e]295 ± 1 K relative rate data taken from Aschmann and Atkinson (2008)[182].

OH radical reactivity (lower panel). Two inset graphs are shown in the upper panel of Figure 2.17 to allow the contributions of the larger carbon number species to be seen more easily. Although the summer data is being shown throughout the remainder of this chapter, care should be taken when interpreting the impacts. It is likely that the summer observations are made up of '*residual*' VOCs remaining after transport from emission source and subsequent photochemical reactions. This could lead to a very slight overestimation of the contribution of diesel-related hydrocarbons and an underestimation of some species, particularly the OVOCs.

The winter has generally higher abundances of hydrocarbons, with summer showing a marked increase in the biogenic source compounds, shown in Figure 2.17. In both winter

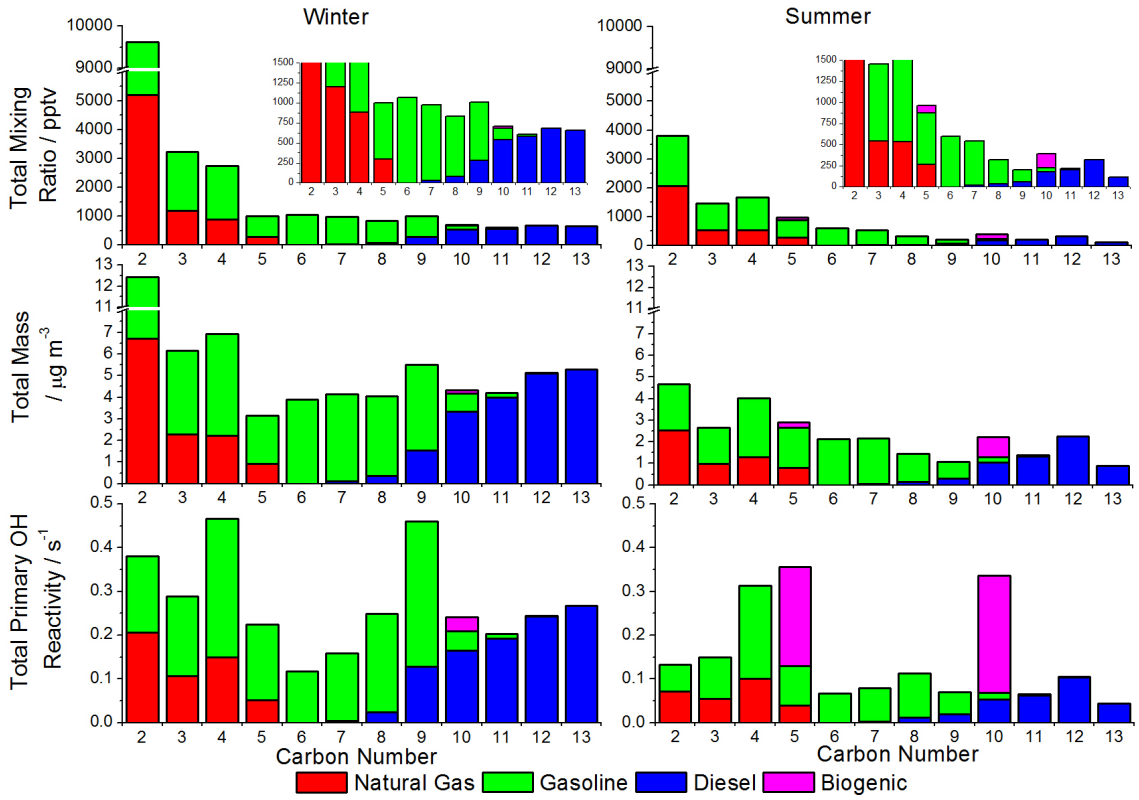

Figure 2.17: Seasonal median values for hydrocarbon mixing ratio, mass concentration and primary hydrocarbon OH radical reactivity in London air grouped by carbon number and potential emission source.

and summer, in mixing ratio terms, the distribution is dominated by high volatility species (over 85% of the total) primarily from natural gas and gasoline sources. When viewed in terms of mass concentration, however, the distribution of combined natural gas and gasoline versus diesel is closer to 70% : 30% in winter and 77% : 23% in summer, the latter due to the increased loss rates for reactive species in summer disproportionately removing larger hydrocarbons.

2.5.5.1 Calculation of unmeasured diesel emissions

The GC measurements stop at C_{13}, however diesel typically has a range of hydrocarbons from C_9 to C_{22} that peaks at C_{16} with *n*-hexadecane as the most abundant compound. Using the observed distribution of C_{10}-C_{13}, allows for an estimate to be made of the remaining, *unobserved* NMHC fraction of gaseous diesel emissions in the C_{14}-C_{22} range, using the fuel composition-based emission factors for the gas phase compounds from Gentner *et al.*, (2013).[172] Assuming no atmospheric loss, a reasonable approximation in winter, it is estimated that the GC×GC-FID technique observes around 25-30% of the total gaseous hydrocarbon emissions from diesel sources. It is then possible to estimate a seasonal av-

erage unmeasured gas phase NMHC mass concentration from diesel sources in London as 76.1-97.8 μg m^{-3} in winter and 26.8-34.3 μg m^{-3} in summer. These values can be compared to typical primary organic aerosol measurements of 1 μg m^{-3},[183,184] indicating that, in ambient air, diesel-related emission of hydrocarbons are overwhelmingly (a factor of 100) to the gas phase, consistent with laboratory and tail pipe studies.[150] In contrast, using gasoline liquid fuel speciation, the combined GC approach can observe over 98% of the mass of gasoline.

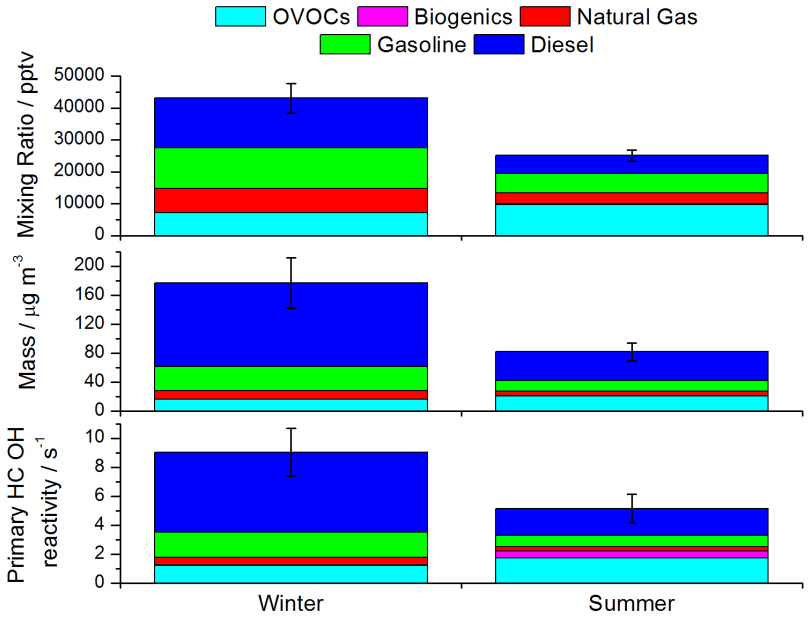

Figure 2.18: Contributions of emission source to total mixing ratio, mass and OH radical reactivity for winter and summer. Diesel is the summation of measured and calculated, with error bars indicating the uncertainty of the unobserved diesel NMHC fraction.

The impact of the unobserved diesel emissions on primary hydrocarbon $^{\bullet}$OH radical reactivity was estimated using the *n*-dodecane rate constant as a proxy. The percentage contributions to mixing ratio (top), mass concentration (middle) and primary hydrocarbon $^{\bullet}$OH radical reactivity (bottom), divided by emission source, including the unmeasured diesel emissions and OVOCs, are shown in Figure 2.18. It is clear that diesel plays an important role in the composition of NMHCs and their subsequent reactivity. The total (measured + calculated) diesel emissions contribute 5.1 and 1.7 s^{-1} to $^{\bullet}$OH radical reactivity in winter and summer respectively compared to 1.7 and 0.8 s^{-1} from gasoline compounds; increasing the contribution of diesel-related hydrocarbons to calculated VOC $^{\bullet}$OH radical reactivity from 23% using the measured VOCs to 61% included the unmeasured I/VOCs in winter and from 8% to 34% in summer (full details can be found in

Table 2.6). In summer, the primary emissions have undergone a degree of loss due to photochemical ageing and so the values are an underestimate of the fuel sources. These diesel-related hydrocarbons may be partly responsible for the missing $^{\bullet}$OH radical reactivity observed between measurements of $^{\bullet}$OH radical lifetime versus the value calculated from observed sinks in many studies,[78,185–189] (discussed in Chapter 3).

Table 2.6: Primary hydrocarbon OH reactivity (s^{-1}) divided by emission source for winter and summer

	Natural Gas	**Gasoline**	**Total Diesel (Measured + Calculated (±error))**	**Biogenic**	**OVOCs**	**Total (±error)**
Winter	0.51	1.73	5.13 (1.02 + 4.10 (±0.51))	0.03	1.23	8.64 (±0.51)
Summer	0.27	0.77	1.726 (0.30 + 1.72 (±0.18))	0.50	1.74	5.00 (±0.18)

2.5.6 Comparison to inventories

Assuming that; the winter observations are made at source (hence atmospheric losses and lifetime differences can be neglected), the measurement location is representative of an urban setting, and the UK inventory correctly estimates the emission for toluene (based on direct flux comparisons made in London by Langford *et al.*, 2010),[190] there appears to be a significant inventory under-reporting for the higher carbon number species. When normalising to toluene, the UK national emissions inventory, which is believed to use best-practice international reporting methodologies, under-reports by a factor of 4.6 for C_9 species, rising to a factor of 74 for C_{12} compounds (see Figure 2.19). Given the clear traffic winter diurnal profile in C_{10}-C_{13} species (seen in Figure 2.14m for C_{13} aliphatics), which essentially encompasses only diesel fuel, the most likely source of these species is gaseous emissions from the diesel vehicle fleet, either evaporative, tailpipe or a combination of the two. These observations provide the first direct evidence of significant diesel hydrocarbons in London's ambient air, something that could previously only be inferred from liquid fuel measurements and exhaust studies. These higher carbon number species, which have been shown to be under represented in emission inventories, are also likely to be either of the wrong magnitude or have inaccurate contributions in the models based on them. The contribution of the actual observations of these species to potential ozone and SOA formation is described in the following two sections.

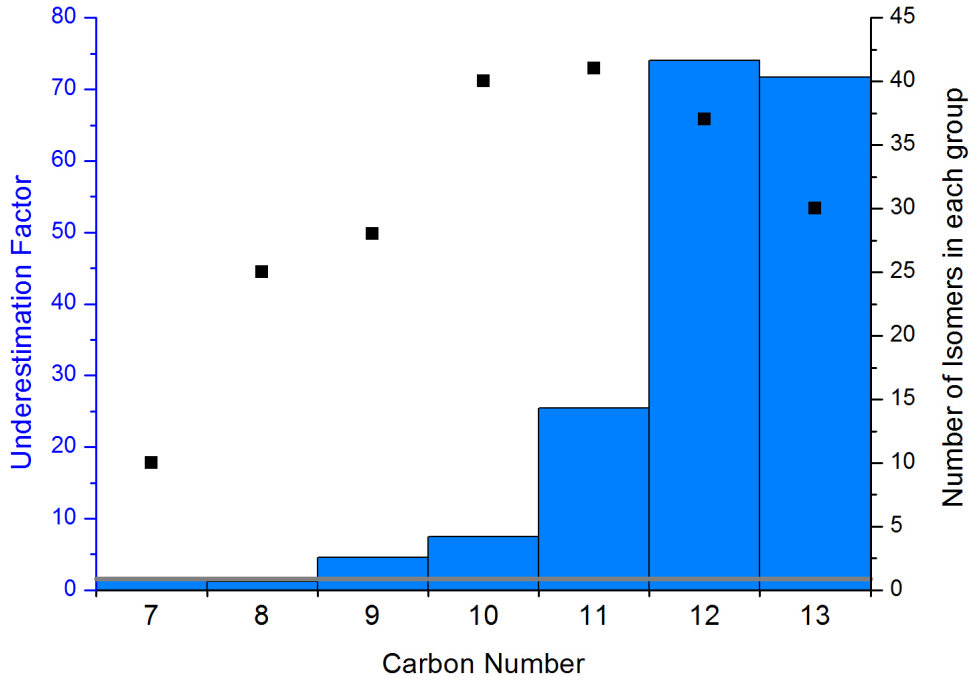

Figure 2.19: Winter emissions inventory underestimation (left axis and blue columns) and the number of isomers included in each grouped set of compounds (right axis and black squares). Grey line shows a factor of 1 *i.e.* inventory emission estimation is consistent with the observations.

2.5.7 Ozone formation potentials

At present, there is insufficient kinetic and mechanistic data to allow for the accurate modelling of the impact diesel hydrocarbons will have on photochemical ozone. Unlike Los Angeles, which is typically impacted by intense single-day episodic photochemical ozone events, in London (and NW Europe), higher ozone levels are usually the result of regional-scale multi-day formation. Therefore, different control strategies and reactivity scales, which take into account transboundary transport, have been developed and applied in Europe.

Photochemical ozone creation potentials (POCPs, *e.g.* Derwent *et al.*, 1998)[191] have been derived using idealized 5-day photochemical trajectory model runs over Europe, incorporating detailed chemical degradation schemes of the emitted VOCs.[61] Individual POCP values depend upon emissions along the trajectory, the reactivity of the VOC and its propensity to form ozone, *i.e.* the number of C-C and C-H bonds in the reactive species. Calvert *et al.*, (2008), using the Master Chemical Mechanism (MCMv3.1, http://mcm.leeds.ac.uk/MCM) and speciated emission inventories (Passant, 2002),[144]

with little speciation of alkanes above C_9, found that alkanes dominated POCP-weighted emissions (33%) on the regional scale in Europe, accounting for slightly more than the aromatics (29%) and significantly more than the alkenes (20%) and oxygenates (17%).[192] They also note that this is in marked contrast with that found on the urban scale in Los Angeles, where alkanes contribute little to the intense episodic ozone formation observed.

The work presented here shows that emission inventories severely underestimate the amount of alkanes emitted from diesel sources, hence these have are not been included in previous studies on ozone formation. Based on the POCP results of Calvert *et al.*, (2008)[192] for shorter chain alkanes, and considering the high OH reactivity of larger hydrocarbons, incorporating the diesel related aliphatics into future calculations is likely to have a significant impact on regional ozone formation in Europe, and likely elsewhere.

However, despite the lack of chemical information available, we can make an assessment of the effects that the new diesel VOC observations have on local ozone productivity by calculating the Ozone Formation Potential (OFP) of each emission source using a Maximum Incremental Reactivity (MIR) scale, as determined by Carter (2010) using the SAPRC-07 mechanism.[193] The MIR scale is based upon one-day photochemical simulations in a box moving over an urban basin and subject to O_3 precursor emissions. The NO_x concentrations are adjusted so that the final O_3 concentration in a simulation showed the maximum sensitivity to changes in emissions of organic compounds, these conditions give the MIR. MIRs represent relatively high NO_x conditions, often experienced in US cities, where control of the emissions of VOCs is the most effective means of reducing O_3 formation.[193]

MIR values for a range of important VOC emission classes (alkanes, alkenes, aromatics, oxygenates) compare well to POCP values calculated using detailed MCMv3.1 chemistry in a one day US urban photochemical trajectory model, giving us confidence in the tuned SAPRC-07 chemistry for predicting photochemical O_3 formation under typical one-day high NO_x, high ozone conditions.[194] However, caution must be observed when applying MIR scales to other conditions (*i.e.* NW Europe), as previously discussed.

For those species included in one of the carbon number and functionality VOC groups, a weighted MIR value has been calculated assuming a composition of 95% branched alkane and 5% alkene. The calculated, unobserved diesel emissions were given a MIR value based on the weighted contributions of the different compound classes from the diesel fuel gaseous emission speciation in Gentner *et al.*, (2013).[172]

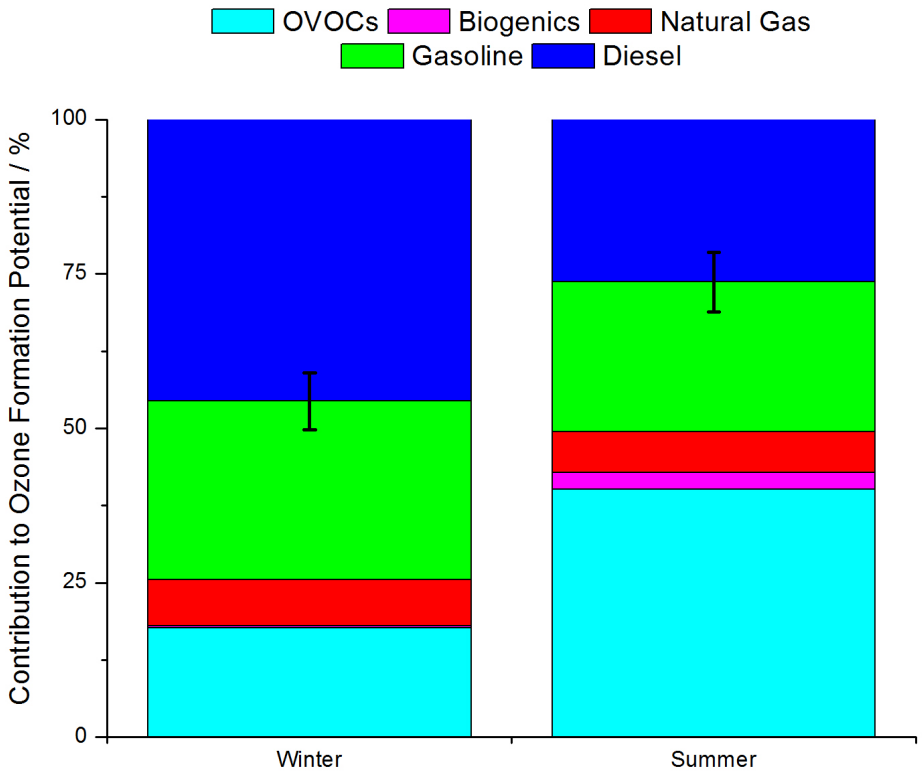

Figure 2.20: Contribution of emission sources to potential ozone formation, where diesel is representative of total diesel emissions and the error bars show the uncertainty of the unobserved diesel fraction calculation.

The calculated OFP values for summer and winter are shown in Figure 2.20, with a clear seasonal difference in the importance of different emission sources. The winter is dominated by emissions from diesel (over 45±4.6%). In contrast, the summer shows a marked increase in contribution from oxygenated species, rising from 18% in winter to 40% in summer. Gentner *et al.*, (2013) concluded that gasoline emissions contributed the majority of potential O_3 formation, however given that gasoline is the primary fuel used in the US (quoted at 73-90% of total fuel use[148]) this is not surprising.[172] Whereas in the UK, diesel fuel accounts for an average of 60% of total fuel use and as such would be expected to contribute a larger percent towards O_3 formation.

Given that many of the higher carbon number species, likely emitted from the combustion of diesel, are not currently included in emissions inventory and as such are missing from many model chemical mechanisms (*e.g.* MCMv3.2), a more rigorous reactivity analysis is not possible (*e.g.* POCPs discussed previously). It is possible to infer from this analysis however, that as winter diesel emissions contribute nearly 50% of the OFP and over 60% of primary hydrocarbon OH reactivity, it is likely that they would have a large impact on the overall reactivity and chemistry of the urban atmosphere.

2.5.8 Potential impacts on secondary organic aerosol formation

Over the last few years, there has been robust debate in the literature over the relative importance of diesel versus gasoline for SOA production, arising in part because of the difficulties of measuring diesel hydrocarbon emissions.[149,151–153,155] Recent studies have shown that unspeciated emissions from combustion sources lead to significantly more SOA production than those that can be speciated by conventional instrumentation. Jathar *et al.*, (2014), used simulation chamber data and source-specific SOA yield parametrizations for these unspeciated emissions to estimate that, in the US, 90% of SOA was from biomass burning and gasoline sources, with 85% of the SOA coming from unspeciated organic emissions.[154]

There is a clear need to improve measurements of larger hydrocarbons that represent a large part of what is referred to in other studies as unspeciated chemicals. In this chapter, the uncertainty in the unspeciated fraction has been reduced by grouping ambient observations of VOCs by carbon number and functionality. The $>C_9$ aliphatic groups are dominated by diesel emissions at this location and so the SOA source strength can be more accurately determined. The potential contributions of the higher hydrocarbons to SOA formation has been estimated by multiplying the median measured VOC mass concentration (Figure 2.21, top panel, black columns) by the corresponding SOA yield (Figure 2.21, top panel, blue circles).[195] The yields applied were measured in high NO_x chamber studies (VOC_0/NO_x (ppbC/ppb) of 0.5) with an organic aerosol mass C_{OA} of 10 μg m^{-3}, representative of urban areas.[195,196] Here it is assumed that NMHCs with less than six carbons and aqueous chemistry of water soluble oxidation products, such as glyoxal, do not contribute to SOA mass.[197] In both winter and summer, the observed levels of aliphatic compounds from diesel sources have the potential to form significant quantities of SOA (Figure 2.21, bottom panel, red columns). If a diesel SOA yield of 0.15[148] is applied to the total diesel emissions (as calculated previously), then gas phase emissions from diesel engines represent the dominant traffic related precursor source of urban SOA in a European megacity such as London, where the use of diesel fuel is prevalent. Each cubic meter of air contains sufficient gas phase hydrocarbons to potentially produce 14.0-24.5 and 4.9-8.6 μg of SOA in winter and summer following atmospheric oxidation.

Recent simulation chamber studies indicate that modern engines fitted with diesel particle filters, such as EURO5 emissions control, have greatly reduced VOC tailpipe emission and form little SOA under chamber conditions.[152,153] However, Carslaw and

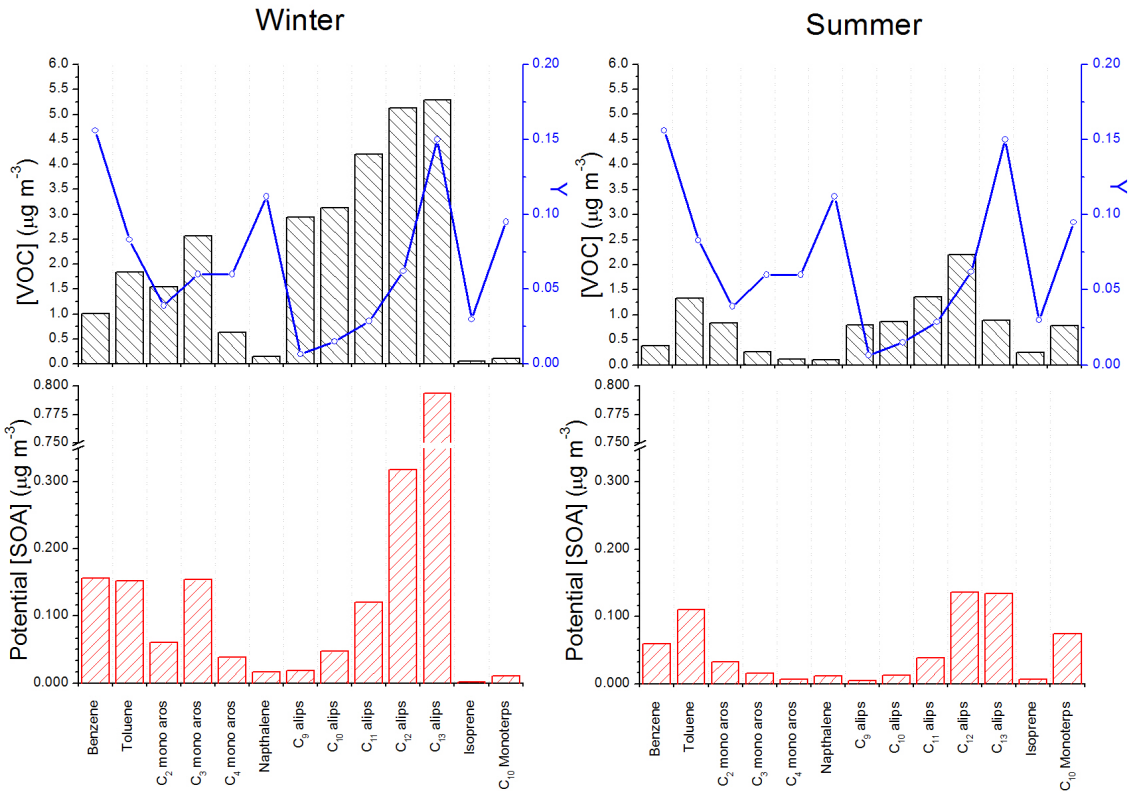

Figure 2.21: Potential SOA mass estimates. Upper: Mean VOC mass concentration [VOC] shown by black columns, and the corresponding SOA yields (Y) for the VOC precursors in blue circles. Lower: Potential SOA mass concentration [SOA], calculated as the product of mean VOC mass and SOA yields. Winter shown on left and summer shown on right hand side panels.

Rhys-Taylor (2013) have recently shown that when vehicles are driven under real-world urban conditions (*i.e.*different engine loads cause variable catalyst temperatures which can lead to limited effectiveness, as opposed to dynamometer tests where the catalyst is held at optimum operating conditions), the emission of NO_x from diesel engines have not been reduced as expected given the new technologies implemented.[198] It is possible to infer that if NO_x emissions are higher than expected, the VOC emission are also likely to be higher. This chapter has shown that there is a significant diesel vehicle source emitting sufficient VOCs to impact ozone and SOA formation in the real world.

2.6 Conclusion

From the results presented, it is possible to conclude that current inventories and emissions estimates do not adequately represent emissions of gas phase higher carbon number species from the diesel fleet under real-world conditions and in a developed urban environment. The calculated impact of these species is significant, particularly in terms of OH reactivity,

ozone formation potential and SOA production.

In the last decade, there has been a steady shift in fuel use in many locations. For example, in the UK diesel fuel use as a fraction of total fuel has risen from 52% in 2005 to 62% in 2011 (See Figure 2.22 and Table 2.7).[178] Although the UK may be considered typical of Europe (where diesel use varies between 45-80%),[199] the average US value was around 29% diesel use[200] in 2013 and the understanding of other geographical regions is poor.

Table 2.7: Fuel use changes for the UK. [a]Total diesel calculated as the sum of buses, diesel cars, HGV and diesel LGV, [b]total petrol calculated as the sum of petrol cars, motorcycles and petrol LGV, [c]% diesel use calculated as (total diesel divided by total fuel (sum total diesel and petrol)) x 100. www.gov.uk/government/statistical-data-sets/road-transport-energy-consumption-at-regional-and-local-authority-level , and was accessed on 30/04/2014.[178]

	Personal Vehicles				Freight					%
Year	Buses	Diesel Cars	Petrol Cars	Motor Cycles	HGV	Diesel LGV	Petrol LGV	Total Diesel[a]	Total Petrol[b]	Diesel Use[c]
2005	1,453.0	5,836.0	17,267.0	198.0	7,577.0	4,250.0	377.0	19,116.0	17,842.0	52
2006	1,476.0	6,314.0	16,687.0	188.0	7,778.0	4,424.0	378.0	19,992.0	17,253.0	54
2007	1,552.0	6,731.0	15,913.0	200.0	7,956.0	4,651.0	345.0	20,890.0	16,458.0	56
2008	1,505.0	7,295.0	14,830.0	183.0	8,054.0	4,652.0	306.0	21,506.0	15,319.0	58
2009	1,501.0	7,370.0	14,373.0	187.0	7,413.0	4,561.0	277.0	20,845.0	14,837.0	58
2010	1,495.0	7,375.0	13,477.0	166.0	7,511.0	4,606.0	252.0	20,987.0	13,895.0	60
2011	1,383.0	7,663.0	12,750.0	167.0	7,311.0	4,678.0	234.0	21,035.0	13,151.0	62

This shift to an increasingly diesel-powered fleet in many developed cities, as a response to energy efficiency drivers, has therefore shifted the balance of hydrocarbons in urban air from short to long chain compounds, and these observations provide direct atmospheric evidence of this effect in London. Previous air quality assessments of diesel-related hydrocarbons in the atmosphere are few in number, and as discussed previously, have been made only in the US where geographic characteristics and vehicle fleet composition are very different to London, and Europe more widely. In many cities the impact of diesel hydrocarbons remains to be determined, but this work demonstrates that it will likely be significant in locations with substantial diesel fleets. An improvement in measurement infrastructure appears to be essential if this source is to be quantified more widely or the impacts of policy evaluated.

Understanding the impact of this change is significantly hindered however by a lack of appropriate physico-chemical data for individual longer chain hydrocarbons. There are already very significant policy challenges for many developed cities relating to the control of NO_2 from modern diesel vehicles, and this chapter indicates that there may also be a

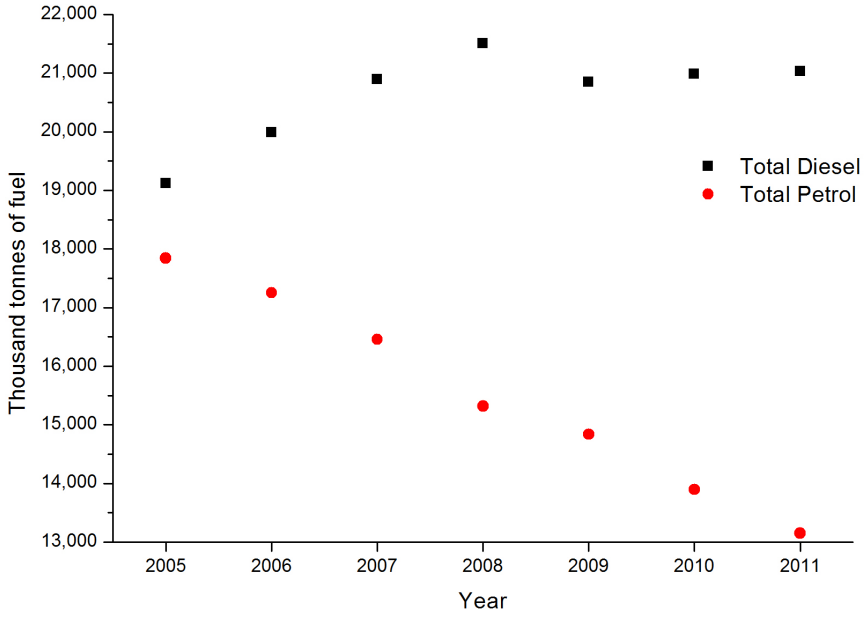

Figure 2.22: Change in fuel use from 2005 to 2011. Statistics from the Department of Energy and Climate Change which give a regional breakdown of the total diesel and fuel consumption from 2005 to 2011. www.gov.uk/government/statistical-data-sets/road-transport-energy-consumption-at-regional-and-local-authority-level , and was accessed on 30/04/2014.[178]

similar, but currently un-recognized, policy challenge to control reactive carbon emissions and their contributions to secondary pollutants.

Chapter 3

Trends in volatile organic compounds and their reactivity in London during ClearfLo

This chapter details further analysis of the large suite of VOC measurements conducted during the ClearfLo campaign. The OVOC species will be discussed in further detail in Chapter 4 and so will only be briefly mentioned throughout this chapter.

Part 1: Trends in volatile organic compounds

In the majority of studies conducted on VOC species (such as those discussed previously in Chapter 2), the focus tends to be on a small subset of species with either a small carbon number range or those species which are easy to measure. A selection of studies, however, have shown that the species which are usually not measured can actually have large impacts. Of particular interest, is the measurement of different functional group species with the same carbon number which may co-elute using a conventional GC instrument but can be separated using the GC×GC instrument. This has been shown by Lewis *et. al.,* (2000) and Hamilton *et. al.,* (2003). The former showed that a GC×GC instrument was able to speciate over 500 different VOC species, compared to a conventional GC instrument that was limited to approximately 30 compounds.[84] Hamilton *et. al.,* (2003) also showed that GC×GC instruments could separate many more individual VOC species than a conventional GC, with particular focus on monoaromatic compounds.[105]

3.1 Seasonal comparison of observed mixing ratio, primary hydrocarbon OH radical reactivity and potential ozone formation

Using the GC×GC instrument described in Chapter 2, in combination with a conventional GC instrument for those species outside the range of the GC×GC, a total of 78 individual and 10 grouped VOC species were quantified. The individual compounds measured during the ClearfLo campaigns have been grouped according to basic functionality as seen in Table 2.2; saturated aliphatics, unsaturated aliphatics and aromatics with the additional grouped UCM species from Table 2.3 as a separate group. The majority of discussion throughout this chapter will reference the group, unless discussion is about an individual compound or grouped UCM species. Figures 3.1 to 3.4 show the average median winter and summer observed mixing ratios (upper panel), calculated primary hydrocarbon OH radical reactivity (middle panel) and potential ozone formation (lower panel) for each individual and grouped UCM species within the four group of VOCs.

The primary hydrocarbon OH radical reactivity has been calculated for each individual and grouped UCM species measured during the ClearfLo campaign. The calculation and comparison based on emission sources was discussed previously in Chapter 2, Section 2.5.5 so only the results, specific to individual compounds, will be discussed in this section. The rate constants used for the reaction of the grouped UCM species with the OH radical

were also discussed in detail. Briefly, the *n*-alkane, α-pinene and 1,3-diethyl benzene rate constants were used for the aliphatic, C_{10} monoterpene and C_4 substituted monoraromatic groups respectively.

OFP can be used to assess the effects of VOC emissions on local ozone production. For the aliphatic grouped UCM species, a weighted MIR value was calculated to represent a composition of the group based on 95% branched alkane and 5% alkene. The OFP from the C_4 substituted monoraromatic and C_{10} monoterpene groups was calculated using the MIR values associated with 1,3-diethyl benzene and α-pinene respectively.

3.1.1 Saturated aliphatic compounds

Figure 3.1 shows the campaign average median winter (black) and summer (red columns) observed mixing ratios (upper), primary hydrocarbon OH reactivity (middle) and potential ozone formation (lower) for the saturated aliphatic compounds. All of these compounds, except for cyclopentane, show a higher winter mixing ratio, OH reactivity and OFP. Cyclopentane has a similar average value in both seasons. This group is dominated by the contribution from the smaller carbon number species; in particular methane, followed by ethane. Both of these compounds have a large emission source from the production, use and storage of natural gas. In general, as the carbon number increases, the mixing ratio decreases. At C_9, this pattern reverses where as the carbon number increases so does the mixing ratio. This is likely due to the emission of *n*-alkanes from diesel fuelled vehicles, as discussed in detail in Chapter 2.

The contribution to primary hydrocarbon OH reactivity (middle panel) shows a similar profile to that observed for the measured mixing ratios. In contrast to the mixing ratios, the increase after C_9 is quite dramatic especially in the winter. This is from the increase in rate constants for the reaction of the specific VOC with the OH radical, for example the rate constant for *n*-decane (1.10×10^{-11} cm^3 molecule^{-1} s^{-1}) is 2 times higher than that of *n*-hexane (5.20×10^{-12} cm^3 molecule^{-1} s^{-1}).[82] Even with this increase in the contribution of the higher carbon number species, the calculated reactivity for each individual species is still approximately a factor of four smaller than that for methane. However, by taking a sum of the C_9-C_{12} saturated aliphatic species, they provide the same amount of reactivity as methane. This is important as these species are not routinely measured but they can contribute a significant portion of the OH reactivity in an urban environment that is influenced by a large diesel vehicle fleet.

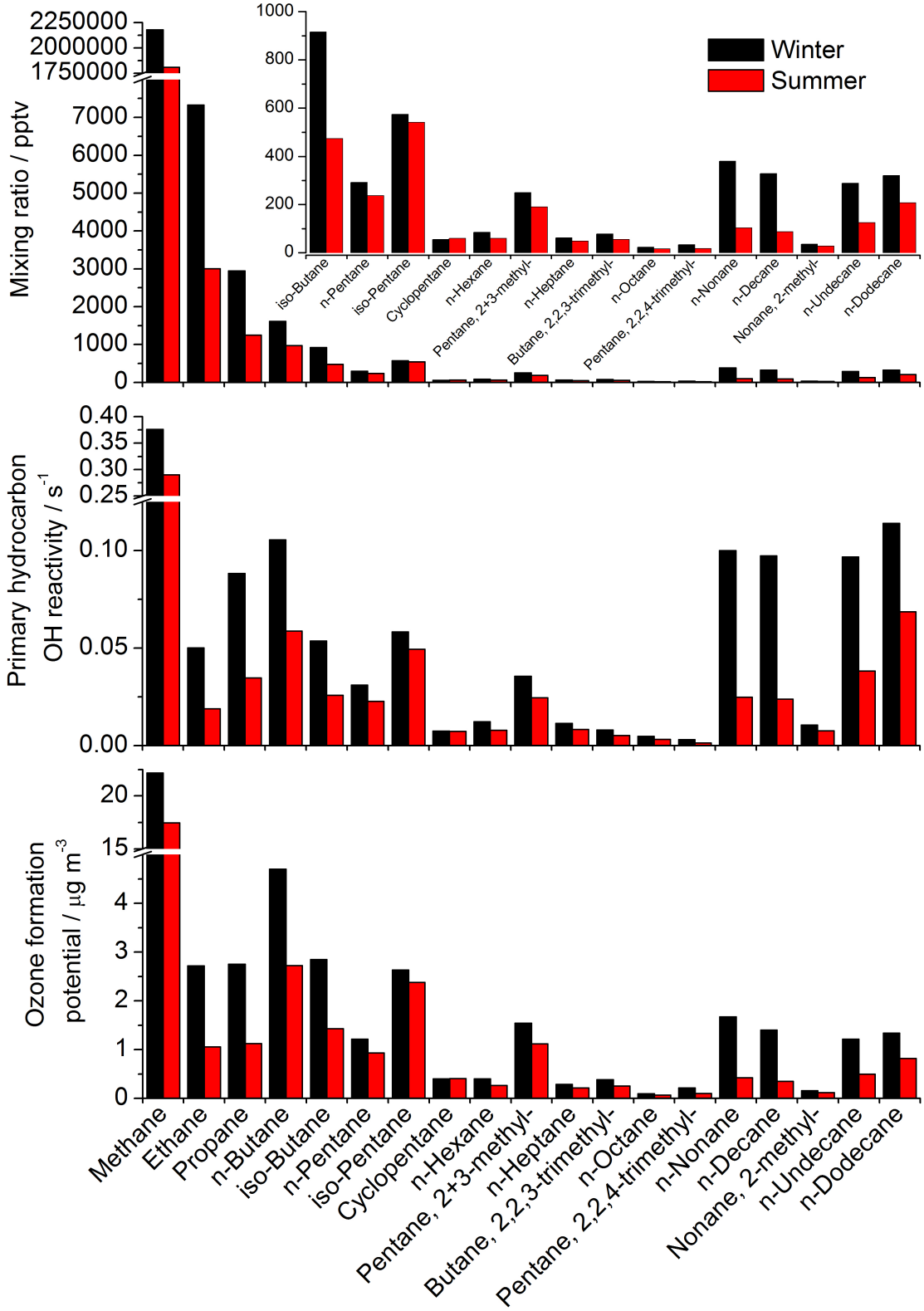

Figure 3.1: Comparison of the contributions of the saturated aliphatic compounds to observed mixing ratio (upper), calculated primary hydrocarbon OH reactivity (middle) and potential ozone formation (lower) in winter (black) and summer (red). The inset graph shows a subset of the contributions of the saturated aliphatics, from *iso*-butane to *n*-dodecane inclusive, to observed mixing ratio

The contribution of the saturated aliphatics to OFP, again shows a similar profile to that seen in the observed mixing ratio and OH reactivity. Methane still dominates, although to a lesser degree. There are a few species which show an increased contribution to OFP than was observed previously, *n*-butane, *iso*-butane and *iso*-pentane. The higher carbon number species, which contributed a large amount of OH reactivity, do not appear to show as large of an importance for OFP.

3.1.2 Unsaturated aliphatic compounds

The winter and summer campaign average median mixing ratios (upper), primary hydrocarbon OH reactivity (middle) and OFP (lower) for the individually quantified unsaturated aliphatic species are shown in Figure 3.2. Two of these compounds were not measured during the winter campaign, propyne and 1,2-butadiene, so they do not have a winter column. The majority of the unsaturated aliphatic species also show a higher winter mixing ratio, OH reactivity and OFP. However, four species have higher summer values; isoprene, styrene, α-pinene and limonene. For styrene, however, there is only a 2 pptv difference between the winter and summer mixing ratios which is not very significant. Isoprene, α-pinene and limonene have a biogenic source that dominates during the summer campaign. Although they have higher summer mixing ratios, there is clearly still a source of these species during the winter. For two of the species, (isoprene and limonene), this is likely to be anthropogenic emission from the use and storage of gasoline (given the traffic related diurnal profiles seen in Figure 2.14).[201] The source of α-pinene, however is less defined, but possibly due to the use of cleaning products as there was no apparent winter traffic related diurnal profile.[202]

The contributions of the unsaturated aliphatics species to OH reactivity (middle panel) show a similar profile to that of the observed mixing ratios. However, some compounds increase (propene) and decrease in importance (acetylene and 1,2-butadiene), due to their rate constants for reaction with the OH radical. The overall range of the group has decreased, with less difference between ethene and the other compounds. The biogenic source compounds show a similar increase in summer, from their increased mixing ratios, but they also dominate over the contributions of the other compounds for OH reactivity. In winter, the contribution of the typically anthropogenic species to the total OH reactivity from this group is 90%, however in summer this falls to 52% as the contribution from the biogenic species increases from 10% to 48% in winter and summer respectively.

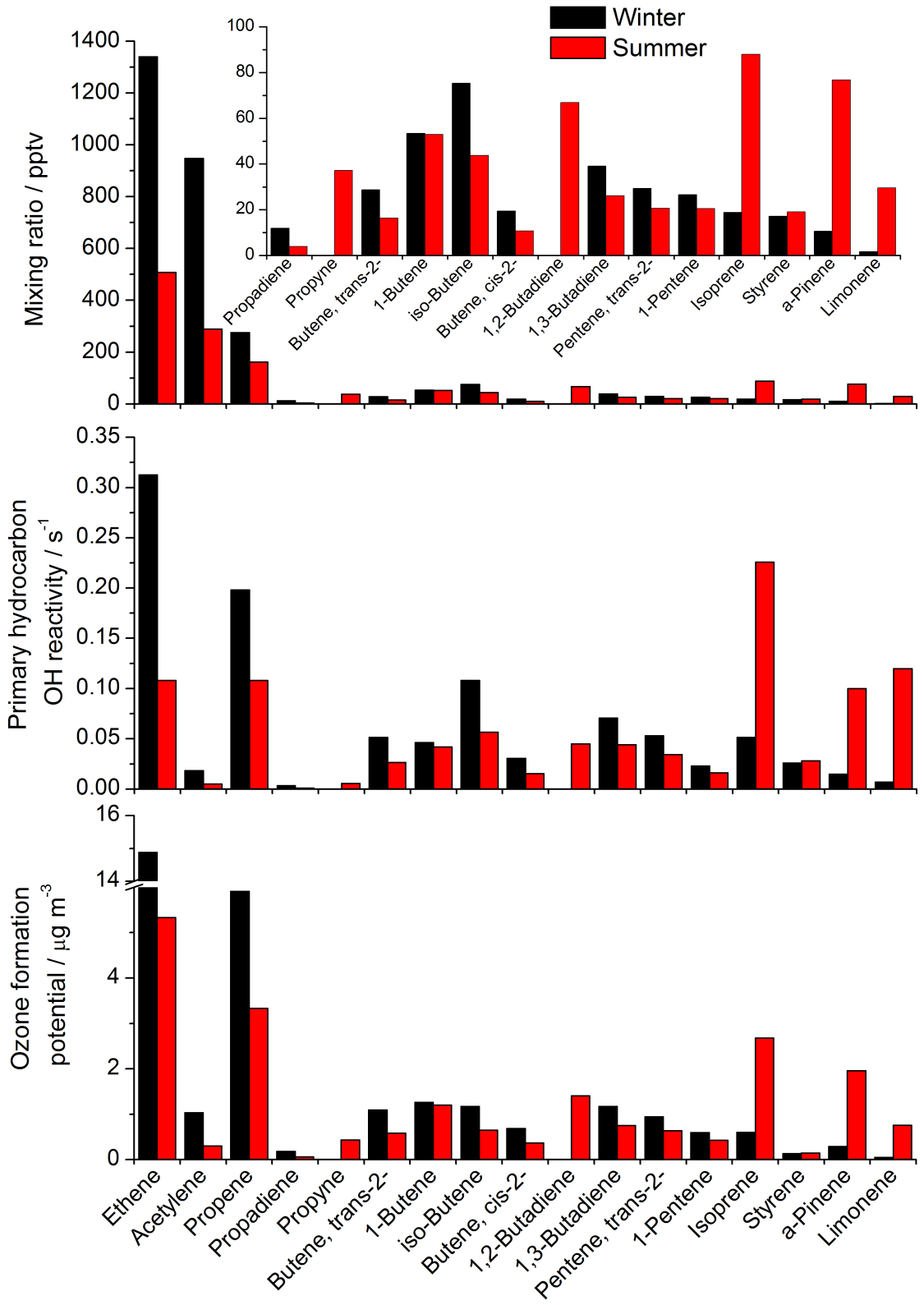

Figure 3.2: Comparison of the contributions of the unsaturated aliphatic compounds to observed mixing ratio (upper), calculated primary hydrocarbon OH reactivity (middle) and potential ozone formation (lower) in winter (black) and summer (red). The inset graph shows a subset of the contributions of the unsaturated aliphatics, from propadiene to limonene inclusive, to observed mixing ratio

The seasonal contributions of the unsaturated aliphatic compounds to OFP (lower) show a similar profile to that for the calculated OH reactivity. Ethene dominates, with a marked increase seen for propene and decrease for acetylene. The compounds in the middle of the figure (propadiene to 1-pentene, inclusive) show a small contribution in both campaigns. The importance of the typically biogenic source compounds (isoprene, α-pinene and limonene) is shown by a large increase in OFP during the summer campaign. In fact, the OFP from isoprene, α-pinene and limonene in summer are factors of 4, 7 and 16 higher than the winter values respectively.

3.1.3 Aromatic compounds

Figure 3.3 shows the average median winter and summer campaign mixing ratios (upper), OH reactivity (middle) and OFP (lower) for the individual aromatic species. Two of these species (*iso*-propyl-benzene and indan) were below the detection limit of the GC×GC during the summer campaign. All bar two of these compounds have a higher winter mixing ratio. One of the compounds, 4-iso-propyl-toluene (also known as *p*-cymene) has a higher summer mixing ratio, likely due to its dominant biogenic source,[203] whereas naphthalene has a similar median mixing ratio in both campaigns. The higher carbon number aromatic species (*i.e.* the C_3 substituted monoaromatics) show higher enhancement in their winter median mixing ratio in comparison to the smaller carbon number species (*i.e.* benzene, toluene and the C_2 substituted monoaromatics). In fact, the C_3 substituted monoaromatics are a factor of 7-15 higher in winter than summer. For the smaller carbon number species, the higher winter median mixing ratio is likely due to their inclusion in gasoline. It is possible that although the higher carbon number species are also included in gasoline, seasonal fuel compositions may limit the amount released during the summer months. These compounds are more likely to evaporate during periods of high temperatures, so fuel compositions are usually changed depending on the season to limit evaporation from storage.[204] For example, during the summer months, compounds that evaporate easily are usually in a smaller quantity in the liquid fuel than would be included in winter resulting in a decrease in the summer observed mixing ratios.[204]

The seasonal contributions of the aromatic species to OH reactivity (middle) shows a similar, but smaller range, trend as seen for the observed aromatic compounds mixing ratio. The major difference between the mixing ratio and OH reactivity is seen in the higher carbon number aromatics (*i.e.* the C_3 substituted monoaromatics), where their

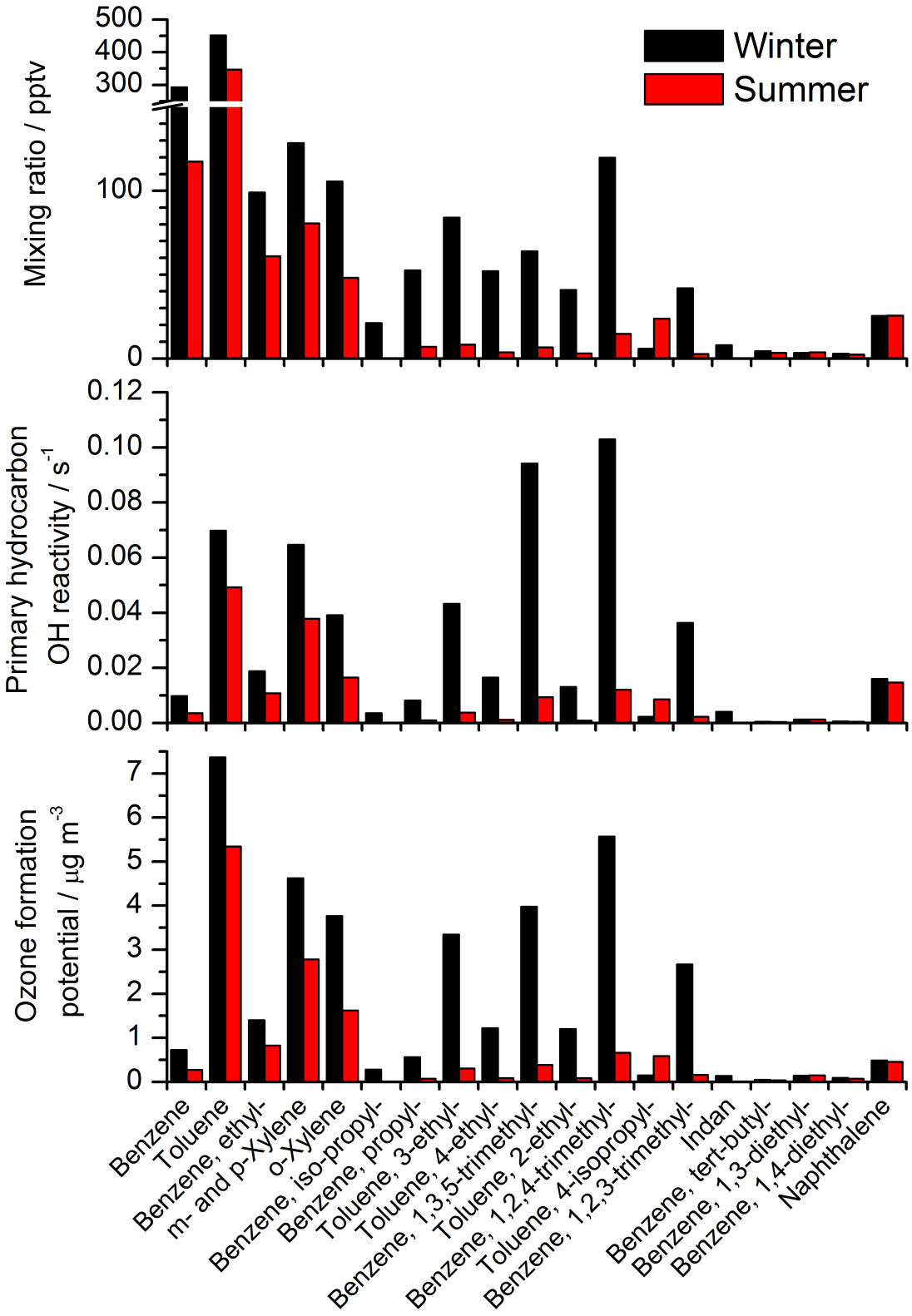

Figure 3.3: Comparison of the contributions of the aromatic compounds to observed mixing ratio (upper), calculated primary hydrocarbon OH reactivity (middle) and potential ozone formation (lower) in winter (black) and summer (red)

winter contributions are higher than those of benzene, toluene, ethyl-benzene and the xylenes. This is due to the faster reaction of these species with the OH radical. For example, the reaction of benzene with the OH radical is much slower than that of 1,3,5-trimethyl-benzene, (1.22×10^{-12} cm^3 molecule^{-1} s^{-1} and 5.67×10^{-11} cm^3 molecule^{-1} s^{-1} respectively).[82] Again, this is important as some of these higher carbon number aromatic compounds are not routinely measured or adequately included in models leading to an underestimation of their importance.

The contributions of the aromatic compounds to OFP (lower) shows a similar profile to that of the calculated OH reactivity. The exception to this is from the smaller carbon number aromatics (*i.e.* benzene, toluene, ethyl-benzene and the xylenes), which increase in importance in comparison to the OH reactivity (where they decrease). The contribution of the C_3 substituted monoaromatics is still important but to a lesser extent that seen for the OH reactivity. The winter still shows higher calculated OFP, from the increased mixing ratios observed during that season.

3.1.4 Grouped unresolved complex mixture species

Figure 3.4 shows the campaign average median winter and summer mixing ratios (upper), OH reactivity (middle) and OFP (lower) for the grouped UCM species. All of these groups bar one, the C_{10} monoterpenes, show higher winter average values. The C_{10} monoterpenes have a higher summer median mixing ratio due to their dominant biogenic source.[19,56,57,70] The aliphatic grouped species show a similar profile as that observed in Figure 3.1 (upper panel) for the individual saturated aliphatic species. In fact, the mixing ratio increases dramatically in the winter campaign from the C_9 to the C_{13} aliphatic species. A similar, but smaller scale, profile is also seen in the summer campaign, pointing to the presence of an anthropogenic source in both campaigns. From Chapter 2, this was determined to be from the combustion and/or evaporation of diesel in vehicles.

The contributions of the grouped species to OH reactivity in the two seasonal campaigns of the ClearfLo project is shown in the middle panel of Figure 3.4. The trend is similar to that seen for the observed mixing ratios. The contributions from the groups increase to C_9, drop then increase dramatically to C_{13}. This is seen in both winter and summer, although the latter has a smaller reactivity due to lower observed mixing ratios for the grouped UCM species in that season. Again, the C_{10} monoterpenes are more important in the summer from an increased emission from biogenic sources.

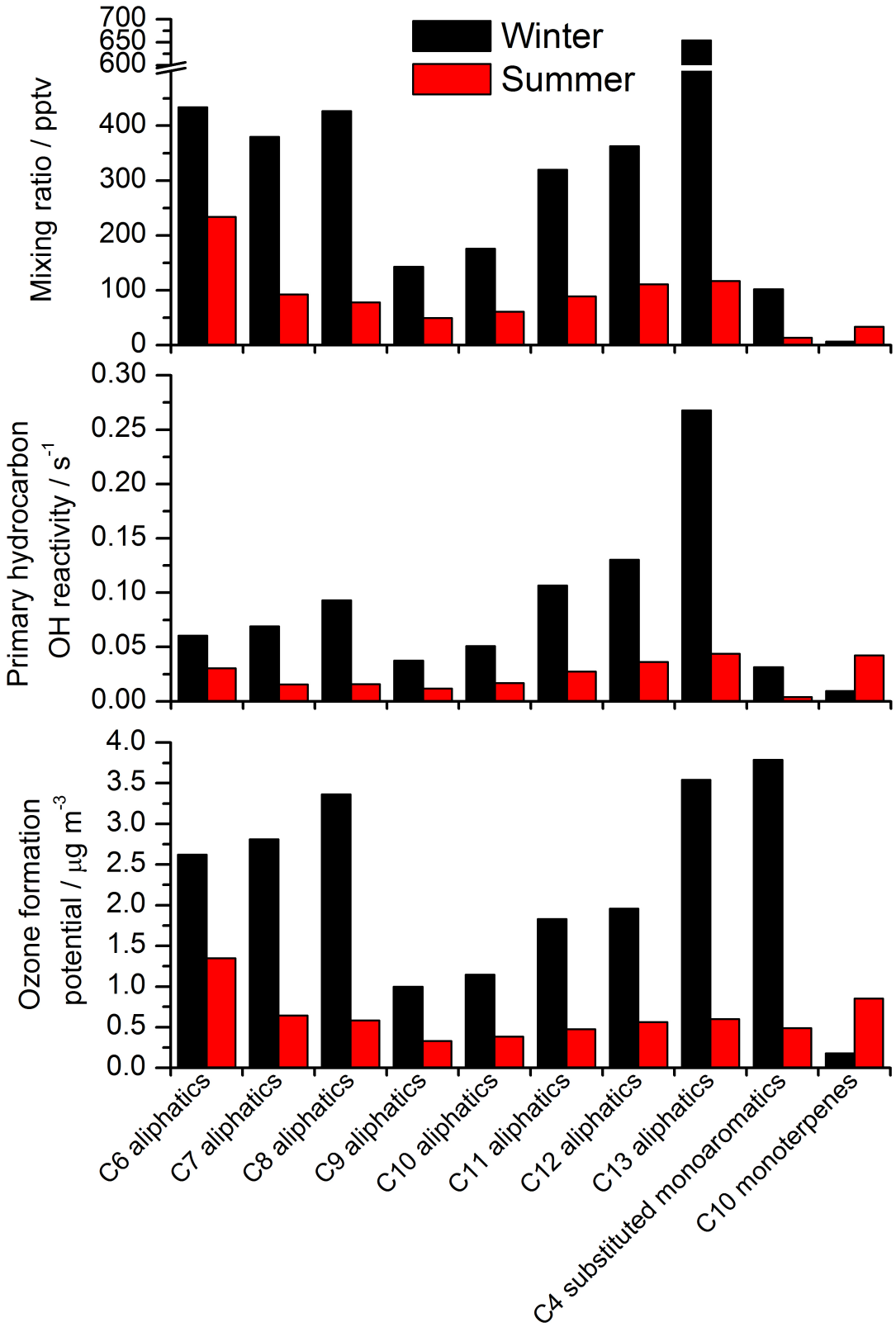

Figure 3.4: Comparison of the contributions of the grouped species to observed mixing ratio (upper), calculated primary hydrocarbon OH reactivity (middle) and potential ozone formation (lower) in winter (black) and summer (red)

The OFP contributions (lower) of the grouped species during the winter and summer campaigns, show a similar trend to the calculated OH reactivity. However, as seen with the aromatic compounds, the contributions from the smaller carbon number groups increase for the OFP when compared to the OH reactivity. At C_9, the contribution decreases then rises dramatically to C_{13}. Dissimilar to that of the OH reactivity, the contribution from the C_4 substituted monoaromatic group shows a large increase during the winter campaign, that is not seen in summer likely due to the smaller mixing ratios observed.

3.2 Air mass analysis

3.2.1 Air mass history

As part of the ClearfLo campaign, air mass history was modelled using the UK Met office's NAME (Numerical Atmospheric dispersion Modelling Environment) dispersion model. The model was originally developed in response to the Chernobyl accident in the late 1980s to provide emergency dispersion predictions for nuclear incidents.[205] This can also be used to give a historical footprint of a site on time scales of hours through to years. The map in Figure 3.5 shows the different gridded sections that air masses were from during the winter and summer campaigns. The NAME model output can be shown as a percentage of the total number of particles that pass over each sector.[205]

The results of the 1 day NAME modelling are shown in Figure 3.6. This was conducted by Dr Zoë Fleming, University of Leicester. The 1 day NAME modelling is shown as the majority of the VOC species of interest (particularly the very reactive and the higher carbon number species) are quite short lived, in the range of hours. For example, isoprene and 1,3,5-trimethyl benzene have lifetimes of $\approx$ 3 and 5 hours, respectively, with the OH radical (at a concentration of 1×10^6 molecule cm^{-3}). Both campaigns are largely dominated by air masses from over London, with a range of other downwind regions influencing the site. This can lead to quite complex air mixtures being observed as they can be comprised of pollutants from a variety of different emission sources, at different levels of chemical processing. The situation is further complicated by the mixing of fresh emissions into plumes of well aged air masses from the regional background.

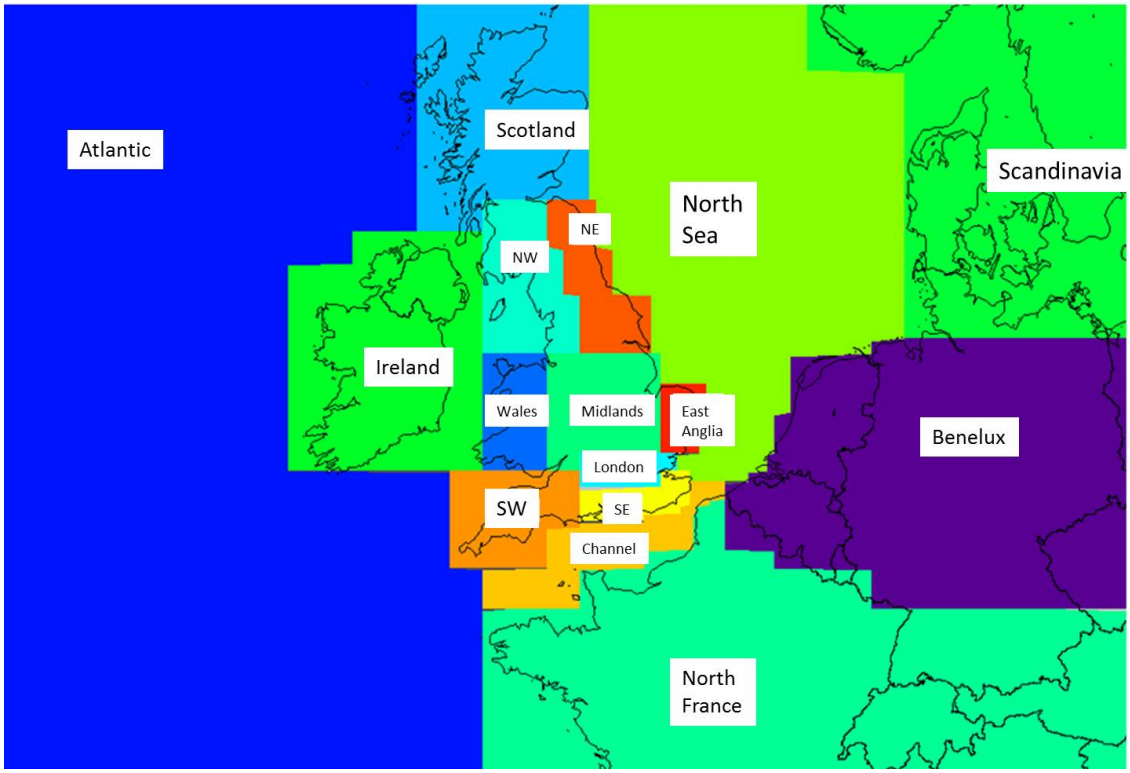

Figure 3.5: Regional grid divisions for the 1 day domain NAME modelling of the North Kensington site; NW is the north west of Britain, NE is the north east, SW is the south west and SE is the south east

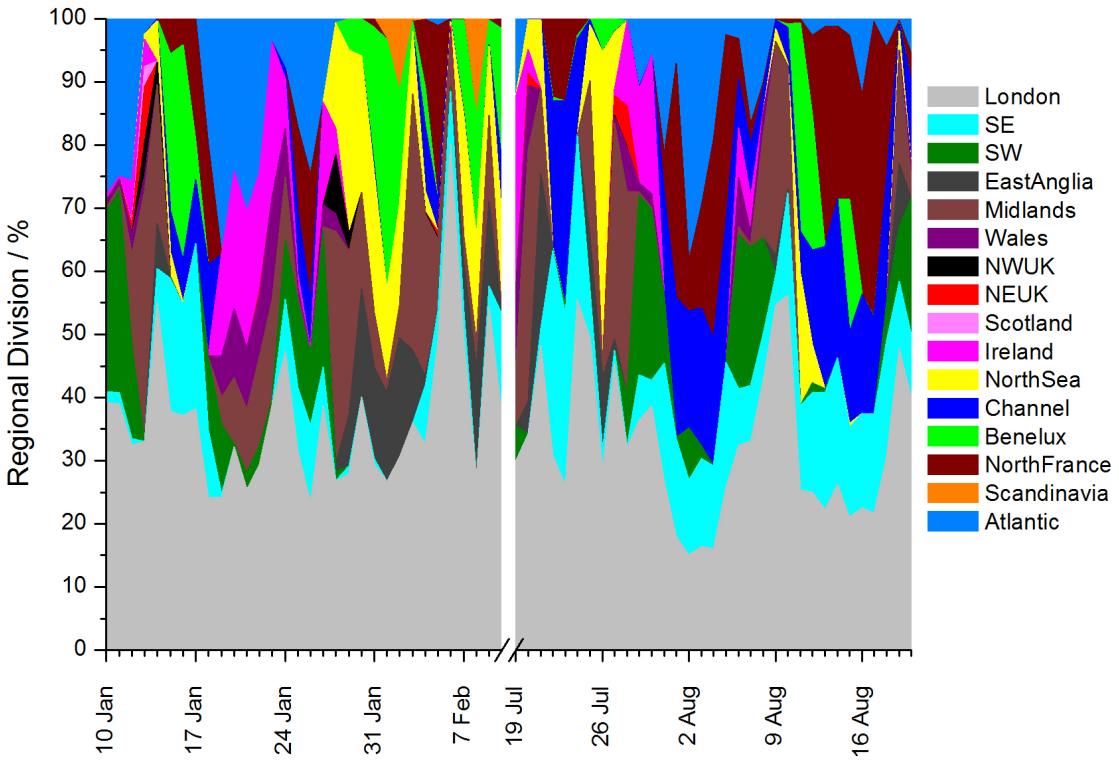

Figure 3.6: Regional division percent contributions for the NK site from the 1 day NAME modelling

3.2.2 Air mass processing ratios

Benzene to toluene ratios (b:t) have been used to indicate the degree of processing that an emission/plume has undergone. Benzene and toluene have a common petrochemical source from gasoline and are now emitted at a ratio of approximately 1:3 (calculated from the 2012 Passant (2002) NAEI emission factors).[144] Toluene is removed from the atmosphere faster due to a quicker reaction rate with the OH radical than benzene (1.22×10^{-12} cm^3 molecule^{-1} s^{-1} compared to 5.63×10^{-12} cm^3 molecule^{-1} s^{-1}).[82] This means that a b:t ratio of 0.33 is indicative of fresh emission while a ratio of 2 indicates highly processed, well aged air masses. This ratio can also be compared to a benzene to 1,3,5-trimethyl-benzene (b:135tmb) ratio. The b:135tmb ratio is usually larger given the even faster reaction rate of 1,3,5-trimethyl-benzene with the OH radical (5.67×10^{-11} cm^3 molecule^{-1} s^{-1}).[82] Benzene and 1,3,5-trimethyl benzene are also emitted from gasoline, at an approximate ratio of 3:1.[144] This means that a b:135tmb of 3 indicates fresh emissions, while ratios of 30 or higher are likely highly processed air masses.

Figure 3.7 shows the b:t (lower panel) and b:135tmb (upper panel) ratios for the winter and summer ClearfLo campaigns. As expected, the b:135tmb ratio is much larger than that of b:t with increased variability observed in both campaigns; however the largest difference is seen in the summer likely due to an increased removal of the higher aromatic species. The b:t ratio calculated during the ClearfLo campaign varied between 0.06 - 2.07 (winter) and 0.15 - 1.18 (summer), with seasonal averages of 0.72 and 0.34 in winter and summer respectively, shown in Table 3.1. The winter b:t ratio is likely higher due to an enhanced background source of benzene from biomass burning (*i.e.* solid fuel combustion in stoves and domestic fires). As seen in Figure 3.7, the b:135tmb ratio shows more variation with a winter ratio of between 0.82 and 50.54 and an average ratio of 7.17. In summer, the range in the ratio is 1.51 to 193.74, with an average of 22.83 (Table 3.1).

Table 3.1: Max, mean and minimum observed ratios during the winter and summer campaign for b:t and b:135tmb.

	Winter			**Summer**		
	Max	**Mean**	**Min**	**Max**	**Mean**	**Min**
b:t	2.066	0.715	0.060	1.181	0.340	0.154
b:135tmb	50.539	7.169	0.823	193.736	22.827	1.513

During the winter campaign the b:t ratio shows a maximum during the early hours of the morning, that rapidly falls after 6 am to a minimum at 9 am. This is likely from the

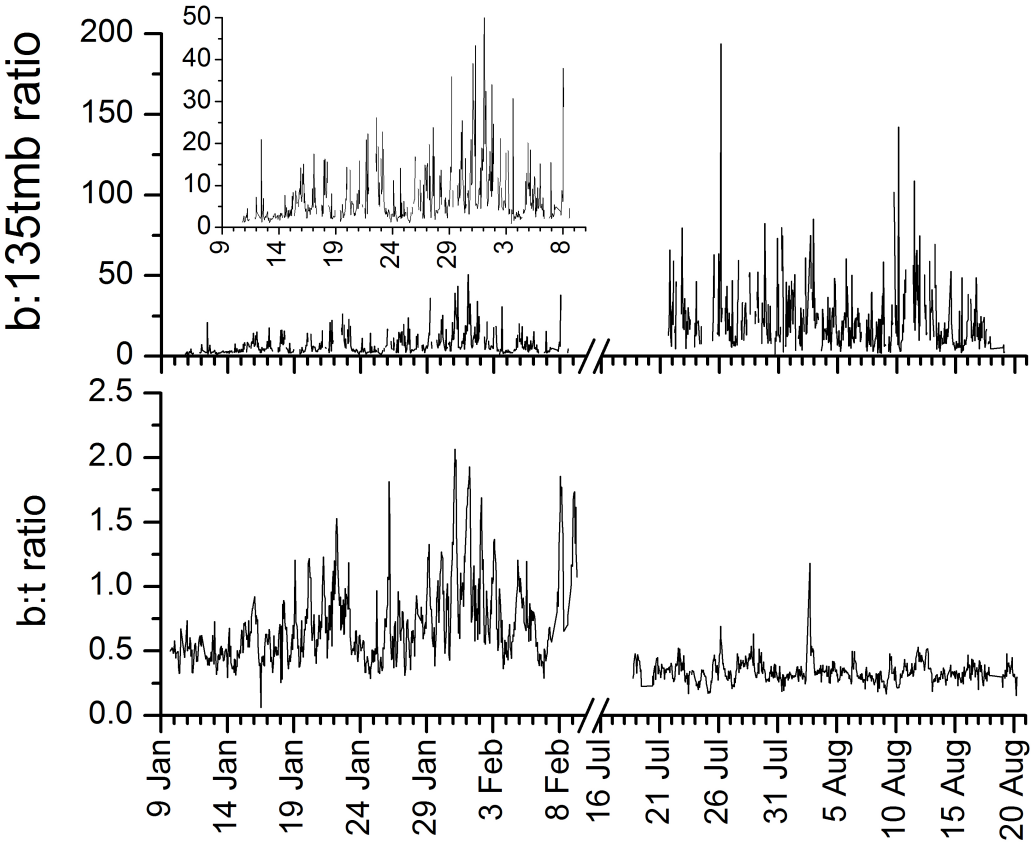

Figure 3.7: Ratios of benzene:toluene (b:t, lower panel) and benzene:1,3,5-trimethyl benzene (b:135tmb, upper panel) from the winter and summer ClearfLo campaigns

increase in fresh emissions from traffic sources during rush hour. In contrast, the summer campaign ratio has a midday maximum. This is likely due to an increase in removal by the OH radical in the summer campaign during periods of increased photochemistry and mixing down of processed air masses from aloft as the boundary layer changes. The b:135tmb ratio shows a similar profile during the winter campaign, with a maximum during the early hours of the day prior to 6 am, which again rapidly falls to a minimum at 9 am when there is an increase in fresh emissions. Smaller b:t ratios indicate an air mass influenced by fresh emissions. However, a large b:135tmb ratio possibly indicates a highly processed air mass, due to the preferential removal of the fast reacting 1,3,5-trimethyl-benzene. This gives further weight to the North Kensington site experiencing a combination of local, highly polluted, and regional, more processed air masses.

The correlations of benzene, toluene, 1,3,5-trimethyl benzene and the two ratios, b:t and b:135tmb are shown in Figure 3.8, along with the linear regression equations and R^2 values. This can provide information about the average air mass processing and age for each campaign. The correlation of benzene and toluene (upper panel) shows that

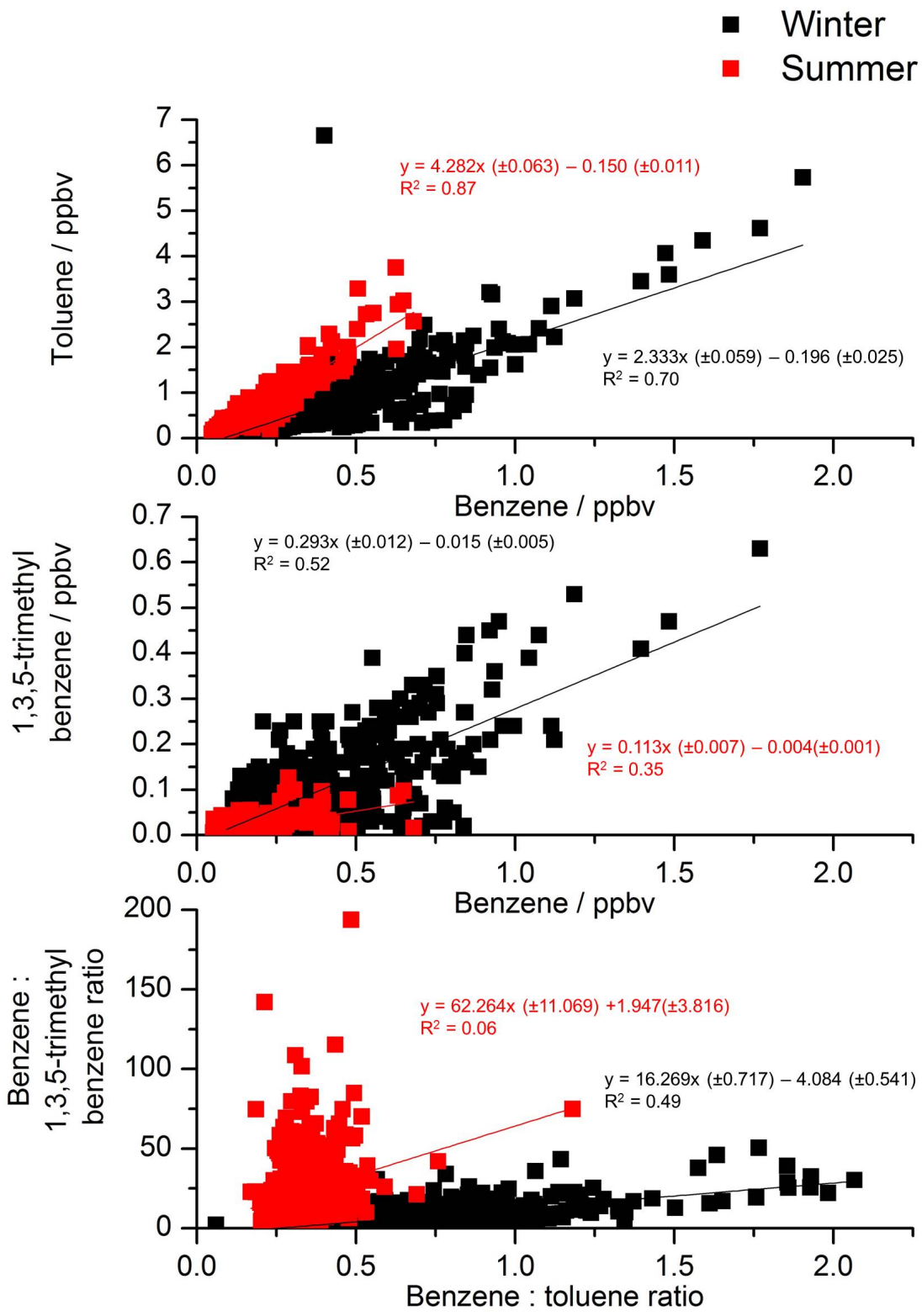

Figure 3.8: Correlations of benzene and toluene (upper panel), benzene and 1,3,5-trimethyl-benzene (middle panel) and the b:t and b:135tmb ratios (lower panel) for the winter (black) and summer (red) campaigns. The equations of R^2 of the lines of best fit are also shown

the summer gradient is almost a factor of two higher than that of winter. This suggests that during the summer campaign, either less toluene was being emitted or that the combustion of solid fuel is enhancing the background concentrations of benzene. This is possibly also seen in the correlation between benzene and 1,3,5-trimethyl benzene (middle panel of Figure 3.8), where the summer gradient is almost a factor of three smaller thus less 1,3,5-trimethyl benzene is observed. This is possibly due to fuel composition changes to limit the evaporative emissions given the higher temperatures experienced in summer, discussed previously.[204] However, the R^2 of the linear regression of benzene to 1,3,5-trimethyl benzene in summer is quite low.

Lee *et al.* (2006) reported b:t and b:135tmb ratios calculated during the Tropospheric ORganic CHemistry (TORCH) campaign in Chelmsford, Essex during August 2003.[206] Both ratios showed a similar variation as that observed during the summer ClearfLo campaign, with a higher b:135tmb than b:t ratio. The authors reported a b:t ratio of between 0.3 and 1.8, which compares quite well to that seen in the summer campaign, see Table 3.1 for campaign mean values. The average b:135tmb during TORCH was 44.6, which is substantially higher than the average from the ClearfLo summer campaign, but is within the range of values. However, this study was conducted in a rural location, downwind of London which would be expected to have experienced more oxidation during transport.

In urban areas, b:t ratios of between 0.23-0.66 are considered to be a good indicator of traffic related emissions of both species.[207,208] Many studies have reported b:t values of below 0.33 and this is considered to be a ratio value that is characteristic of traffic emissions around the world.[207–215] The ClearfLo average b:t ratios in winter and summer are well within the range. The mean ratios from ClearfLo are also similar to those found around the world such as: Bari 0.5,[210] Rome 0.36,[216] Izmir 0.5-0.53,[208] Santiago 0.50,[217] Sydney 0.25,[218] Ankara 0.23,[219] China 0.26,[220] Windsor 0.23[221], within Belgium 0.26-0.23,[222] and Osaka 0.14.[223] The b:t ratios are very varied between different cities and this can reflect changes in vehicle types and fuel composition.[215]

3.3 Anthropogenic volatile organic compounds

Figure 3.9 shows the winter and summer observed mixing ratios for a selection of species that show the range of species measured (*i.e.* large and small carbon number species, aliphatic and aromatic), these have been plotted on the same y-axis scale for each com-

pound in both seasons to allow for a direct comparison. These four species show similar profiles, with higher winter concentrations that are typical of anthropogenic source species. The majority of species measured during the ClearfLo campaign show a similar profile in winter that is largely influenced by the stagnant and high pressure periods (highlighted in Figure 3.9) at the start and end of the measurement period. This was due to low wind speeds, with an average of 1.76 ms^{-1}, resulting in little transport of species which were emitted into a shallow boundary layer. The exception, are those species dominated by a biogenic source during summer; isoprene, α-pinene, limonene, 4-*iso*-propyl-toluene, the majority of the OVOC species, dichloromethane, trichloroethylene and the grouped C_{10} monoterpenes. The biogenic species will be discussed in more detail in Section 3.4.

3.3.1 Correlations between anthropogenic volatile organic compounds

Correlations between all of the individual and grouped VOC species measured during the ClearfLo campaigns were calculated and can be seen in Appendix A, Tables A.1 to A.21. These correlations are linear fits of the data, where the R^2 values are a statistical measure of how well the linear line fits the real data. The following will be a discussion of what specific correlations show during the winter and summer campaigns. The correlations of compounds previously suggested to have a biogenic source in the summer campaign (isoprene, α-pinene, limonene, 4-*iso*-propyl-toluene and the C_{10} monoterpene group) will be discussed in Section 3.4.1.

During the winter campaign, the majority of species measured correlate well with each other (R^2 of 0.50-0.99). Of the 2016 correlations calculated, 88% (1765) have an R^2 value of greater than 0.50. This suggests either a common emission source or different emission sources which have similar temporal fluctuations. Given the diurnal profiles of some of these species (shown in Chapter 2, Figure 2.14), the sources are likely related to the combustion of fuels (gasoline and diesel). As the vehicle fleet is not limited to only one fuel, *i.e.* is it a combination of both gasoline and diesel, is it possible that the increased R^2 correlations are from common emission times when both types of vehicles are on the road at the same time.

During the summer campaign, half of the correlations calculated show R^2 values between 0.50-0.99. The majority of these correlations are similar to those seen in the winter campaign, although the values are typically smaller. This suggests that these species are still emitted from the same source but that, in summer, there is an increased removal

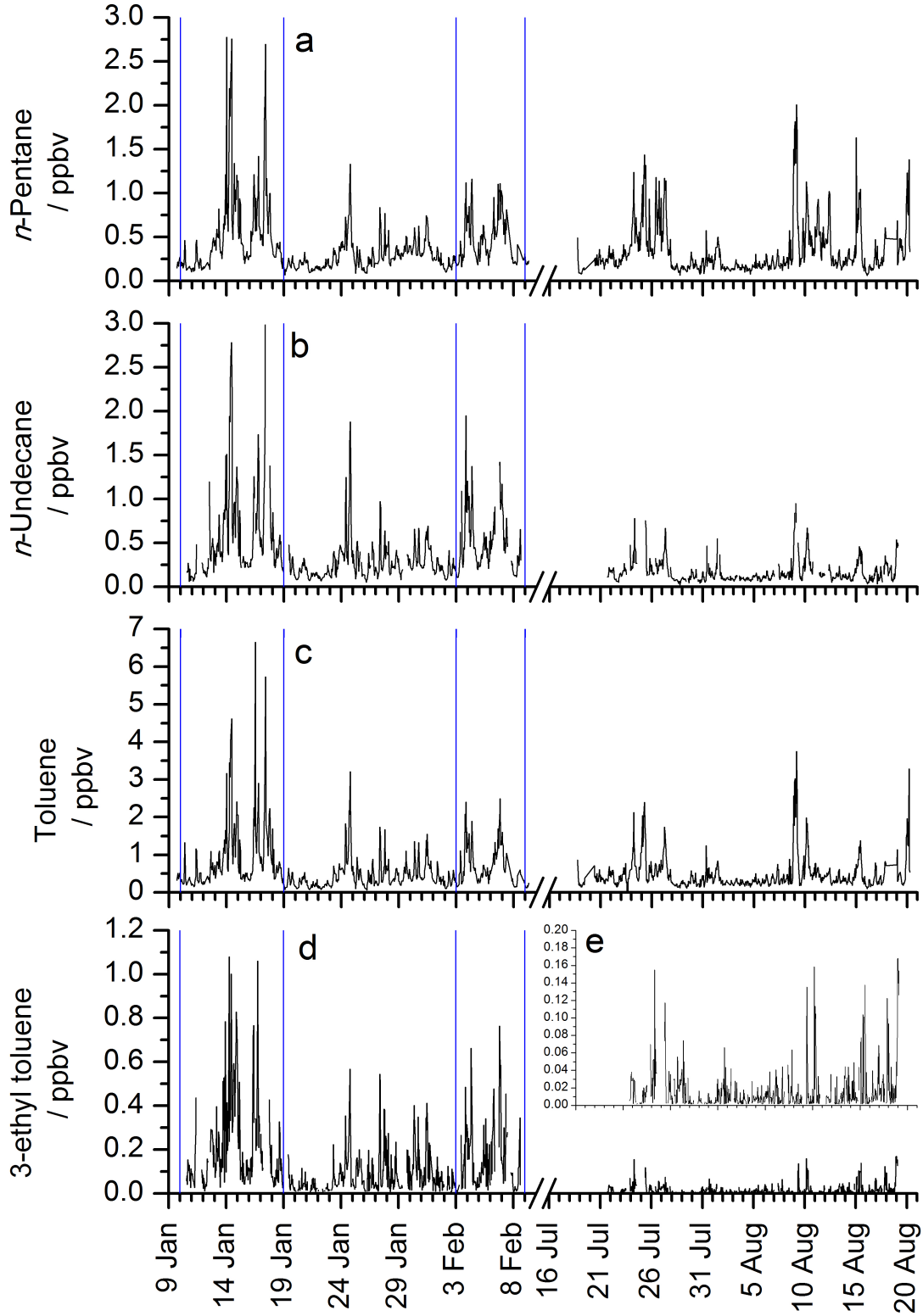

Figure 3.9: Time series of selected anthropogenic source compounds: (a) *n*-pentane, (b) *n*-undecane, (c) toluene and (d) 3-ethyl-toluene ((e) is a zoomed in graph of the summer 3-ethyl-toluene observed mixing ratio)

resulting in lower observed mixing ratios.

Of the aromatic species, one compound *tert*-butyl-benzene, does not show correlations of any significance with any of the other individual and grouped species measured during the winter and summer campaigns. The winter and summer correlations of all other measured species with this compound are below an R^2 of 0.14 and 0.32 respectively. The only exception to this is the correlation of *tert*-butyl-benzene with propyne, R^2 of 0.67. The NAEI suggests that the emission sources for *tert*-butyl-benzene are coating manufacture, industrial adhesives and coatings, landfill and printing. However, these are all shared with other measured compounds, while the correlations suggest that *tert*-butyl-benzene may have a unique emission source. It is worth noting that although the observed mixing ratios of *tert*-butyl-benzene do show profiles consistent with an anthropogenic source, the median values in both campaigns are quite small (winter 4 pptv and summer 3 pptv) and this may be distorting the correlation plot.

All of the grouped species, except the C_{10} aliphatics, show strong winter correlations with the majority of other species. This suggests that the monoterpene compounds included in the grouped analysis have an anthropogenic source, likely from their inclusion in gasoline given the traffic related diurnal profiles observed during the winter campaign (see Chapter 2, Figure 2.14 o). The correlations of the C_{10} aliphatic group are very varied and typically below R^2 values of 0.50. During the summer, the majority of correlations between the grouped species and the other VOCs are similar but the R^2 values are smaller. The correlations of the grouped species with the higher carbon number aliphatic and aromatic compounds are much smaller, a factor of 2 in some cases. This may be from seasonal differences in fuel composition, discussed previously.

3.4 Biogenic volatile organic compounds

Compounds that have a dominant biogenic source have higher observed mixing ratios during the summer campaign, a selection are shown in Figure 3.10. These have also been plotted on the same y-axis scale for each individual species and group in both seasons. All these species show an anthropogenic source during the winter campaign. For isoprene, limonene and the C_{10} monoterpenes this appears to be traffic related, likely from the combustion and evaporation of gasoline as the temporal profile match that seen with the anthropogenic species. The winter source of α-pinene however, is less apparent but was suggested to be from use as a fragrance in cleaning products.[202] These winter profiles

are also influenced by the meteorological conditions mentioned previously, with higher mixing ratios observed during those periods at the start and end of the winter campaign, highlighted in Figure 3.10. The summer profiles of these species and group show much higher observed mixing ratios. For all, but particularly evident in the profile of isoprene, there is an diurnal oscillation present that corresponds with emission due to higher levels of photosynthetic active radiation during the middle of the day when maximum levels of sunlight and temperature are recorded. This was seen in the diurnal profiles of these species shown in Chapter 2, Figure 2.14.

3.4.1 Correlations of biogenic volatile organic compounds

The winter correlations of the typically biogenic source compounds, isoprene, limonene, 4-*iso*-propyl-toluene and the C_{10} monoterpene group, with the other largely anthropogenic species indicate the contribution of an anthropogenic source. The correlations of the three species except 4-*iso*-propyl-toluene, show strong correlations with the majority of species. The average R^2 values were 0.76 for isoprene from the 63 correlations with all other VOC species (except the OVOCs), 0.68 for limonene and 0.80 for the C_{10} monoterpenes. 4-*iso*-propyl-toluene has an average R^2 value of 0.37, indicating that although it may share a common anthropogenic source with the other species, it may also have other sources.

During the winter campaign, α-pinene does not correlate with any of the individual or grouped set of species measured. All of the correlations of α-pinene have R^2 values below -0.04. It is possible that α-pinene either has a unique emission source that is not shared by any other compound (*i.e.* cleaning products discussed previously)[202] or the fact that the measured concentrations were close to the limit of detection and as such may skew the analysis.

Summer correlations of the biogenic species are quite different, they show high correlations with each other and much smaller correlations with the other anthropogenic species. This suggests that the biogenic source of these species is dominant during the summer campaign. Interestingly, the three unsaturated compounds, isoprene, α-pinene and limonene, do not correlate with each other except for isoprene and α-pinene which has an R^2 value of 0.72. Limonene does correlate with the aromatic biogenic compound, 4-*iso*-propyl-toluene (R^2 0.58). There have been limited reports on the emission of 4-*iso*-propyl-toluene from various plant species,[224–226] which may indicate that they either share a common biogenic emission source or are emitted concurrently with each other.

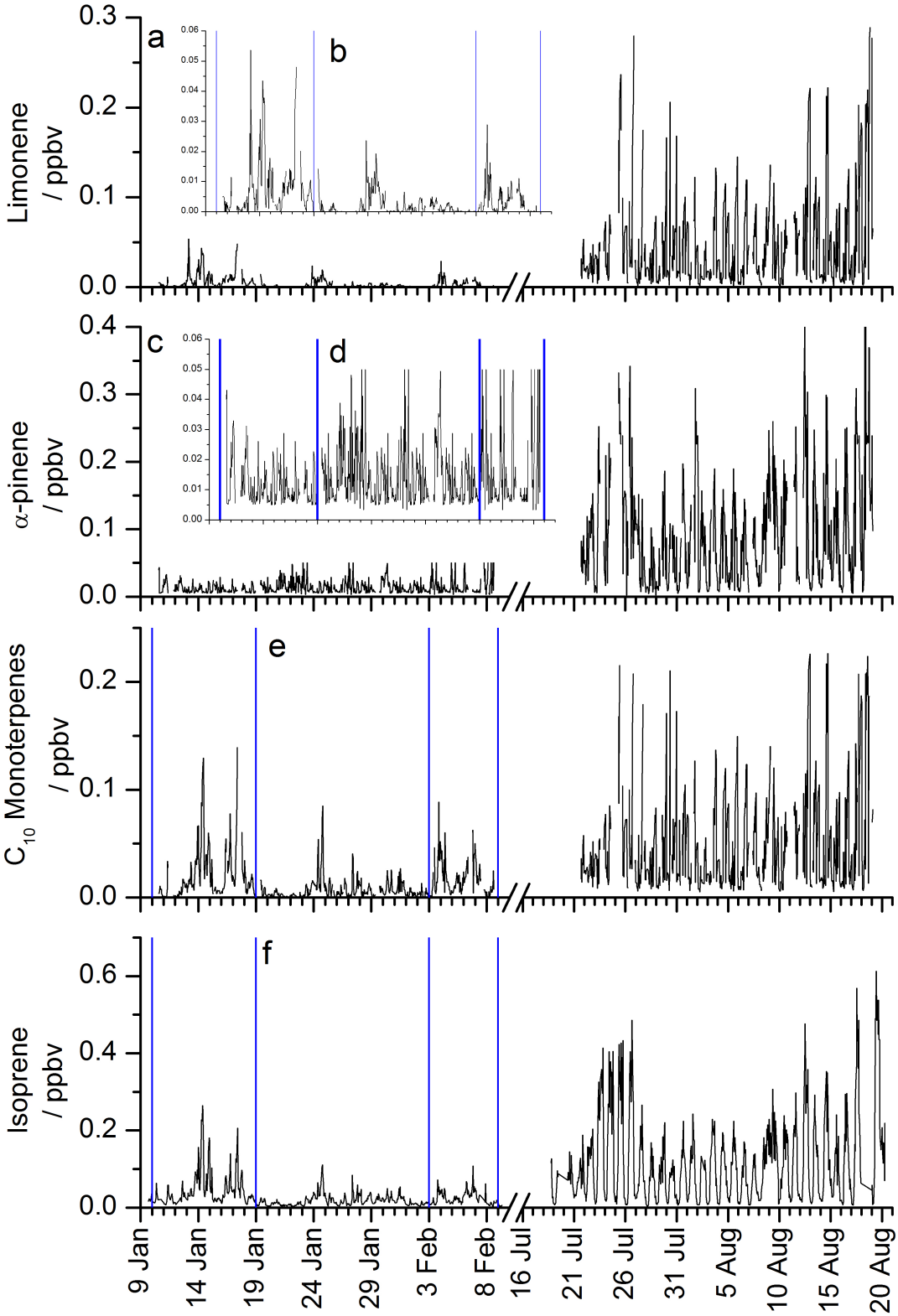

Figure 3.10: Time series of selected biogenic source compounds: (a) limonene, (b) zoomed in graph of the winter limonene observed mixing ratio, (c) α-pinene, (d) zoomed in graph of the winter α-pinene observed mixing ratio, (e) C_{10} monoterpenes and (f) isoprene

3.4.2 Relationship of biogenic species with temperature

The considerable summer diurnal variation in the emission of biogenic species from vegetation has been shown previously in this thesis and other studies,[69,206,227] where the maximum emission is at approximately midday. This diurnal variation is attributed to the fact that the emission is dependent on both light and temperature.[227] Figure 3.11 shows the correlation relationship of the four biogenic compounds with temperature during the summer campaign. These species often show an exponential relationship with temperature, with isoprene having the strongest correlation assuming an exponential fit to the data (R^2 of 0.47). The correlation is much smaller with the other three species, suggesting that there is not much of a relationship between these compounds and temperature.

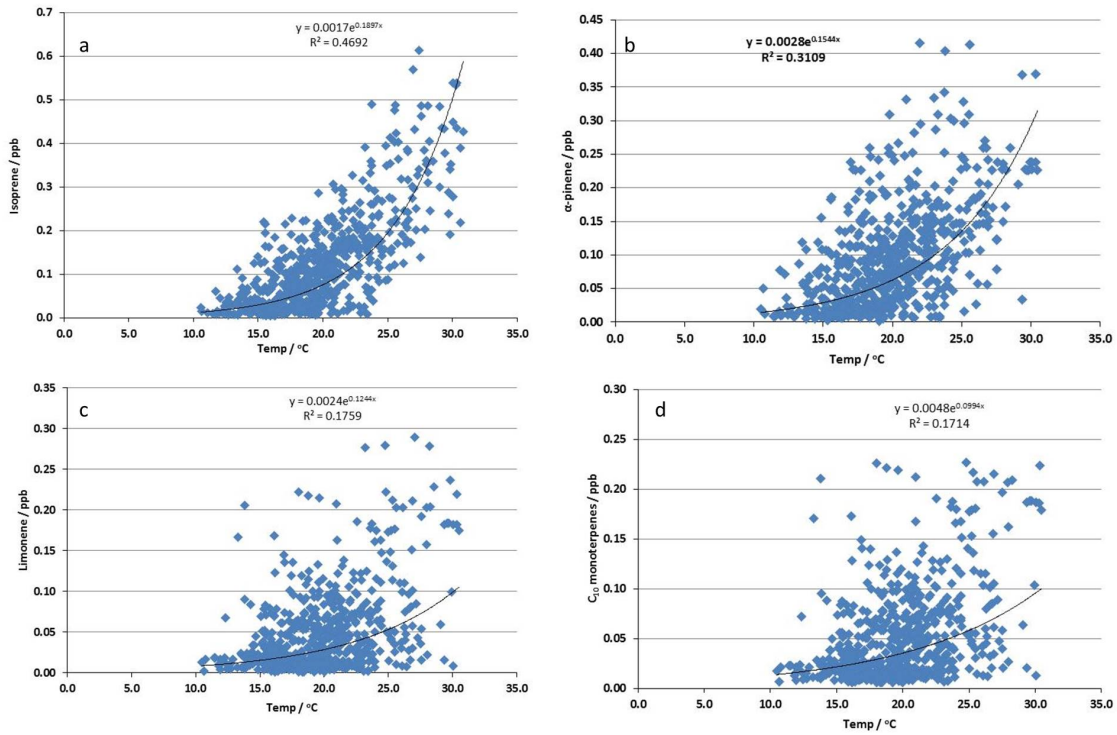

Figure 3.11: Correlation graphs of typically biogenic source compounds with temperature specifically (a) isoprene, (b) α-pinene, (c) limonene and (d) C_{10} monoterpenes. Equations and R^2 values of the line of best fit are shown on the specific graphs to which they correspond

Although this relationship is present during the summer ClearfLo campaign, the correlations of the biogenic species with temperature is smaller than those seen in other studies. A study by Jones *et al.*, (2011) showed correlations of isoprene, α-pinene and limonene with temperature from a tropical rainforest.[227] The correlations were found to be much stronger than those presented here. The correlation of isoprene and temperature had an

R^2 value of 0.78 whilst in London the correlation had an R^2 value of only 0.47. The R^2 value from the correlation of α-pinene with temperature from Jones *et al.*, was 0.70,[227] while in London this was only 0.31. The correlation of limonene with temperature was also much smaller in London (0.18) than seen in Jones *et al.*, (0.70).[227]

It is possible that the rather short lifetimes of these compounds with the OH radical in the atmosphere could be skewing the data towards a less prominent relationship with temperature. With a concentration of 1×10^6 molecules cm^{-3} for the OH radical, the lifetimes of the compounds are 5.3 hours for α-pinene, 2.8 hours for isoprene and 1.7 hours for limonene. These lifetime values also suggest that the biogenic source of these compounds must be local to the site as it is unlikely that they could be transported from further afield, although this may explain the poor correlations between these species and temperature in London. Obviously the ClearfLo campaign was carried out in a highly urbanised city which may not be expected to have strong biogenic sources of these compounds. However, a relationship between these compounds and temperature was still observed. The importance of biogenic isoprene in London was recently discussed by von Schneidemesser *et al.*, (2011), where they found that there were relatively large levels of isoprene in particular. However, for the majority of the year, anthropogenic sources dominate while in summer months with high levels of sunlight and temperatures significant OFP can be attributed to isoprene.[201]

Part 2: Impacts of additional volatile organic compounds on modelled OH radical reactivity

3.5 Introduction

For the majority of VOCs, reaction with the OH radical is the dominant removal mechanism in the atmosphere. A key method to study the impact of potential sources of secondary chemistry is OH reactivity. Previously, OH reactivity could only be inferred from calculations or modelling of OH sink species.[78] In the past two decades however, new instrumentation has allowed direct measurement of OH reactivity.[228] These results can then be compared to calculated and modelled results to test the understanding of the chemistry of the atmosphere. Total OH reactivity from measured species can be calculated using Equation 3.1, discussed previously in Chapter 1, Section 1.2.2.1. Briefly, this is the sum of all observed species which react with OH (*i.e.* VOCs, NO_2, CO *etc.*) where $[X]_i$ is the concentration and k_{OH+X} is the bimolecular rate coefficient for the species X when reacting with the $^{\bullet}$OH radical.

$$k_{OH} = \sum_{i=1}^{n} k_{X,OH} \cdot [X]_i \tag{3.1}$$

By restricting the species included in calculations and models to only those that are actually measured in the field, in-situ OH reactivity measurements can be directly compared. For modelled OH reactivity, this will also include some unmeasured OH sinks that are often OVOCs formed after the oxidation of the directly emitted species. The difference found between the actual measurement and that calculated or modelled is often referred to as 'missing' OH reactivity. This is due to the fact that the measurement is usually higher than predicted from the calculation or model. By analysing the degree of difference, some distinction can be made about whether the 'missing' reactivity is from either primary emissions that were not full characterised or unmeasured oxidised intermediates.

In the majority of studies in urban areas where a comparison was made with measured OH reactivity, most compared with calculated rather than modelled reactivity. A number of these studies showed good agreement between the measured and calculated OH reactivity.[185,229,230] Modelling of the OH reactivity can provide an estimate of the contributions model generated intermediates make to total OH loss. However, given the closure obtained using only the calculated reactivity from primary emissions, the suggestion is made that the oxidised intermediates do not always have significant contributions to total OH reactivity in some cities.

However, all urban cities are not identical and some can have large percentages of

'missing' reactivity. For example, Chatani *et al* (2009) and Dolgourouky *et al* (2012) both reported missing reactivity of ≈ 30% in Tokyo and 75% in Paris respectively.[187,231] In both of these studies, only measured sink species were used to calculate the OH reactivity and directly compared to that measured. However, care must be taken when comparing missing reactivity that is reported in the literature. The chemical detail and range of measured sink species (*e.g.* VOCs, CO, O_3) that have been used to calculate the OH reactivity can vary significantly. By comparing the OH reactivity calculated and modelled using different sets of VOCs, the magnitude of changes for the range of species included can be shown.

3.6 Experimental

3.6.1 OH reactivity observations

During the ClearfLo campaign a variety of species were measured as detailed in Chapter 2. OH reactivity was also measured using a discharge flow technique, where water vapour is photolysed to produce OH radicals. The subsequent decay of these radicals, from the reaction with ambient sink species such as VOCs, is then observed by Laser induced florescence (LIF). This technique has been described in detail in Ingham *et al.*, (2009).[228] This measurement was conducted by Dr Lisa Whalley from the University of Leeds.

3.6.2 OH reactivity modelling

A zero-dimensional photochemical box model, based on the Master Chemical Mechanism (MCMv3.2), was used to predict the OH radical concentrations and reactivity. A sub-set of the MCM was run which treated the degradation of 135 concurrently measured trace VOC species, CH_4 and CO after oxidation by OH, O_3 and NO_3. This included approximately 17000 reactions and 6700 species. The model was constrained to measurements made of NO, NO_2, O_3, HONO, CO, CH_4, VOC species from the DC-GC and GC×GC instruments, PAN, formaldehyde (HCHO), water vapour, temperature, pressure, photolysis rates and aerosol surface area. Model inputs were every 15 minutes with data averaged or interpolated to 15 minute intervals if the species was measured more or less frequently, respectively.

The model was run for the entire summer ClearfLo campaign in 7 day overlapping segments. Prior to comparison of model outputs to measurements, the model was run for

5 days from the initial measurement day (22nd July) to allow for the model generated intermediates (that are not measured) to maintain steady state concentrations. This modelling was also conducted by Dr Lisa Whalley from the University of Leeds.

3.6.3 Volatile organic compounds sets in the model

Three sets of VOC observations were used during the modelling of OH reactivity: (1) the standard set of VOCs that have been routinely measured using the DC-GC instrument in previous campaigns, (2) an extended set which includes additional individual species measured using the GC×GC instrument and (3) an extended + grouped VOC set that includes all the individual VOCs of the extended set plus the grouped species discussed in Chapter 2. Table 3.2 shows the first two sets of individual VOCs; set 1 in normal font and the extra VOCs included in set 2 in bold. The grouped species included in VOC set 3 are detailed in Table 3.3 along with the OH rate constant applied to each group. The rate constants for the corresponding *n*-alkanes was applied to the aliphatic groups, α-pinene for the C_{10} monoterpene group and that of propyl-benzene for the C_4 substituted monoaromatic group. The *n*-alkane rate constants were used for the aliphatic groups, as the average rate constant for 354 C_{12} aliphatic isomers were found to be within the error limits given for the *n*-alkane (calculated using SARs and discussed in detail in Chapter 2, Section 2.5.5). Full details of both instrument set ups are described in Chapter 2, Section 2.3. Even though over 70 VOCs were measured during the ClearfLo campaign, some of them are not included as their reaction mechanisms with the OH radical are not known and they are not included in the MCM.

Table 3.2: VOC species included in the MCM modelling of OH reactivity during the ClearfLo summer campaign with their associated OH rate constants.[82] These have been split by basic functionality and ordered by increasing rate constant values. Compounds in normal font are from the (1) Standard VOC suite. The (2) Extended suite contains all compounds in normal font and the additional VOCs in bold. Compounds measured using the DC-GC are denoted with † and those measured using the GC×GC with ‡.

Compound	$10^{12} \times k_{OH}$ (cm^3 $molecules^{-1}$ s^{-1})	Compound	$10^{12} \times k_{OH}$ (cm^3 $molecules^{-1}$ s^{-1})	Compound	$10^{12} \times k_{OH}$ (cm^3 $molecules^{-1}$ s^{-1})	Compound	$110^{12} \times k_{OH}$ (cm^3 $molecules^{-1}$ s^{-1})
CO	0.24	**Alkene and Alkynes**		**Aromatics**		**Alcohols**	
NO	7.94	Acetylene†	0.705	Benzene†	1.22	Methanol†	0.94
NO_2	14.5	Ethene†	8.52	Toluene†	5.63	Ethanol†	3.2
Alkanes		Ethene†	8.52	**Benzene, propyl‡**	5.8	Propanol†	5.8
Methane†	0.0064	Propene†	26.3	**Benzene, *iso*-propyl-‡**	6.3	Butanol†	8.5
Methane, dichloro‡	0.142	1-Butene†	31.4	Benzene, ethyl- †	7	**Carbonyls**	
Ethane†	0.248	1-Pentene†	31.4	**Toluene, 4-ethyl-‡**	11.8	Acetone†	0.17
Propane†	1.09	*iso*-Butene†	51.4	**Toluene, 2-ethyl‡**	11.9	**Butanone‡**	1.15
iso-Butane†	2.12	*cis*-2-Butene†	56.4	**Benzaldehyde‡**	12.9	**Acetate, ethyl-‡**	1.6
n-Butane†	2.36	*trans*-2-Butene†	64	*o*-Xylene†	13.6	**2-Pentanone‡**	4.9
iso-Pentane†	3.6	*trans*-2-Pentene†	67	**Toluene, 3-ethyl-‡**	18.6	**2-Hexanone‡**	9.1
n-Pentane†	3.8	**Dialkenes**		*m/p*-Xylene†	18.7	Formaldehyde	9.37
n-Hexane†	5.2	1,3-Butadiene†	66.6	Benzene, 1,2,4-trimethyl-†	32.5	**Pentanone, 4-methyl-2-‡**	14.4
Pentane, 2-methyl-†	5.2	Isoprene†	100	Benzene, 1,2,3-trimethyl-†	32.7	Acetaldehyde†	15
n-Heptane†	6.76	**Biogenics**		Benzene, 1,3,5-trimethyl-†	56.7	Ketone, methyl-vinyl‡	18.8
n-Octane†	8.11	**α-Pinene‡**	52.3	**Styrene‡**	58	**Butanal‡**	23.5
***n*-Nonane‡**	9.7	**Limonene‡**	164			**Propanal, 2-methyl-‡**	26.3
***n*-Decane‡**	11					**Pentanal‡**	28.5
***n*-Undecane‡**	12.3					Methacrolein‡	33.5
***n*-Dodecane‡**	13.2						

Table 3.3: Grouped VOC species included in the MCM modelling of OH reactivity of the (3) extended+grouped set during the ClearfLo summer campaign with their associated OH rate constants.[82]

Grouped species	$\mathbf{10^{12} \times k_{OH}}$ ($\mathbf{cm^3\ molecules^{-1}\ s^{-1}}$)
C_6 aliphatics	5.2
C_7 aliphatics	6.76
C_8 aliphatics	8.11
C_9 aliphatics	9.7
C_{10} aliphatics	11
C_{11} aliphatics	12.3
C_{12} aliphatics	13.2
C_{13} aliphatics	15.1
C_4 substituted monoaromatics	5.8
C_{10} monoterpenes	52.3

3.7 Results

Figure 3.12 shows the summer campaign measurements of OH reactivity taken during ClearfLo. The average reactivity observed was approximately 18 s^{-1} during the measurement period, however periods of high reactivity were seen highlighted by the data spikes of up to 40-60 s^{-1} in Figure 3.12. The maximum OH reactivity was 116 s^{-1} with a minimum value of 4 s^{-1}. Typically, throughout the campaign south westerly winds ranging from 1 ms^{-1} at night to between 4-6 ms^{-1} in the afternoon were observed. During the two periods highlighted in Figure 3.12, the wind direction changed to an easterly flow that brought air passing over central London to the site. The wind speeds also dropped, with enhancements seen in temperature and solar radiation.[159] The OH reactivity was also enhanced during these periods. There have been several observations of OH reactivity in urban cities throughout the last decade.[185,187,229–236] These showed that some of the highest levels (> 120 s^{-1}) of observed OH reactivity were recorded in megacities such as Mexico City and Paris.[187,234] In many of these large cities, the OH reactivity was found to be dominated by contributions from anthropogenic VOCs, CO and NO_x. The OVOCs have also been highlighted as a significant sink of OH.[230]

The average diurnal profile of the measured OH reactivity is shown in Figure 3.13. This shows a distinct peak between 6-7 am, which then drops to a minimum during the afternoon. A secondary peak is observed in the evening, where the observed reactivity rises from $\approx$ 6 pm throughout the night. This closely follows the summer diurnal profile of

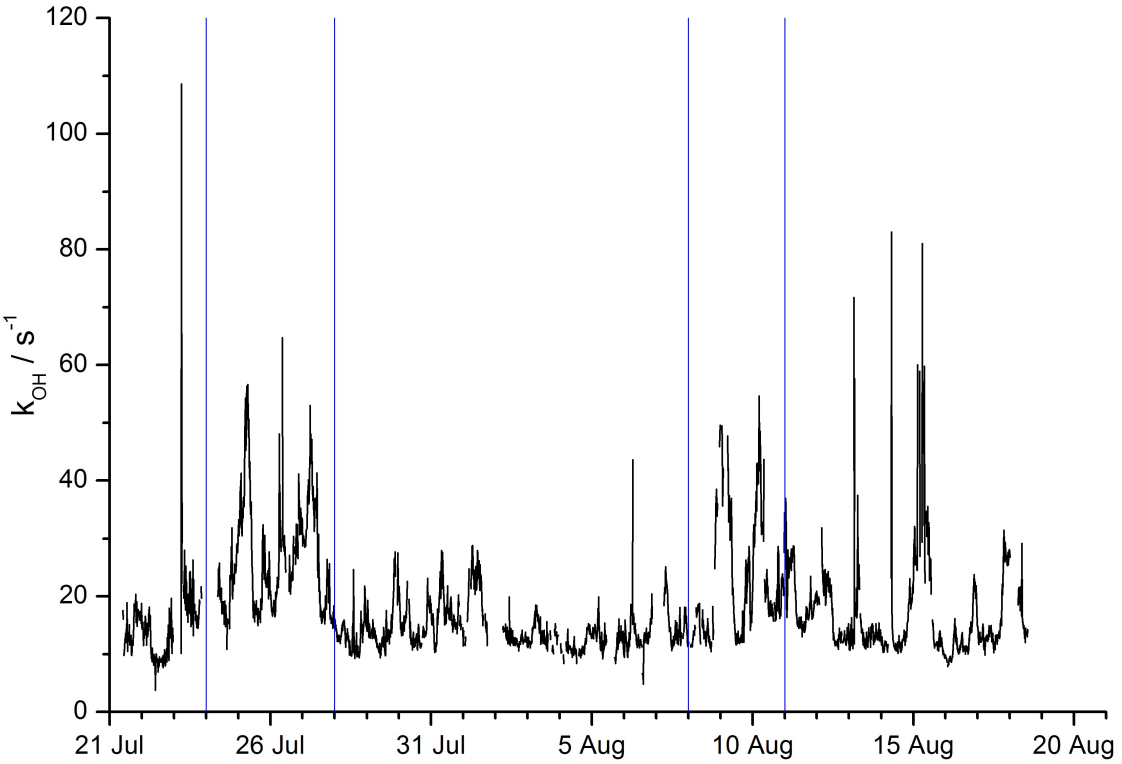

Figure 3.12: Time series of the measured OH reactivity during the summer campaign

NO_x, shown in Chapter 2, Figure 2.14 d. This profile has also been seen in several other observations of OH reactivity in urban areas.[187,231,237]

3.7.1 Impact of using different sets of volatile organic compounds to calculate and model OH reactivity

To compare the impact of the three sets of VOCs to the observed OH reactivity, a calculated and modelled reactivity were determined for all sets. For the calculated reactivity, each VOC was multiplied by its respective rate constant for reaction with OH (as shown previously in Chapter 2, Section 2.5.5). The rate constants for the calculated OH reactivity were taken from the most recent literature and are detailed in Table 3.2 and Table 3.3. The modelled reactivity uses temperature dependent rates constants when available. These were calculated for each time point where VOC measurements were taken during the summer campaign then a campaign diurnal averaged. The VOCs have been grouped together according to functionality, as the rate of loss of OH with each individual VOC is relatively small. This allows the contributions of different VOC classes (alcohol, alkanes, alkenes, aromatics, biogenics, carbonyls and dialkenes) to the removal of OH, hence their influence

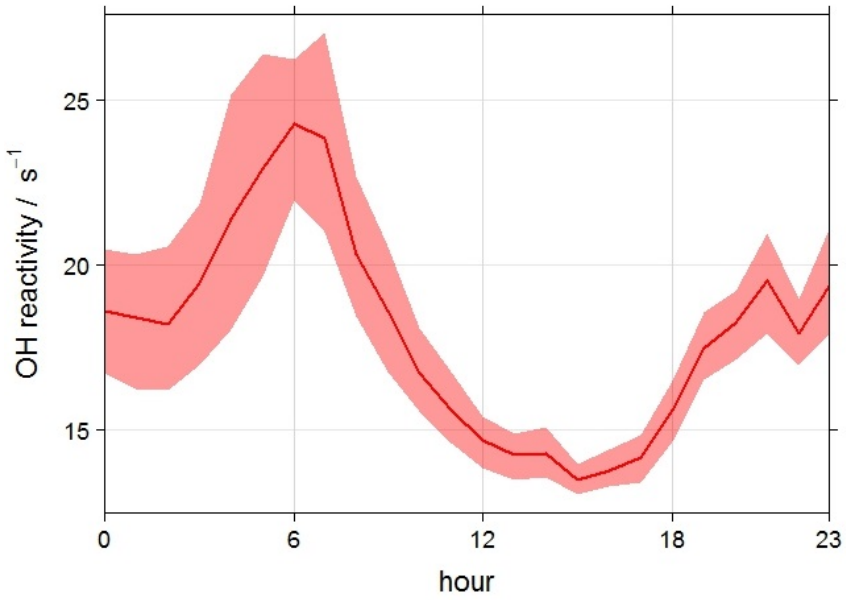

Figure 3.13: Diurnal profile of the measured OH reactivity during the summer campaign. This figure was constructed using the OpenAir project for R where the solid line represents the mean daily concentration and the shaded regions shows the 95% confidence intervals surrounding the mean.[166–168]

on the oxidising capacity to be evaluated.

3.7.1.1 Standard and extended volatile organic compounds sets

Figure 3.14 shows an average diurnal profile for the measured OH reactivity and that calculated using Equation 1.24 from the standard VOC set (upper left panel) and the extended VOC set (lower left panel), during the summer ClearfLo campaign. The right panel graphs show the same graph but with the contributions from the inorganic species (NO_2, NO and CO) removed. This allows the diurnal profile contributions of the other groups to be seen.

The calculated OH reactivity from both sets of VOCs show a similar profile (left panels of Figure 3.14) which is driven by the contribution from NO_x. This provides a characteristic traffic 'rush hour' peak in the morning, as well as a smaller peak in the late evening. By removing the inorganic species, right panels, the profiles of the other groups can be pulled out. The other groups, except the dialkenes, show a similar profile to that of the inorganic species driven by the emission from traffic sources. In contrast, the dialkane group, which is dominated by the contribution from isoprene, shows a peak at noon. This suggests that this group has a temperature/sunlight driven biogenic source. An enhanced and similar profile is seen for the extended biogenic group (α-pinene and limonene) which

would be expected.

The combined inorganic species (NO_2, NO and CO) contribute an average 5.8 s^{-1}, which is almost matched by the combination of all the other groups from the standard VOC set (5.5 s^{-1}). The carbonyl group has the largest contribution of the organic species to reactivity, seen in the upper right panel of Figure 3.14. This group is dominated by two individual VOCs, acetaldehyde and formaldehyde (54% and 40% respectively), and when considered as a group provides a similar contribution as NO_2 to the total calculated OH reactivity (3.34 s^{-1} for the carbonyl group and 3.82 s^{-1} for NO_2). The other groups (alcohols, alkanes, alkenes, aromatics, biogenics and dialkenes) contribute less, an average of between 0.2-0.6 s^{-1}.

The combined contributions of the inorganic species and the standard VOC set cannot reconcile the observed OH reactivity. There is an average 'missing' OH reactivity of 6.8 s^{-1}, which is 38% of the total measured value. Previous studies postulated this underestimation to be caused by higher carbon number species, particularly aromatic and/or biogenic compounds such as terpenes.[78] However, even though 23 additional individual VOCs are included in the calculation of OH reactivity from the extended VOC set (shown in lower left panel fo Figure 3.14), there is still 'missing' OH reactivity. The contributions from the alkane, aromatic and carbonyl groups increased by 0.21, 0.05 and 0.05 s^{-1} respectively. The largest increase observed using the extended VOC set was for the biogenic group, which contains α-pinene and limonene. The reactions of OH with these two species increased the total calculated OH reactivity by 0.25 s^{-1}.

Even with the additional VOC species included in the extended VOC set, there is a significant difference between the calculated and measured reactivity. The 'missing' OH reactivity from the extended VOC set is 6.21 s^{-1}, 34% of the total observed reactivity. This points to a need for either the measurement of more OH radical sinks or the addition of intermediate sinks which are extremely difficult to measure. The reaction of these intermediates (usually second or third generation degradation products) with the OH radical, can be estimated through the use of a model which deals with the chemical degradation of the measured species.

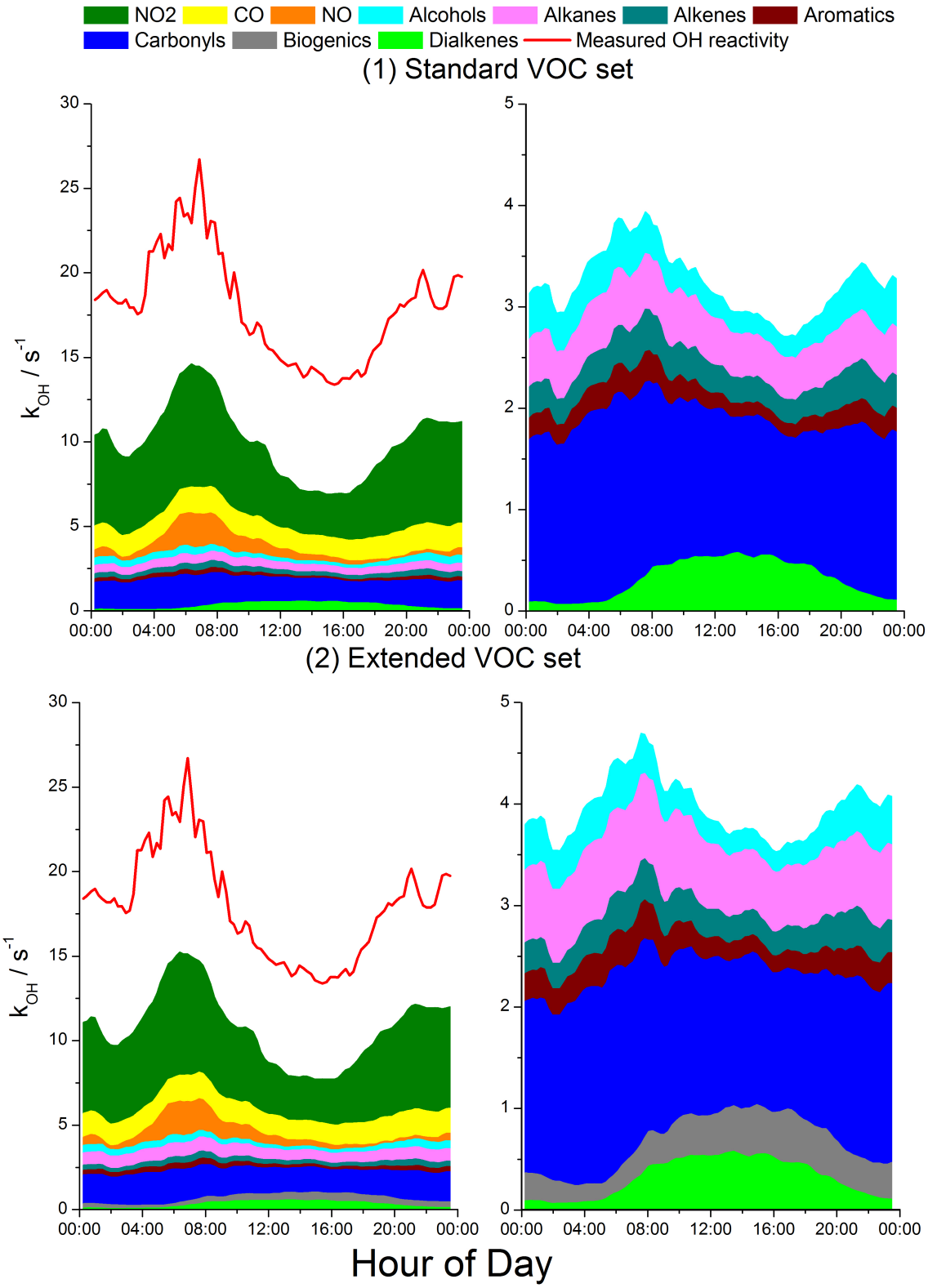

Figure 3.14: Daily average summer IOP campaign profile of the measured OH reactivity (red line) compared to that calculated (filled areas) using the (1) standard (upper left panel) and (2) extended (lower left panel) VOC sets. The right panels show the same graph with the contributions from the inorganic species (NO_2, NO and CO) removed to allow the diurnal profiles of the other species to be easily seen

3.7.1.2 Impact of model generated intermediates

Using the MCM box model, the OH reactivity was estimated using the (1) standard VOC set and (2) extended VOC set with the model generated intermediates shown in navy at the bottom of each plot in Figure 3.15. These are intermediate secondary species that are formed from the reaction of parent VOCs with the OH radical and are not easily measured as they have very short lifetimes in the atmosphere or are not well suited to current analytical methods. By including these model generated intermediate species, the model performs better. The left hand plots of Figure 3.15 shows the comparison of all species to the measured OH reactivity for the standard (upper left) and extended (lower left) VOC sets. As previously, the right hand plots show the contributions of the organic species only.

The total contribution to OH reactivity of the inorganic species and the standard VOC set, including the model generated intermediates, is now an average reactivity of 12.0 s^{-1}. The diurnal profile is similar to that seen previously, where the contribution from NO_2 drives the shape, the majority of the other species show smaller traffic related profiles and both the dialkenes and model generated intermediates show a profile characteristic of a temperature/sunlight driven biogenic source (upper right panel of Figure 3.15). The model generated intermediates from the standard VOC set add an additional 0.7 s^{-1}, which is 4% of the total measured OH reactivity. This intermediate group is largely made up of oxygenated compounds such as methyl glyoxal, glyoxal and glycoaldehyde which derive from aromatic species, isoprene and methyl vinyl ketone. However, the modelled reactivity from the standard VOC set is still missing an average of 34% of the total measured OH reactivity.

When model generated intermediates are included with the extended set of VOCs (Figure 3.15 lower left panel), the model predicts both the shape and magnitude well. The profile is again similar to those seen previously. However, the profile of the model generated intermediates from the extended VOC set (lower right panel of Figure 3.15) does not show a diurnal that is driven by biogenic emission/photochemical production, unlike that seen for the model generated intermediates from the standard VOC set. In contrast, the model generated intermediates show a rather flat profile.

The model generated intermediates from the higher carbon number species provide an additional 3.3 s^{-1} of reactivity on average (compared to 0.75 s^{-1} from the standard VOC set). This shows that the contributions from the intermediates generated from modelling of

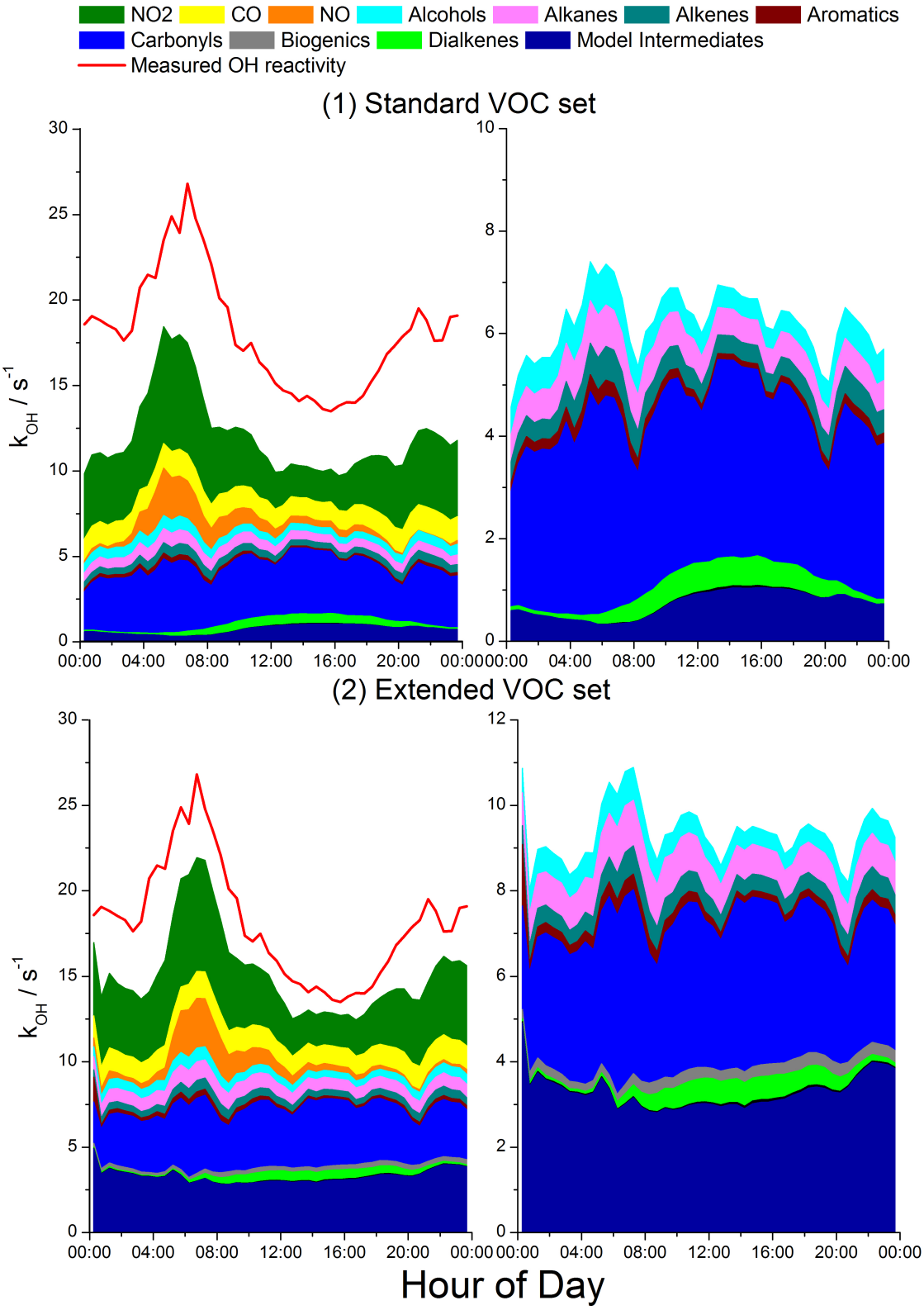

Figure 3.15: Daily average summer IOP campaign profile of the measured OH reactivity (red line) compared to that modelled (filled areas) using the (1) standard (upper left panel) and (2) extended (lower left panel) VOC sets, including model generated intermediates. The right panels show the same graph with the contributions from the inorganic species (NO_2, NO and CO) removed to allow the diurnal profiles of the other species to be easily seen

the extended VOC set are significant and can almost close the gap between measured and modelled OH reactivity. This is due to the extended VOC set making a greater number of intermediate species, due to their larger size and the increased number of potential VOC-NO_x-O_3 cycles that can be completed. Thus the NO_x:VOC ratio is decreased, resulting in more propagation than termination reactions occurring.

It is possible to determine the parent VOC source of the dominant oxygenated model generated intermediates. For the extended VOC set, although the contribution from the individual VOCs in the biogenic group (α-pinene and limonene) was small, their oxidation products were found to account for more than 1.7 s^{-1} ($\approx$ 50%) of the OH reactivity from all the model generated intermediates.

There is better agreement between the modelled and measured OH reactivity (lower left panel of Figure 3.15), when the model is constrained to the extended VOC set. This not only demonstrates the significant contribution that model generated intermediates can make to the total OH reactivity, but also highlights that BVOCs in London can have a noteworthy impact when secondary oxidised products are considered. The role that monoterpenes can play towards increasing OH reactivity has not previously been demonstrated at urban sites. This may be due to the fact that BVOCs other than isoprene are not routinely measured at urban sites concurrent with OH reactivity measurements.[187,229,230,232,237] It is also possible that, if only the reaction of the parent BVOC species with OH is considered, the contribution that the larger BVOC species can make to total OH reactivity is quite small.[231] Also, the influence of biogenic emissions in London has been shown to be important as discussed previously in this chapter. The ultimate fate of these oxidised intermediates derived from biogenic VOCs is highly uncertain, but if they remain in the gas-phase, as opposed to partitioning onto particles, their potential to increase the rate of radical propagation and in situ ozone production is significant.

Although the model results from the extended VOC set are better, there is still a small amount of 'missing' reactivity 2.9 s^{-1} which is approximately 16% of the total observed OH reactivity. The 'missing' reactivity could be from either the real-world physical loss of the model generated intermediates being smaller than that in the model or the presence of further unmeasured primary OH sinks, such as the additional grouped species measured using the GC×GC.

3.7.2 Impact of the grouped volatile organic compounds

As discussed in Chapter 2, the additional grouped species can have a large impact on primary hydrocarbon OH reactivity and potential ozone and SOA formation. This analysis was not without uncertainties though. The main issue when dealing with the analysis of the grouped species is that each individual species including in this mixture can not have its own rate constants and reaction mechanisms applied. However, by applying the rate constants and mechanisms of the *n*-alkane, propyl-benzene and α-pinene, it is possible to approximate the contributions of these groups to OH reactivity. Figure 3.16 (upper left panel) a shows the OH reactivity calculated from the (3) extended+grouped set of VOCs, where the grouped species have been included in the coloured functional group most representative of each (all aliphatics into the alkane, C_4 substituted monoaromatics into the aromatic and C_{10} monoterpenes into the biogenic). As previously, the right hand panel shows the contribution of the organic fraction only.

The calculated OH reactivity from the (3) extended+grouped VOC set is closer to the observed OH reactivity than seen previously for calculated reactivity, however there is still 5.6 s^{-1} (31%) missing. By including the additional grouped UCM species, the contribution from the alkane group increases by 0.41 s^{-1}. The aromatic and biogenic groups also increased, but to smaller degree of only $\approx$ 0.1 s^{-1} combined.

The inclusion of the model generated intermediates from the modelling of this set (Figure 3.16 lower left panel), improves the overall agreement between the measured and modelled OH reactivity with just 6% of the total OH reactivity still unaccounted for. The contribution of the model generated intermediates increased by 1.1 s^{-1}, compared to the extended VOC set. There is a small overestimation of the OH reactivity in the earlier afternoon ($\approx$ 16:00). It is possible that some of the higher carbon number species, especially those included in the grouped analysis of the UCM, partition into the aerosol phase after a degree of chemical processing. After only two cycles of oxidation, these C_{10}-C_{13} species are likely to form SVOC if they undergo functionalisation versus fragmentation reactions.[139] Higher carbon number species have the potential to form a significant amount of SOA. This is not something that is considered as part of the gas-phase MCM modelling. However, by incorporating a gas-to-particle partitioning model alongside the MCM, this discrepancy may be improved.

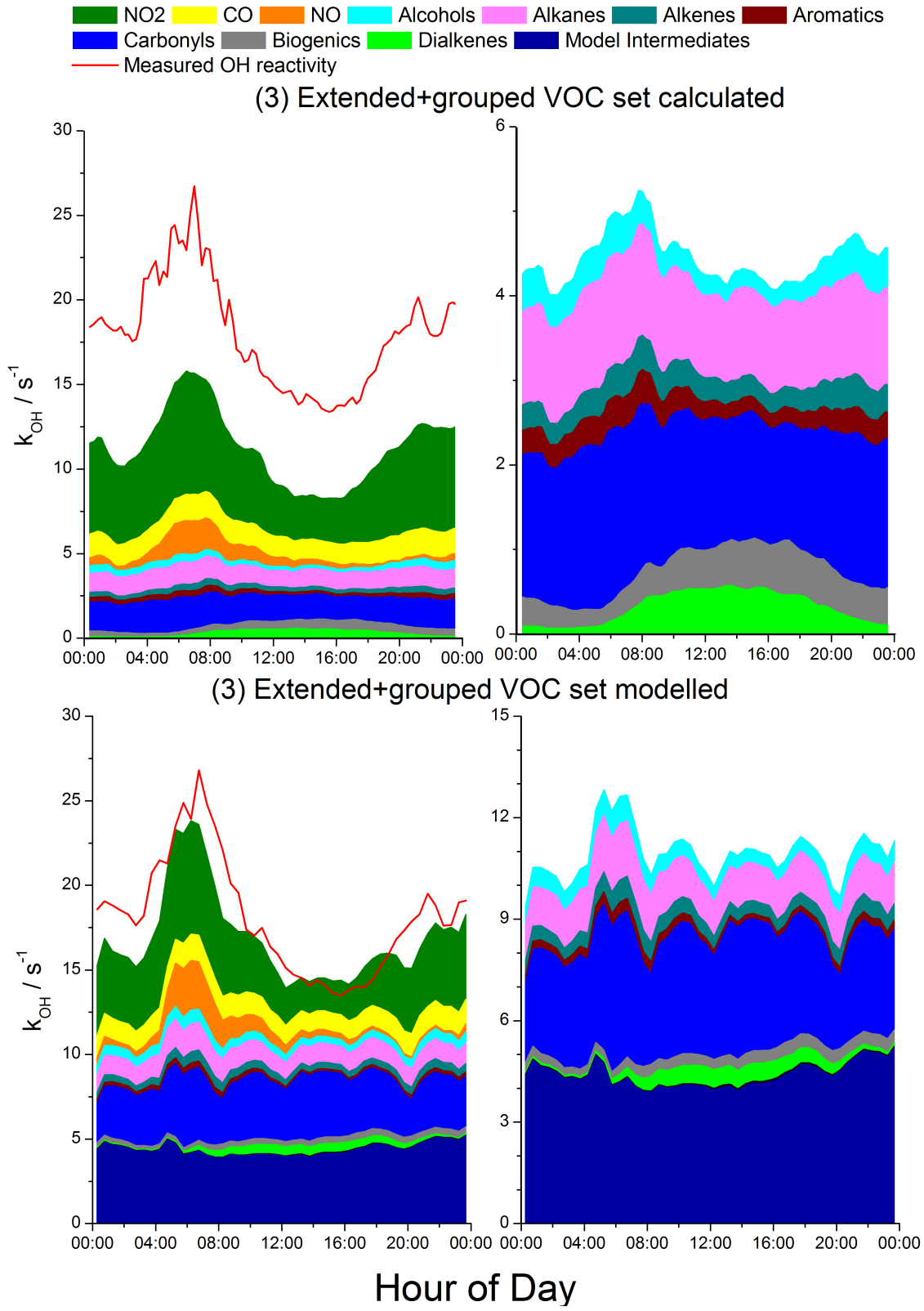

Figure 3.16: Daily average summer IOP campaign profile of the measured OH reactivity (red line) compared to that calculated and modelled (filled areas) using the (3) extended+grouped VOC set, upper left panel, calculated and lower left panel, modelled with model generated intermediates. The right panels show the same graph with the contributions from the inorganic species (NO_2, NO and CO) removed to allow the diurnal profiles of the other species to be easily seen

3.7.3 Influence of air mass origin on OH reactivity

Figure 3.17 shows the average diurnals experienced during the two different air mass flows highlighted in Figure 3.12. Although the contributions of the different groups of species to the total OH reactivity do not change significantly between the two regimes, during the more polluted easterly flow they represent larger OH sinks. The diurnal profile during the easterly flow (right panel) is more polluted, which is likely from a combination of more significant changes in the boundary layer height over days with low wind speeds.

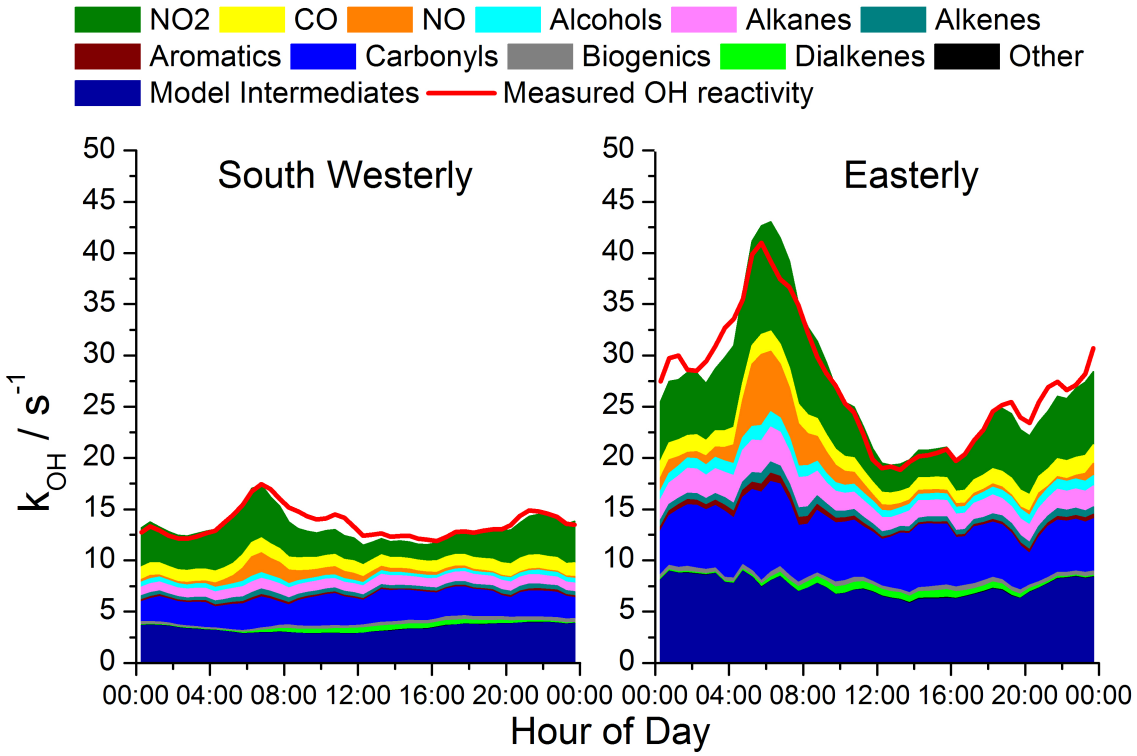

Figure 3.17: Average diurnal profile of measured OH reactivity (red line) compared to that modelled (filled areas) using the (3) extended+grouped VOC set with model generated intermediates; left panel, average diurnal during south westerly flows and right, average diurnal during easterly flows

There is a slight model over prediction observed during the easterly flow, at approximately 6 am. However, the overall agreement between the modelled and measured OH reactivity is very good during the easterly flow in both shape and magnitude. Conversely, there is a very small under prediction (average difference of 2%) throughout most of the diurnal during south westerly conditions. This could suggest that there are either more unmeasured VOC species during this period or the physical loss of the model generated intermediates should be treated differently during the two different air masses.

Conclusion

The quantification of a larger suite of VOC measurements than the majority of studies previously has allowed for a more in depth analysis to be carried out. The majority of previous studies focus on either a small, select sub group of VOCs and/or have a limited carbon number or functionality range. The VOCs quantified in this study cover C_1 to C_{12} and have a variety of different functionalities, including a large number of monoaromatic species. The contributions of these individual and grouped species to VOC mixing ratio, OH reactivity and potential ozone formation have shown that some of these species, which are not routinely measured, are very important. In particular, the higher carbon number species in all four groups of species discussed. For example, the C_4 substituted monoaromatics group is rarely measured. However, Figure 3.4 shows that, although this group does not contribute greatly to VOC mixing ratio or OH reactivity, the contribution is substantial for the potential ozone formation in winter. This shows that, although some compounds are not measured routinely given low mixing ratios, they can be important in terms of atmospheric reactivity.

Two different air mass characteristics; trajectory history and processing ratios, were analysed to provide information about whether the North Kensington measurement site was influenced by local, fresh or transported and aged emissions. On the whole, the site appeared to be largely influenced by local emissions with specific periods of both campaigns showing more well aged emissions that had been transported from further afield. Both anthropogenic and biogenic sources have been identified and found to have large impacts on the total VOC loading in an urban atmosphere such as London. The major anthropogenic emission source is likely to be a combination of fuel combustion from gasoline and diesel. This is evident from correlations between the different species identified as being emitted from anthropogenic sources with those species known to be emitted in large quantities from fuel combustion such as toluene and benzene. During the summer campaign, several species are shown to have a biogenic source that dominates over the anthropogenic source

present during the winter campaign.

An OH reactivity measurement was also made concurrent with this large suite of VOC measurements. A modelling study was conducted to compare three different sets of VOC species (standard, extended and extended+grouped) with the actual OH reactivity measurement. The results show that the discrepancy between the modelled and measured OH reactivity is decreased when additional VOC species are included in the model. This analysis suggests that if either oxidised VOCs are not included or the measured VOC suite is not comprehensive enough to sufficiently represent the actual primary VOC emissions, predictions of in situ ozone formation may be underestimated and in some cases this would be substantial. In particular, the contributions of BVOCs and additional grouped VOC species were shown to have significant contributions to total OH reactivity, and therefore are likely to play a critical role in increasing local ozone production. Additionally, the inclusion of model generated intermediate species, which are usually extremely short-lived in the atmosphere and thus very difficult to measure, with all three groups of VOCs improves the model performance. However, with the extended+grouped VOC set there was a small amount of overestimation during the early afternoon (Figure 3.16 lower left panel). It is likely this is due to the presence of either the grouped VOC species or the model generated intermediates as the mechanisms for each unidentified VOC species cannot be applied to these groups, so an estimate has to be made. During the ClearfLo project, there were several days during which the observed ozone exceeded the EU air quality recommended guideline of 60 ppbv. Future abatement strategies and policies must consider the role of both anthropogenic and biogenic emissions, as well as more than a standard set of VOCs in ozone production, even in the relatively temperate location of London.

Chapter 4

Investigating the magnitude and sources of oxygenated volatile organic compounds in London during ClearfLo

This chapter details further analysis of the large group of oxygenated VOCs measured during the ClearfLo campaign and the detailed analysis of one specific compound, ethanol.

Part 1: Analysis of oxygenated volatile organic compounds

OVOCs are a group of functionalised VOC species that can be either directly emitted to the atmosphere by both biogenic and anthropogenic sources or formed in the atmosphere through the oxidation of VOCs.[238,239] These species have been shown to contribute a large fraction of the total organic carbon measured in the troposphere, with some studies showing that the OVOCs were between 2-5 times more abundant than the other VOCs observed combined.[240–242] OVOCs can also highly influence the oxidising capacity and potential ozone formation in the atmosphere.[242,243] In several recent studies, OVOCs have also been found to be an important component of SOA.[176,242] Despite the importance of OVOCs in the atmosphere, there are still large uncertainties and gaps relating to the sources, sinks and the chemical reactivity of OVOC species.[241,244] This is mainly due to difficulties associated with measuring OVOC species and the fact there is are a vast amount of different OVOC configurations.[242] The importance of the OVOC species measured during the ClearfLo campaign has been shown in Chapter 2, where this group of species contributed as large percentage of potential ozone formation (see Figure 2.20). The OVOC species will be analysed in further detail in this chapter.

4.1 Seasonal comparison of oxygenated volatile organic compound observations

A total of 21 individual OVOCs were measured during the ClearfLo campaign. The campaign averages for the observed mixing ratios are shown in the upper panel of Figure 4.1. The top five most abundant OVOCs in winter and summer were ethanol (mean 5005 and 4978 pptv in winter and summer respectively), acetaldehyde (2256 and 4301 pptv), methanol (1246 and 3376 pptv), butanol (1157 and 484 pptv) and acetone (1076 and 2405 pptv). These accounted for 95% and 96% of the total measured OVOC loading in winter and summer respectively. Higher average mixing ratios were observed during the summer campaign for the majority of species except ethanol which had a similar average mixing ratio in both seasons and benzaldehyde, propanol and butanol which were higher during the winter campaign, suggesting the presence of a dominant anthropogenic source.

Valach *et al* (2014) also measured a suite of OVOCs using a Proton Transfer Reaction-Mass Spectrometer (PTR-MS) during the winter ClearfLo campaign at the North Kensington (NK) site and also at the Marylebone Road (MR) site (see Figure 2.4 for a map of these locations).[245] The MR site is a highly polluted kerbside site, while the NK site is

representative of an urban background. The PTR-MS was based at the NK site between 16-25/01/2012 and at the MR site between 25/01-07/02/2012. They reported that both sites were dominated by concentrations of methanol, acetaldehyde and acetone with average values shown in Table 4.1.[245] For acetaldehyde, this is quite significant as it implies that at a kerbside site, the concentrations can be enhanced by up to a factor of 2.5. Possibly due to the fact that the GC×GC was at the NK site for the entire winter campaign, the average acetaldehyde concentration was much higher (2256 pptv) than that reported by Valach *et al.* Assuming a similar enhancement from urban background to kerbside sites, the MR site could potentially have experienced acetaldehyde concentrations of nearly 6 ppbv.

Table 4.1: NK and MR mixing ratios in pptv measured using a PTR-MS[245]

	Methanol	**Acetaldehyde**	**Acetone**
NK	6400	620	1340
MR	4670	1610	1250

Figure 4.1 also shows the contributions of the OVOC species to calculated OH reactivity (middle panel) and OFP (lower panel). Species which have high concentrations do not necessarily contribute more to OH reactivity or OFP as they may have a slow rate constant for reaction with the OH radical or have less potential for ozone formation. For example, methanol is 15% of the total OVOC loading in winter, but only contributes 2% of the total OVOC OH reactivity and OFP. The OH reactivity shows a similar trend to that of the average mixing ratio, with the majority of species having higher summer contributions. Ethanol again shows a somewhat similar contribution in both seasons. The OFP (lower panel) shows the same profile that is dominated by the contribution from acetaldehyde, the four alcohol and acetone providing the next biggest contributions in both seasons. Interestingly, benzaldehyde has a negative OFP in both seasons. This is due to NO_x removal through the formation of peroxybenzoylnitrate during benzaldehyde oxidation.[246]

In both seasons, the contribution of acetaldehyde to OH reactivity and OFP dominates. Acetaldehyde provides 55% and 68% of the total OH reactivity from the OVOC during winter and summer respectively. The contribution to OFP is slightly smaller but still significant, 50% in winter and 63% in summer. This overall dominance by acetaldehyde shows that it is a very important OVOC species and can have large impacts on, not just

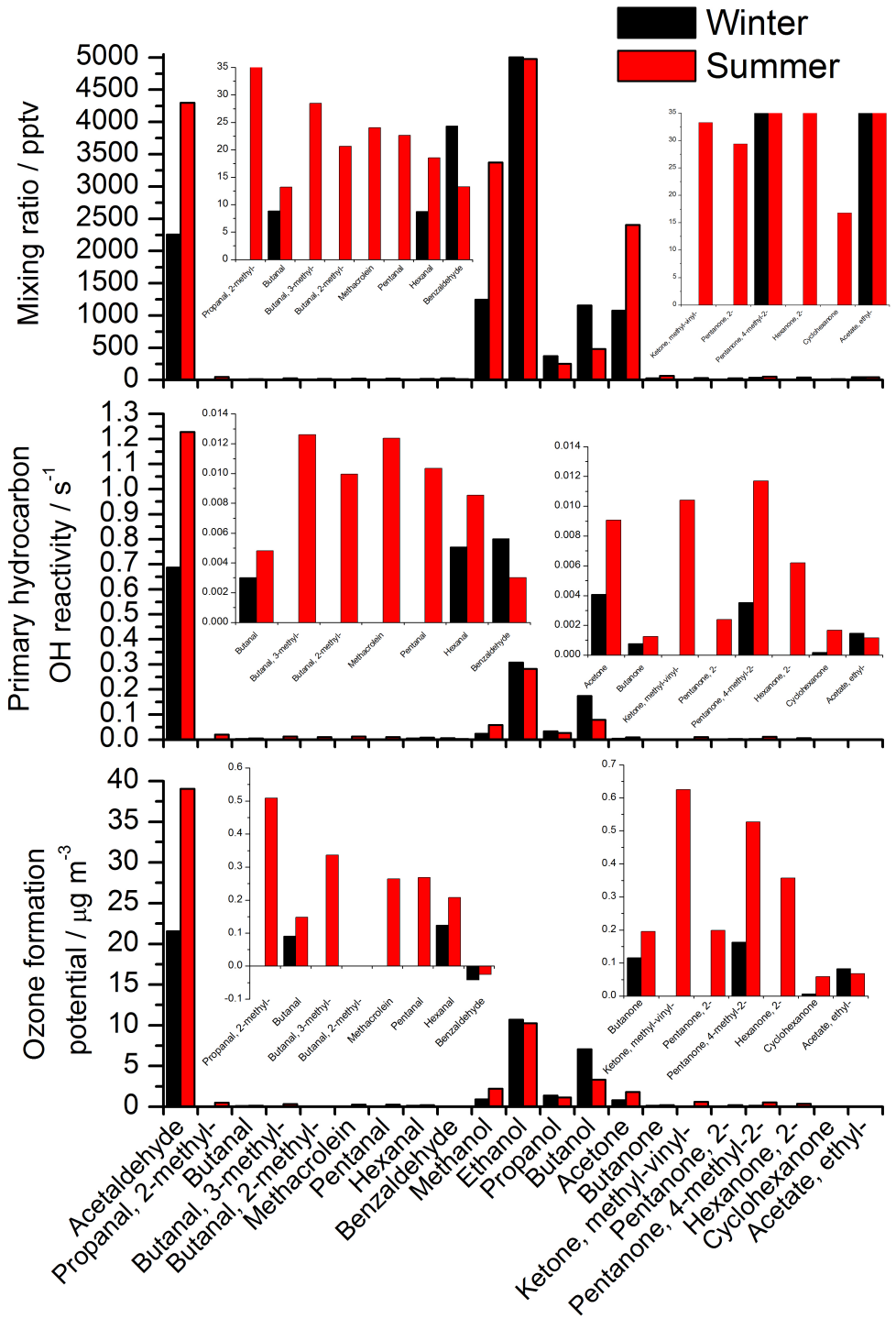

Figure 4.1: Winter (black columns) and summer (red columns) average mixing ratios (upper), primary hydrocarbon OH reactivity (middle) and potential ozone formation (lower) for the OVOC species during the ClearfLo campaign. The mixing ratio inset plot on the left shows a zoomed in section for 2-methyl-propanal to benzaldehyde and the plot on the right shows the same for methyl-vinyl-ketone to ethyl-acetate. The OH reactivity inset plot on the left shows a zoomed in section for butanal to benzaldehyde and the plot on the right shows the same for acetone to ethyl-acetate. The OFP inset plot on the left shows a zoomed in section for 2-methyl-propanal to benzaldehyde and the plot on the right shows the same for butanone to ethyl-acetate

the oxidative capacity of the atmosphere, but also air quality.

The time series of the OVOCs are shown in Figure 4.2. The time series have been plotted onto the same y-axis scale for each individual compound to allow for direct comparison of the two seasons, where necessary an inset plot has been added to allow for the smaller concentration time series to be viewed. Several of the OVOCs were below the detection limit of the GC×GC instrument and as such do not have a winter time series present. As already mentioned, the majority of species show a higher observed mixing ratio in the summer indicating their main source is secondary production in the atmosphere. Butanal, benzaldehyde, propanol and butanol have higher winter mixing ratios. This is most likely due to an anthropogenic emission source that contributes during the winter campaign. Ethanol displays a similar profile in both seasons, likely from its inclusion in gasoline. This will be discussed in further detail in Section 4.2.

Some of the winter profiles appear to show quite spiky data indicating the possible presence of local or point sources. In particular, the profiles of butanal, methanol, propanol and butanol. For the latter two, especially butanol, this local source is likely due to a fugitive emission from the Condensation Particle Counter (CPC) unit in the long-term measurement cabin or University of Manchester container based at the NK site. This source is not as apparent in the summer campaign, as the release of exhaust emissions were improved. The winter time series of propanol shows some extremely large spikes, over 12 ppbv in some cases. For propanol, this source could potentially be from cleaning of scientific instruments with iso-propanol on site. The DC-GC, used to quantify propanol, can not distinguish between the two structural isomers. Methanol also has two samples during the winter campaign, 21/01/2012 08:22 and 30/01/2012 06:53 where values of 19.3 and 30.7 ppbv respectively were observed. These are quite significant as they are a factor of 16 and 26 above the campaign averaged observed for methanol (1.2 ppbv) respectively. Butanal has a lower average median mixing ratio in winter than summer but the winter data is very spiky in nature.

During the summer campaign, the profiles observed for the majority of OVOCs follow a temperature/sunlight driven photochemical production pattern. This is seen in the oscillating nature of the profiles, that peak around midday day and fall to almost zero over night. However, there are some species that do not have this profile.

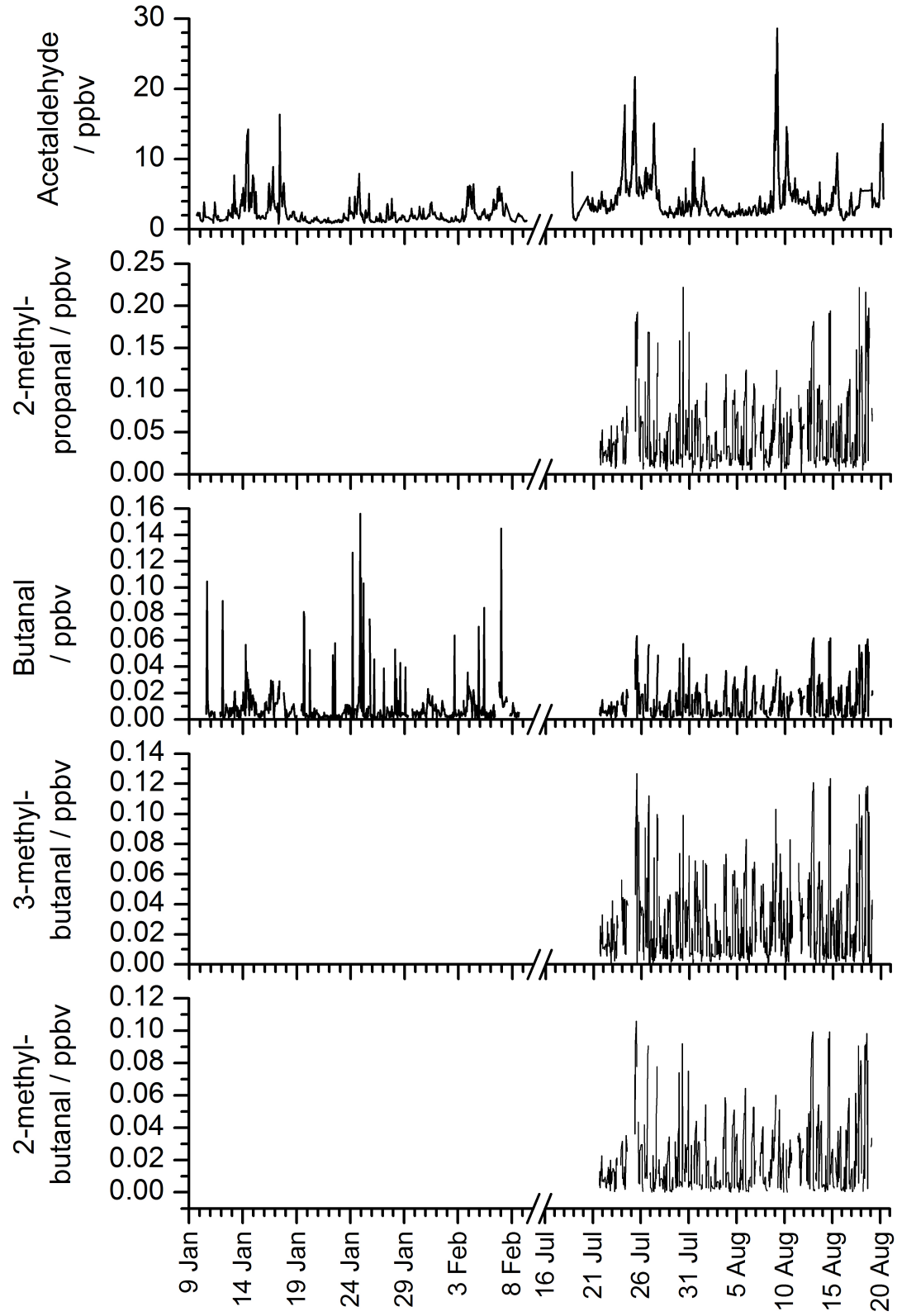

Figure 4.2: Time series of OVOCs from the winter and summer campaigns

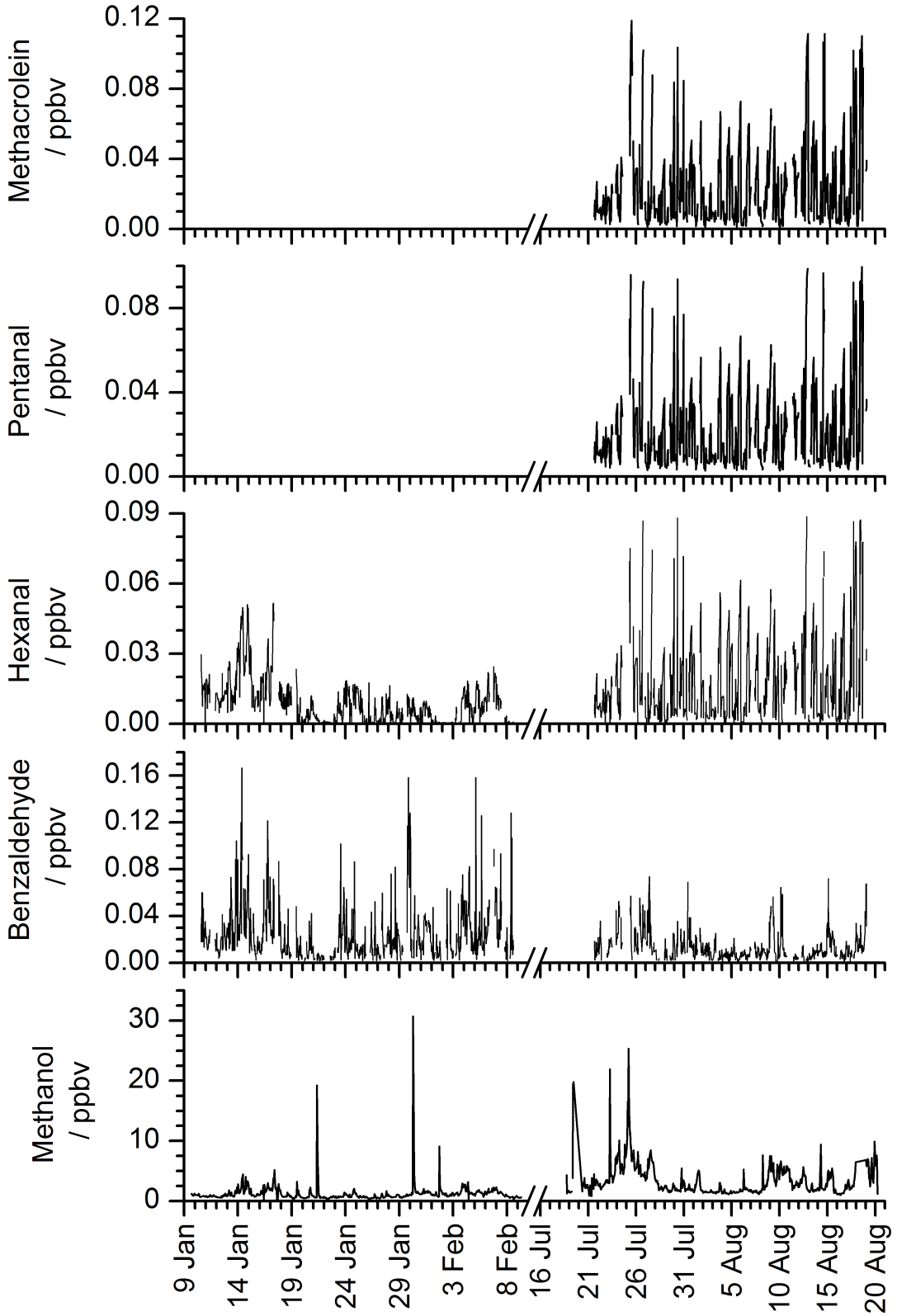

Figure 4.2: cont.

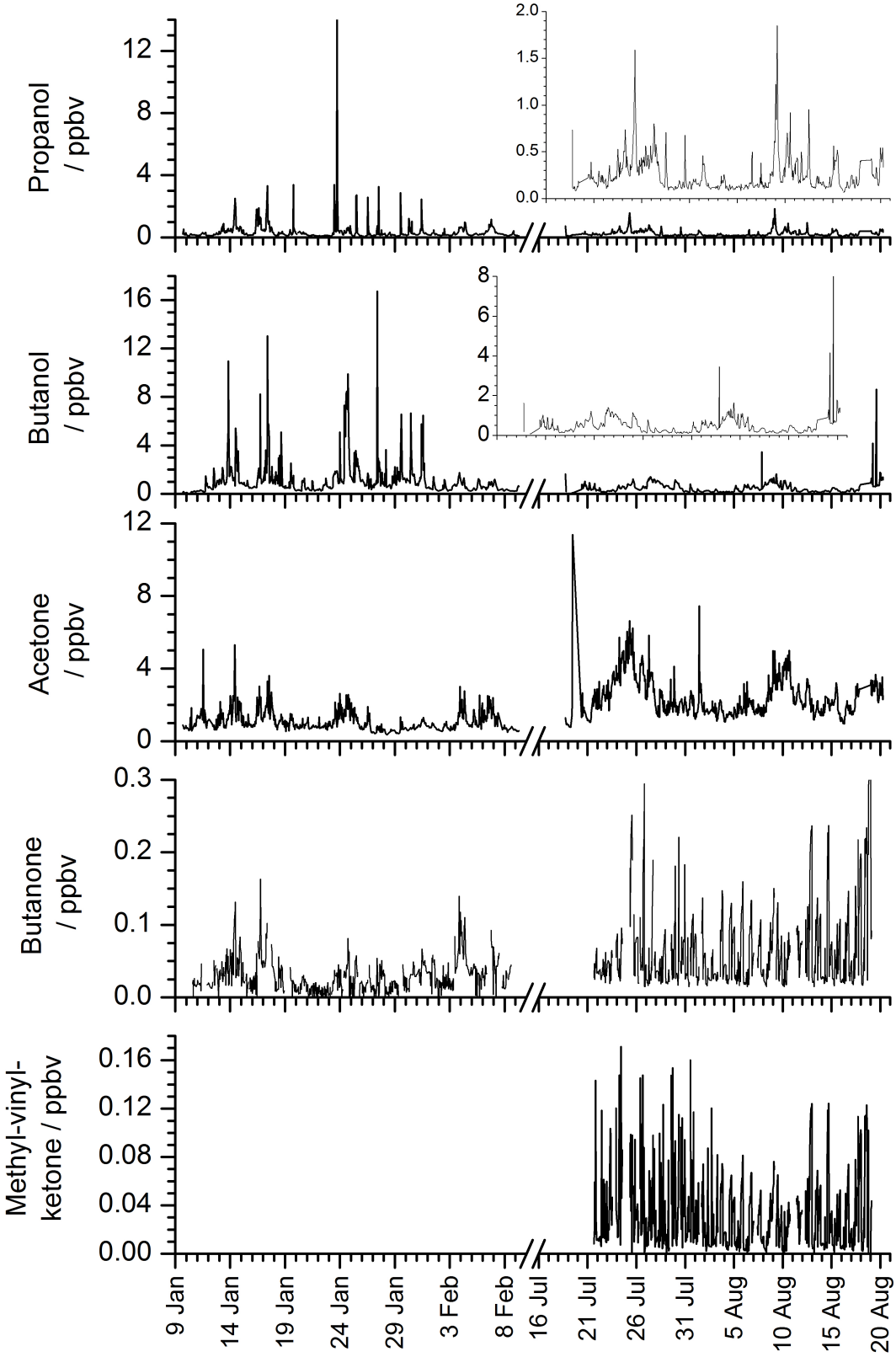

Figure 4.2: cont.

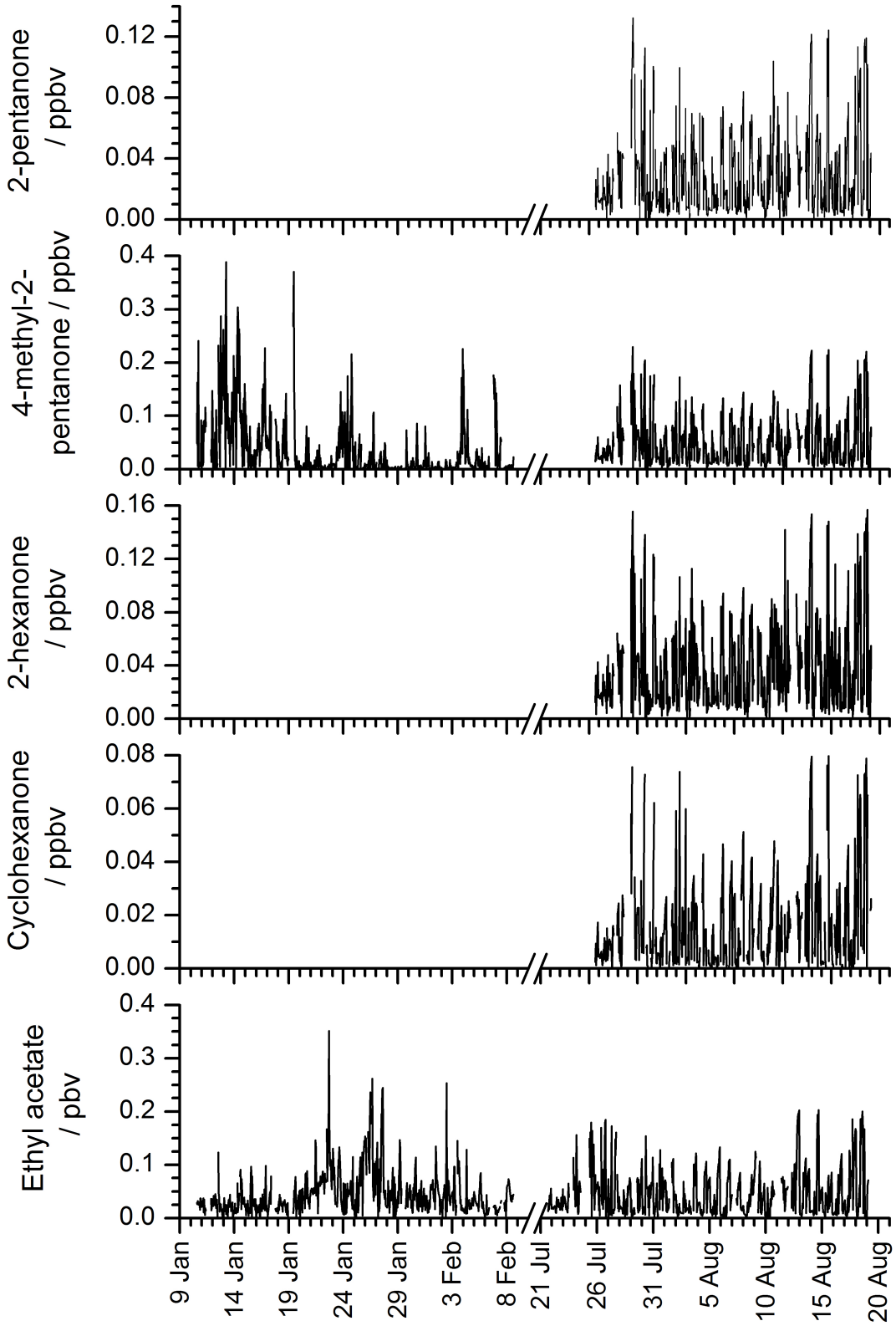

Figure 4.2: cont.

4.1.1 Diurnal profiles

The average diurnal profiles of OVOCs are shown in Figure 4.3 for the winter and summer campaigns. The winter diurnals generally show three different profiles: traffic related (acetaldehyde, benzaldehyde, ethanol, methanol), a flat profile (hexanal) and an 'other' profile that is not necessarily indicative of any particular emission source but for some appears to be driven by rapid fluctuations in their mixing ratios (butanone, ethyl acetate, butanal *etc.*). During the summer campaign, two distinct diurnal profiles are observed: species with anthropogenic emission and photochemical removal during the middle of the day, and those species that are formed from photochemical reactions showing a maxima around midday. The specific profiles in Figure 4.3 relating to the five categories are labelled with traffic, flat, other, anthropogenic and photochemical (production).

The main traffic related OVOCs during the winter campaign are; acetaldehyde, benzaldhyde and possibly methanol and 4-methyl-2-pentanone. For the latter two species, this profile is less obvious however there small rush-hour peaks seen in Figure 4.3 s and 4.3 ag. The emission of 4-methyl-2-pentanone from light-duty vehicles has been quanitified to be 0.01 mg per kg of fuel combusted.[247,248] For acetaldehyde and benzaldehyde, the traffic source is more apparent, particularly in the winter diurnal of acetaldehyde (Figure 4.3 a). Benzaldehyde and methanol (Figure 4.3 q and 4.3 s) have more spiky profiles, likely driven by some local point sources that distort the average diurnal. Benzaldehyde has been shown to be emitted from both gasoline vehicles and to a larger extent from medium-duty diesel trucks (1.27[249] and 3.80[250] mg per kg of fuel combusted respectively[248]). In summer, the main OVOCs that show a diurnal profile consistent with anthropogenic emission and photochemical removal during the middle of the day are; acetaldehyde, benzaldehyde and methanol. It is likely that these species are also emitted by the traffic-related sources in summer as seen during the winter campaign.

During the winter campaign one compound shows an almost flat diurnal profile, that of hexanal (Figure 4.3 o). This profile is mostly level during the entire diurnal, with a small 'dip' seen at approximately 12 noon. This may correspond to the changes seen in the boundary layer height (Figure 2.9), which begins to rise at around 10:00 reaches a maximum just after 12 noon and then falls to a consistent level over night from 18:00. Looking at the time series of hexanal, the mixing ratio does appear to be enhanced during the stagnant period as the start of the winter campaign.

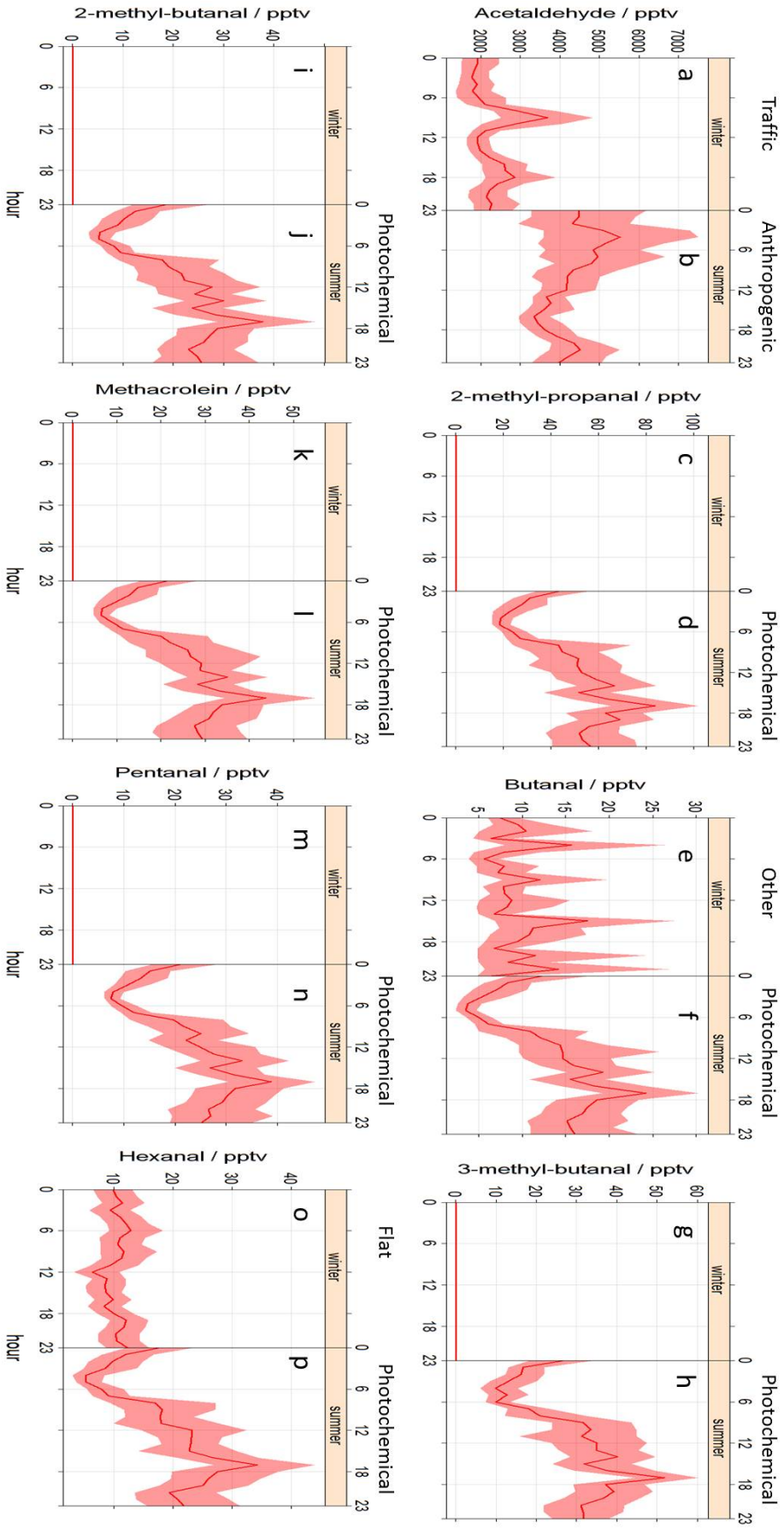

Figure 4.3: Diurnal profiles of the OVOCs in winter (left-hand side of each plot) and summer (right-hand side of each plot). Winter and summer are plotted on the same y-axes to show seasonal differences. a and b; acetaldehyde (n = 659 and 681; winter and summer, respectively), c and d; 2-methyl-propanal (n = 0 and 629), e and f; butanal (n = 647 and 613), g and h; 3-methyl-butanal (n = 0 and 624), i and j; 2-methyl-butanal (n = 0 and 583), k and l; methacrolein (n = 0 and 620), m and n: pentanal (n = 0 and 616), o and p; hexanal (n = 571 and 672). These profiles have been labelled with either traffic, flat, other, anthropogenic and photochemical (production) to help distinguish between them during discussion throughout the text. This figure was constructed using the OpenAir project for R where the solid line represents the mean daily concentration and the shaded regions shows the 95% confidence intervals surrounding the mean.[166–168]

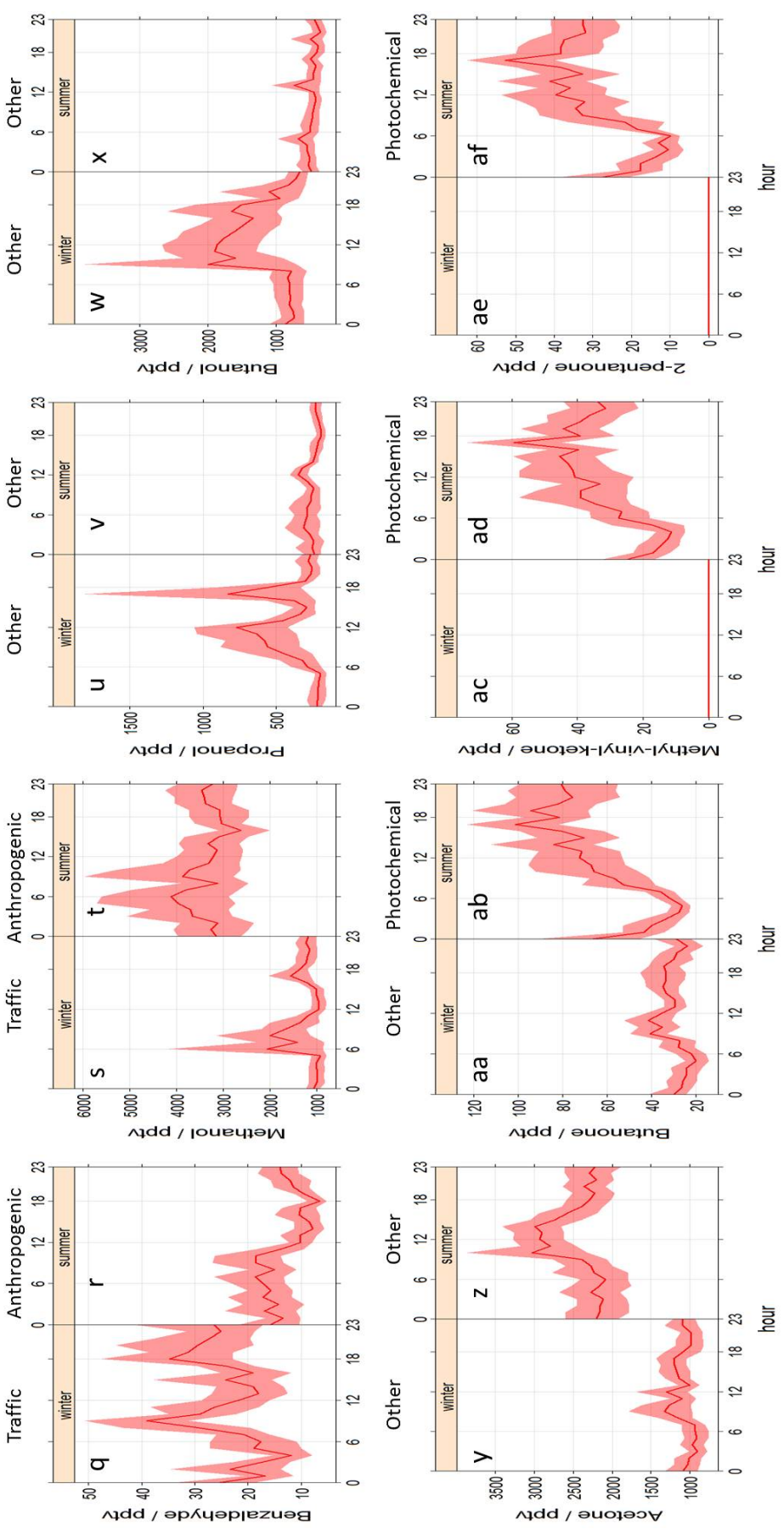

Figure 4.3: cont. q and r; benzaldehyde ($n = 627$ and 574; winter and summer, respectively), s and t; methanol ($n = 660$ and 680), u and v; propanol ($n = 657$ and 679), w and x; butanol ($n = 655$ and 668), y and z: acetone ($n = 660$ and 681), aa and ab; butanone ($n = 658$ and 634), ac and ad: methyl-vinyl-ketone ($n = 0$ and 621), ae and af; 2-pentanone ($n = 0$ and 626). These profiles have been labelled with either traffic, flat, other, anthropogenic and photochemical (production) to help distinguish between them during discussion throughout the text

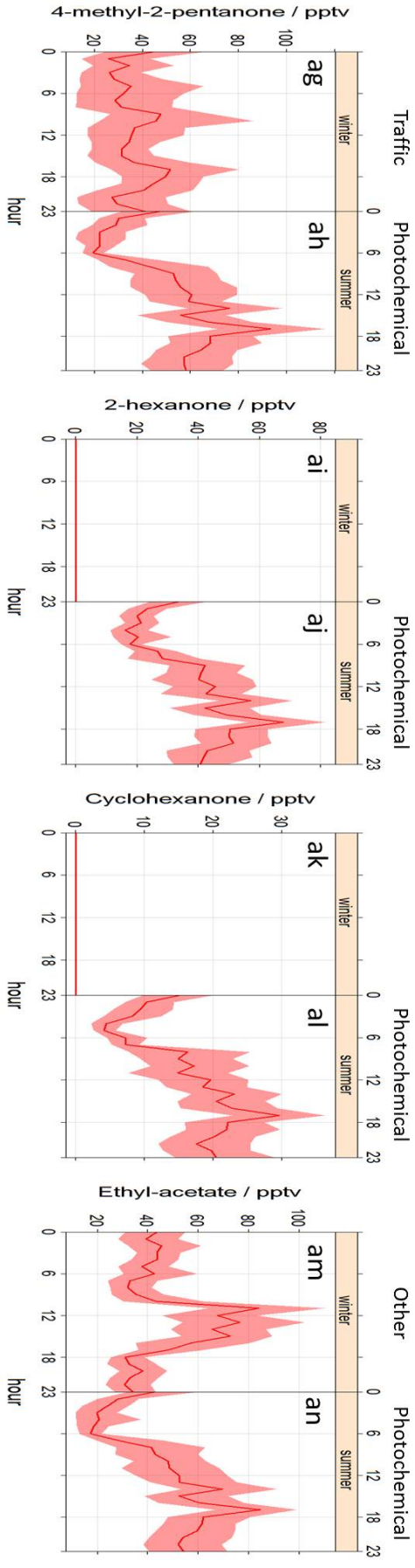

Figure 4.3: cont. ag and ah; 4-methyl-2-pentanone (n = 675 and 626; winter and summer, respectively), ai and aj; 2-hexanone (n = 0 and 626), ak and al; cyclohexanone (n = 0 and 535), am and an; ethyl-acetate (n = 675 and 620). These profiles have been labelled with either traffic, flat, other, anthropogenic and photochemical (production) to help distinguish between them during discussion throughout the text

The majority of the other OVOCs measured during the summer campaign show profiles that are consistent with secondary formation in the atmopshere from photochemical reactions of the other VOC species (2-methyl-propanal, butanal, 3-methyl-butanal, 2-methyl-butanal, methacrolein, pentanal, hexanal, butanone, methyl-vinyl-ketone, 2-pentanone, 4-methyl-2-pentanone, 2-hexanone, cyclohexanone and ethyl-acetate). These diurnal profiles show a maxima around midday, with a minimum in the early hours of the morning (just before or $\approx$ 6am).

Those OVOCs that have not been previously discussed fall into the 'other' category, where their diurnal profiles do not have any of the profiles seen in the other four categories. In both seasons, these species are propanol, butanol and acetone and additionally in winter, butanal, butanone and ethyl-acetate. The winter diurnals of butanal, propanol and butanol (Figure 4.3 e, 4.3 u and 4.3 w) are likely driven by the spiky nature of the overall time series, discussed previously. This is also likely to be the case for the summer profiles of the latter two species (Figure 4.3 v and 4.3 x). The winter profiles of butanone and ethyl-acetate (Figure 4.3 aa and 4.3 am) and profiles of acetone in both seasons (Figure 4.3 y and 4.3 z) appear to show that these species are formed during the day, with a maximum during the middle of the day at approximately 12 noon. That being said, the winter profiles of acetone and butanone could also show a small traffic related source although this is not clear.

From the diurnal profiles, three distinct groups of OVOCs became apparent: (1) direct anthropogenic emission, (2) OVOCs formed during secondary reactions and (3) OVOCs that have other sources. In an attempt to strengthen the links and evidence behind these three groups, correlations have been calculated. Correlations from both between the OVOCs and between the OVOCs and the other VOCs in the winter and summer campaigns are shown in Appendix A, Tables A.23 to A.33. During both ClearfLo campaigns, there were several OVOC and VOC species either below the detection limit of the GC×GC or not measured and as such have not been included in any of the tables. Correlations with an R^2 value of greater than or equal to 0.50 are highlighted in bold.

4.1.2 Direct anthropogenic emission of oxygenated volatile organic compounds

The OVOCs identified as having a direct anthropogenic emission are: acetaldehyde, benzaldehyde, methanol, 4-methyl-2-pentanone during the winter and only the former three in

summer. In winter, acetaldehyde shows good correlations with benzaldehyde (R^2 of 0.51) and 4-methyl-2-pentanone (R^2 of 0.56) but not methanol (R^2 of 0.26). In fact, methanol does not show much of a correlation with any of the other OVOC species, with all R^2 values of below 0.26 (except ethanol, R^2 of 0.43). In summer, the three OVOC species have better correlations with each other particularly methanol. Acetaldehyde has an R^2 of 0.58 and 0.67 with benzaldehyde and methanol respectively and the latter two have a smaller correlation with each other, R^2 of 0.49. This suggests that the anthropogenic emission contribution of methanol may be higher during the summer campaign.

With the other individual and grouped VOC species, acetaldehyde shows the strongest correlations, an average R^2 of 0.75 with 64 species. Benzaldehyde and 4-methyl-2-pentanone have smaller correlations with average R^2 values of 0.45 and 0.48 respectively. Methanol has very poor correlations with most of the other VOC species (average R^2 of 0.23). This suggests that although methanol shows a possible traffic-related diurnal profile, it only has a small proportion of its observed mixing ratio from the same source as the other three compounds. A similar pattern is followed for the three OVOC species, acetaldehyde, benzaldehyde and methanol in summer although the overall correlations are smaller for the former two and larger for methanol. From correlations with 65 VOC species, acetaldehyde has an average R^2 of 0.63, benzaldehyde 0.47 and methanol 0.45. This also suggest that methanol has more emission from anthropogenic sources in summer.

4.1.3 Secondary oxygenated volatile organic compounds

During the summer campaign, the majority of the other OVOC species measured showed diurnal profiles that were expected from species formed in the atmosphere through photochemical reactions. These were 2-methyl-propanal, butanal, 3-methyl-butanal, 2-methyl-butanal, methacrolein, pentanal, hexanal, butanone, methyl-vinyl-ketone, 2-pentanone, 4-methyl-2-pentanone, 2-hexanone, cyclohexanone and ethyl-acetate. They show strong correlations with each other during the summer and very little correlation with the anthropogenic source OVOCs. In fact, the correlations of these secondary OVOCs with the anthropogenic source OVOCs are all below an R^2 of 0.09. The average correlations of the secondary OVOCs with each other are all above R^2 of 0.86, with the majority above 0.90. There were three VOC species that do show strong correlations with the secondary OVOCs, limonene, 4-*iso*-propyl-toluene and the grouped C_{10} monoterpenes with average R^2 values of 0.84, 0.62 and 0.83 respectively. Although these three species do have strong

correlations with the secondary OVOCs, this does not necessarily mean they share a common source. The VOC species are emitted from temperature/sunlight driven biogenic sources, while the OVOCs are formed with sunlight. This means that they would share a common temporal/diurnal profile during the summer campaign.

4.1.4 Other oxygenated volatile organic compounds

The other category includes propanol, butanol and acetone in both seasons and additionally butanal, hexanal, butanone and ethyl-acetate in winter. The winter correlations of hexanal with the other OVOCs and VOC species appear to suggest a anthropogenic source that may be traffic-related. With the anthropogenic source OVOCs, the average winter correlation is R^2 of 0.46 and with the other individual and grouped VOC species, the average R^2 is 0.60. During the winter campaign, ethyl acetate does not show much of a correlation with any of the other species measured (average R^2 of -0.16). It is possible that this OVOC compound has a unique anthropogenic source in winter and given its mainly negative correlations it may be that ethyl acetate is emitted/formed at opposite times to the other species.

For the other OVOCs included in this category during winter, there appears to be two different subcategories. The first subgroup includes three species (butanal, propanol and butanol) that do not correlate with any of the other OVOC or VOC species, all R^2 values are below 0.21 and 0.33 with the OVOCs and VOCs respectively. This may suggest that these species are highly driven by very local sources as seen in the spiky influenced time series and diurnal profiles. The second subgroup includes two species (acetone and butanone) that show good correlations with the anthropogenic source OVOCs (average R^2 of 0.63) and VOCs (average R^2 of 0.61 with 64 species). In contrast, the correlations of the second subgroup with the other OVOCs is poor, average R^2 values of 0.25 for acetone and 0.24 for butanone.

In summer, the three species included in the other category are propanol, butanol and acetone. Butanol and acetone show similar summer correlations as those seen for the two species during the winter campaign. Again, butanol shows poor correlations with the other OVOC (R^2 0.08) and VOC species (R^2 0.30). Likewise acetone, again shows good, but smaller, correlations with the anthropogenic source OVOC (average R^2 of 0.66) and VOC species (average R^2 of 0.45 with 65 species) but poor correlations with the other OVOC species (average R^2 of 0.19). In contrast to the winter, propanol now has good

correlations with the anthropogenic OVOCs (average R^2 of 0.69) and the majority of the other VOC species (average R^2 of 0.58 with 65 species).

Part 2: Atmospheric ethanol in London and the potential impacts of future fuel formulations

4.2 Introduction

There is growing global consumption of non-fossil fuels such as ethanol made from renewable biomass. In the UK, gasoline currently contains 5% ethanol (E5), with the expectation that this will rise to 10% by 2020 to meet EU guidelines on renewable fuel sources.[251,252] These guidelines were implemented to meet two of Europe's key energy policy challenges; firstly, to tackle climate change by replacing fossil fuel consumption with sources of energy that emit less carbon, and secondly, to ensure there are adequate supplies of energy to reduce our reliance on imported fossil fuels.[251] In the UK, there is also the Renewable Transport Fuel Obligation (RTFO), in place since April 2008. This ensures that fuel suppliers use a minimum percentage of biofuel.[251]

The term biofuel is a generic definition to describe any solid, liquid or gaseous fuel source that is derived from biomass and used as a replacement for gasoline and diesel fuels. For gasoline, this is usually ethanol although butanol has also been considered and for diesel, this is fatty acid methyl esters (FAMEs). There are a variety of feedstocks that can be used to make biofuels, and these are categorised as first and second generation biofuels. The former are produced from biomass that is part of the foodchain such as sugar and/or starch crops, *i.e.* maize, wheat or seeds such as oil seeds or palm oil for bioethanol. The latter are made from biomass that is not part of the foodchain. These biofuels can be used in two forms for the transport sector, either in a pure form or, more usually, blended with gasoline and diesel.[251]

Ethanol can be blended with gasoline in a variety of mixtures, the most common in Europe is E5, in North America E10 (10% ethanol) and Brazil E85 (85% ethanol) or pure ethanol. In fact, the US and Brazil combined represent more than 90% of the world's production and consumption of bioethanol.[253,254] Although, high strength blends are used around the globe, this fuel is generally not used in the EU. The situation in Brazil is more complex due to the introduction of flexible fuelled vehicles (FFV). These vehicles can run on normal gasoline, pure ethanol and any blends of the two using only one fuel tank. The engines in FFVs can automatically adapt and make changes to the ignition timing based on the specific fuel blend using a ethanol/gasoline sensor.[255]

Blending gasoline with ethanol has many advantages; it increases the combustive potential of the fuel,[256] improves some of the engines running processes and can decrease the emission of certain pollutants to the air.[253] The emissions of CO, tailpipe PM and hydrocarbons are generally reduced, however the emissions of NO_x are more variable, with

some studies suggesting a reduction,[253] while others report increases.[257]

Studies of low strength ethanol blended fuels suggest that there is no consistent change in the emissions of NO_x and that emissions of other regulated pollutants are decreased (CO -13%, total hydrocarbon -5%, PM, benzene -12% and 1,3-butadiene -6%). However, there is a significant increase in the emission of acetaldehyde (+159%), an unregulated and toxic pollutant. This large scale emission of aldehydes during combustion is the main disadvantage of using alcohol blended fuels.[1,251] Despite the increase in use of ethanol, there have only been sporadic measurements around the globe, largely focused in Brazil and the US as they use large quantities of ethanol-blended fuels.[253]

Both pure ethanol and blended ethanol generate significant concentrations of acetaldehyde, formaldehyde, considerable levels of vaporized ethanol, and also benzaldehyde during combustion.[258,259] There have been no large-scale studies on the toxicological effects of atmospheric concentrations of these pollutants. However, acetaldehyde and formaldehyde are suspected carcinogens due to their ability to form adducts with DNA.[260] These pollutants have also been associated with respiratory irritation, asthma aggravating effects[261] and bronchitis in both outdoor and indoor environments.[253] Benzaldehyde is also a known nerve-toxin that can cause brain damage when people are exposed to high concentrations.[262]

Still the main concern when using biethanol blends remains the emission of acetaldehyde. By combining the degradation rates of acetaldehyde and its products, the exposure to ethanol combustion products can be estimated to be approximately 10 days.[253] This is a considerable time period where a large amount of the urban and rural population could be exposed, of specific concern to the increasing number of asthma and allergy sufferers present in urban areas. Depending on the local atmospheric conditions, acetaldehyde degradation can vary from 11 hours to up to 5 days.[39] As part of the degradation process, acetic acid is generated which has a lifetime of $\approx$ 130 hours.[253] This is also a product of bioethanol combustion.[252]

The UK NAEI currently does not include a road transport or evaporative gasoline source for ethanol,[144] rather its main source is spirit manufacture, shown in Figure 4.4. This is likely due to the fact that the VOC source apportionment part of the emission inventory was last updated in 2002 and ethanol was first introduced in gasoline blends in 2003. An assumption is made that the speciation profile of each emission source sector is unchanged each year, except for the specific VOCs benzene and 1,3-butadiene.[263] Ac-

etaldehyde, in contrast has approximately 70% contribution from road transport to total UK emissions, Figure 4.5.

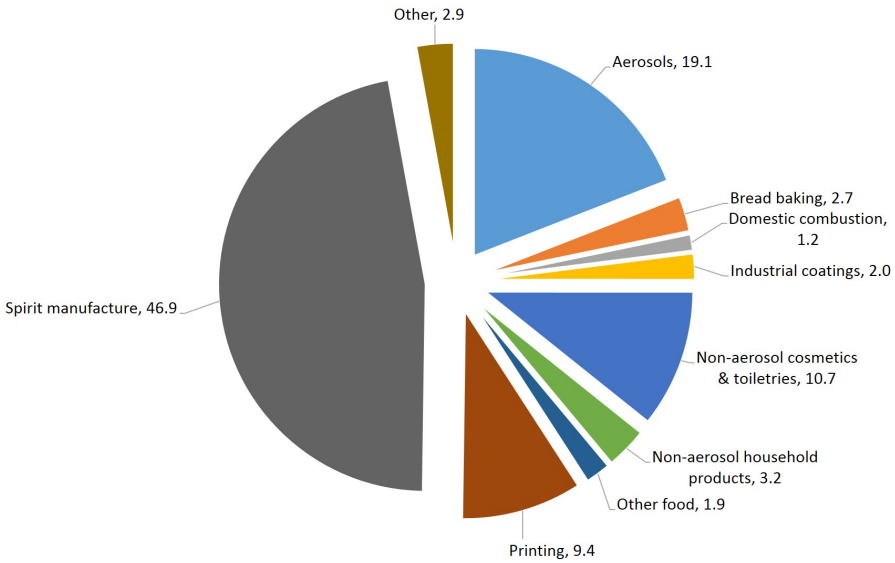

Figure 4.4: Emission source contributions for ethanol from the NAEI. The Other category refers to the sum of categories that have less than 1% each: agrochemicals use, brewing, chemical industry, cider manufacture, coating manufacture, domestic adhesives, film coating, glass, industrial adhesives, landfill, non-aerosol automotive products, other industrial combustion (wood), paper printing, solvent and oil recovery, textile coating and wine manufacture.[144]

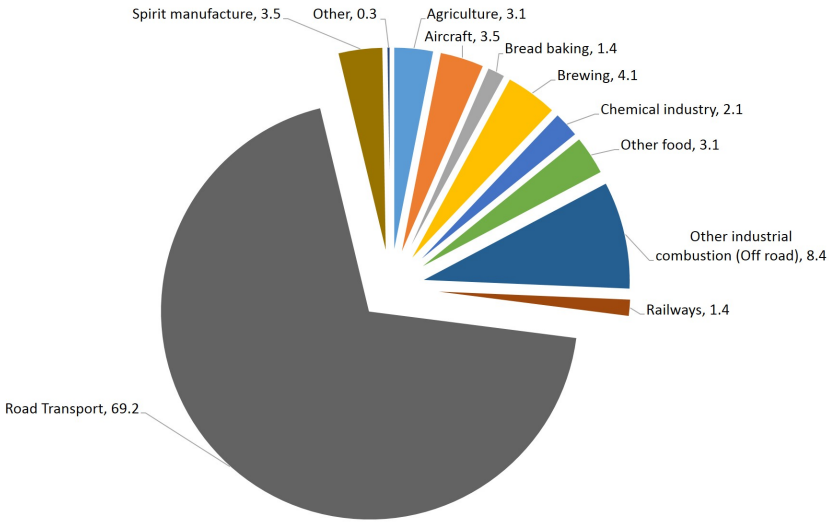

Figure 4.5: Emission source contributions for acetaldehyde from the NAEI. The Other category refers to the sum of categories that have less than 1% each: cement (non-de-carbonising), glass, house and garden machinery, miscellaneous-landfill gas, power stations, public services and solvent and oil recovery.[144]

The MCM degradation scheme for the reaction of ethanol with the OH radical is shown in Figure 4.6.[71] Ethanol, acetaldehyde and formaldehyde are highlighted in the

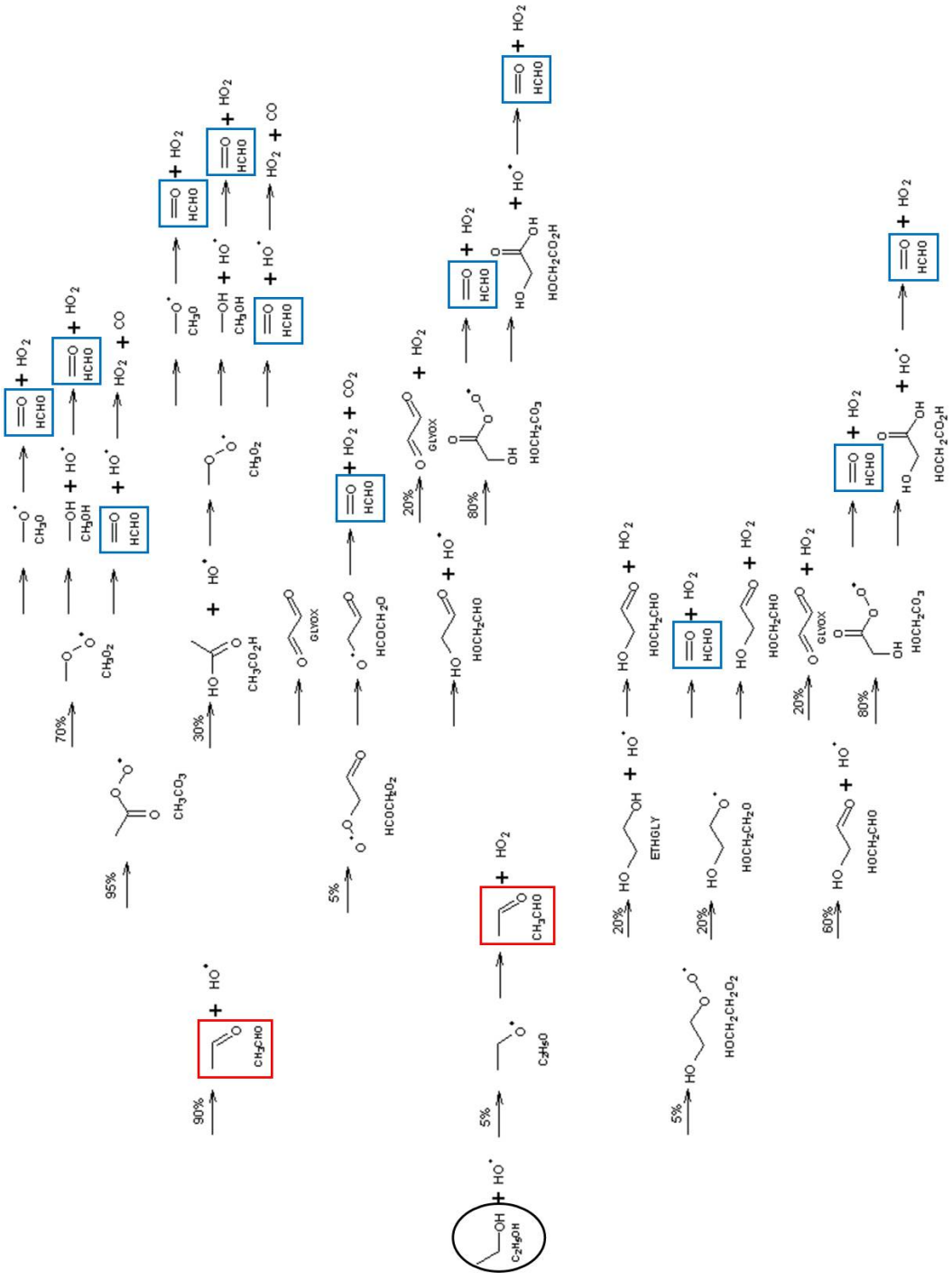

Figure 4.6: Chemical mechanism reaction pathways for the degradation of ethanol with the OH radical. [71] Ethanol is circled in black, with acetaldehyde boxed in red and formaldehyde boxed in blue

scheme with a black circle, red boxes and blue boxes respectively. This scheme shows that potentially 95% of ethanol can directly form acetaldehyde through reactions with the OH radical. The degradation of ethanol also has multiple routes to form formaldehyde. Given that the acetaldehyde measured during the ClearfLo campaigns can provide an average of 0.96 s^{-1} OH reactivity and 30.3 $\mu g\ m^{-3}$ potential ozone formation, the degradation of ethanol into acetaldehyde can have significant effects on air quality.

4.3 Results

Figure 4.7 shows the winter and summer time series of atmospheric ethanol mixing ratios in London measured during ClearfLo. There are extended periods during both campaigns with high levels of ethanol. During the winter and summer IOPs, the mean and maximum ethanol mixing ratios observed were: winter mean 5 ppb, winter maximum 38 ppb, summer mean 5 ppb and summer maximum 34 ppb. The high sustained levels of ethanol during the winter campaign correspond to the low wind, stagnant periods discussed in Chapter 2, Section 2.5.3.1. Ethanol is the most abundant VOC present in London air and may be a significant contributor to the OH sink budget and potential O_3 formation.

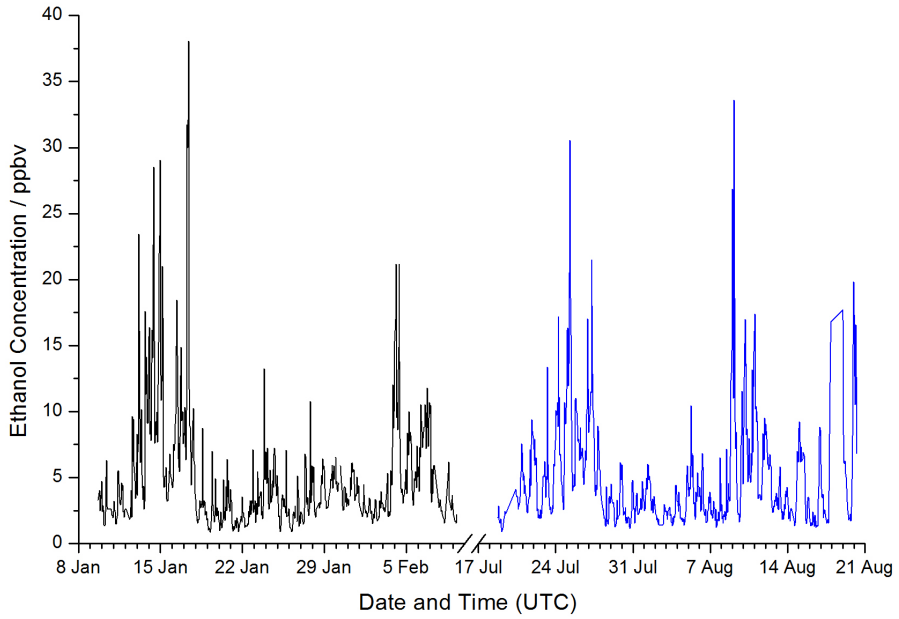

Figure 4.7: Time series of ethanol in the winter (left panel, black) and summer (right panel, blue)

The campaign average contributions of ethanol to mixing ratio, primary hydrocarbon OH reactivity and potential O_3 formation are shown in Figure 4.8. For all three statistics, the winter contribution is higher although only slightly for mixing ratio. As the most

abundant VOC, ethanol contributes 11% and 14% to the winter and summer observed total VOC mixing ratios respectively. For OH reactivity and OFP, the contribution of ethanol is smaller due to its lower reactivity (k_{OH} of 3.2×10^{12} cm^3 molecule^{-1} s^{-1}) and potential O_3 formation (MIR value of 1.53 g O_3 g VOC^{-1}). In winter, ethanol contributes 6.7% to both OH reactivity and OFP, whereas in summer the contribution is larger, 7.8 and 8.8%, respectively. It is likely the summer increase is due to a disproportionate loss of other reactive hydrocarbons, while the observed ethanol mixing ratio is consistent in both seasons.

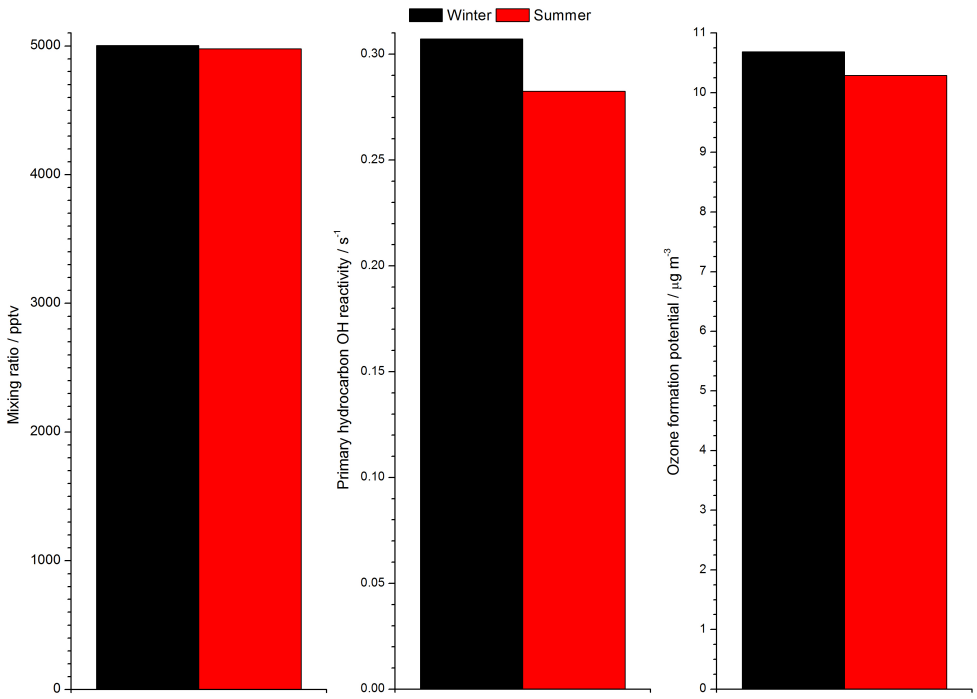

Figure 4.8: Winter (black column) and summer (red column) campaign average mixing ratio, primary hydrocarbon OH reactivity and ozone formation potential for ethanol

The average winter diurnal profiles of ethanol and acetaldehyde are shown in Figure 4.9. These profiles suggest a dominant traffic related source given the apparent rush-hour peaks observed. In summer however, the average diurnals are largely influenced by meteorology (*i.e.* the fluctuations in the boundary layer height throughout the day) and photochemical processes.

In both seasons, ethanol has high correlations with gasoline related species, such as benzene, toluene, xylenes, acetylene and small carbon number aliphatic compounds. Interestingly, the correlation of ethanol with isoprene, limonene and grouped C_{10} monoterpenes is high in winter, due to a dominant traffic emission, but very low in summer when a bio-

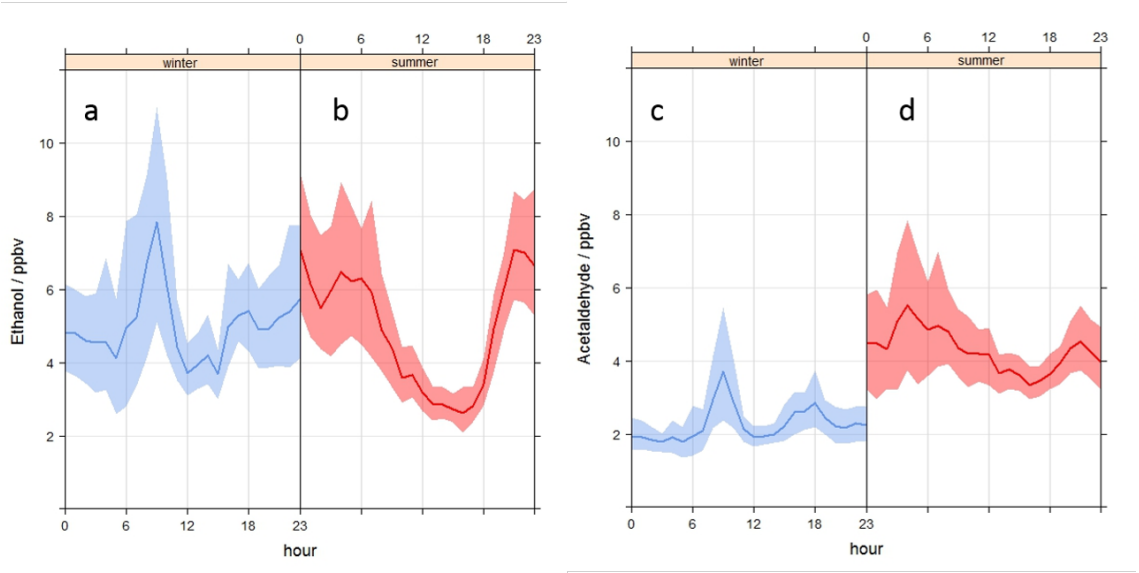

Figure 4.9: Diurnal profiles of ethanol (a and b) and acetaldehyde (c and d) in winter (left-hand side of each plot, blue) and summer (right-hand side, red). All four plots have the same y-axis scale to aid direct comparison. This figure was constructed using the OpenAir project for R where the solid like represents the mean daily concentration and the shaded regions show the 95% confidence intervals surrounding the mean.[166–168]

genic source is dominant for the other species. These correlations are shown in Table 4.2 and 4.3, for the individual and groups species respectively. Values in bold indicate correlations with R^2 values of greater than 0.75. During both campaigns, ethanol has a poor correlation with many of the other OVOC species likely due to the fact that ethanol has a direct anthropogenic source that is present in both seasons while the majority of the OVOCs, particularly in summer, are dominated by a photochemical production source.

The relationship between the mixing ratios of ethanol and acetaldehyde is shown in Figure 4.10. The winter equation of the linear regression is y = 2.12 (± 0.07) x + 0.24 (± 0.19) and for summer is y = 1.12 (± 0.03) x + 0.17 (± 0.14). The correlation of the these two species is high with R^2 values of 0.78 in winter and 0.82 in summer. The approximate ratio of ethanol:acetaldehyde changes from 2:1 in winter to 1:1 in summer. The correlation values of selected species with ethanol are shown in Figure 4.11, for winter (left column) and summer (right column). These species have first been ordered according to emission source, then by carbon number. In both seasons, ethanol has high correlations with gasoline related species, such as benzene, toluene, *iso*-octane (2,2,4-trimethyl pentane) and small carbon number aliphatic compounds, *n*-butane and 1,3-butadiene. Ethanol shows a stronger relationship in winter with petrol species that have a dominant combustion emission source (*n*-butane and 1,3-butadiene), whereas those with a more evaporation

Table 4.2: Correlation of all individually quantified VOCs with ethanol during the ClearfLo campaign, values in bold indicate R^2 correlations of greater than 0.75

	Correlation with Ethanol			Correlation with Ethanol	
Compound	**Winter**	**Summer**	**Compound**	**Winter**	**Summer**
Saturated			**Aromatics continued**		
Methane	**0.88**	0.75	m- and p-Xylene	**0.88**	**0.90**
Ethane	**0.86**	**0.81**	o-Xylene	**0.86**	**0.90**
Propane	**0.89**	**0.89**	Benzene, iso-propyl-	0.71	-
n-Butane	**0.89**	**0.85**	Benzene, propyl-	**0.84**	0.67
iso-Butane	**0.86**	**0.84**	Toluene, 3-ethyl-	**0.85**	0.68
n-Pentane	**0.91**	**0.88**	Toluene, 4-ethyl-	**0.77**	0.66
iso-Pentane	**0.89**	**0.87**	Benzene, 1,3,5-trimethyl-	**0.82**	0.73
Cyclopentane	**0.76**	**0.82**	Toluene, 2-ethyl-	**0.78**	0.63
n-Hexane	**0.91**	**0.79**	Benzene, 1,2,4-trimethyl-	**0.79**	0.60
Pentane, 2+3-methyl-	**0.89**	**0.88**	Toluene, 4-isopropyl-	0.63	0.31
n-Heptane	**0.80**	**0.84**	Benzene, 1,2,3-trimethyl-	**0.88**	**0.72**
Butane, 2,2,3-trimethyl-	**0.83**	**0.85**	Indan	**0.84**	-
n-Octane	**0.90**	**0.85**	Benzene, tert-butyl-	0.28	0.41
Pentane, 2,2,4-trimethyl-	**0.80**	**0.87**	Benzene, 1,3-diethyl-	**0.86**	0.61
n-Nonane	**0.88**	**0.77**	Benzene, 1,4-diethyl-	**0.86**	**0.79**
n-Decane	**0.89**	0.65	Naphthalene	**0.83**	0.66
Nonane, 2-methyl-	**0.83**	0.66	**Oxygenates**		
n-Undecane	**0.88**	**0.86**	Acetaldehyde	**0.89**	**0.91**
n-Dodecane	**0.88**	**0.79**	Propanal, 2-methyl-	-	0.14
Unsaturated			Butanal	0.49	0.19
Ethene	**0.88**	**0.85**	Butanal, 3-methyl-	-	0.18
Acetylene	**0.90**	**0.86**	Butanal, 2-methyl-	-	0.17
Propene	**0.86**	**0.81**	Methacrolein (MACR)	-	0.16
Propadiene	**0.88**	**0.81**	Pentanal	-	0.19
Propyne	-	**0.79**	Hexanal	**0.87**	0.24
Butene, trans-2-	**0.88**	**0.82**	Benzaldehyde	0.69	0.72
1-Butene	**0.91**	**0.82**	Methanol	0.66	0.81
iso-Butene	**0.90**	**0.89**	Ethanol	-	-
Butene, cis-2-	**0.88**	**0.82**	Propanol	0.54	**0.85**
1,2-Butadiene	-	-0.17	Butanol	0.49	0.62
1,3-Butadiene	**0.88**	**0.75**	Acetone	**0.80**	0.75
Pentene, trans-2-	0.43	**0.83**	Butanone	**0.81**	0.31
1-Pentene	0.49	**0.88**	Ketone, methyl-vinyl- (MVK)	-	0.19
Isoprene	**0.90**	0.11	Pentanone, 2-	-	0.15
Styrene	**0.80**	0.41	Pentanone, 4-methyl-2-	0.70	0.22
α-Pinene	-0.37	0.36	Hexanone, 2-	-	0.17
Limonene	**0.90**	0.27	Cyclohexanone	-	0.18
Aromatics			Acetate, ethyl-	-0.48	0.23
Benzene	**0.87**	**0.91**	**Halogenated**		
Toluene	**0.89**	**0.91**	Methane, dichloro	**0.85**	**0.78**
Benzene, ethyl-	**0.85**	**0.90**	Trichloroethylene	-	**0.85**

Table 4.3: Correlation of the grouped species with ethanol during the ClearfLo campaign, values in bold indicate R correlations of greater than 0.75

	Correlation with Ethanol	
Grouped species	**Winter**	**Summer**
C_6 Aliphatics	**0.79**	0.74
C_7 Aliphatics	**0.85**	**0.77**
C_8 Aliphatics	**0.87**	**0.78**
C_9 Aliphatics	**0.85**	0.73
C_{10} Aliphatics	0.71	0.70
C_{11} Aliphatics	**0.87**	0.65
C_{12} Aliphatics	**0.85**	0.65
C_{13} Aliphatics	**0.88**	0.70
C_4 substituted monoaromatics	**0.86**	0.72
C_{10} Monoterpenes	**0.87**	0.17

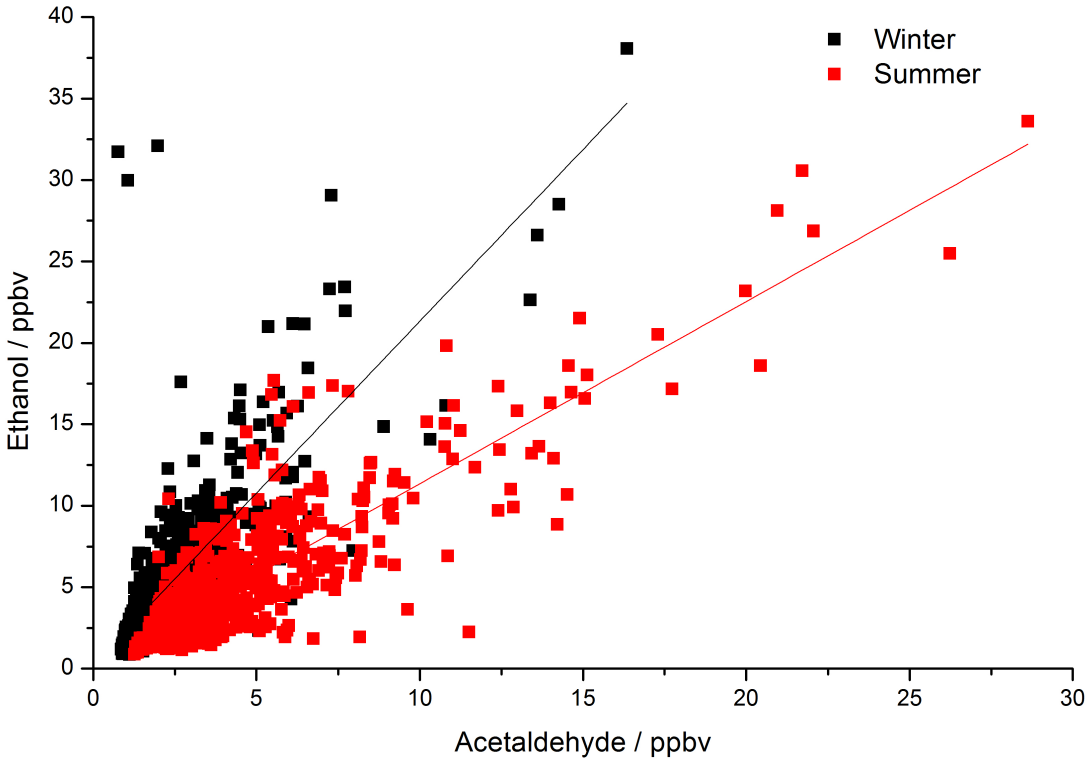

Figure 4.10: Correlation of ethanol and acetaldehyde in the winter (black) and summer (red) campaigns

related emission have higher summer correlation values (benzene, toluene and *iso*-octane). The correlation between ethanol and CO, a combustion tracer, is stronger in winter than summer, but the summer value is still high (R of 0.90 and 0.83 in winter and summer respectively). Interestingly, the correlation between ethanol and isoprene is high in winter, due to a dominant traffic emission, but very low in summer when the biogenic emission

source is dominant for isoprene.

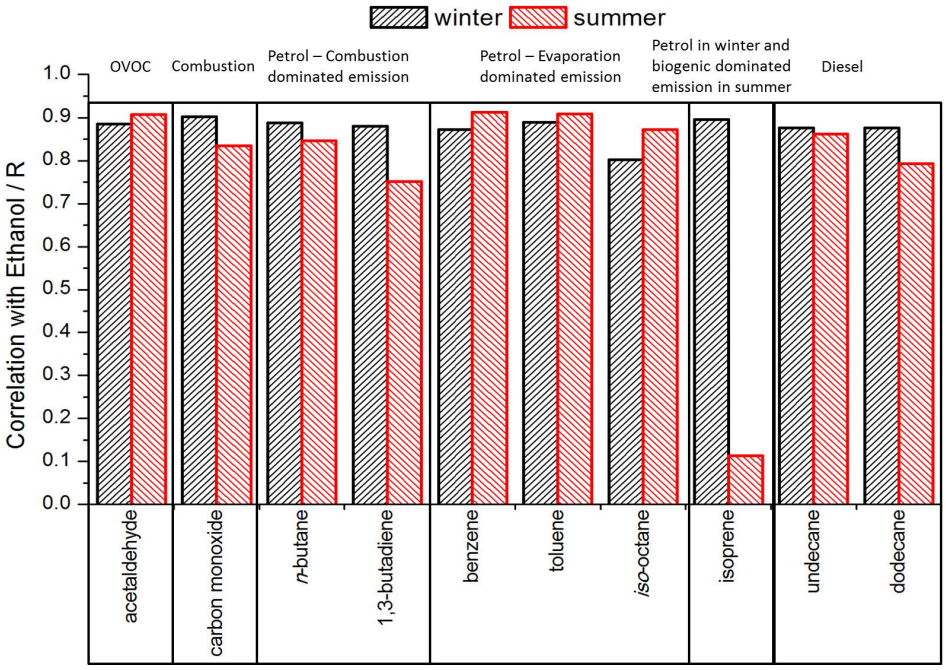

Figure 4.11: Correlation of selected compounds with ethanol in winter (left column) and summer (right column), grouped by emission source and ordered by carbon number

The most likely anthropogenic source of ethanol in London is related to gasoline use given the diurnal profiles (Figure 4.9) and strong correlation with other gasoline related emissions (Figure 4.11). The correlation between ethanol and benzene, toluene and *iso*-octane in summer are marginally higher than those in winter, which could be indicative of mutual evaporative emission from gasoline use and storage during periods of higher ambient temperatures (average summer temperature of 19.7 °C). In contrast, in winter (where temperatures are much lower, average winter temperature of 4.8 °C) a higher correlation is seen for compounds more likely to be from the combustion of gasoline, *i.e.* 1,3-butadiene and CO. This suggests that the emission of ethanol is a combination of both emission sources, with combustion of ethanol-blended fuels a larger source in winter and evaporation more important in summer.

4.3.1 Effect of ethanol content on acetaldehyde

Vasconcellos *et al.*, (2005) studied the use of ethanol-blended fuels in Brazil. Generally, in urban areas there are higher observed mixing ratios of formaldehyde than acetaldehyde. However, in Brazil, where there is significant use of ethanol-blended fuels, the formaldehyde/acetaldehyde (f/a) ratio was usually quite low (in some cases less than 1), suggesting

that large quantities of acetaldehyde were either being directly emitted or formed in the atmosphere through photochemical processes.[264] Some studies use f/a ratios to suggest what the sources of these compounds are, a ratio of less than one is taken as direct emission while a ratio greater than one is representative of in situ photochemical formation.[264–266] Figure 4.12 shows the f/a ratio from the winter (left, black) and summer (right, blue) ClearfLo campaigns in London.

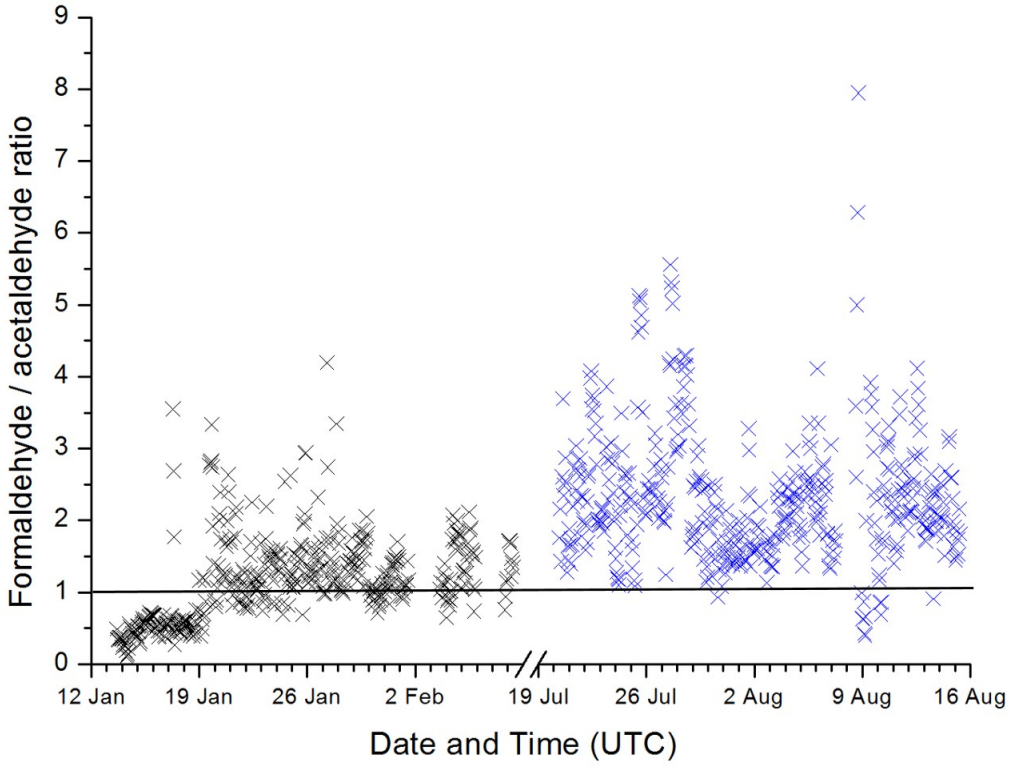

Figure 4.12: Time series of the formaldehyde/acetaldehyde ratio from the winter (left, black) and summer (right, blue) campaigns.

The measurements from London show a mix of the two different ratio conditions, with significant periods during the winter campaign where the ratio is <1. This suggests that the use of 5% ethanol in gasoline in the UK is directly emitting acetaldehyde into the atmosphere. However, during the summer campaign, the ratio is much larger overall with very few points below 1. However, the values are also < 1 during the period of the 8-9th August, where the atmospheric concentrations are dominated by emission into a low boundary layer and limited chemistry. The ratio values in summer could suggest that the majority of acetaldehyde observed during this season is formed in the atmosphere through photochemical processing of a range of VOCs, however, this is not what has been shown from the diurnal profile of acetaldehyde or correlations of this species with other

compounds measured during the ClearfLo campaigns (discussed in Section 4.1.2). This could also be due to the evaporative emission of ethanol from gasoline use/storage into the atmosphere, which reacts with the OH radical to form acetaldehyde directly. Interestingly, the large portion of less than 1 ratios in the winter campaign, is during the stagnant, high pressure highly polluted periods. It is possible that this ratio is due to the accumulation of large concentrations of acetaldehyde in a lower boundary layer than would normally be observed. It must be noted, however, that these ratios are most useful for determining the source of acetaldehyde in areas where there is a large use of high ethanol blended gasoline, such as Brazil where the most used blend is E85. This is not the case in the UK, or London, where only E5 is used. However the fact that the f/a ratio is quite low and at some points below 1, does indicate that there is a significant source of the acetaldehyde directly emitted into the atmosphere.

4.3.2 Impacts of ethanol blended fuel use on air quality

4.3.2.1 Modelling using the Master Chemical Mechanism

A zero-dimensional photochemical box model, based on MCMv3.2 was used to investigate the local impact of current ethanol use on acetaldehyde concentrations. The MCM model was run in an analogous way as to that described in Lee *et al.* (2015).[267] Full details of the kinetic and photochemical data used as part of the model mechanism are available from the MCM website (http://mcm.leeds.ac.uk/MCM). A subset of the MCM was used in the model that treated the degradation of simultaneously measured trace VOC species, CH_4 and CO following oxidation initiated by OH, O_3 and NO_3, which included ~15,000 reactions and ~3,800 species. The model was constrained to *in-situ* measurements made at the North Kensington site of; NO, NO_2, O_3, HONO, CO, CH_4, 64 individually quantified VOC species from both GC systems, many more VOCs quantified in a grouped analysis (as detailed in Dunmore *et al.* (2015)[268]) PAN, HCHO, water vapour, temperature, pressure and photolysis rates. Model inputs were made every 15 minutes with the measured data either averaged or interpolated to 15 minute intervals if the species was measured more or less frequently, respectively. Only the summer IOP was modelled here, owing to the availability of extensive radical measurements. The model was constrained to the measured concentrations of all species, except acetaldehyde. Acetaldehyde formed photochemically from ethanol in the model simulations was tagged in the resulting data, so that it could be identified as being formed directly from ethanol.

Modelling results of the impacts of measured ethanol emissions on the concentrations of atmospheric acetaldehyde in London are shown in Figure 4.13. On average, 6.5% of the acetaldehyde observed in London was a result of the photochemical oxidation of ethanol. Although the levels of acetaldehyde from the model degradation of ethanol (Figure 4.13, black filled area) are relatively consistent and show a stable diurnal pattern throughout the campaign, there are periods where ethanol produces up to 18% of the observed acetaldehyde. The profile of the total modelled acetaldehyde (black and red filled areas) shows a diurnal variation typical of photochemical production and loss, with ethanol contributing around 16% of the acetaldehyde produced in the model. However, it is clear that the detailed photochemical model simulation significantly under estimates the levels of acetaldehyde observed in London. This discrepancy is most likely due to a direct emission of acetaldehyde into the atmosphere from vehicle emissions, given the diurnal profile observed in Figure 4.9. This also means it is possible that the percentage of the acetaldehyde produced from ethanol oxidation is underestimated. This has been investigated further in Dunmore *et al.,* (2015) using a GEOS-Chem chemical model to simulate the regional, rather than local, impacts of ethanol blended gasoline use.[269]

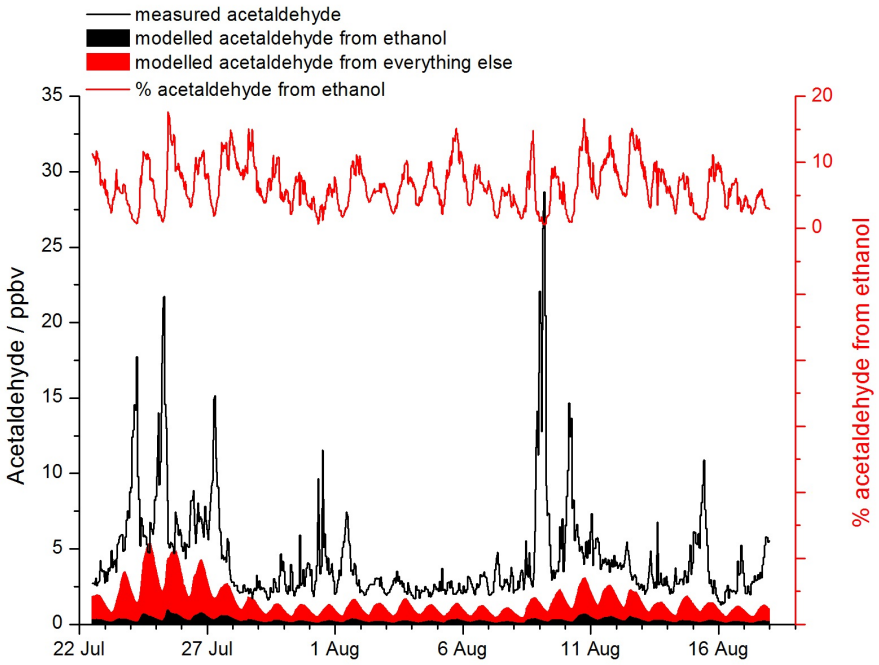

Figure 4.13: Modelling results of the impacts of current levels of ethanol observed in London. The measured acetaldehyde during the summer campaign (black), acetaldehyde formed in the model from the reaction of OH and ethanol (black filled area) and other photochemical acetaldehyde sources in the model (red filled area) are plotted on the left y axis. The percentage of the measured acetaldehyde that was directly formed from ethanol (red) is plotted on the right y axis

A study by de Gouw *et al.,* (2012) found that the ethanol emitted from the use of E10 in the US produced 20% of the acetaldehyde formed from other sources on the first day of photochemistry. They also found that on the second day this value increased to 90%, suggesting that the larger impact of ethanol emissions from fuel would be felt further away from the emission source.[254] It is worth noting that the US study only inputs 800 ppt of ethanol, while an average of 5 ppb of ethanol was observed during both ClearfLo campaigns implying that the impact of ethanol blended gasoline use in the UK could be more significant. Also worth noting is that while ethanol does not react particularly fast with the OH radical (kOH (298 K) = 3.2×10^{-12} cm^3 molecule^{-1} s^{-1})[270] or produce significant quantities of O_3 (1.53 g O_3 g VOC^{-1}[193] a relatively low maximum incremental reactivity (MIR) coefficient, a proxy for O_3 formation), the direct emission and photochemical production of large quantities of acetaldehyde (a compound which reacts rapidly with OH, kOH (298 K) = 15×10^{-12} cm^3 molecule^{-1} s^{-1},[270] and has a high MIR coefficient, 6.54 g O_3 g VOC^{-1})[193] indicates that the impacts of the use of ethanol fuels should not be judged solely on the reactions of ethanol.[271]

Conclusion

A total of 21 OVOC species were quantified as part of the ClearfLo study. From the analysis of this large suite of OVOC species, it is possible to conclude that there are significant quantities of these species both directly emitted to and formed through secondary processes in the atmosphere. During both ClearfLo campaigns, the dominant OVOCs measured were ethanol, acetaldehyde, methanol, butanol and acetone. These five species provided 95% and 96% of the total observed OVOC loading during winter and summer respectively. In terms of OH reactivity and potential ozone formation, the contribution of acetaldehyde was shown to be dominant in both seasons and as such it is a very important OVOC species. There were two main categories of OVOC species identified, those with a direct anthropogenic emission source and those formed in the atmosphere through photochemical reactions. The species identified as being directly emitted from an anthropogenic source are acetaldehyde, benzaldehyde and methanol in both seasons and 4-methyl-2-pentanone in winter. This was postulated to be from traffic emissions given their diurnal profiles and correlations with traffic-related VOC tracers. The majority of the other OVOC species fall into the second category, especially during the summer campaign, as being directly formed in the atmosphere. However, there were some compounds which did not fall into either category. These compounds were either highly influenced by large fluctuations in the observed data suggesting a very local emission source (propanol, butanol and the winter observation of butanal) or possibly had a small contribution from traffic emissions (acetone and the winter observation of butanone). OVOCs are not routinely measured in urban areas, however this chapter has shown that they can have significant impacts of the oxidative capacity of the atmosphere given their fast reactions with the OH radical and can form considerable amounts of ozone thus impacting air quality.

Two OVOCs of particular interest are ethanol and its oxidation product, acetaldehyde. The first half of this chapter has shown that both compounds were very important contributors to the total OVOC mixing ratio. Acetaldehyde was also the major contributor

to OH reactivity and potential ozone formation. As part of the UK government's commitment to renewable and sustainable fuel use, gasoline that is currently sold in UK forecourts must contain approximately 5% ethanol that is manufactured as a biofuel. Ethanol was the most abundant VOC in London's atmosphere during the winter and summer ClearfLo campaigns, and significant amounts of acetaldehyde were also observed. The diurnal profiles and correlation of these two species with other VOCs have shown that their main emission source is likely to be a combination of combustion and evaporative emissions from the use of ethanol blended gasoline. Detailed photochemical MCM simulations of the local scale impacts of measured ethanol has shown that, although ethanol does not seem to produce significant local levels of acetaldehyde, the model can not accurately reproduce the observed profile of acetaldehyde, due to the presence of a direct emission into the atmosphere, with strong evidence that this is related to traffic emissions. It is clear that there are significant traffic related emissions of ethanol in urban areas and that these are not currently included in emission inventories. Given the long lifetime of ethanol in the atmosphere, the full effects of its emission and the subsequent production of acetaldehyde may not be seen at the emission source location but rather downwind. Although increased use of bioethanol in European fuel may help reduce net carbon dioxide emissions there is a suggestion that there is the potential for an inadvertent impact on air quality, which should be monitored through the transition.

Chapter 5

Development of a combined heart-cut and comprehensive two dimensional gas chromatography system to extend the carbon range of volatile organic compounds analysis in a single instrument

This chapter details the development of a GC-GC×GC-2FID instrument to measure a wider carbon number range of VOCs in a tropical atmosphere, with particular emphasis on the quantification of isoprene.

5.1 Introduction

VOCs play a central role in the atmosphere through reactions which can produce secondary pollutants such as SOA and O_3, both of which are detrimental to health. VOC measurements can be either; offline, where the sample is collected and stored in a canister for analysis back at the lab, or online in the field. There are a variety of instruments designed to measure the atmospheric concentrations of VOCs. One of the most common methods of VOC analysis, both off and online, is TD-GC-FID/MS.[100]

Commonly, VOC measurements span a range of C_2-C_8; including alkanes, alkenes and simple aromatic compounds such as benzene, toluene and xylenes. This select group of VOCs are routinely measured in many countries for compliance with air quality policy, however there are potentially many thousands of VOC compounds that are not measured and as a result their influence on local processes and secondary pollution generation is not well established. The situation is further complicated by the exponential increase in structural isomers with increasing carbon number.[103]

Measurement of higher carbon number VOCs is much rarer than small chain hydrocarbons. The previous measurement approach, detailed in Chapter 2, was using GC×GC,[268] which can increase the number of VOC species identified in complex mixtures, such as urban air, when compared to single column GC.[110] The combination of two GC columns with different selectivities is particularly effective at resolving compounds with similar boiling points but different polarities, such as alkanes from aromatics and also OVOCs.[109]

Figure 5.1 shows the isoprene mixing ratios observed from the two GC instruments deployed during the ClearfLo campaign (see Chapter 2 for details). The DC-GC instrument (lower panel) was capable of accurately measuring the concentrations of isoprene, however the GC×GC instrument was not, with the signal looking like noise (seen in the upper panel of Figure 5.1). It is likely this is due to the incomplete separation of isoprene from the aliphatic band in the unresolved 'blob' at the start of the chromatogram, shown in Figure 5.2.

Isoprene has been shown to be extremely important in tropical regions, particularly those with forested areas.[272] The instrument would eventually be deployed to characterise a tropical, marine influenced atmosphere, where the observation of isoprene is rather important. However, it has been shown in Figure 5.1 for isoprene, that this method could not accurately analyse small carbon chain VOCs. Due to this, the instrument would need to be further developed. The overall aim of this development was to extend the carbon

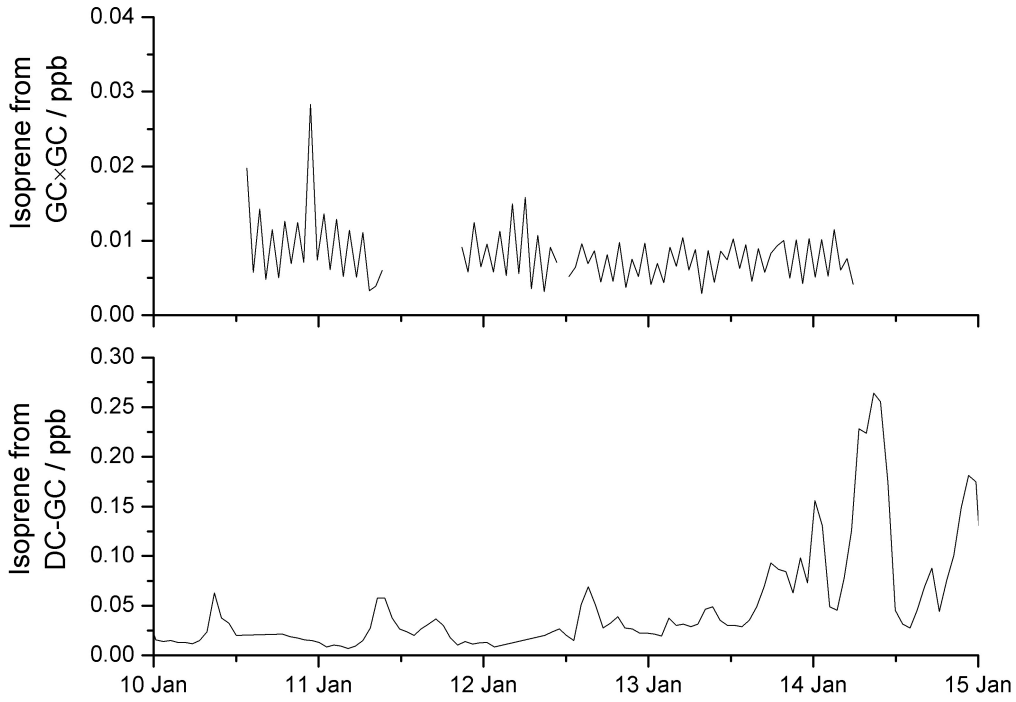

Figure 5.1: Isoprene concentrations from the DC-GC (lower) and GC×GC (upper) instruments during the winter ClearfLo campaign. Note: very different scales.

range of VOCs that could be quantified using a single instrument, however, the particular focus was to be able to accurately and reproducible measure isoprene as well as larger carbon number species. This is not routinely done using a single GC×GC setup, which is where a combined multidimensional GC system would be ideal.

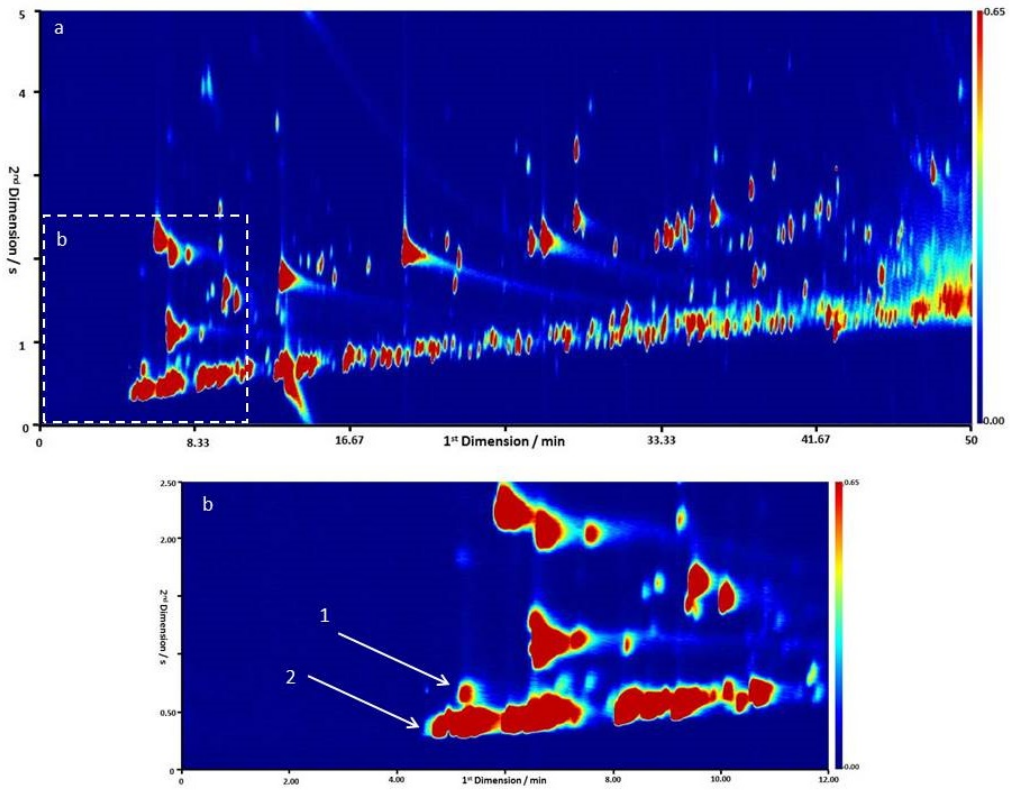

Figure 5.2: Typical GC×GC plot from the ClearfLo campaign, a: full time scale image with box around isoprene area, b: zoom in on isoprene (arrow 1) to display lack of separation from rest of aliphatic band (arrow 2)

5.1.1 Multidimensional gas chromatography

The aim of developing new advanced instrumentation and techniques is to overcome the limitations of current systems.[273,274] Conventional 1D GC has limited peak capacity leading to an inadequate resolution and separation of complex mixture components.[275] Co-elution is the main issue to overcome when there is only a 1D separation. This can be particularly problematic when conducting trace analysis as compound identification is difficult.[274,276–278] This led to a move to MDGC systems,[279] where peak capacity is increased thus expanding the available separation space.[278]

MDGC systems provide the user with greater separation through two quite different methods; either classical MDGC or the more recent, GC×GC.[274] MDGC systems are typically comprised of heart-cut GC (GC-GC), where targeted and discrete sections of the 1D column separation are transferred either for further separation on a second dimension (2D) and/or to a different detection system.[274,280] The columns are connected through the use of either a switching valve or pressure-driven switching device.[278] The targeted regions are subjected to a greater separation than would be possible in 1D GC.[280] The

principles of MDGC systems are shown graphically in Figure 5.3.[281]

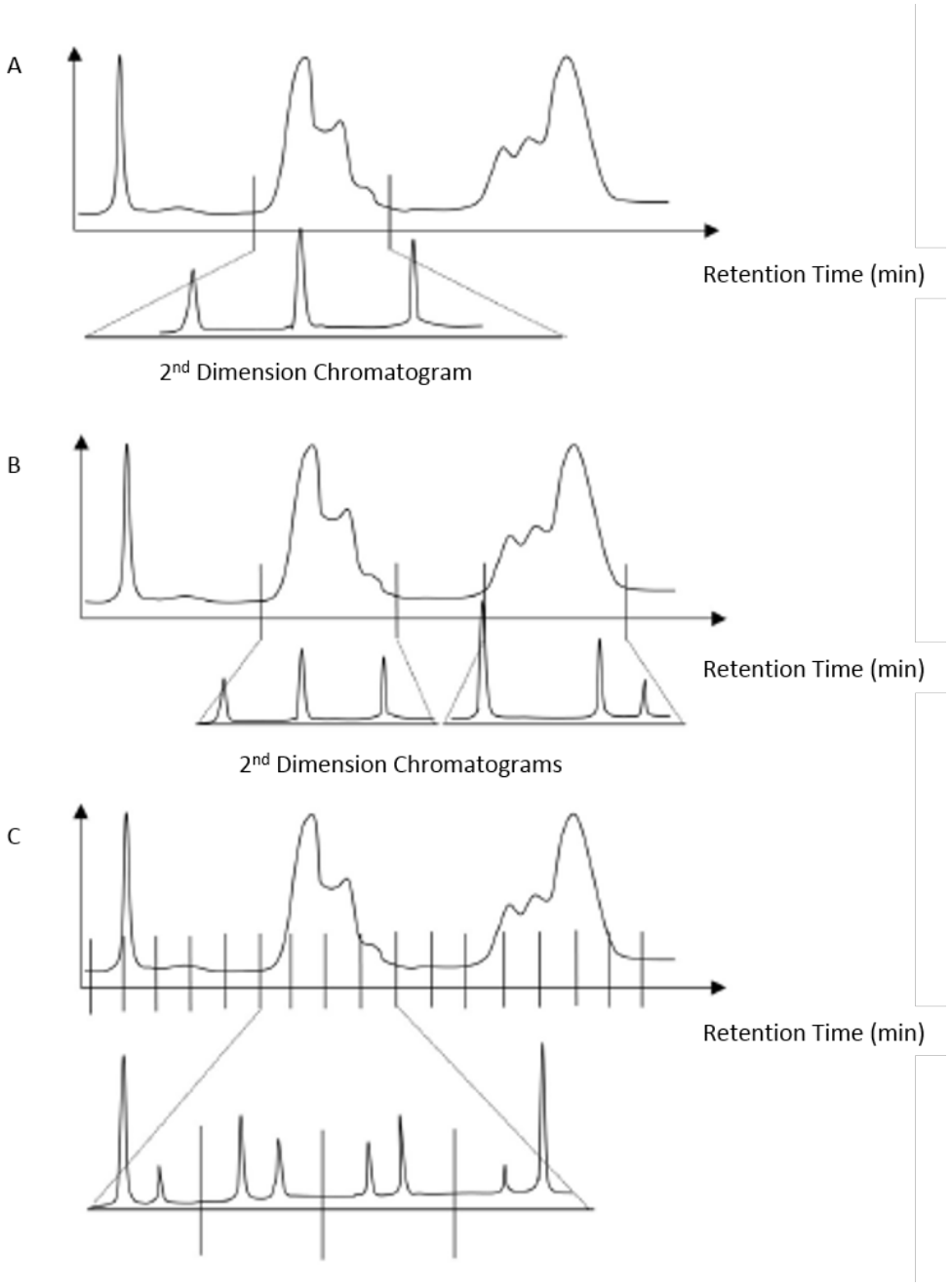

Figure 5.3: Graphical representation of MDGC concepts. A, a single heart-cut 1D GC analysis. B, multiple heart-cut GC representation, in this case dual heart-cut. C, GC×GC analysis. Adapted from Gorecki *et al.*, (2004).[281]

The second separation increases the separation power and peak capacity of MDGC methods over those of traditional 1D GC, where the primary column separation could be considered to be a pre-fractionation step.[278,282] The maximum peak capacity of a GC-GC system is the sum of the peak capacities of the two individual 1D columns, Equation 5.1.[278] This can still often be less than the number of sample constituents and co-elution will still

be observed. It is possible for the primary column effluent to be sampled multiple times onto a secondary column,[282] (panel B of Figure 5.3), which could increase the systems peak capacity as the peak capacity of the secondary column is multiplied by the number of transferred fractions (n_{tf} in Equation 5.2).[278]

$$n_{tot} = n_{c1} + n_{c2} \tag{5.1}$$

$$n_{tot} = n_{c1} + (n_{c2} \times n_{tf}) \tag{5.2}$$

The need for a larger separation space to increase the number of individual compounds that can be detected made the introduction of MDGC techniques a logical response.[278] These hyphenated GC techniques can enhance the accuracy of the method and simplify the implementation without having to use different systems.[280]

However, although MDGC techniques have been available for a long period of time, they have not been used to the fullest extent possible. It is likely this is due to a preference for conventional GC techniques over MDGC.[278] Another reason could be that heart-cut MDGC is not a truly comprehensive technique. A single, or at most a few, selected regions of the 1D separation are transferred onto the 2D column for further analysis as the two columns would usually have different selectivities.[278] The 2D separation would only be comprehensive if the entire sample were analysed using two or more mutually independent separations and if the 1D separation was maintained throughout the entire analysis,[278] such as with GC×GC.

5.1.1.1 Comprehensive two dimensional gas chromatography

Unlike GC-GC or MDGC, GC×GC instruments subject the entire sample under analysis to separation in both dimensions,[278,279] as discussed previously in Chapter 1, Section 1.3.2. This technique is an exceptional method to analyse samples that are highly complex[282,283] and that may not have been separated well using 1DGC or MDGC, particularly when performing trace analysis.[274] However, in some applications GC×GC can still not provide a complete separation of analytes and co-elution occurs. In these situations, a targeted or heart-cut MDGC analysis may be required.[284]

5.1.1.2 Hybrid gas chromatography systems

The coupling of either multiple GC techniques or detectors into a hyphenated system provide an excellent method for studying complex samples, such as the composition of the atmosphere.[280] These systems could be a combination of 1DGC, GC-GC and/or GC×GC in a single instrument that can be implemented to prove the best resolution and separation of a sample.[280]

The three different hybrid systems described below make use of a detector not previously discussed, olfactormetry. This is where a human participant's nose is used to identify different odours, when the odour eluets from the GC column. Using a nose to detect odours is sometimes necessary as the threshold that humans can detect smells can be much lower than instrumental detectors.[285] In some complex odour related samples, such as essential oils, wines, fragrances *etc*, the compounds responsible for the odours can be identified using conventional GC coupled to a olfactormetry in conjunction with an FID or MS. However, this analysis can be limited as peaks in the odour regions can co-elute.[286] Combining GC×GC with olfactormetry assessments has found little use due to the large difference between the slow breathing cycle of the human assessor and the rapid elution of peaks from the GC×GC system. This is where MDGC systems are ideally suited. These systems can resolve the co-eluting peaks and still allow for an olfactory assessment; through the use of heart-cutting and cryo-trapping devices that isolate and transfer target compounds from the first to second dimension columns. The second dimension column is then equipped with a sniff port outlet to allow olfactory analysis.[280,286–288]

A study by Maikhunthod *et al.*, (2010) described a switchable GC×GC and targeted MDGC system for essential oil analysis. This could be switched between the three modes (GC, GC×GC and targeted MDGC) multiple times during a single analysis to provide the best separation possible.[274,280] The instrument set up and an events chart is shown in Figure 5.4. This system was designed to provide an overview of the entire sample using GC×GC, however due to the nature of the sample (odour related) a slower sensory analysis is required for some individual peaks.[274] By incorporating the Deans switch (DS) prior to the cryotrapping device, eluent from the first dimension column can be analysed by either one or two second dimension columns. The shorter second dimension column (^2D_s) for GC×GC and the longer (^2D_l) for targeted MDGC analysis. The design allows for those specific odour regions to be analysed using the ^2D_l.[274]

Chin *et al.* (2012) discussed a set up that incorporated conventional GC, GC×GC

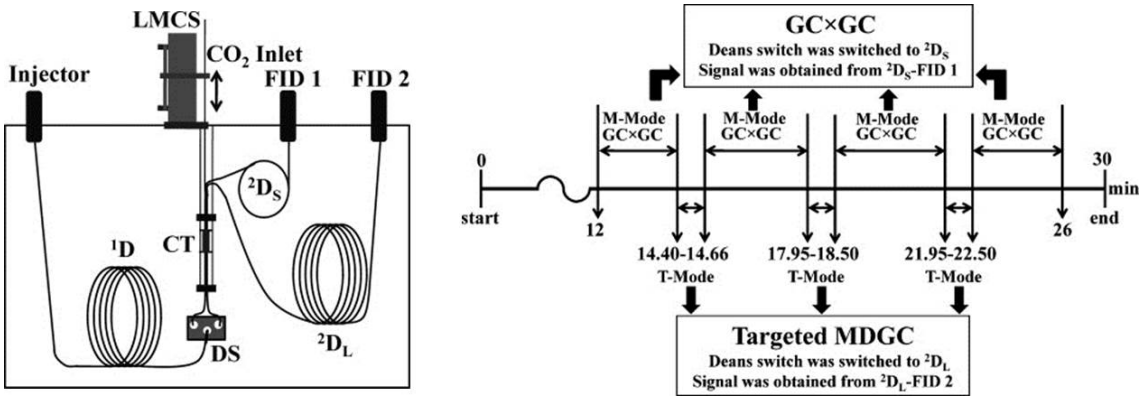

Figure 5.4: The left panel shows a schematic diagram of the Maikhunthod *et al* switchable targeted MDGC/GC GC×GC system. DS: Deans switch, CT: cryotrap, ^{1}D: first dimension column, ^{2}D$_s$: short second dimension column (for the GC×GC mode) terminated at FID 1, ^{2}D$_l$: long second dimension column (for targeted MDGC mode) terminated at FID2. The right panel shows an events chart for the switching operation between GC×GC and targeted MDGC separations.[274]

and targeted heart-cut MDGC with three detectors, FID, MS and olfactormetry (O).[280] The combination of these GC methods into a single system was found to provide a high resolution and separation of the sample under analysis, Shiraz wine. Similar to the previous method, the entire sample was analysed using GC×GC-FID and compared to a conventional GC analysis using parallel O and FID detectors.[274,280] However, in contrast to the previous example, selected regions were heart-cut from the primary column eluent to a long secondary column to be analysed using parallel O and MS detectors. By including these multiple GC techniques into a hyphenated single system, the analytical method was simplified, accuracy was improved and the overall robustness of the system was enhanced.[280]

This system was further developed by Capobiagno *et al* (2015) for the analysis of banana *Terra* spirit.[286] This design was a multi-hyphenated system incorporating MDGC and GC×GC, also with the three detectors, FID, MS and O, schematic shown in Figure 5.6. The odour regions were specifically targeted for full analysis and identification using heart-cut MDGC to parallel O and MS detectors.[286] Using retention indexing, compounds were identified by comparison of the GC-FID/O and MDGC-MS/FID/O chromatograms. This study found 18 different aroma regions, that were further separated using MDGC with parallel O and MS analysis. The MDGC-O/MS analysis generally provided a more successful isolation and identification of the odour specific compounds.[286]

The result of a study combining GC×GC with two different second dimension columns is shown in Figure 5.7. This shows how different columns can provide a better resolution

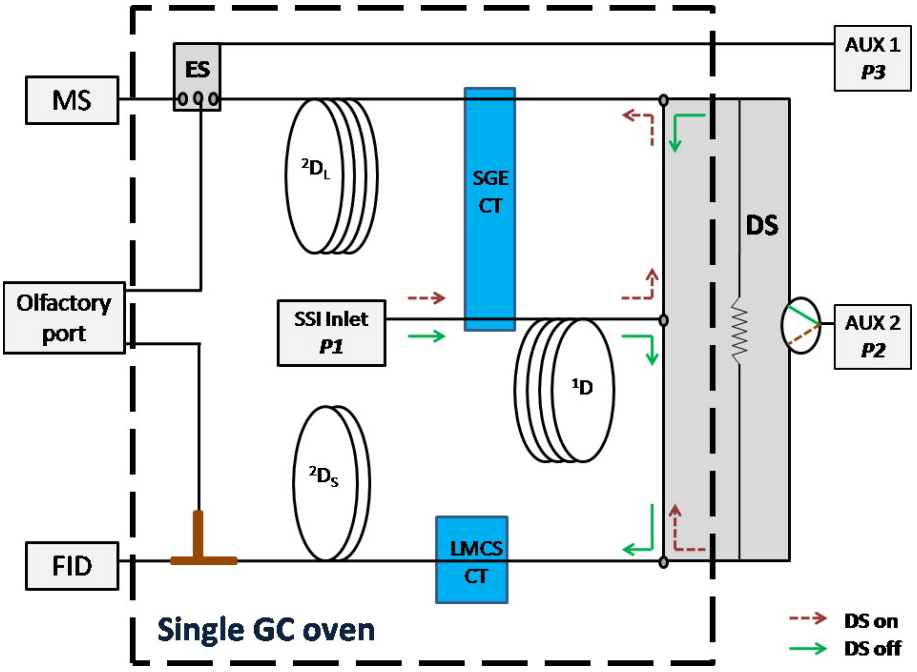

Figure 5.5: Schematic of the Chin *et al* integrated GC×GC/MDGC system with olfactory and MS detections. DS: Deans switch, ES: effluent splitter, AUX: auxillary pressure port, ^{1}D: first dimension column, ^2D_l: second dimension long column, ^2D_s: second dimension short column, CT: cryotrap, SSI: split/splitless injector: FID.[280]

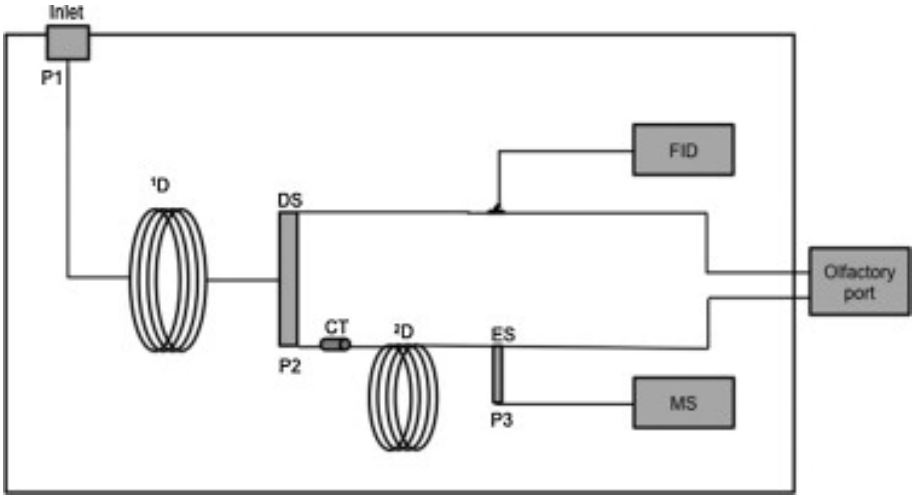

Figure 5.6: Schematic of Capobiagno *et al* integrated GC-FID and MDGC-MS with olfactometry detector. DS: Deans switch, ES: effluent splitter, CT: cryotrap, P1-3: pressure applied at respective junctions.[286]

and separation of specific compounds. The highlighted compounds (in circles) have better separation from the other species using the two different columns. Using set up A, with a BPX50 second dimension column (left plot), there is one compound that is better resolved from the aliphatic band than seen in the other plot. Set up B, using a BP20 second dimension column (right plot), has four aromatics compounds that are not well resolved from the other compounds in set up A.

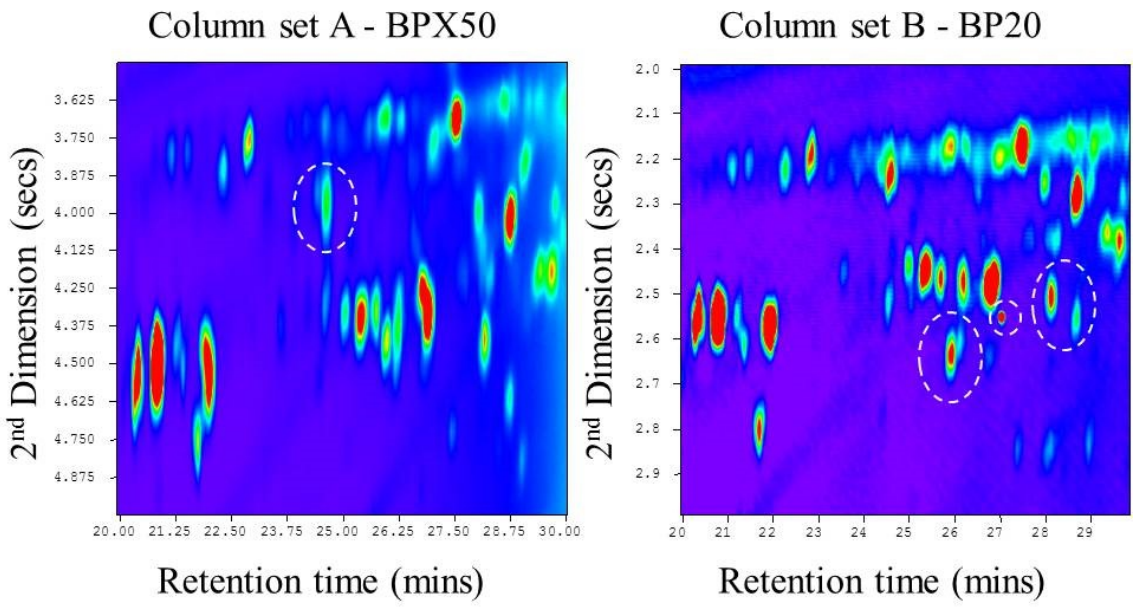

Figure 5.7: GC×2GC plots with the second dimension column of BPX50 (left) and BP20 (right). The highlighted compounds, in circles, show compounds that were more resolved using the different second dimension columns

All of these hybrid GC systems have shown that the combination of different GC methods can have to overcome system disadvantages. Thus the difficulties in separating isoprene experienced by the Dunmore *et al* GC×GC instrument could be improved through combining the existing set-up with another type of GC.[268]

5.1.2 Measurement of volatile organic compounds in rural atmospheres

Bachok, Malaysia is at the centre of a vitally important region of the globe, often referred to as the Maritime Continent (MC) in south east Asia which comprises many islands, peninsulas and shallow seas between approximately 10° S to 20° N and 90 to 150° E. This region is subject to a complex mix of anthropogenic and biological emissions including; industrial emissions from the rapidly-developing nations in Asia, particularly the south east, biomass burning emissions from tropical forests, and emissions from natural and cultivated terrestrial and marine ecosystems. The conditions in the MC are further compounded by its presence within the Tropical Warm Pool (TWP, located within the western Pacific and eastern Indian Ocean) which exhibits some of the highest water temperatures of the world ocean. The TWP region has been shown to be increasing given the warming of the global climate. However, the consequences of atmospheric changes in these regions, and globally, cannot be fully quantified due to limited observations of the atmospheric composition, in comparison to the rest of the world.[289]

Sturges and Reeves (2009) have identified the tropical regions of the globe as being highly important for atmospheric research.[290] Of particular interest is the atmospheric oxidation of many gaseous compounds (*e.g.* VOCs) which, given the high levels of radicals and photochemical radiation present in the tropics, is at a maximum. This often leads to the atmospheric lifetimes being controlled by degradation/destruction rates in the tropics.[291] The transport of atmospheric species in this region is controlled by the oscillation of the intertropical convergence zone and the accompanying monsoon seasons. Of particular interest during the winter months, is the flow of air from highly industrialised and populated regions in China, Japan, Korea and Taiwan over the South China Sea (shown in the left panel of Figure 5.8). This, in conjunction with the increasing anthropogenic emissions from these countries, due to the rapid development they are undergoing, could be potentially significant when considering regional radiative forcing.

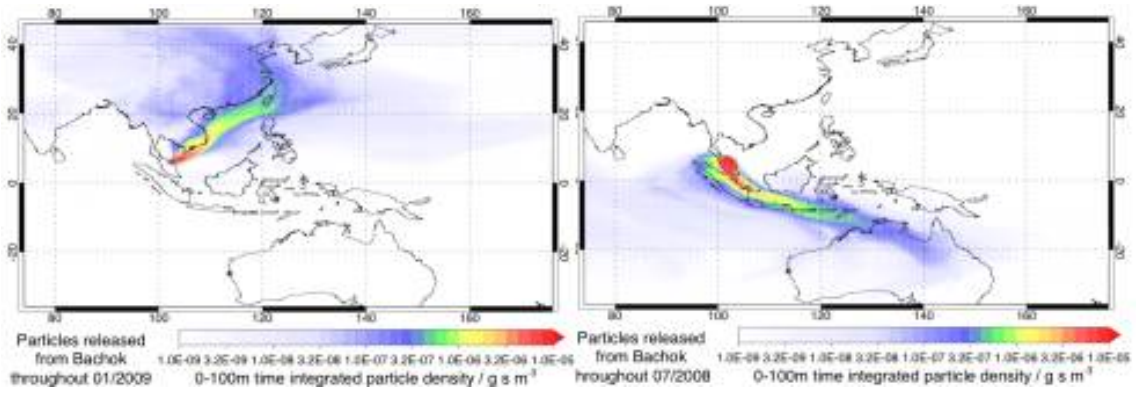

Figure 5.8: NAME back-trajectories in lowest 100m from Bachok during January 2009 (left) and July 2008 (right). Warmer colours show the likelihood of air masses from that area in the previous 12 days. Image provided by Professor William Sturges, University of East Anglia

Even though this region is of high interest, there have so far being a limited number of studies conducted. Logistically, this region is quite complex and there are a limited number of countries which have a strong enough scientific infrastructure to support atmospheric measurement networks. Malaysia has good scientific infrastructure with an existing Global Atmospheric Watch (GAW) global station, based at Bukit Atur (BA) in the Danum Valley rainforest in Borneo shown in Figure 5.9.

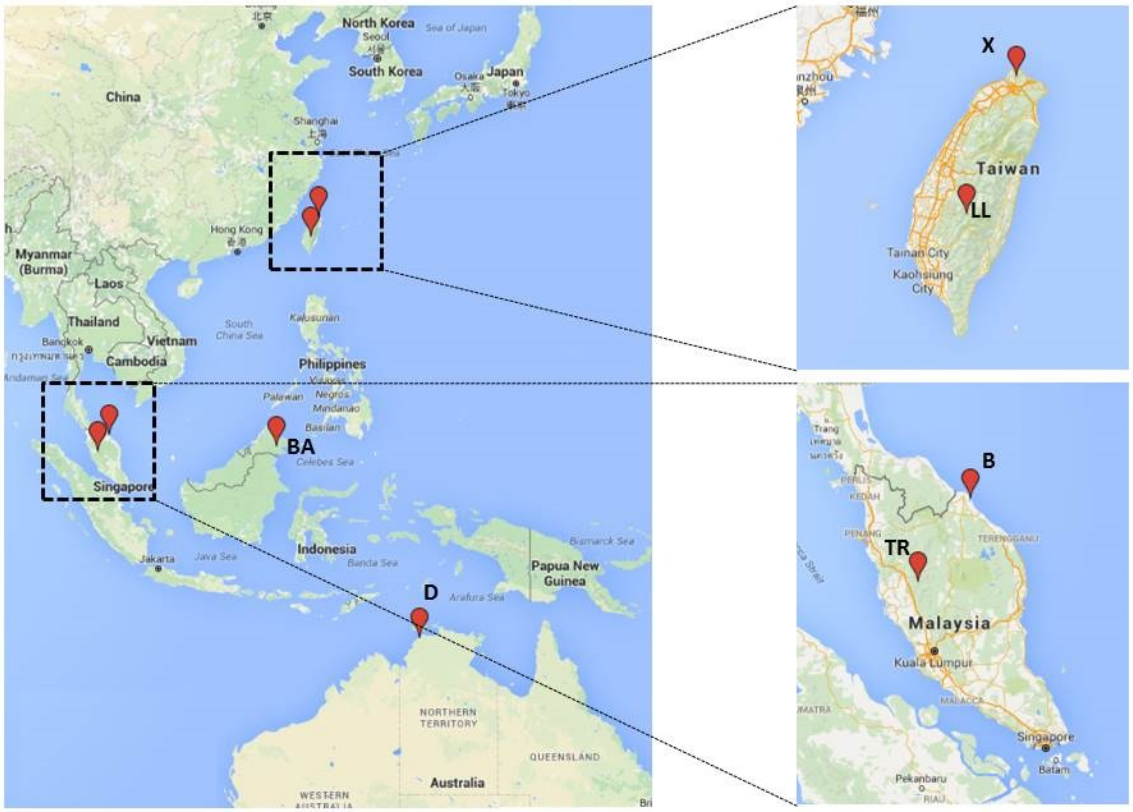

Figure 5.9: Location of measurements sites across South East Asia: Bachok Marine and Atmospheric research station (B), regional station at Tana Ratah (TR), Global Atmospheric Watch (GAW) station based at Bukit Atur (BA) in the Danum Valley rainforest in Borneo, GAW station at Gun Point in Darwin, Australia (D), coastal site on Taiwan (X) and a global GAW station at Lu-Lin, Taiwan (LL).

This chapter details the development of a new combined heart-cut and GC×GC instrument to measured a wider range of VOCs. This new instrument was compared to the DC-GC-FID described in Chapter 2, Section 2.3. The deployment of the instrument to a newly developed research facility located at the Bachok Marine and Atmospheric Research Station of the University of Malaya (shown in Figure 5.9). The campaign during January and February 2014 was designed to capture the composition of air flowing from industrialised regions to the north of the South China Sea. As the flow of air during this period is from these regions (shown in Figure 5.8, left panel), the composition is likely to be highly chemically processed air due to the presence of intense tropical sunlight combined with a complex mixture of NO_x, O_3, and natural and anthropogenic VOCs.

5.2 Experimental

5.2.1 Instrument comparisons

The GC-GC×GC instrument developed was compared to a well-established DC-GC that is operated by NCAS FGAM. A detailed reporting of the DC-GC set up and calibration is provided by Hopkins *et al.*, (2003).[161] Briefly this instrument has three GC columns; an aluminium oxide PLOT column and two, in series, LOWOX columns for the analysis of NMHCs and OVOCs respectively.

The GC-GC×GC instrument was set up as discussed in Section 5.3. Thermal desorption of ambient samples was achieved using a Markes TT24-7 unit with an air server attachment (Markes International, Llantrisant, UK), sampling at a rate of 100 mL min^{-1} for 55 min, to give a total sample volume of 5.5L. Trapping temperature was set at -10 °C, and then heated to 200 °C at 100 °C min^{-1} to desorb all analytes of interest. Outside air was sampled from a manifold attached to the roof of the Wolfson Atmospheric Chemistry Laboratory based on the University of York, Heslington West campus. This was pumped through a glass finger in an ethylene glycol bath held at -30 °C, to remove any moisture present. An optimised oven temperature programme for the GC-GC×GC instrument was developed to optimise the separation and resolution of analytes. The initial temperature was 50 °C, held for 3 min, ramped at 2.5 °C min^{-1} to 130 °C, held for 2 min then ramped at 10 °C min^{-1} to 200 °C, and held for 6 min; giving a total run time of 50 minutes. The total analysis time was 55 minutes.

5.2.2 Bachok demonstration 'International Operating Fund' campaign

The GC-GC×GC was deployed to the Bachok Marine and Atmospheric Research Station, located on the eastern coast of Peninsular Malaysia, within 100 m of the South China Sea (Figure 5.9). This site is owned and operated by the University of Malaya (UM) as part of the Institute of Ocean and Earth Sciences (IOES). The IOP demonstration activity ran during January and February 2014, was funded by NERC and UM and involved several UK universities (East Anglia, Cambridge, York, Leeds, Leicester and Royal Holloway University of London), NCAS, UM and the Malaysia Meteorological Department. Measurements were taken from an atmospheric observation tower (7 floors, ≈ 15 m) on the beach side of the site, using the GC-GC×GC method described in the previous section. The tower and its position relative to the main building and sea is shown in Figure 5.10.

Figure 5.10: Photo of the location of the tower with respect to the main building and sea (left) and a full image of the tower (right)

5.3 Instrument design

The GC-GC×GC-2FID system comprised of an Agilent 7890 GC with two FIDs operating at 200 Hz (Agilent Technologies, Wilmington, DE, USA). It had two operating modes, volatile heart-cut stage (GC-, first 5 minutes) and a normal GC×GC stage (5 to 50 minutes) as shown in Figure 5.11. For the heart-cut stage, effluent was injected down the primary column (BPX-5, SGE, Australia; column pressure of 60psi), through two 4-port, 2-way valves (Valco Instruments, Houston, TX, USA), onto a PLOT column to the 1st FID. At 5 minutes, the valves switch position and the PLOT column used an auxiliary helium flow of 11 psi to push effluent to the detector and the GC×GC stage starts. This comprises of the primary column flow through a total transfer flow modulator (6-port, 2-way diaphragm valve modulator, Valco Instruments) to a secondary column (BP-20, SGE; 23 psi) then to the 2nd FID. All column pressures were controlled by the GC EPC. The modulator was held at 100 °C with a 5 s modulation period. Valve actuation, modulation and cryo re-focussing (discussed in the next section) were controlled using LabVIEW software (National Instruments), allowing for autonomous operation. The GC×GC-FID set-up has been discussed previously in Lidster *et al.*, (2011) and Dunmore *et al.*, (2015).[131,268]

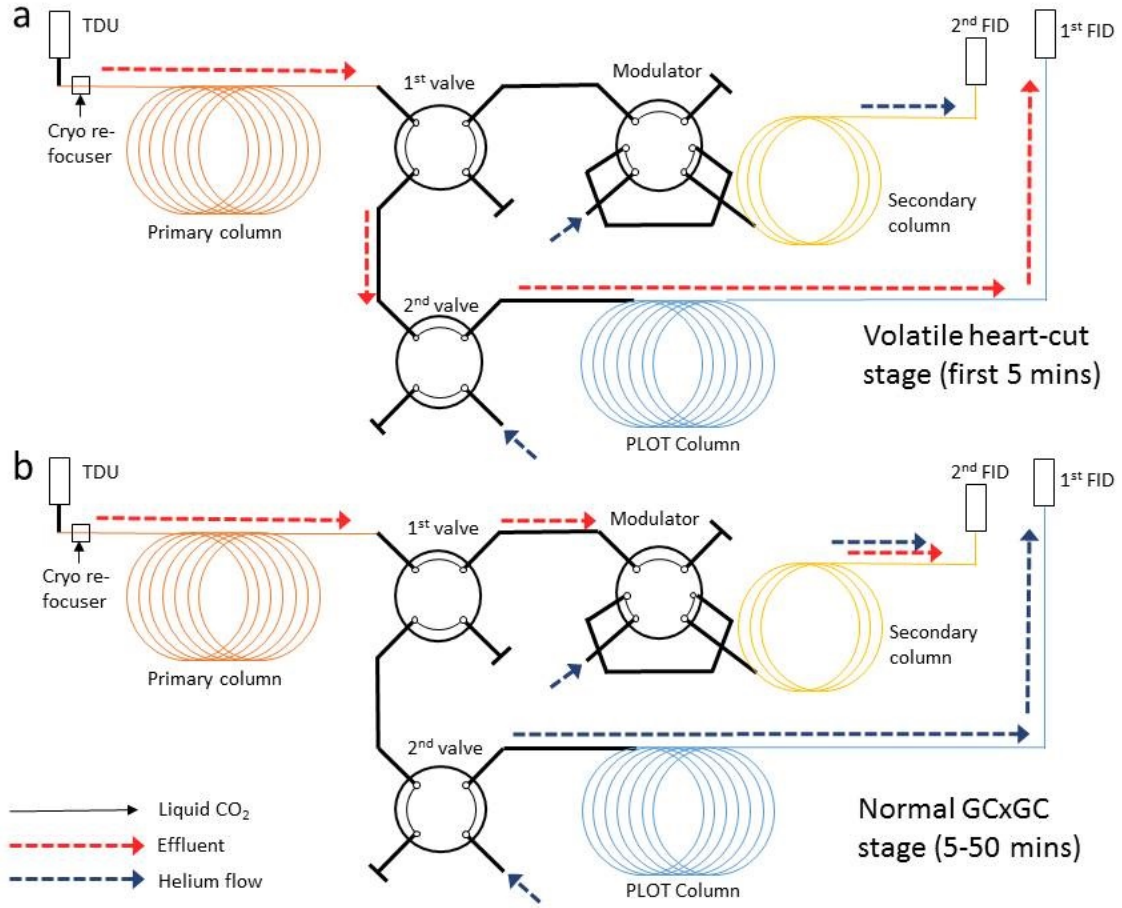

Figure 5.11: GC-GC×GC-2FID schematic: a, details the volatile heart-cut stage from the first 5 minutes of operation, b, details the standard GC×GC-FID operation from 5 to 50 minutes. TDU represents the thermal desorption unit.

5.3.1 Cryo re-focussing step

One of the issues encountered when sampling ambient air using a thermal desorption unit then injecting onto a relatively narrow primary column (BPX-5) is that the plug of sample can be subject to a high degree of band broadening, ultimately resulting in poor chromatographic resolution. A cryo-focussing step was introduced after the TDU, to allow for the sample to be re-focused and held at the front of the primary column before any separation occurs as shown in Figure 5.11. This allowed the sample to be injected as a narrow plug by turning off the cryogen, creating better separation. To make this step suitable for field work, a re-focussing T-piece (SGE Analytical Science Pty Ltd, Ringwood, Victoria, Australia) was used in conjunction with liquid CO_2. As shown in Figure 5.12, the primary column is threaded through the T-piece and liquid CO_2 is sprayed around the column at sample injection using solenoid activation. In order for the trapped analytes to

be released, the T piece was housed within the GC oven to allow for rapid temperature equilibration after the cryogen is switched off.

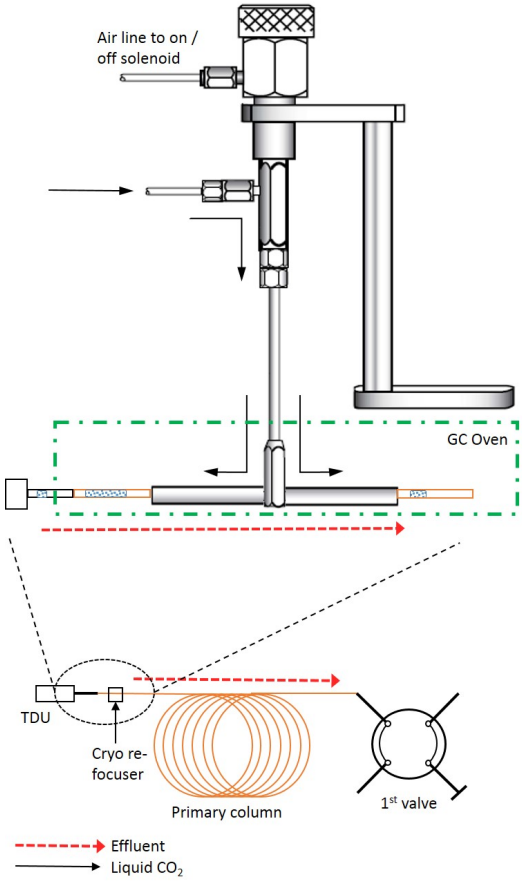

Figure 5.12: Schematic of the liquid CO_2 re-focussing T-piece

Duplicate injections were run using a toluene gas sample to investigate the effects the cryo re-focussing would have on separation in the first and second dimensions during GC×GC analysis, Figure 5.13. When the cryo re-focussing is on (Figure 5.13 d), the toluene peak is much narrower in the second dimension, with only 6 modulated peaks as opposed to over 16 without re-focussing (Figure 5.13 c). The first dimension retention time is also slightly pushed to the right with re-focussing.

The optimum re-focussing time was investigated by changing only the cryo re-focussing time period from 0 s to 120 s at 30 s increments. A 60 s time period was found to be the ideal, with reduced peak widths and little/to no distortion. For compounds which are weakly retained, a cryo-focusing period of over 60 seconds results in progressively more band broadening. Conversely, for strongly retained compounds, there was no significant amount of re-focussing until 120 seconds. However with longer time periods, the T-piece

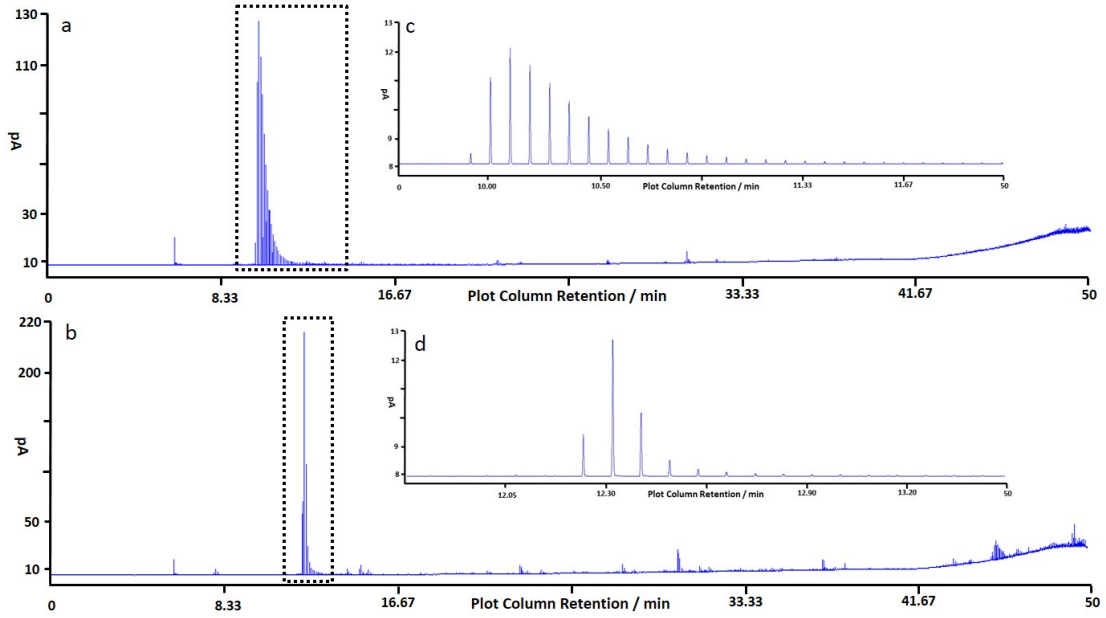

Figure 5.13: Duplicate injections of a toluene sample with cryo re-focussing off (a) and on (b) to investigate the effects of re-focussing on separation using GC×GC, (c) and (d) show zoomed in portions of plots (a) and (b) respectively

became blocked which reduced the efficiency of the re-focussing step. Therefore to obtain the best conditions for analysis, a 60 second time period was chosen to allow for re-focussing without any band broadening effects to occur.

5.3.2 Instrument suitability

Figure 5.14 shows a typical chromatogram of the gas standard from the GC-GC×GC-2FID instrument. This shows the 1D GC-FID trace in the upper panel, where the x-axis is retention time along the PLOT column (separation based on boiling point) and the y-axis is peak amplitude. The lower panel shows a typical GC×GC-FID chromatogram where the x and y-axis are the retention times on the primary (separation based on boiling point) and secondary (based on polarity) columns, respectively and the coloured contour is compound intensity. The red section at the start of the chromatogram is indicative of the first 5 minutes of the run when the system is in heart-cut mode, such that no GC×GC separation occurs. This chromatogram shows good separation of the species of interest and the ability to separate and resolve isoprene. The 1D GC-FID chromatogram (upper panel) contains C_3-C_7 compounds, inclusive of isoprene and benzene, while the GC×GC plot (lower panel) consists of higher carbon number species; such as larger aromatics and aliphatics, along with other functional groups.

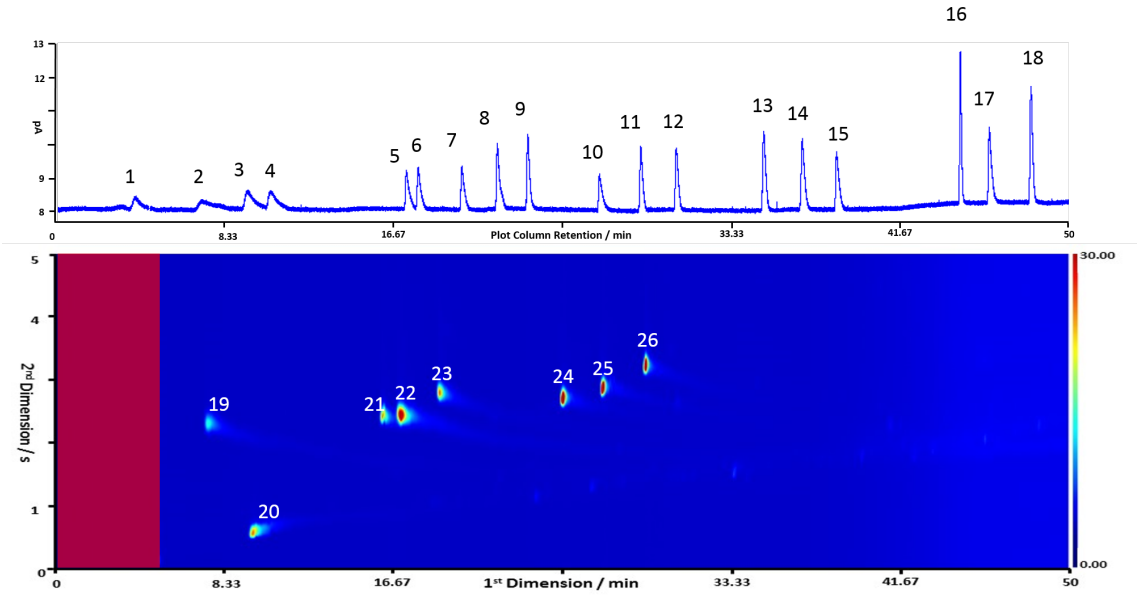

Figure 5.14: Chromatogram from the GC-GC×GC-2FID instrument run with an NPL 30 ozone precursor component standard: upper panel is a one-dimensional GC plot from the volatile heart-cut stage and the lower panel is a two-dimensional GC plot from the GC×GC stage. Compounds are identified as follows: 1 *n*-propane, 2 *iso*-butane, 3 *n*-butane, 4 acetylene, 5 *trans*-2-butene, 6 1-butene, 7 *cis*-butene, 8 *iso*-pentane, 9 *n*-pentane, 10 1,3-butadiene, 11 *trans*-2-pentene, 12 *cis*-2-pentene, 13 2+3-methyl pentane, 14 *n*-hexane, 15 isoprene, 16 *n*-heptane, 17 benzene, 18 2,2,4-trimethyl pentane, 19 toluene, 20 *n*-octane, 21 ethyl benzene, 22 *m+p*-xylene, 23 *o*-xylene, 24 1,3,5-trimethyl benzene, 25 1,2,4-trimethyl benzene and 26 1,2,3-trimethyl benzene.

5.3.3 Compound identification

38 individual VOCs were identified and quantified in ambient air, however this only represents a fraction of the total VOC mass loading in the atmosphere. The majority of compounds were identified from the two NPL standards described in Chapter 2, Section 2.3.1.1, Table 2.1. The other compounds, not included in the standards, were identified by comparison with the previous GC×GC set up used during the ClearfLo campaign and quantified using retention factors (discussed in Chapter 2, Section 2.3.1.2).

Using the grouping techniques described in Dunmore *et al.*, (2015),[268] 7 groups have been collectively quantified; C_9-C_{13} aliphatics, C_4 substituted mono-aromatics and C_{10} monoterpenes. This was discussed previously in Chapter 2, Section 2.5.1. An example of the grouping from the GC-GC×GC instrument is shown in Figure 5.15, which only shows the GC×GC portion of the chromatogram. There were three less groups (the C_6-C_8 aliphatics) quantified than previously. This is a direct result of the new instrument set up where compounds that elute prior to toluene are analysed on the PLOT column, which is not conducive to the grouping analysis. This figure shows that there is still a large

number of higher carbon number aliphatics that have not been included in the grouping (as they have not been identified), although this is obscured by possible column bleed.

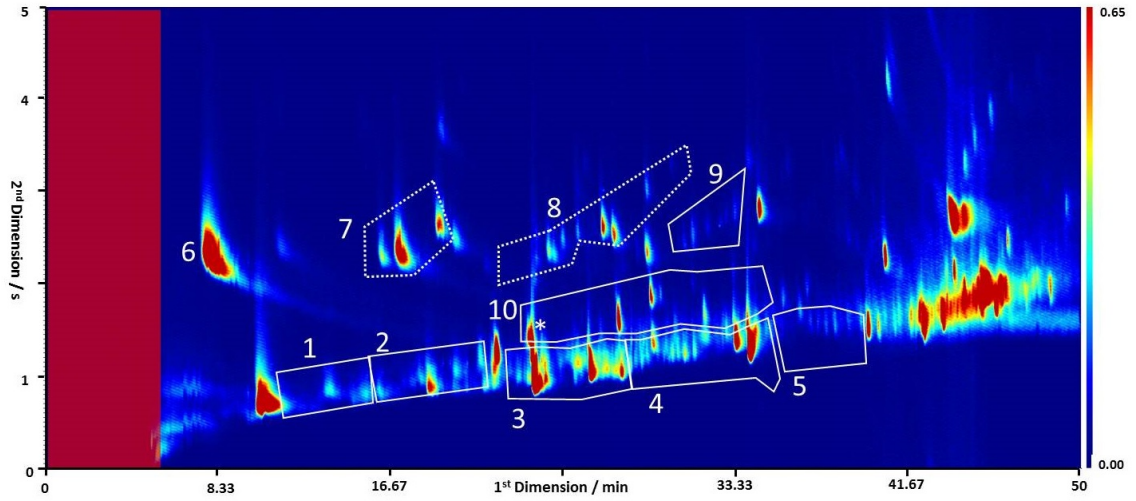

Figure 5.15: GC-GC×GC-FID chromatogram, demonstrating the grouping of compounds. Labelled peaks and groups are identified as follows, with the dashed and solid lines indicating compounds that were identified individually and as a group respectively; (1-5) aliphatic groups from C_9 to C_{13}, (6) toluene, (7) C_2 substituted monoaromatics, (8) C_3 substituted monoaromatics, (9) C_4 substituted monoaromatics, and (10) C_{10} monoterpenes with * corresponding to α-pinene which is the start of that group. The remaining compounds, not enclosed in a box contain hetero-atoms, primarily oxygenates and some larger carbon number aliphatics that have not been identified. The grouping of compounds was accomplished using the lasso technique in Zoex GC image software (Zoex, USA). This technique allows the software to calculate the area of all peaks included in the lasso.

5.3.3.1 Validation of method

When making any atmospheric measurements there is an associated bias. In order to develop a method to accurately quantify species measured, any errors must be minimised. The bias in VOC observations is calculated as the sum of uncertainty in the collection of samples and the analytical quantitation method,[292] in this case measurement using GC. The uncertainty in the GC method has been detailed in Chapter 2 and Dunmore *et al.*, (2015).[268] It is very important to remove, or at least decrease any sources of bias. This is particularly true for the sampling of VOCs using sorbent traps as this is usually the first analysis step, and as such is extremely important.[292] As discussed previously, VOCs can be collected and analysed either off-line or on-line. There are two primary means of accomplishing this; using Whole Air Sampling (WAS) cannisters or via sorbent tubes/traps. For this chapter, the focus will be on sorbent sampling. These traps can be used in a variety of ways, both on and off-line. On-line sorbent tube sampling via a thermal desorption unit is a common practice for in-situ field campaigns.

A breakthrough test can be carried out to test the validity of using sorbent tubes to sample ambient air. The breakthrough test is used to determine what parameters should be maintained to ensure that none of the analyte of interest is lost or undetected.[292] If not carried out the wrong sampling volume may be used (*i.e.* too high a volume could cause sample to leach out of the sampling tube) or the sorbent could become saturated with analyte leading to a false quantification.

To test the sorbent tubes used, in this case Air toxic traps (Markes International), a set of serial calibrations were conducted. These traps are designed to trap both polar and non-polar VOCs that typically range from propene to tridecane. A particular focus of this testing was to determine what breakthrough would occur with the more volatile compounds being targeted by the new set-up (*i.e.* C_3 - C_6). Using a NPL standard containing 30 ozone precursor compounds (C_3-C_9), the breakthrough was tested for some of the more volatile species.

Figure 5.16 shows the breakthrough test results for the main species of interest, isoprene, and three volatile species that appear on the PLOT column. The correlations and equations of best fit for the breakthrough of all compounds investigated are given in Table 5.1. From this table it is possible to determine that this method is not suitable for the analysis of species with 4 or less carbon atoms, as the R^2 values for those compounds are below 0.85.

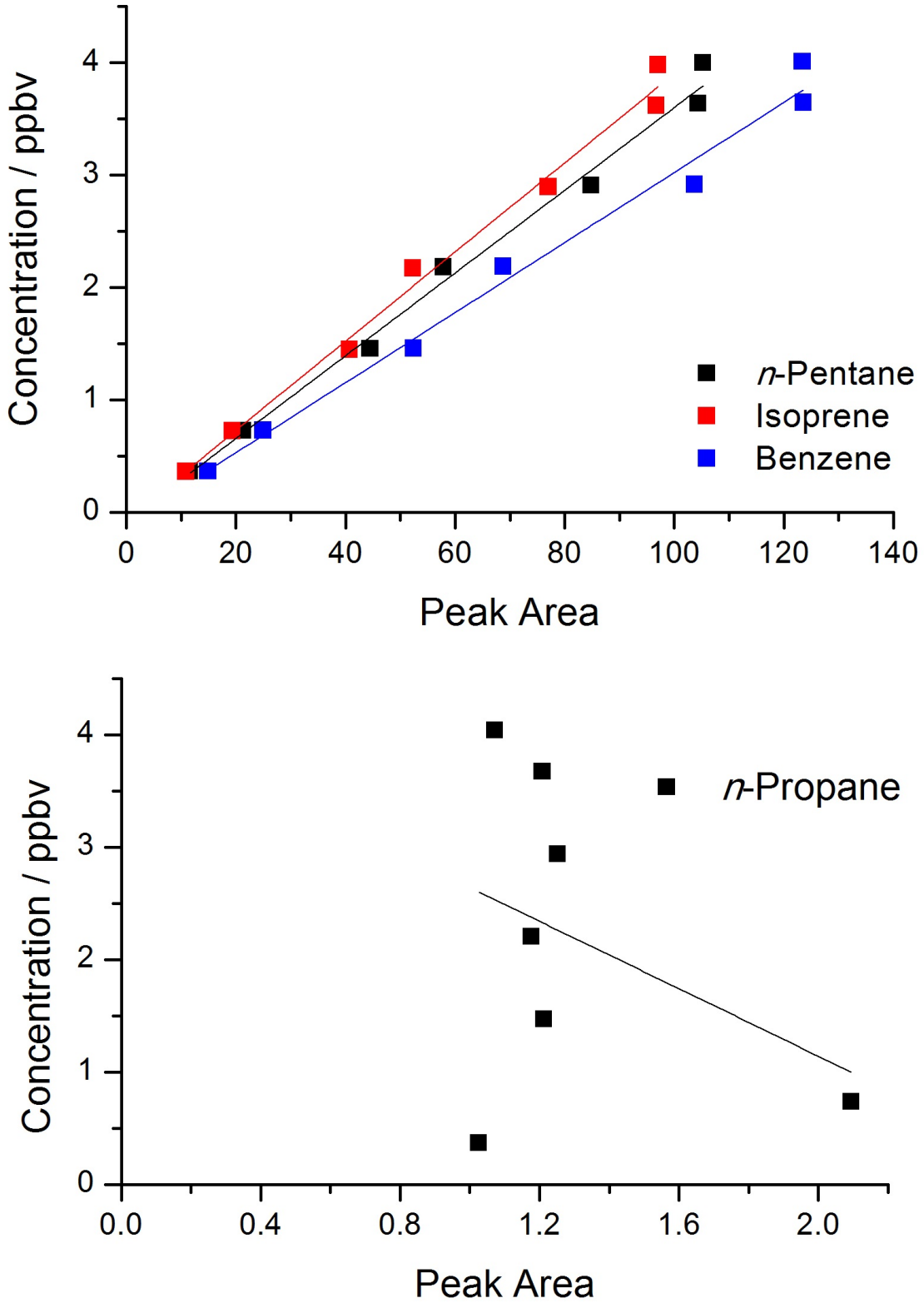

Figure 5.16: Breakthrough test results for *n*-Pentane, Isoprene and Benzene (upper) and *n*-Propane (lower). Correlations and equation of the lines are given in Table 5.1

Table 5.1: Gradient, intercepts and R^2 values for breakthrough test compounds. Numbers correspond to the identified peaks in Figure 5.14, acetylene and *cis*-2-pentene are not included

	Compounds	Gradient	Intercept / 10^{-15}	R^2
1	*n*-Propane	-1.5010	4.1427	0.15
2	*iso*-Butane	-1.8479	4.5295	0.17
3	*n*-Butane	-0.3147	4.5533	0.58
5	*trans*-2-Butene	0.0995	-0.7799	0.81
6	1-Butene	0.1419	-1.0857	0.69
7	*cis*-Butene	0.0937	-0.7115	0.83
8	*iso*-Pentane	0.0916	-0.9669	0.87
9	*n*-Pentane	0.0368	-0.0771	0.99
10	1,3-Butadiene	0.0654	0.2000	0.43
11	*trans*-2-Pentene	0.0393	-0.0736	0.99
13	2/3-methyl Pentane	0.0322	-0.1313	0.99
14	*n*-Hexane	0.0302	-0.0658	0.99
15	Isoprene	0.0397	-0.0623	0.99
16	*n*-Heptane	0.0264	-0.0751	0.99
17	Benzene	0.0312	-0.0910	0.99
18	2,2,4-trimethyl-Pentane	0.0231	-0.0602	0.99

5.3.4 Intercomparison of two gas chromatography instruments

By comparing this new instrument against a well established instrument,[162] its performance can be evaluated. The two instruments observed 15 of the same compounds using the PLOT column; small alkanes, an alkene and one aromatic. The measured mixing ratios of two of the compounds measured by both instruments, *n*-Pentane and Isoprene, are shown in Figure 5.17. The two instruments compare well for both compounds. There does appear to be a slight discrepancy between them, however the rapidly fluctuating data, especially at the end of the *n*-Pentane time series, makes this difficult to say accurately. This analysis was carried out at the Department of Chemistry, University of York so it may be that there were some emissions of *n*-Pentane from solvent use in the department that may be influencing the time series.

Figure 5.18 shows a correlation for *n*-pentane (upper) and isoprene (lower) observations from the two instruments. The correlation shows a good agreement between the two instruments with R^2 values of 0.99 for both species. From this it is possible to conclude that the new instrument can accurately measure and quantify the overlapping species with more than 4 carbon atoms. One thing to note about the correlations between the two systems, is the offset of the intercept from the equation of the line of best fit. This suggests that the two instruments quantify slightly different concentrations of the species

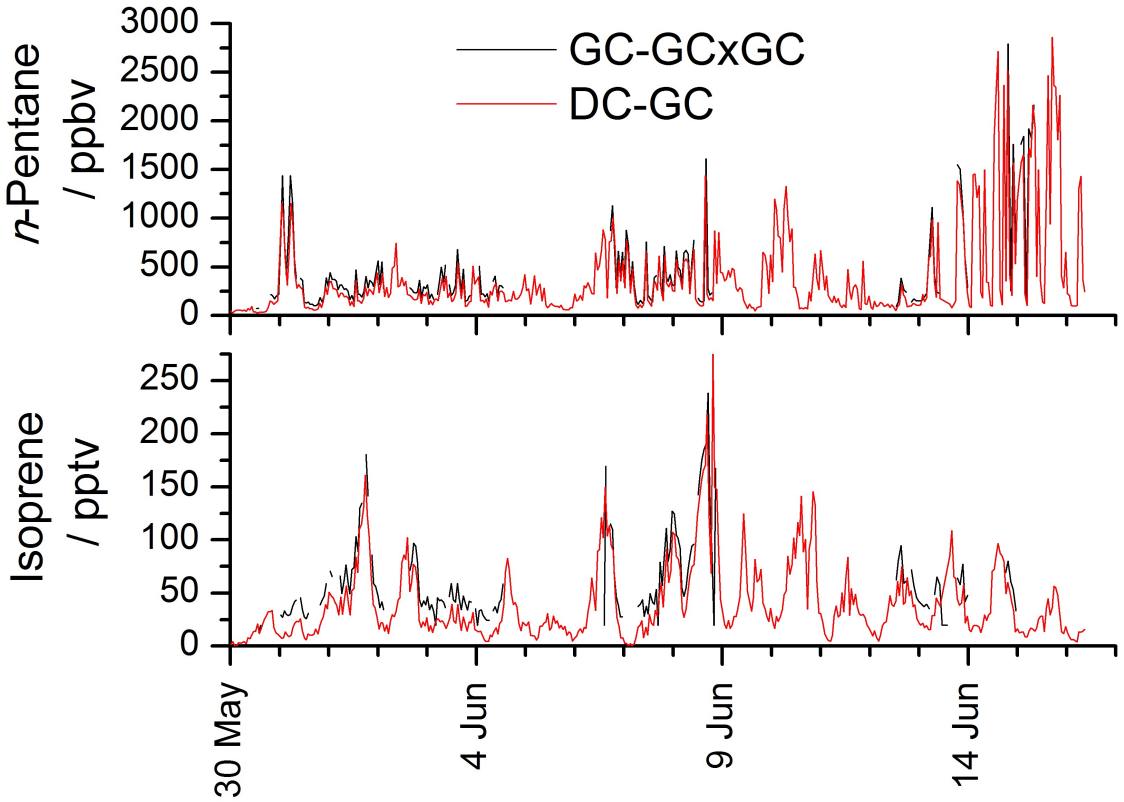

Figure 5.17: Time series of *n*-Pentane (upper) and Isoprene (lower) from the GC-GC×GC (black) and DC-GC (red) instruments

measured. It is possible that this discrepancy is from either differences in sampling times between the two instruments, a result of sorting the two time series to the same time stamp for direct comparison or that there may be some variation at low pptv levels that still needs to be resolved.

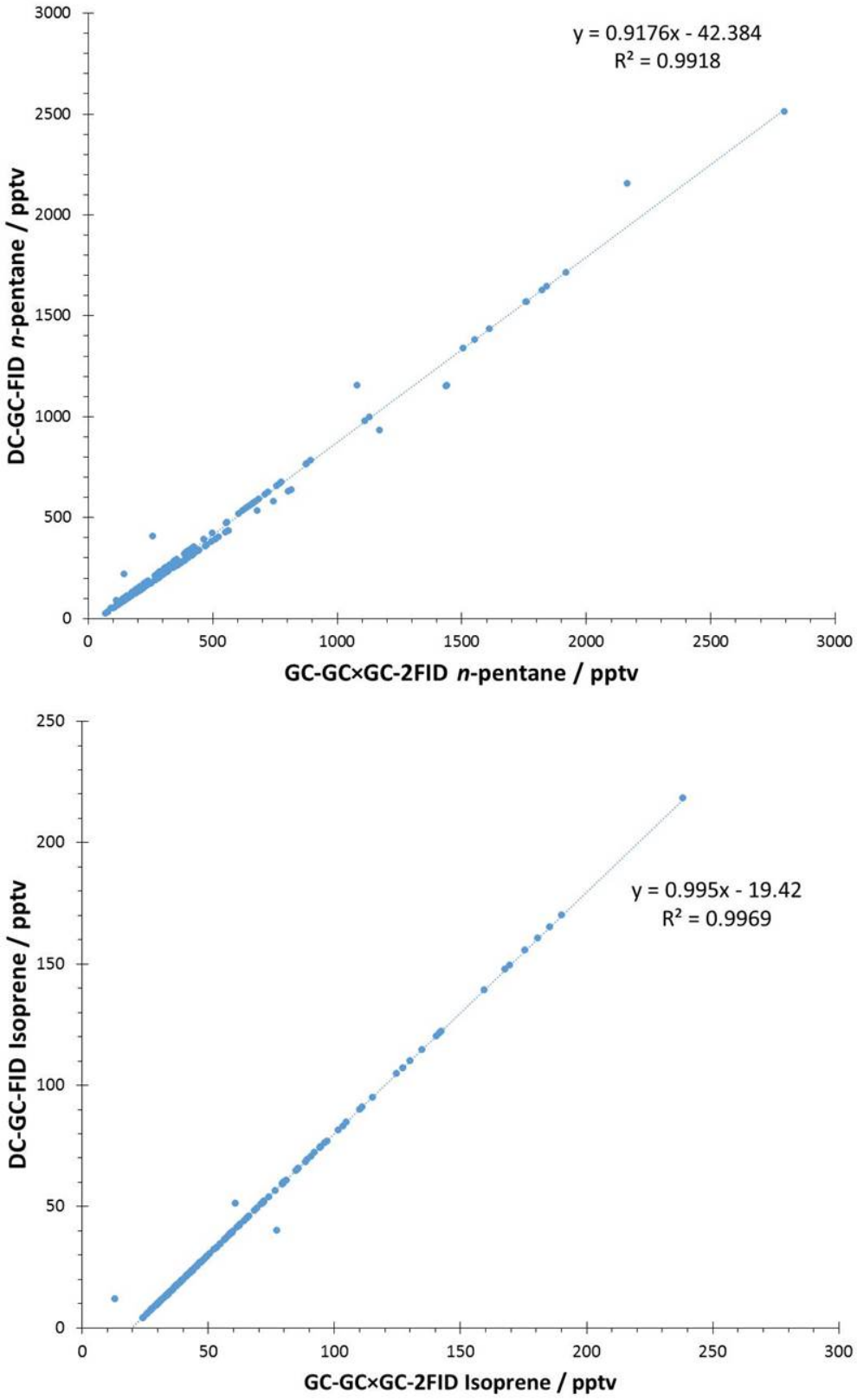

Figure 5.18: Correlation between the two GC instruments for *n*-Pentane (upper) and Isoprene (lower), a linear regression line has been fitted to the data with the equation of the line and R^2 for each correlation shown

5.4 Bachok demonstration campaign

A sample GC-GC×GC-2FID chromatogram from the Bachok campaign is shown in Figure 5.19. This shows the presence of approximately a hundred individual species. Several of these are highly polar, with high retention times in the second dimension in the GC×GC plot, indicating they are most likely aromatic or oxygenated compounds. The zoomed in plot of the 1D GC trace (c in Figure 5.19) shows that although it is dominated by one specific compound, there are also many other compounds present with less than 6 carbon atoms.

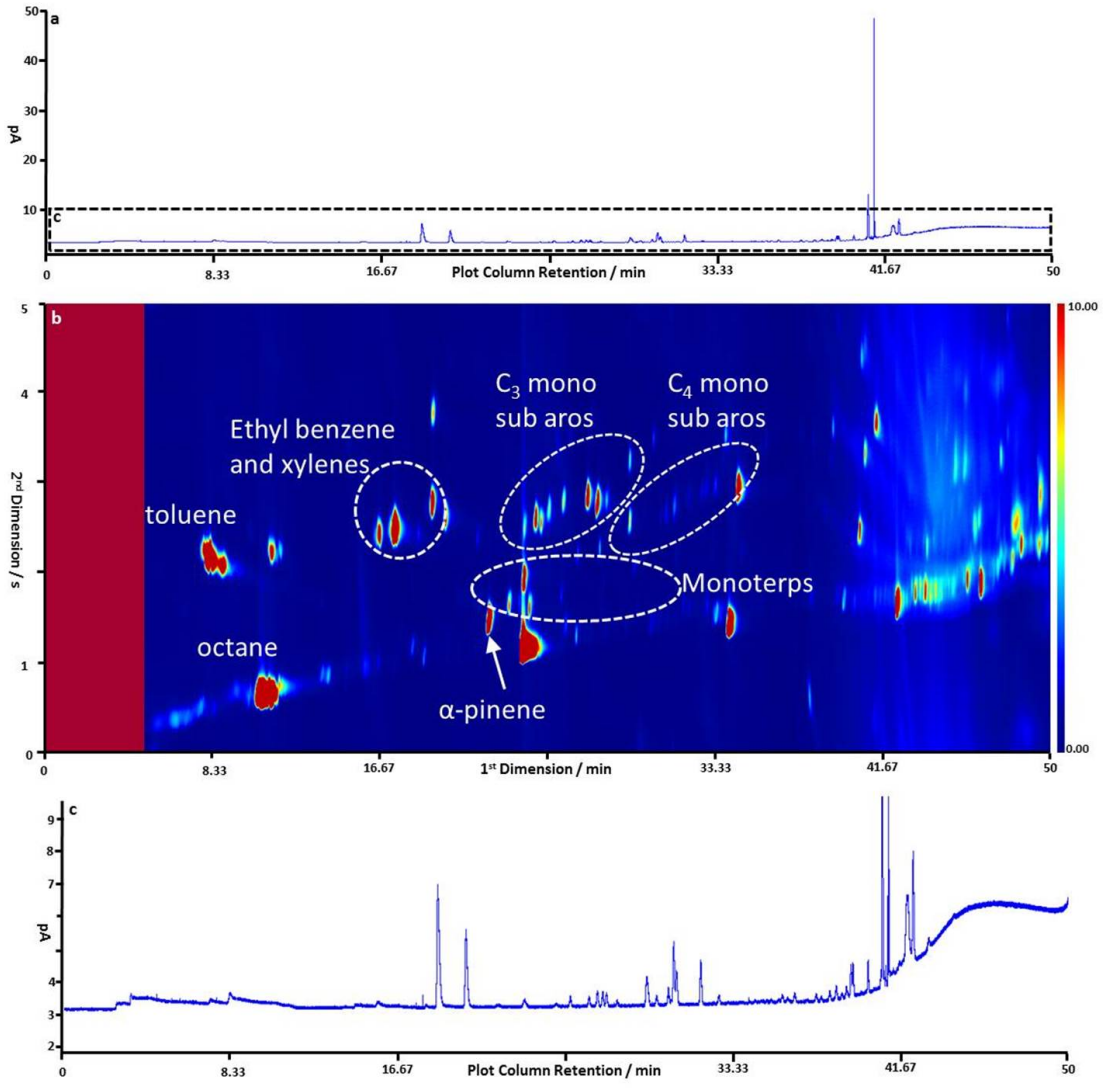

Figure 5.19: Typical GC-GC×GC chromatogram from Bachok from 01/02/2014 at 22:32 (local time), a: 1D GC plot from the volatile heart-cut stage, b: 2D GC plot from the GC×GC stage and c: shows a zoomed in section of the 1D GC plot, highlighted by the box in plot a

Two different meteorological periods were experienced at the site, classified as clean and

polluted by the Malaysian Met Office due to a switch in air mass trajectory. The changes in air mass back trajectories are shown in Figure 5.20. These are NAME back trajectories conducted by Alistair Manning (Met Office) for the Bachok site. The trajectory at the start of the campaign, during the polluted period (20/01/2014, a), shows air masses transported from over China and across Thailand, Vietnam and Cambodia. These regions can be highly polluted from increasing development and industrialisation. Also, there are some periods where these areas experience large biomass burning events, shown in Figure 5.20 c. In contrast, during the clean period at the end of the campaign (06/02/2014, b) the majority of the air mass is from the South China Sea and so would likely be less polluted.

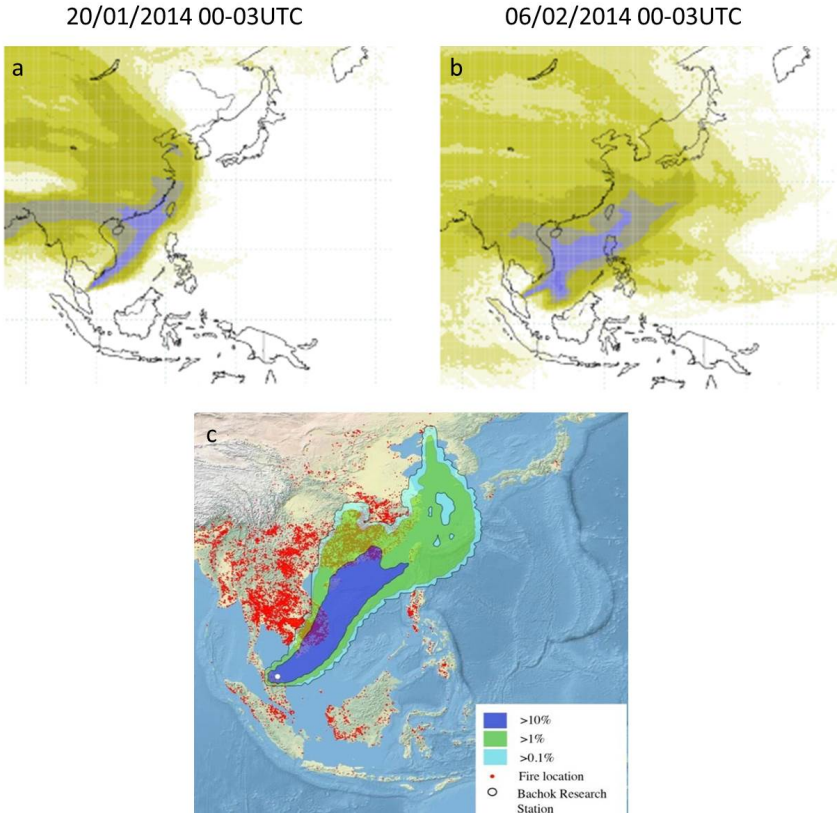

Figure 5.20: Different meteorological periods experienced at Bachok, Malaysia, a and b show NAME back trajectories for 20/01/2014 (a) and 06/02/2014 (b), and c shows fire points (red dots) for the period of 01/01/14 to 09/02/14 with the cumulative trajectory for January shown by the coloured 'plume'. Plots a and b were provided by Alistair Manning, Met Office, while plot c was provided by Rebecca Brownlow from Royal Holloway, University of London

Figures 5.21 and 5.22 show the difference between the clean and polluted samples respectively. The GC×GC plots (plot b in both figures) are scaled to the same level so that any differences can be easily seen. This is not done for the 1D GC plots (plot a in each figure) for the same reason, the polluted sample (Figure 5.22) shows peak amplitudes

that are up to a factor of three higher than those seen in the clean sample (Figure 5.21). There are some obvious differences between the GC×GC plots for the two samples; the polluted sample shows both an increased presence (approximately 50 more species can be observed) and intensity of species, while the clean sample is indicative of a less polluted, marine influenced air mass. There are only two hours between the two different samples which shows how quickly the air masses can change in this region.

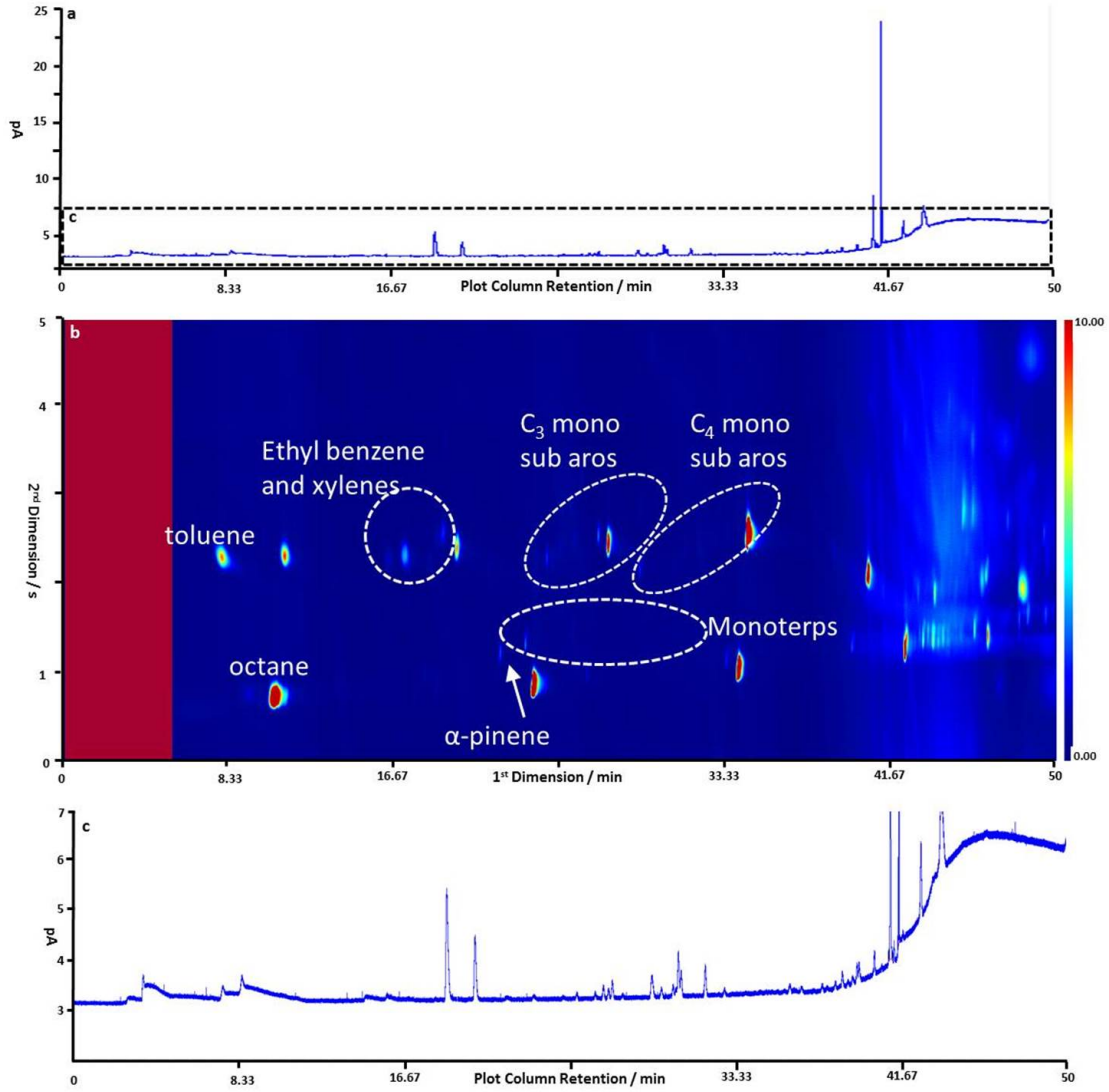

Figure 5.21: GC-GC×GC chromatogram from Bachok that is representative of a clean marine influenced air mass from 19/01/2014 at 07:24 (local time), a: 1D GC plot from the volatile heart-cut stage, b: 2D GC plot from the GC×GC stage and c: shows a zoomed in section of the 1D GC plot, highlighted by the box in plot a

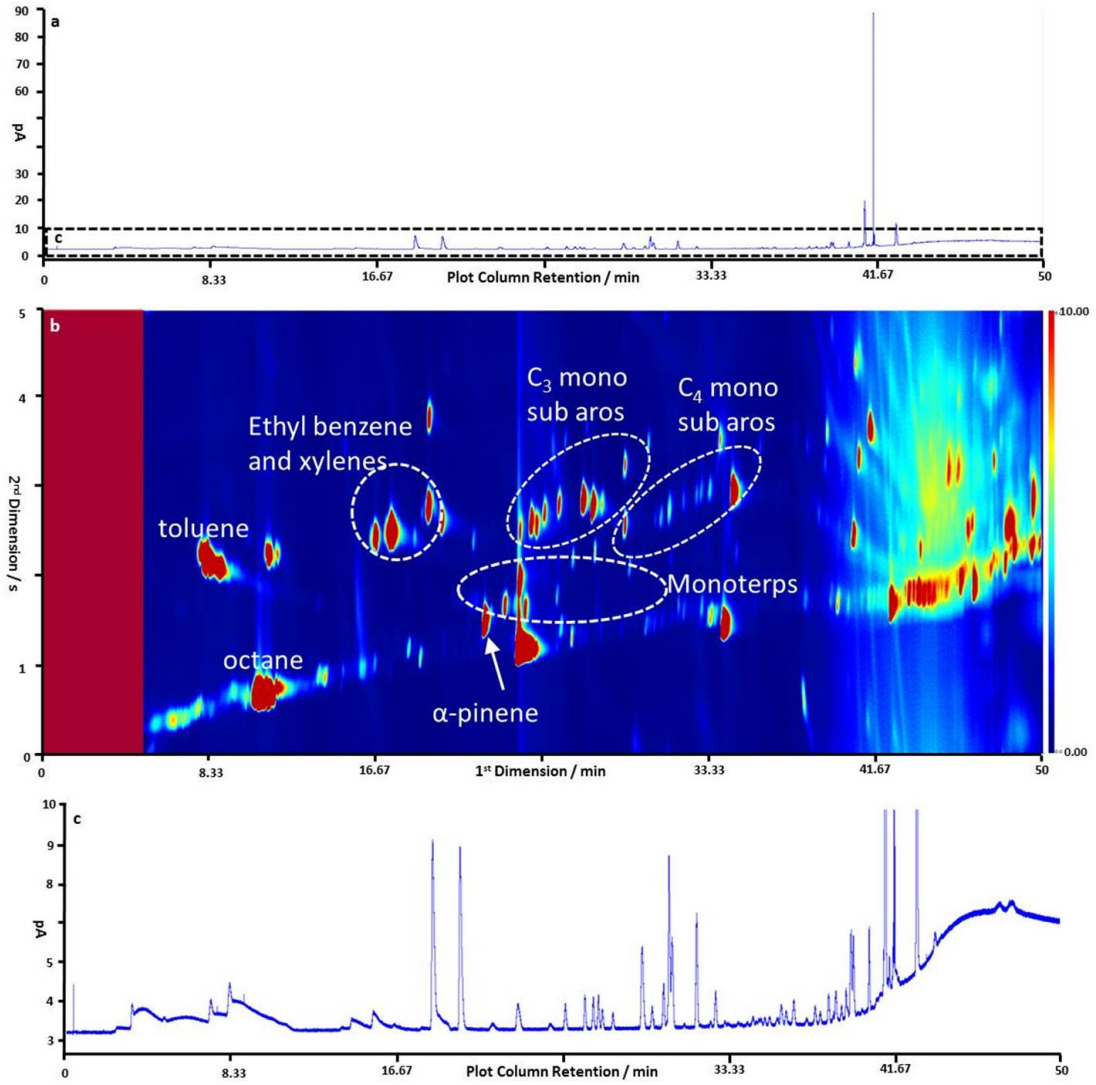

Figure 5.22: GC-GC×GC chromatogram from Bachok that is representative of a highly polluted air mass from 20/01/2014 at 09:21 (local time), a: 1D GC plot from the volatile heart-cut stage, b: 2D GC plot from the GC×GC stage and c: shows a zoomed in section of the 1D GC plot, highlighted by the box in plot a

5.4.1 Time series

Figure 5.23 shows time series for isoprene and toluene measured using the GC-GC×GC during the Bachok campaign. Measurement gaps in these profiles were due to either concentrations below the detection limit of the instrument or blockages in the sampling line. These blockages were caused by a build up of ice in the glass finger as a result of very high levels of ambient relative humidity. However, even with these gaps, there were high levels of both compounds observed during the first four days of the campaign and throughout the rest of the campaign for isoprene. This was also observed in all other VOC species measured during the Bachok campaign, where anthropogenic species

had very high levels at the start of the campaign and biogenic species had high levels throughout. Isoprene, and other BVOCs, are likely enhanced during this campaign as this is a region with many biogenic sources and emissions are increased due to high levels of temperature and sunlight. The increased levels of both species during the first four days of the campaign were influenced by air masses transported from China and Thailand that were highly polluted.

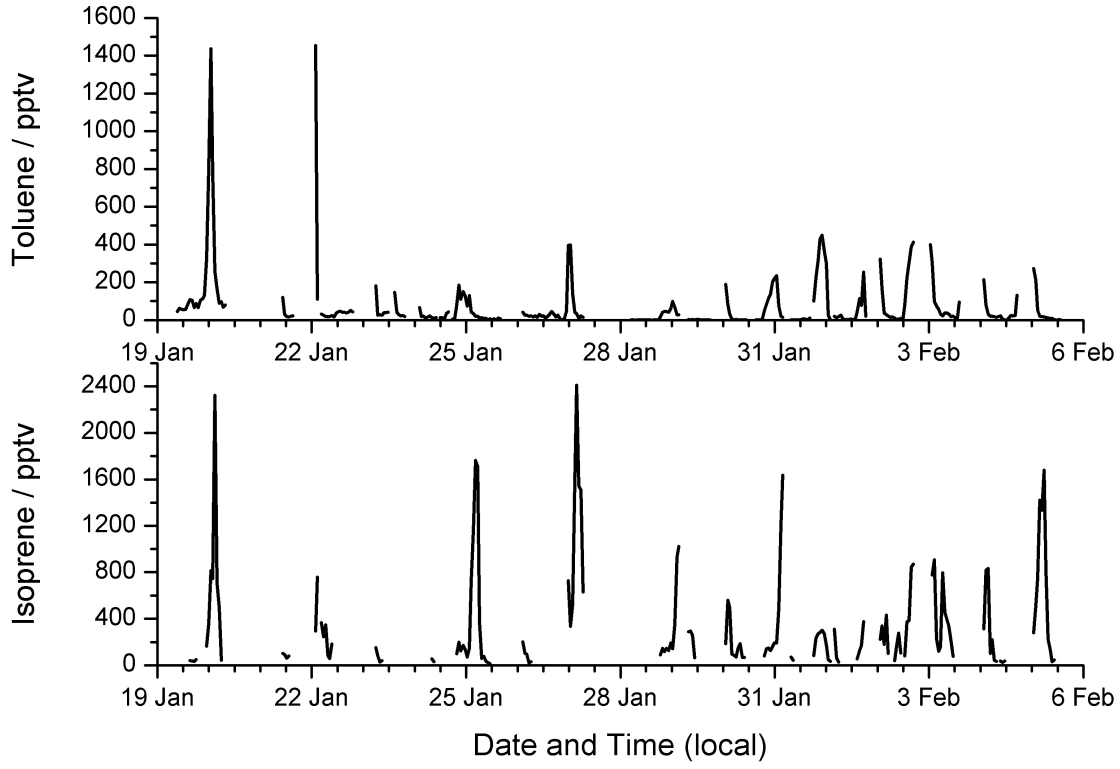

Figure 5.23: Time series of isoprene (lower) and toluene (upper) during the Bachok campaign.

5.4.2 Diurnal profiles

Figure 5.24 shows the diurnal profiles observed at Bachok from selected VOCs and NO_x. The profiles of NO_x and the anthropogenic source VOCs show a morning peak at approximately 7 am, with a sharp decrease seen around 10 am where the concentrations are sustained at a minimum until the next morning, except for NO which begins to increase from $\approx$ 20:00 to the maximum early in the morning. The diurnal profile of isoprene shows a maxima just before midday that is not present in those species of anthropogenic origin, consistent with the presence of an overwhelming biogenic source. However, the profile still drops off faster than expected.

There were no reliable meteorology measurements made at the Bachok site, however

from personal experiences there was a switch in wind direction made each day at approximately midday. During the morning hours, the air was coming over the land and showed very high levels of NO_x and the anthropogenic VOCs. The sources of these were local burning of rubbish (see Figure 5.25), seen by the peaks in all species at approximately 8 am. When the wind direction changes, a rapid switch is seen, particularly in the profiles of NO_x and the anthropogenic species where a dramatic decrease is observed.

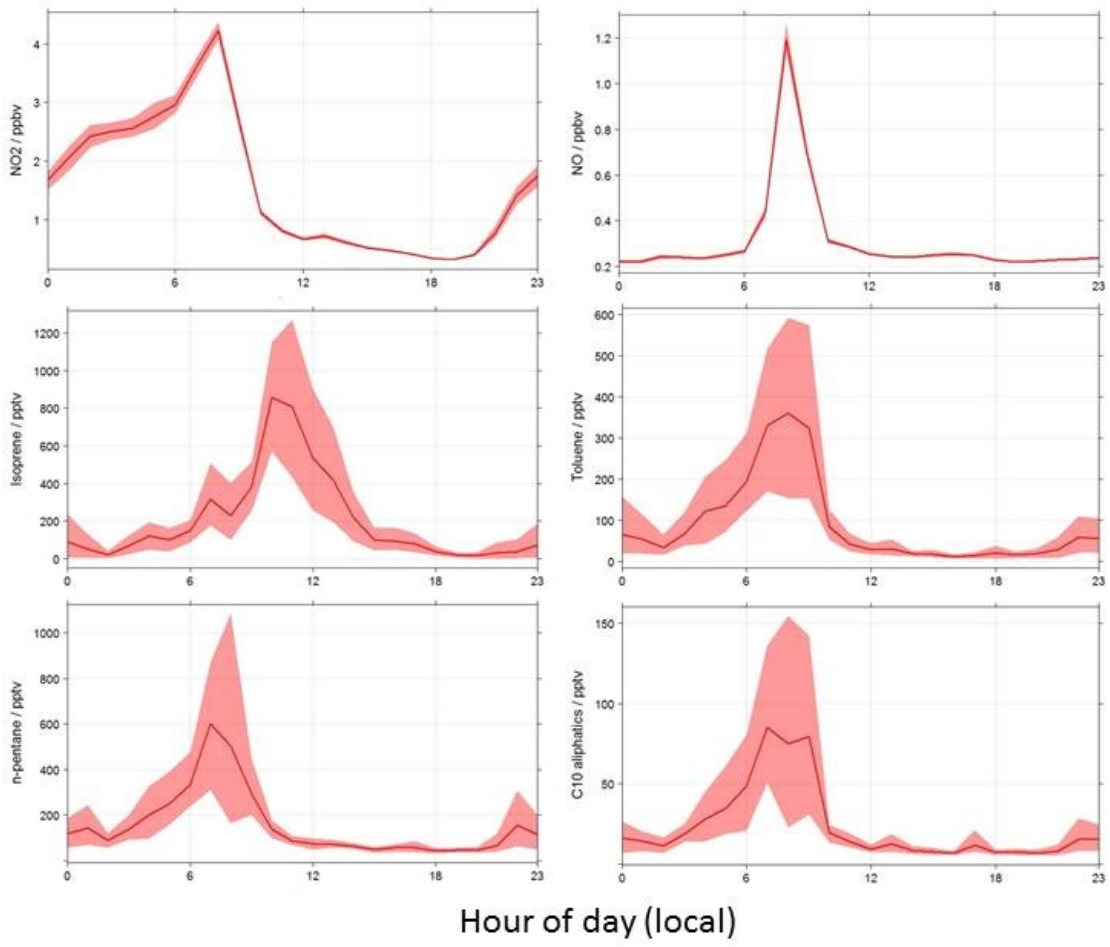

Figure 5.24: Diurnal profiles of NO, NO_2, isoprene, toluene, *n*-pentane and C_{10} aliphatic species, constructed using the openair project for R where the solid line represents the mean daily concentration and the shaded regions shows the 95% confidence intervals surrounding the mean.[166–168]

Figure 5.25: Images of local rubbish burning from the surrounding area. The left image shows burning just beyond the fence surrounding the site. The right shows sampling from burning of waste wood from a local pallet manufacturing company (just down the road from the site, ≈ 0.5 km)

5.4.3 Comparison to proton-transfer-reaction mass spectrometer

During the Bachok demonstration campaign, the University of East Anglia also measured VOCs using a PTR-MS. Some of these species overlapped with those measured using the GC-GC×GC instrument. Figure 5.26 shows a comparison time series (left panel) and correlation (right panel) of toluene and isoprene from the PTR-MS and GC-GC×GC instruments. The PTR-MS was offline during the middle part of the campaign indicated by the break in the x-axis, due to a power supply failure. During the periods where both instruments were operational, both show similar time series trends and profiles, though the PTR-MS does have more structured data due to its faster time resolution (approximately minute data as opposed to almost hourly resolution from the GC-GC×GC). Both instruments show the sharp decrease after midday, assumed to be when the wind direction changed from land to ocean influenced air masses. The PTR-MS does show significantly higher observed mixing ratios of isoprene than the GC-GC×GC instrument. It was speculated that this was due to interferences from furan, which also appears at m/z 69 (the integer mass that corresponds to isoprene). The quantification of multiple species at a single mass can be a common occurrence when using a PTR-MS.[293] This is also seen in the correlation plot for isoprene (Figure 5.26, right panel lower plot) which has a high intercept (+401 pptv) on the line of best fit for the PTR-MS. In contrast, the correlation for toluene from both instruments shows that they compare quite well,(R^2 of 0.7377). and there is only a very small offset (+30 pptv) in the intercept. The R^2 for isoprene (0.3207) shows that is it likely that there were interferences on the PTR-MS instrument.

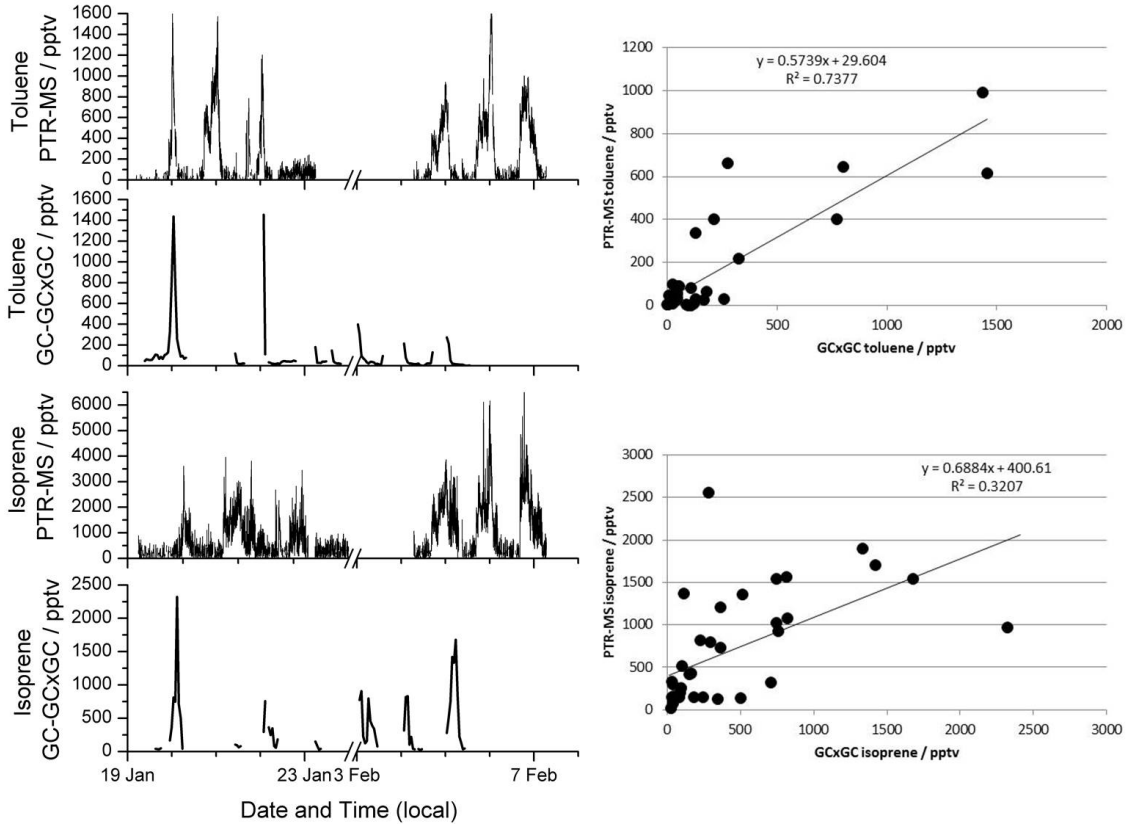

Figure 5.26: Comparison time series (left panel) and correlations (right panel) of toluene and isoprene from the PTR-MS and GC-GC×GC instruments.

5.5 Conclusion

The original GC×GC instrument described in previous chapters performed well for the majority of compounds, however it was unable to accurately quantify isoprene due to the incomplete separation and resolution of the species from surrounding compounds. Combining conventional 1D GC with GC×GC not only allows for a much wider range of VOCs to be measured using a single instrument (GC-GC×GC), but also provides a method that could quantify isoprene. Comparison to an existing instrument demonstrated that this new GC-GC×GC can accurately measure C_5-C_{13} VOC species with have a wide range of functionalities. This GC-GC×GC instrument was shown to be able to quantify isoprene with a LOD of 13 pptv. Approximately hourly measurements were conducted in a remote environment, Bachok, Malaysia. Despite difficulties faced by the GC-GC×GC instrument from high levels of humidity and power failures, it was possible to measure and quantify isoprene (LOD = 14 pptv). This region was shown to be influenced by both clean marine air masses, local anthropogenic and biogenic emission sources and transported

emissions from across highly polluted regions. There appears to be a dramatic shift in air mass direction each day, which has been shown to influence the diurnal profiles of species measured at the Bachok site. A PTR-MS was also deployed to Bachok and compared to the new GC-GC×GC instrument. The correlation between the two instruments for isoprene was shown to be rather poor ((R^2 of 0.3207), likely from integer mass interference on the PTR-MS. This was not seen with other compounds that both instruments measured, such as toluene (R^2 of 0.7377). Overall, this new GC-GC×GC instrument has been shown to perform well in lab comparisons and in situ operation, despite difficulties from observations in un-ideal locations.

Chapter 6

Conclusions and future work

The increased use of diesel world-wide, and particularly in megacities, has changed the profile of VOC emissions from short to long chain compounds. The large suite of VOC measurements carried out during the ClearfLo campaign has provided direct evidence of this effect on the atmospheric composition of London. These species have also been shown to have significant impacts on OH reactivity, ozone formation potential and SOA production in London. The emission of the higher carbon number VOCs from diesel are underestimated by current emission inventories and as such there needs to be an improvement made to the existing measurement infrastructure so that these species can be accurately quantified. There are already policy challenges relating to the emission of NO_2 from diesel vehicles. This thesis demonstrates that there is likely another challenge regarding the emission of higher carbon number VOCs and their impacts on urban air pollution.

This thesis details the quantification of a much larger suite of VOCs than is usually seen in the majority of studies, allowing for a very in depth analysis of London's atmosphere. VOCs ranging from C_1 to C_{12}, with a wide variety of functionalities (including multiple OVOCs and aromatic species) have been observed. Several of these species, both individually and as functional groups, are not routinely measured as part of air quality strategies and were shown to be important to total VOC mixing ratio, OH reactivity and potential ozone formation. The NK site, an urban background location in London, was shown to be largely influenced by fresh local emissions but also some periods where aged emissions were transported from further afield. Both anthropogenic and biogenic emissions sources were found to be important in London. The anthropogenic emissions were dominated by traffic-related sources, with the impact of emissions from diesel vehicles further strengthened. There also appears to be a local source of biogenic emissions in London that significantly affects the composition of the atmosphere during the summer. Species emitted from both these sources can have a considerable effects on the OH reactivity and potential ozone formation of the local region.

A direct measurement of OH reactivity was also made during the summer ClearfLo campaign, concurrent with the VOC measurements. This was compared to modelled OH reactivity from three different sets of VOC species; a standard VOC set that contains VOCs that have been routinely measured, an extended VOC set that includes additional individual higher carbon number VOCs measured using the GC×GC and an extended plus grouped UCM VOC set. This last VOC set includes all of the individually quantified

VOCs and also those included in a grouped quantification analysis using the GC×GC. The comparison showed that OH reactivity, and subsequent ozone formation, can be accurately modelled if the VOCs included are fully representative of the primary VOC emissions. There were substantial underestimations found when the OH reactivity was modelled using the standard and extended VOC sets, something not shown with the extended + grouped UCM VOC set. The additional grouped VOC species and BVOCs were highlighted as being particularly important for OH reactivity and the majority of these are not routinely measured in the atmosphere. Thus the current measurement infrastructure needs to be improved to provide a wider characterisation of the VOC loading, particularly in urban areas and megacities such as London.

An extensive set of OVOC species were measured during the ClearfLo campaign, with 21 individual compounds quantified. Five of these species provided the majority of the total OVOC mixing ratio loading during both the winter and summer campaigns, while acetaldehyde was the dominant contributor to the OH reactivity and OFP from the OVOCs. Analysis showed that there were two distinct groups of OVOCs present in London's atmosphere, those directly emitted and those formed in the atmosphere. These two groups had different diurnal profiles and correlations with other OVOC and VOC species that corroborated their different sources. Some OVOC species did not fall into either category and they shown to be largely influenced by high levels of fluctuation in their time series. Measurements of OVOC species is not common in urban areas but this analysis has shown that they are vitally important to urban air quality, as they can have a high influence on the oxidative potential of the atmosphere and produce significant quantities of ozone.

The work presented in this thesis has shown that the composition of the atmosphere in a developed megacity, London, is highly complex. This situation is further complicated by the increased combustion of diesel throughout Europe. In the US, however, diesel has only found limited use. It would be interesting to measure this large suite of VOCs in other megacities around the globe that have varying levels of diesel usage. This could provide more detailed information to be used in models, such as the MCM for OH reactivity, and to update emission inventories that are lacking this significant source of higher carbon number species. Chamber studies could be used for detailed analysis of the compositional changes between gasoline and diesel, and also how those changes can affect the production of secondary pollutants such as ozone and SOA.

The use of biofuel worldwide, and specifically in the UK, has been increasing over the last decade. The UK currently uses 5% ethanol blended gasoline, however the impacts this would have on UK air quality have not been fully investigated. Ethanol was the most abundant VOC species measured during the winter and summer ClearfLo campaigns. Diurnal profiles and correlations of both ethanol and acetaldehyde (the main product of the reaction of ethanol with the OH radical) with other VOC species demonstrated that the main emission source was from either the combustion of or evaporative emissions from ethanol blended gasoline. A highly detailed MCM model simulation was carried out to determine what the local scale impacts of the measured ethanol would have. It was found that, although the ethanol included in the model did not produce large quantities of acetaldehyde, the model outputted acetaldehyde did not match that observed. It is likely that this discrepancy is due to the presence of a direct emission source of acetaldehyde, with evidence pointing to traffic-related emissions. The results have shown that there is a large traffic-related emission source of ethanol, and likely acetaldehyde, in urban areas. If a chemical transport model (*i.e.* GEOS-Chem) were used, which would take into account the long lifetime of ethanol in the atmosphere, it is possible that an enhanced acetaldehyde plume downwind of emission source would be produced. Further analysis that could be carried out would be to use a chemical transport model to attempt a prediction of the longer range transport of ethanol, its impact on acetaldehyde and subsequent ozone production. This should be investigated further as increased bioethanol use in Europe is likely to help reduce the net carbon dioxide emissions from vehicles.

A hybrid GC system was developed, combining heart-cut GC and GC×GC in a single instrument (GC-GC×GC) to measure a wider range of VOC species. This new instrument was compared to a well established DC-GC instrument and found to be suitable to measure C_5-C_{13} VOC species, as well as accurately quantify isoprene (with a LOD of 13 pptv). The GC-GC×GC was deployed to Bachok, Malaysia, a rural location, and approximately hourly time-resolved measurements were carried out. The results showed that the measurement site was influenced by local anthropogenic and biogenic emissions, while switching of air mass trajectories brought both highly polluted and cleaner air masses. A further comparison to a PTR-MS instrument proved that the GC-GC×GC was well suited to in situ observations of a wide range of VOC species. The measurement of isoprene in Bachok using the GC-GC×GC was more accurate than the PTR-MS, which suffered from mass interferences. This new instrument could be developed further in an attempt to overcome

the difficulties experienced during water removal from samples. Also, this instrument can be deployed to other remote or urban areas around the globe to provide a more detailed characterisation of the atmospheric VOC loading than could be accomplished using the previous GC×GC set up.

Appendix A

Correlations of individual and grouped volatile organic compounds

Correlation values for all the measured individual and grouped VOC species are shown in Tables A.1 to A.21. Several species were not measured or were below the detection limit of the instrument and have not been included in the relevant tables. Correlations that are greater than 0.50 have been highlighted in a bold font.

A.1 Winter correlations between volatile organic compounds

Table A.1: Winter correlations of saturated aliphatic species, values in bold indicate correlations greater than 0.50.

	Methane	Ethane	Propane	*iso*-Butane	*n*-Butane	*n*-Pentane	*iso*-Pentane	Cyclopentane	*n*-Hexane	Pentane, 2+3-methyl-	*n*-Heptane	Butane, 2,2,3-trimethyl-	*n*-Octane	Pentane, 2,2,4-trimethyl	*n*-Nonane	*n*-Decane	Nonane, 2-methyl-	*n*-Undecane
Ethane	**0.95**																	
Propane	**0.91**	**0.93**																
***iso*-Butane**	**0.81**	**0.81**	**0.92**															
***n*-Butane**	**0.73**	**0.72**	**0.87**	**0.98**														
***n*-Pentane**	**0.87**	**0.85**	**0.90**	**0.91**	**0.85**													
***iso*-Pentane**	**0.80**	**0.79**	**0.87**	**0.92**	**0.86**	**0.98**												
Cyclopentane	**0.68**	**0.71**	**0.68**	**0.63**	**0.57**	**0.68**	**0.67**											
***n*-Hexane**	**0.81**	**0.76**	**0.84**	**0.88**	**0.82**	**0.96**	**0.94**	**0.59**										
Pentane, 2+3-methyl-	**0.77**	**0.75**	**0.83**	**0.88**	**0.83**	**0.95**	**0.98**	**0.64**	**0.94**									
***n*-Heptane**	**0.60**	**0.58**	**0.65**	**0.69**	**0.65**	**0.74**	**0.75**	**0.51**	**0.73**	**0.76**								
Butane, 2,2,3-trimethyl	**0.63**	**0.61**	**0.68**	**0.71**	**0.67**	**0.76**	**0.76**	**0.52**	**0.74**	**0.79**	**0.62**							
***n*-Octane**	**0.79**	**0.77**	**0.84**	**0.88**	**0.81**	**0.94**	**0.95**	**0.68**	**0.92**	**0.96**	**0.74**	**0.78**						
Pentane, 2,2,4-trimethyl	**0.58**	**0.56**	**0.64**	**0.70**	**0.66**	**0.74**	**0.77**	**0.52**	**0.72**	**0.80**	**0.59**	**0.67**	**0.77**					
***n*-Nonane**	**0.70**	**0.68**	**0.75**	**0.80**	**0.76**	**0.85**	**0.87**	**0.59**	**0.83**	**0.89**	**0.70**	**0.88**	**0.89**	**0.76**				
***n*-Decane**	**0.77**	**0.73**	**0.78**	**0.78**	**0.73**	**0.84**	**0.81**	**0.65**	**0.81**	**0.83**	**0.68**	**0.80**	**0.85**	**0.73**	**0.88**			
Nonane, 2-methyl-	**0.63**	**0.61**	**0.68**	**0.71**	**0.67**	**0.76**	**0.76**	**0.52**	**0.74**	**0.79**	**0.62**	**0.99**	**0.78**	**0.67**	**0.88**	**0.80**		
***n*-Undecane**	**0.70**	**0.68**	**0.75**	**0.80**	**0.76**	**0.85**	**0.87**	**0.59**	**0.83**	**0.89**	**0.70**	**0.88**	**0.89**	**0.76**	**0.99**	**0.88**	**0.88**	
***n*-Dodecane**	**0.74**	**0.69**	**0.76**	**0.76**	**0.71**	**0.82**	**0.80**	**0.61**	**0.79**	**0.82**	**0.67**	**0.80**	**0.84**	**0.72**	**0.88**	**0.97**	**0.80**	**0.88**

Table A.2: Winter correlations of saturated and unsaturated aliphatic species, values in bold indicate correlations greater than 0.50. Two of the unsaturated aliphatic species were not measured during the winter campaign, propyne ad 1,2-butadiene, and as such have not been included in this table.

	Ethene	Acetylene	Propene	Propadiene	Butene, *trans*-2-	1-Butene	*iso*-Butene	Butene, *cis*-2-	1,3-Butadiene	Pentene, *trans*-2-	1-Pentene	Isoprene	Styrene	α-Pinene	Limonene
Methane	**0.80**	**0.77**	**0.71**	**0.74**	**0.73**	**0.76**	**0.78**	**0.73**	**0.71**	**0.69**	**0.63**	**0.80**	**0.57**	-0.14	**0.75**
Ethane	**0.70**	**0.74**	**0.63**	**0.70**	**0.74**	**0.71**	**0.77**	**0.72**	**0.70**	0.17	0.21	**0.78**	**0.58**	-0.10	**0.76**
Propane	**0.78**	**0.81**	**0.75**	**0.78**	**0.81**	**0.81**	**0.85**	**0.81**	**0.77**	0.20	0.25	**0.84**	**0.60**	-0.11	**0.78**
***iso*-Butane**	**0.79**	**0.81**	**0.75**	**0.81**	**0.87**	**0.83**	**0.90**	**0.87**	**0.79**	0.22	0.28	**0.85**	**0.60**	-0.12	**0.76**
***n*-Butane**	**0.74**	**0.76**	**0.71**	**0.77**	**0.82**	**0.78**	**0.86**	**0.82**	**0.74**	0.21	0.26	**0.79**	**0.55**	-0.11	**0.70**
***n*-Pentane**	**0.86**	**0.85**	**0.83**	**0.88**	**0.93**	**0.89**	**0.94**	**0.93**	**0.85**	0.25	0.31	**0.91**	**0.65**	-0.15	**0.80**
***iso*-Pentane**	**0.83**	**0.82**	**0.81**	**0.88**	**0.97**	**0.89**	**0.97**	**0.97**	**0.86**	0.26	0.33	**0.92**	**0.66**	-0.15	**0.78**
Cyclopentane	**0.55**	**0.53**	**0.51**	**0.56**	**0.63**	**0.58**	**0.64**	**0.60**	**0.58**	0.16	0.19	**0.69**	**0.59**	-0.12	**0.67**
***n*-Hexane**	**0.86**	**0.86**	**0.85**	**0.87**	**0.90**	**0.90**	**0.92**	**0.90**	**0.83**	0.26	0.33	**0.86**	**0.59**	-0.17	**0.75**
Pentane, 2+3-methyl-	**0.85**	**0.84**	**0.84**	**0.90**	**0.97**	**0.90**	**0.97**	**0.97**	**0.87**	0.28	0.35	**0.90**	**0.68**	-0.16	**0.77**
***n*-Heptane**	**0.68**	**0.69**	**0.66**	**0.71**	**0.91**	**0.71**	**0.75**	**0.92**	**0.66**	0.26	0.33	**0.69**	**0.52**	-0.13	**0.62**
Butane, 2,2,3-trimethyl-	**0.73**	**0.73**	**0.69**	**0.77**	**0.76**	**0.75**	**0.79**	**0.79**	**0.70**	0.22	0.28	**0.70**	**0.65**	-0.14	**0.65**
***n*-Octane**	**0.88**	**0.86**	**0.86**	**0.91**	**0.94**	**0.93**	**0.96**	**0.94**	**0.90**	0.27	0.34	**0.90**	**0.69**	-0.14	**0.79**
Pentane, 2,2,4-trimethyl-	**0.72**	**0.69**	**0.71**	**0.80**	**0.79**	**0.76**	**0.82**	**0.80**	**0.74**	0.21	0.26	**0.77**	**0.57**	-0.11	**0.62**
***n*-Nonane**	**0.81**	**0.79**	**0.78**	**0.86**	**0.87**	**0.85**	**0.89**	**0.88**	**0.82**	0.26	0.33	**0.82**	**0.75**	-0.16	**0.75**
***n*-Decane**	**0.84**	**0.83**	**0.78**	**0.85**	**0.79**	**0.83**	**0.83**	**0.79**	**0.80**	0.24	0.29	**0.81**	**0.70**	-0.15	**0.79**
Nonane, 2-methyl-	**0.73**	**0.73**	**0.69**	**0.77**	**0.76**	**0.75**	**0.79**	**0.79**	**0.70**	0.22	0.28	**0.70**	**0.65**	-0.14	**0.65**
***n*-Undecane**	**0.81**	**0.79**	**0.78**	**0.86**	**0.87**	**0.85**	**0.89**	**0.88**	**0.82**	0.26	0.33	**0.82**	**0.75**	-0.16	**0.75**
***n*-Dodecane**	**0.83**	**0.83**	**0.76**	**0.85**	**0.79**	**0.81**	**0.82**	**0.79**	**0.78**	0.23	0.28	**0.78**	**0.70**	-0.16	**0.77**

Table A.3: Winter correlations of saturated aliphatic and aromatic species, values in bold indicate correlations greater than 0.50.

	Benzene	Toluene	Benzene, ethyl-	*m*- and *p*-Xylene	*o*-Xylene	Benzene, *iso*-propyl-	Benzene, propyl-	Toluene, 3-ethyl-	Toluene, 4-ethyl-	Benzene, 1,3,5-trimethyl-	Toluene, 2-ethyl-	Benzene, 1,2,4-trimethyl-	Toluene, 4-*iso*-propyl-	Benzene, 1,2,3-trimethyl-	Indan	Benzene, *tert*-butyl-	Benzene, 1,3-diethyl-	Benzene, 1,4-diethyl-	Napthalene
Methane	**0.78**	**0.77**	**0.68**	**0.74**	**0.76**	0.46	**0.54**	**0.56**	0.46	**0.60**	**0.54**	**0.51**	0.38	**0.70**	**0.62**	0.04	**0.67**	**0.69**	**0.63**
Ethane	**0.73**	**0.74**	**0.67**	**0.72**	**0.74**	0.43	**0.50**	**0.50**	0.45	**0.58**	**0.54**	0.46	0.36	**0.68**	**0.59**	0.06	**0.64**	**0.68**	**0.61**
Propane	**0.80**	**0.82**	**0.75**	**0.80**	**0.81**	**0.52**	**0.59**	**0.60**	**0.52**	**0.65**	**0.57**	**0.55**	0.37	**0.74**	**0.68**	0.07	**0.71**	**0.74**	**0.68**
***iso*-Butane**	**0.82**	**0.88**	**0.81**	**0.86**	**0.86**	**0.61**	**0.65**	**0.66**	**0.59**	**0.70**	**0.62**	**0.61**	0.34	**0.79**	**0.80**	0.07	**0.74**	**0.76**	**0.71**
***n*-Butane**	**0.77**	**0.83**	**0.76**	**0.81**	**0.80**	**0.61**	**0.61**	**0.62**	**0.55**	**0.66**	**0.56**	**0.56**	0.31	**0.74**	**0.81**	0.07	**0.69**	**0.71**	**0.67**
***n*-Pentane**	**0.88**	**0.94**	**0.85**	**0.91**	**0.91**	**0.62**	**0.70**	**0.72**	**0.62**	**0.75**	**0.67**	**0.68**	0.39	**0.83**	**0.78**	0.08	**0.79**	**0.81**	**0.76**
***iso*-Pentane**	**0.86**	**0.96**	**0.88**	**0.94**	**0.94**	**0.65**	**0.70**	**0.73**	**0.65**	**0.78**	**0.69**	**0.67**	0.35	**0.84**	**0.80**	0.08	**0.81**	**0.83**	**0.76**
Cyclopentane	**0.57**	**0.65**	**0.62**	**0.66**	**0.68**	0.41	0.37	0.36	0.37	**0.53**	**0.50**	0.35	0.21	**0.60**	**0.58**	0.03	**0.56**	**0.62**	**0.52**
***n*-Hexane**	**0.86**	**0.92**	**0.83**	**0.89**	**0.88**	**0.59**	**0.71**	**0.76**	**0.62**	**0.72**	**0.63**	**0.70**	0.39	**0.81**	**0.75**	0.07	**0.77**	**0.78**	**0.74**
Pentane, 2+3-methyl-	**0.87**	**0.97**	**0.91**	**0.96**	**0.95**	**0.69**	**0.73**	**0.76**	**0.70**	**0.80**	**0.72**	**0.70**	0.37	**0.86**	**0.83**	0.09	**0.83**	**0.84**	**0.79**
***n*-Heptane**	**0.70**	**0.76**	**0.71**	**0.76**	**0.95**	**0.68**	**0.55**	**0.55**	**0.53**	**0.59**	**0.50**	**0.50**	0.25	**0.67**	**0.82**	0.04	**0.65**	**0.67**	**0.62**
Butane, 2,2,3-trimethyl-	**0.76**	**0.80**	**0.75**	**0.79**	**0.78**	**0.73**	**0.73**	**0.70**	**0.67**	**0.76**	**0.68**	**0.63**	0.44	**0.82**	**0.89**	0.07	**0.79**	**0.79**	**0.99**
***n*-Octane**	**0.87**	**0.96**	**0.91**	**0.96**	**0.96**	**0.71**	**0.73**	**0.73**	**0.68**	**0.80**	**0.69**	**0.68**	0.38	**0.87**	**0.84**	0.10	**0.83**	**0.86**	**0.78**
Pentane, 2,2,4-trimethyl-	**0.75**	**0.82**	**0.76**	**0.81**	**0.78**	**0.51**	**0.57**	**0.62**	**0.59**	**0.67**	**0.60**	**0.53**	0.29	**0.75**	**0.69**	0.01	**0.70**	**0.72**	**0.67**
***n*-Nonane**	**0.82**	**0.91**	**0.86**	**0.90**	**0.87**	**0.83**	**0.79**	**0.79**	**0.77**	**0.86**	**0.81**	**0.73**	0.47	**0.92**	**0.88**	0.02	**0.89**	**0.90**	**0.88**
***n*-Decane**	**0.87**	**0.84**	**0.78**	**0.83**	**0.83**	**0.72**	**0.73**	**0.74**	**0.69**	**0.77**	**0.71**	**0.69**	0.42	**0.85**	**0.84**	0.06	**0.82**	**0.87**	**0.80**
Nonane, 2-methyl-	**0.76**	**0.80**	**0.75**	**0.79**	**0.78**	**0.73**	**0.73**	**0.70**	**0.67**	**0.76**	**0.68**	**0.63**	0.44	**0.82**	**0.89**	0.07	**0.79**	**0.79**	**0.99**
***n*-Undecane**	**0.82**	**0.91**	**0.86**	**0.90**	**0.87**	**0.83**	**0.79**	**0.79**	**0.77**	**0.86**	**0.81**	**0.73**	0.47	**0.92**	**0.88**	0.02	**0.89**	**0.90**	**0.88**
***n*-Dodecane**	**0.86**	**0.83**	**0.78**	**0.82**	**0.81**	**0.75**	**0.72**	**0.73**	**0.69**	**0.79**	**0.73**	**0.66**	0.45	**0.86**	**0.84**	0.05	**0.84**	**0.86**	**0.80**

Table A.4: Winter correlations of saturated aliphatic and the grouped species, values in bold indicate correlations greater than 0.50.

	C_6 aliphatics	C_7 aliphatics	C_8 aliphatics	C_9 aliphatics	C_{10} aliphatics	C_{11} aliphatics	C_{12} aliphatics	C_{13} aliphatics	C_4 substituted monoaromatics	C_{10} monoterpenes
Methane	**0.51**	**0.67**	**0.71**	**0.67**	0.34	**0.69**	**0.64**	**0.70**	**0.68**	**0.69**
Ethane	**0.51**	**0.65**	**0.69**	**0.65**	0.30	**0.67**	**0.64**	**0.69**	**0.67**	**0.67**
Propane	**0.59**	**0.72**	**0.75**	**0.71**	0.39	**0.75**	**0.71**	**0.76**	**0.74**	**0.74**
***iso*-Butane**	**0.66**	**0.77**	**0.79**	**0.76**	0.45	**0.79**	**0.78**	**0.81**	**0.79**	**0.80**
***n*-Butane**	**0.63**	**0.72**	**0.74**	**0.71**	0.44	**0.75**	**0.74**	**0.76**	**0.74**	**0.75**
***n*-Pentane**	**0.69**	**0.81**	**0.83**	**0.80**	0.43	**0.84**	**0.82**	**0.86**	**0.83**	**0.84**
***iso*-Pentane**	**0.72**	**0.83**	**0.84**	**0.82**	0.44	**0.85**	**0.85**	**0.87**	**0.85**	**0.86**
Cyclopentane	0.40	**0.57**	**0.59**	**0.57**	0.16	**0.58**	**0.55**	**0.59**	**0.59**	**0.59**
***n*-Hexane**	**0.67**	**0.79**	**0.81**	**0.77**	0.47	**0.82**	**0.80**	**0.84**	**0.81**	**0.82**
Pentane, 2+3-methyl-	**0.75**	**0.85**	**0.87**	**0.84**	0.47	**0.87**	**0.87**	**0.89**	**0.88**	**0.88**
***n*-Heptane**	**0.59**	**0.65**	**0.68**	**0.68**	0.44	**0.69**	**0.68**	**0.70**	**0.68**	**0.69**
Butane, 2,2,3-trimethyl-	**0.78**	**0.80**	**0.85**	**0.80**	0.48	**0.87**	**0.84**	**0.88**	**0.84**	**0.84**
***n*-Octane**	**0.72**	**0.84**	**0.86**	**0.83**	0.48	**0.87**	**0.85**	**0.89**	**0.88**	**0.88**
Pentane, 2,2,4-trimethyl-	**0.63**	**0.68**	**0.72**	**0.68**	0.40	**0.75**	**0.74**	**0.76**	**0.75**	**0.77**
***n*-Nonane**	**0.89**	**0.94**	**0.98**	**0.93**	**0.51**	**0.97**	**0.97**	**0.99**	**0.97**	**0.98**
***n*-Decane**	**0.71**	**0.81**	**0.87**	**0.81**	0.40	**0.86**	**0.81**	**0.89**	**0.86**	**0.87**
Nonane, 2-methyl-	**0.78**	**0.80**	**0.85**	**0.80**	0.48	**0.87**	**0.84**	**0.88**	**0.84**	**0.84**
***n*-Undecane**	**0.89**	**0.94**	**0.97**	**0.93**	**0.51**	**0.97**	**0.97**	**0.99**	**0.97**	**0.98**
***n*-Dodecane**	**0.73**	**0.81**	**0.86**	**0.81**	0.41	**0.86**	**0.80**	**0.89**	**0.85**	**0.87**

Table A.5: Winter correlations of unsaturated aliphatic species, values in bold indicate correlations greater than 0.50. Two of the unsaturated aliphatic species, propyne and 1,2-butadiene, were not measured during the winter campaign and as such have not been included.

	Ethene	Acetylene	Propene	Propadiene	Butene, *trans*-2-	1-Butene	*iso*-Butene	Butene, *cis*-2-	1,3-Butadiene	Pentene, *trans*-2-	1-Pentene	Isoprene	Styrene	α-Pinene
Acetylene	**0.89**													
Propene	**0.93**	**0.81**												
Propadiene	**0.90**	**0.91**	**0.84**											
***trans*-2-Butene**	**0.83**	**0.83**	**0.82**	**0.91**										
1-Butene	**0.94**	**0.88**	**0.96**	**0.91**	**0.91**									
***iso*-Butene**	**0.87**	**0.87**	**0.85**	**0.94**	**0.98**	**0.93**								
***cis*-2-Butene**	**0.84**	**0.83**	**0.84**	**0.91**	**0.99**	**0.92**	**0.98**							
1,3-Butadiene	**0.85**	**0.84**	**0.83**	**0.91**	**0.89**	**0.91**	**0.92**	**0.90**						
***trans*-2-Pentene**	**0.78**	**0.79**	**0.78**	**0.86**	**0.97**	**0.86**	**0.94**	**0.97**	**0.81**					
1-Pentene	**0.77**	**0.79**	**0.75**	**0.87**	**0.95**	**0.86**	**0.93**	**0.95**	**0.80**	**0.96**				
Isoprene	**0.81**	**0.79**	**0.80**	**0.86**	**0.91**	**0.88**	**0.93**	**0.91**	**0.89**	**0.90**	**0.86**			
Styrene	**0.61**	**0.57**	**0.58**	**0.63**	**0.68**	**0.66**	**0.67**	**0.68**	**0.63**	**0.64**	**0.62**	**0.63**		
α-**Pinene**	-0.17	-0.12	-0.16	-0.13	-0.13	-0.15	-0.14	-0.13	-0.10	-0.06	-0.05	-0.13	-0.15	
Limonene	**0.72**	**0.70**	**0.70**	**0.71**	**0.76**	**0.77**	**0.78**	**0.75**	**0.73**	**0.66**	**0.61**	**0.79**	**0.70**	-0.13

Table A.6: Winter correlations of unsaturated aliphatic and aromatic species, values in bold indicate correlations greater than 0.50. Two of the unsaturated aliphatic species were not measured during the winter campaign, propyne and 1,2-butadiene, and as such have not been included.

	Benzene	Toluene	Benzene, ethyl-	*m-* and *p*-Xylene	*o*-Xylene	Benzene, *iso*-propyl-	Benzene, propyl-	Toluene, 3-ethyl-	Toluene, 4-ethyl-	Benzene, 1,3,5-trimethyl-	Toluene, 2-ethyl-	Benzene, 1,2,4-trimethyl-	Toluene, 4-*iso*-propyl-	Benzene, 1,2,3-trimethyl-	Indan	Benzene, *tert*-butyl-	Benzene, 1,3-diethyl-	Benzene, 1,4-diethyl-	Napthalene
Ethene	**0.91**	**0.87**	**0.81**	**0.86**	**0.84**	**0.59**	**0.66**	**0.68**	**0.68**	**0.68**	**0.59**	**0.65**	0.46	**0.76**	**0.70**	0.09	**0.73**	**0.76**	**0.73**
Acetylene	**0.94**	**0.85**	**0.77**	**0.82**	**0.83**	**0.54**	**0.66**	**0.67**	**0.61**	**0.65**	**0.55**	**0.62**	0.43	**0.75**	**0.72**	0.08	**0.70**	**0.71**	**0.73**
Propene	**0.81**	**0.85**	**0.79**	**0.85**	**0.81**	**0.56**	**0.64**	**0.69**	**0.65**	**0.66**	**0.55**	**0.62**	0.44	**0.74**	**0.64**	0.08	**0.72**	**0.75**	**0.69**
Propadiene	**0.95**	**0.92**	**0.86**	**0.91**	**0.90**	**0.65**	**0.71**	**0.73**	**0.67**	**0.76**	**0.64**	**0.67**	0.42	**0.81**	**0.76**	0.07	**0.77**	**0.80**	**0.77**
***trans*-2-Butene**	**0.87**	**0.96**	**0.90**	**0.95**	**0.94**	**0.67**	**0.70**	**0.71**	**0.68**	**0.79**	**0.71**	**0.64**	0.36	**0.83**	**0.79**	0.08	**0.80**	**0.82**	**0.76**
1-Butene	**0.87**	**0.92**	**0.86**	**0.91**	**0.89**	**0.63**	**0.72**	**0.75**	**0.69**	**0.75**	**0.64**	**0.67**	0.45	**0.81**	**0.75**	0.09	**0.79**	**0.82**	**0.75**
***iso*-Butene**	**0.89**	**0.98**	**0.91**	**0.96**	**0.96**	**0.69**	**0.73**	**0.75**	**0.69**	**0.81**	**0.71**	**0.69**	0.38	**0.86**	**0.82**	0.08	**0.82**	**0.84**	**0.79**
***cis*-2-Butene**	**0.86**	**0.97**	**0.91**	**0.96**	**0.94**	**0.68**	**0.71**	**0.74**	**0.69**	**0.81**	**0.72**	**0.66**	0.37	**0.84**	**0.80**	0.09	**0.81**	**0.82**	**0.79**
1,3-Butadiene	**0.85**	**0.89**	**0.85**	**0.88**	**0.87**	**0.62**	**0.70**	**0.69**	**0.64**	**0.74**	**0.62**	**0.59**	0.32	**0.78**	**0.75**	0.10	**0.74**	**0.79**	**0.70**
***trans*-2-Pentene**	**0.83**	**0.89**	**0.88**	**0.94**	**0.92**	**0.67**	**0.70**	**0.68**	**0.62**	**0.74**	**0.70**	**0.57**	0.31	**0.79**	**0.77**	0.04	**0.77**	**0.79**	**0.74**
1-Pentene	**0.83**	**0.86**	**0.87**	**0.92**	**0.91**	**0.67**	**0.68**	**0.67**	**0.60**	**0.72**	**0.66**	**0.56**	0.29	**0.76**	**0.75**	0.02	**0.75**	**0.76**	**0.73**
Isoprene	**0.82**	**0.91**	**0.84**	**0.90**	**0.90**	**0.59**	**0.72**	**0.71**	**0.60**	**0.74**	**0.63**	**0.63**	0.30	**0.80**	**0.80**	0.08	**0.75**	**0.83**	**0.70**
Styrene	**0.59**	**0.69**	**0.67**	**0.71**	**0.66**	**0.64**	**0.57**	**0.52**	**0.61**	**0.70**	**0.69**	**0.50**	0.46	**0.69**	**0.65**	0.01	**0.74**	**0.74**	**0.65**
α-Pinene	-0.15	-0.16	-0.15	-0.16	-0.12	-0.18	-0.13	-0.10	-0.17	-0.16	-0.14	-0.07	-0.11	-0.16	-0.12	-0.04	-0.16	-0.17	-0.14
Limonene	**0.68**	**0.77**	**0.72**	**0.78**	**0.74**	**0.55**	**0.64**	**0.59**	**0.62**	**0.70**	**0.72**	**0.51**	0.35	**0.76**	**0.74**	0.05	**0.77**	**0.77**	**0.65**

Table A.7: Winter correlations of unsaturated aliphatic and grouped species, values in bold indicate correlations greater than 0.50. Two of the unsaturated aliphatic species were not measured during the winter campaign, propyne and 1,2-butadiene, and as such have not been included.

	C_6 aliphatics	C_7 aliphatics	C_8 aliphatics	C_9 aliphatics	C_{10} aliphatics	C_{11} aliphatics	C_{12} aliphatics	C_{13} aliphatics	C_4 substituted monoaromatics	C_{10} monoterpenes
Ethene	**0.69**	**0.75**	**0.78**	**0.74**	0.49	**0.79**	**0.76**	**0.82**	**0.78**	**0.79**
Acetylene	**0.67**	**0.72**	**0.76**	**0.71**	**0.52**	**0.78**	**0.74**	**0.80**	**0.76**	**0.77**
Propene	**0.66**	**0.75**	**0.76**	**0.74**	0.49	**0.78**	**0.75**	**0.79**	**0.77**	**0.78**
Propadiene	**0.75**	**0.79**	**0.82**	**0.78**	0.48	**0.84**	**0.82**	**0.87**	**0.83**	**0.85**
***trans*-2-Butene**	**0.75**	**0.83**	**0.84**	**0.83**	0.44	**0.86**	**0.86**	**0.88**	**0.86**	**0.87**
1-Butene	**0.72**	**0.81**	**0.83**	**0.81**	**0.51**	**0.84**	**0.82**	**0.86**	**0.83**	**0.84**
***iso*-Butene**	**0.75**	**0.84**	**0.86**	**0.84**	0.47	**0.88**	**0.87**	**0.89**	**0.88**	**0.89**
***cis*-2-Butene**	**0.76**	**0.84**	**0.85**	**0.83**	0.46	**0.87**	**0.87**	**0.88**	**0.87**	**0.88**
1,3-Butadiene	**0.69**	**0.78**	**0.79**	**0.79**	0.47	**0.81**	**0.79**	**0.82**	**0.82**	**0.82**
***trans*-2-Pentene**	**0.68**	**0.79**	**0.76**	**0.80**	0.33	**0.79**	**0.83**	**0.83**	**0.84**	**0.84**
1-Pentene	**0.67**	**0.77**	**0.73**	**0.77**	0.36	**0.77**	**0.81**	**0.81**	**0.82**	**0.82**
Isoprene	**0.65**	**0.79**	**0.81**	**0.79**	0.40	**0.81**	**0.79**	**0.82**	**0.81**	**0.82**
Styrene	**0.64**	**0.72**	**0.74**	**0.71**	0.34	**0.74**	**0.72**	**0.75**	**0.75**	**0.75**
α-Pinene	-0.15	-0.16	-0.16	-0.14	-0.07	-0.17	-0.16	-0.16	-0.16	-0.17
Limonene	**0.56**	**0.74**	**0.76**	**0.74**	0.38	**0.73**	**0.71**	**0.76**	**0.74**	**0.76**

Table A.8: Winter correlations of the aromatic species, values in bold indicate values greater than 0.50.

	Benzene	Toluene	Benzene, ethyl-	*m*- and *p*-Xylene	*o*-Xylene	Benzene, *iso*-propyl-	Benzene, propyl-	Toluene, 3-ethyl-	Toluene, 4-ethyl-	Benzene, 1,3,5-trimethyl-	Toluene, 2-ethyl-	Benzene, 1,2,4-trimethyl-	Toluene, 4-*iso*-propyl-	Benzene, 1,2,3-trimethyl-	Indan	Benzene, *tert*-butyl-	Benzene, 1,3-diethyl-	Benzene, 1,4-diethyl-
Toluene	**0.89**																	
Benzene, ethyl-	**0.80**	**0.93**																
***m*- and *p*-Xylene**	**0.86**	**0.98**	**0.99**															
***o*-Xylene**	**0.88**	**0.97**	**0.93**	**0.98**														
Benzene, *iso*-propyl-	**0.62**	**0.72**	**0.69**	**0.75**	**0.72**													
Benzene, propyl-	**0.67**	**0.72**	**0.69**	**0.72**	**0.65**	**0.59**												
Toluene, 3-ethyl-	**0.67**	**0.75**	**0.66**	**0.74**	**0.69**	**0.61**	**0.73**											
Toluene, 4-ethyl-	**0.61**	**0.70**	**0.69**	**0.72**	**0.67**	**0.69**	**0.58**	**0.53**										
Benzene, 1,3,5-trimethyl-	**0.70**	**0.82**	**0.80**	**0.83**	**0.78**	**0.79**	**0.70**	**0.73**	**0.67**									
Toluene, 2-ethyl-	**0.57**	**0.72**	**0.68**	**0.73**	**0.66**	**0.74**	**0.57**	**0.57**	**0.72**	**0.77**								
Benzene, 1,2-4-trimethyl-	**0.64**	**0.71**	**0.61**	**0.69**	**0.62**	**0.52**	**0.67**	**0.74**	**0.58**	**0.60**	**0.50**							
Toluene, 4-*iso*-propyl-	0.40	0.37	0.33	0.36	0.24	0.36	0.35	0.41	0.38	0.44	0.38	0.41						
Benzene, 1,2,3-trimethyl-	**0.76**	**0.87**	**0.84**	**0.88**	**0.86**	**0.77**	**0.72**	**0.80**	**0.71**	**0.83**	**0.79**	**0.72**	0.42					
Indan	**0.74**	**0.84**	**0.79**	**0.85**	**0.83**	**0.77**	**0.70**	**0.66**	**0.65**	**0.79**	**0.76**	**0.53**	0.21	**0.89**				
Benzene, *tert*-butyl-	0.08	0.09	0.11	0.09	0.04	0.05	0.03	0.02	0.01	0.04	0.00	0.03	0.04	-0.01	0.07			
Benzene, 1,3-diethyl-	**0.72**	**0.83**	**0.80**	**0.84**	**0.80**	**0.82**	**0.73**	**0.76**	**0.74**	**0.87**	**0.79**	**0.66**	0.45	**0.89**	**0.84**	0.03		
Benzene, 1,4-diethyl-	**0.74**	**0.85**	**0.80**	**0.85**	**0.82**	**0.78**	**0.79**	**0.78**	**0.72**	**0.84**	**0.73**	**0.70**	0.45	**0.88**	**0.86**	0.01	**0.85**	
Napthalene	**0.76**	**0.80**	**0.75**	**0.79**	**0.78**	**0.73**	**0.73**	**0.70**	**0.67**	**0.76**	**0.68**	**0.63**	0.44	**0.82**	**0.89**	0.07	**0.79**	**0.79**

Table A.9: Winter correlations of the aromatic and grouped species, values in bold indicate correlations greater than 0.50.

	C_6 aliphatics	C_7 aliphatics	C_8 aliphatics	C_9 aliphatics	C_{10} aliphatics	C_{11} aliphatics	C_{12} aliphatics	C_{13} aliphatics	C_4 substituted monoaromatics	C_{10} monoterpenes
Benzene	**0.72**	**0.74**	**0.79**	**0.74**	0.48	**0.81**	**0.78**	**0.83**	**0.79**	**0.81**
Toluene	**0.79**	**0.86**	**0.88**	**0.85**	**0.50**	**0.89**	**0.89**	**0.91**	**0.89**	**0.90**
Benzene, ethyl-	**0.75**	**0.81**	**0.83**	**0.80**	0.46	**0.84**	**0.84**	**0.86**	**0.85**	**0.85**
***m*- and *p*-Xylene**	**0.77**	**0.85**	**0.87**	**0.84**	0.47	**0.88**	**0.88**	**0.90**	**0.88**	**0.89**
***o*-Xylene**	**0.71**	**0.83**	**0.85**	**0.83**	0.45	**0.86**	**0.85**	**0.88**	**0.87**	**0.87**
Benzene, *iso*-propyl-	**0.68**	**0.75**	**0.80**	**0.74**	0.35	**0.82**	**0.79**	**0.83**	**0.82**	**0.83**
Benzene, propyl-	**0.67**	**0.72**	**0.77**	**0.72**	0.43	**0.77**	**0.75**	**0.78**	**0.77**	**0.77**
Toluene, 3-ethyl-	**0.64**	**0.72**	**0.75**	**0.72**	0.43	**0.76**	**0.74**	**0.79**	**0.77**	**0.78**
Toluene, 4-ethyl-	**0.70**	**0.72**	**0.74**	**0.71**	0.47	**0.76**	**0.76**	**0.78**	**0.77**	**0.78**
Benzene, 1,3,5-trimethyl-	**0.75**	**0.78**	**0.83**	**0.78**	0.40	**0.85**	**0.83**	**0.87**	**0.85**	**0.86**
Toluene, 2-ethyl-	**0.69**	**0.75**	**0.79**	**0.76**	0.30	**0.80**	**0.79**	**0.82**	**0.81**	**0.82**
Benzene, 1,2,4-trimethyl-	**0.59**	**0.64**	**0.67**	**0.61**	0.42	**0.71**	**0.69**	**0.73**	**0.70**	**0.71**
Toluene, 4-*iso*–propyl-	0.42	0.41	0.45	0.39	0.29	0.46	0.44	0.47	0.44	0.45
Benzene, 1,2,3-trimethyl-	**0.78**	**0.86**	**0.90**	**0.85**	0.48	**0.91**	**0.89**	**0.92**	**0.91**	**0.92**
Indan	**0.69**	**0.85**	**0.87**	**0.83**	0.41	**0.87**	**0.84**	**0.88**	**0.89**	**0.89**
Benzene, *tert*-butyl-	0.01	0.02	0.01	0.01	0.00	0.02	0.01	0.03	0.00	0.00
Benzene, 1,3-diethyl-	**0.76**	**0.84**	**0.88**	**0.83**	0.47	**0.88**	**0.85**	**0.89**	**0.88**	**0.89**
Benzene, 1,4-diethyl-	**0.73**	**0.84**	**0.87**	**0.84**	0.43	**0.88**	**0.85**	**0.89**	**0.89**	**0.89**
Napthalene	**0.78**	**0.80**	**0.85**	**0.80**	0.48	**0.87**	**0.84**	**0.88**	**0.84**	**0.84**

Table A.10: Winter correlations of the grouped species, values in bold indicate correlations greater than 0.50.

	C_6 aliphatics	C_7 aliphatics	C_8 aliphatics	C_9 aliphatics	C_{10} aliphatics	C_{11} aliphatics	C_{12} aliphatics	C_{13} aliphatics	C_4 substituted monoaromatics
C_7 aliphatics	**0.83**								
C_8 aliphatics	**0.87**	**0.95**							
C_9 aliphatics	**0.84**	**0.94**	**0.93**						
C_{10} aliphatics	**0.54**	**0.50**	**0.51**	**0.50**					
C_{11} aliphatics	**0.88**	**0.92**	**0.96**	**0.91**	**0.51**				
C_{12} aliphatics	**0.90**	**0.92**	**0.95**	**0.91**	**0.52**	**0.96**			
C_{13} aliphatics	**0.90**	**0.93**	**0.96**	**0.92**	**0.51**	**0.98**	**0.98**		
C_4 substituted monoaromatics	**0.87**	**0.93**	**0.95**	**0.91**	0.49	**0.96**	**0.97**	**0.97**	
C_{10} monoterpenes	**0.87**	**0.93**	**0.96**	**0.92**	**0.50**	**0.97**	**0.98**	**0.98**	**0.99**

Table A.11: Winter correlations of measured species with dichloromethane, values in bold indicate correlations greater than 0.50. Two of the unsaturated aliphatic compounds, propyne and 1,2-butadiene were not measured during the winter campaign and as such have not been included.

Methane, dichloro					
Methane	**0.65**	**Ethene**	**0.66**	**Benzene**	**0.65**	**C_6 aliphatics**	**0.61**
Ethane	**0.63**	Acetylene	**0.62**	Toluene	**0.72**	**C_7 aliphatics**	**0.69**
Propane	**0.67**	**Propene**	**0.63**	**Benzene, ethyl-**	**0.66**	**C_8 aliphatics**	**0.73**
***iso*-Butane**	**0.67**	**Propadiene**	**0.67**	***m*- and *p*-Xylene**	**0.73**	**C_9 aliphatics**	**0.69**
***n*-Butane**	**0.61**	***Trans*-2-Butene**	**0.68**	***o*-Xylene**	**0.67**	**C_{10} aliphatics**	0.37
***n*-Pentane**	**0.72**	**1-Butene**	**0.70**	**Benzene,.*iso*-propyl-**	**0.57**	**C_{11} aliphatics**	**0.73**
***iso*-Pentane**	**0.71**	***iso*-Butene**	**0.71**	**Benzene, propyl-**	**0.64**	**C_{12} aliphatics**	**0.71**
Cyclopentane	**0.50**	***cis*-2-Butene**	**0.69**	**Toluene, 3-ethyl-**	**0.65**	**C_{13} aliphatics**	**0.75**
***n*-Hexane**	**0.70**	**1,3-Butadiene**	**0.61**	**Toluene, 4-ethyl-**	**0.61**	**C_4 substituted monoaromatics**	**0.73**
Pentane, 2+3-methyl-	**0.73**	***trans*-2-Pentene**	**0.64**	**Benzene, 1,3,5-trimethyl-**	**0.69**	**c_{10} monoterpenes**	**0.74**
***n*-Heptane**	**0.59**	**1-Pentene**	0.44	**Toluene, 2-ethyl-**	**0.61**		
Butane, 2,2,3-trimethyl-	**0.67**	**Isoprene**	**0.67**	**Benzene, 1,2,4-trimethyl-**	**0.56**		
***n*-Octane**	**0.73**	**Styrene**	**0.62**	**Toluene, 4-*iso*-propyl-**	0.38		
Pentane, 2,2,4-trimethyl-	**0.60**	α-Pinene	-0.14	**Benzene, 1,2,3-trimethyl-**	**0.75**		
***n*-Nonane**	**0.75**	**Limonene**	**0.67**	**Indan**	**0.65**		
***n*-Decane**	**0.74**			**Benzene, *tert*-butyl-**	0.05		
Nonane, 2-methyl-	**0.67**			**Benzene, 1,3-diethyl-**	**0.75**		
***n*-Undecane**	**0.75**			**Benzene, 1,4-diethyl-**	**0.77**		
***n*-Dodecane**	**0.73**			**Napthalene**	**0.67**		

A.2 Summer correlations between volatile organic compounds

Table A.12: Summer correlations of saturated aliphatic species, values in bold indicate correlations greater than 0.50.

	Methane	Ethane	Propane	*n*-Butane	*iso*-Butane	*n*-Pentane	*iso*-Pentane	Cyclopentane	*n*-Hexane	Pentane, 2+3-methyl-	*n*-Heptane	Butane, 2,2,3-trimethyl-	*n*-Octane	Pentane, 2,2,4-trimethyl	*n*-Nonane	*n*-Decane	Nonane, 2-methyl-	*n*-Undecane
Ethane	**0.84**																	
Propane	**0.76**	**0.83**																
***n*-Butane**	**0.55**	**0.61**	**0.90**															
***iso*-Butane**	**0.55**	**0.61**	**0.88**	**0.95**														
***n*-Pentane**	**0.60**	**0.63**	**0.84**	**0.78**	**0.79**													
***iso*-Pentane**	**0.56**	**0.64**	**0.82**	**0.79**	**0.80**	**0.96**												
Cyclopentane	0.48	**0.56**	**0.65**	**0.60**	**0.63**	**0.66**	**0.70**											
***n*-Hexane**	**0.53**	0.47	**0.71**	**0.65**	**0.66**	**0.88**	**0.79**	**0.51**										
Pentane, 2+3-methyl-	**0.63**	**0.66**	**0.86**	**0.78**	**0.83**	**0.97**	**0.96**	**0.69**	**0.88**									
***n*-Heptane**	**0.62**	**0.65**	**0.82**	**0.75**	**0.75**	**0.81**	**0.82**	**0.64**	**0.71**	**0.84**								
Butane, 2,2,3-trimethyl-	**0.55**	**0.59**	**0.73**	**0.67**	**0.65**	**0.74**	**0.76**	**0.53**	**0.61**	**0.78**	**0.70**							
***n*-Octane**	**0.57**	**0.54**	**0.79**	**0.68**	**0.68**	**0.80**	**0.76**	**0.54**	**0.75**	**0.87**	**0.76**	**0.65**						
Pentane, 2,2,4-trimethyl	**0.51**	**0.59**	**0.77**	**0.75**	**0.79**	**0.83**	**0.86**	**0.65**	**0.67**	**0.88**	**0.78**	**0.72**	**0.73**					
***n*-Nonane**	**0.51**	**0.54**	**0.62**	**0.56**	**0.54**	**0.62**	**0.64**	**0.51**	**0.53**	**0.68**	**0.60**	**0.82**	**0.51**	**0.53**				
***n*-Decane**	0.37	0.42	0.46	0.42	0.40	**0.51**	**0.50**	0.33	0.41	**0.52**	0.44	**0.62**	0.36	0.40	**0.67**			
Nonane, 2-methyl-	0.36	0.42	**0.51**	0.45	0.45	**0.55**	**0.54**	0.32	0.48	**0.56**	0.48	**0.62**	0.46	**0.51**	**0.52**	**0.57**		
***n*-Undecane**	**0.55**	**0.61**	**0.76**	**0.71**	**0.68**	**0.75**	**0.78**	**0.56**	**0.62**	**0.80**	**0.73**	**0.96**	**0.68**	**0.73**	**0.86**	**0.60**	**0.55**	
***n*-Dodecane**	**0.61**	**0.66**	**0.69**	**0.62**	**0.61**	**0.70**	**0.71**	**0.53**	**0.59**	**0.75**	**0.67**	**0.83**	**0.53**	**0.62**	**0.98**	**0.76**	**0.55**	**0.88**

Table A.13: Summer correlations of saturated and unsaturated aliphatic species, values in bold indicate correlations greater than 0.50.

	Ethene	Acetylene	Propene	Propadiene	Propyne	Butene, *trans*-2-	1-Butene	*iso*-Butene	Butene, *cis*-2-	1,2-Butadiene	1,3-Butadiene	Pentene, *trans*-2-	1-Pentene	Isoprene	Styrene	α-Pinene	Limonene
Methane	**0.58**	**0.50**	**0.50**	0.47	0.41	**0.50**	0.46	**0.53**	**0.52**	0.05	0.35	**0.57**	**0.57**	-0.14	0.20	-0.06	-0.16
Ethane	**0.56**	**0.57**	0.48	**0.52**	**0.61**	**0.61**	**0.50**	**0.63**	**0.62**	0.00	0.48	**0.71**	**0.71**	-0.07	0.16	0.01	-0.04
Propane	**0.78**	**0.77**	**0.72**	**0.68**	**0.77**	**0.72**	**0.71**	**0.83**	**0.73**	-0.02	**0.53**	**0.77**	**0.81**	0.09	0.26	0.14	-0.03
***n*-Butane**	**0.73**	**0.73**	**0.69**	**0.68**	**0.70**	**0.70**	**0.70**	**0.82**	**0.71**	0.08	0.49	**0.70**	**0.75**	0.24	0.29	0.24	-0.01
***iso*-Butane**	**0.73**	**0.75**	**0.71**	**0.67**	**0.73**	**0.72**	**0.70**	**0.83**	**0.72**	0.04	0.49	**0.73**	**0.76**	0.22	0.26	0.22	-0.01
***n*-Pentane**	**0.84**	**0.80**	**0.82**	**0.72**	0.48	**0.83**	**0.85**	**0.89**	**0.84**	-0.03	**0.60**	**0.84**	**0.90**	0.29	0.25	0.31	0.08
***iso*-Pentane**	**0.80**	**0.80**	**0.78**	**0.72**	0.38	**0.90**	**0.88**	**0.93**	**0.90**	0.00	**0.68**	**0.89**	**0.94**	0.39	0.27	0.37	0.12
Cyclopentane	**0.57**	**0.56**	**0.57**	**0.54**	**0.78**	**0.70**	**0.57**	**0.68**	**0.68**	-0.01	**0.58**	**0.73**	**0.70**	0.13	0.13	0.20	0.06
***n*-Hexane**	**0.77**	**0.68**	**0.79**	**0.62**	**0.61**	**0.68**	**0.76**	**0.75**	**0.69**	-0.03	0.45	**0.67**	**0.73**	0.18	0.19	0.20	0.06
Pentane, 2+3-methyl-	**0.86**	**0.87**	**0.84**	**0.79**	**0.55**	**0.88**	**0.88**	**0.93**	**0.89**	-0.05	**0.79**	**0.88**	**0.92**	0.25	0.23	0.29	0.08
***n*-Heptane**	**0.76**	**0.75**	**0.73**	**0.68**	**0.71**	**0.73**	**0.74**	**0.80**	**0.73**	-0.02	**0.58**	**0.74**	**0.79**	0.22	0.25	0.21	0.01
Butane, 2,2,3-trimethyl-	**0.71**	**0.71**	**0.64**	**0.60**	0.15	**0.67**	**0.70**	**0.73**	**0.67**	-0.04	0.39	**0.68**	**0.74**	0.18	0.36	0.20	0.06
***n*-Octane**	**0.75**	**0.70**	**0.74**	**0.65**	**0.66**	**0.60**	**0.71**	**0.73**	**0.61**	-0.01	0.36	**0.61**	**0.72**	0.13	0.24	0.19	0.03
Pentane, 2,2,4-trimethyl-	**0.76**	**0.80**	**0.71**	**0.76**	**0.78**	**0.80**	**0.78**	**0.90**	**0.82**	-0.02	**0.65**	**0.81**	**0.86**	0.27	0.25	0.29	0.09
***n*-Nonane**	**0.64**	**0.62**	**0.59**	**0.52**	0.18	**0.60**	**0.61**	**0.60**	**0.59**	-0.04	0.29	**0.60**	**0.64**	0.13	0.32	0.17	0.06
***n*-Decane**	**0.57**	**0.50**	**0.51**	0.42	**0.65**	0.49	**0.50**	0.47	0.47	-0.05	0.25	0.46	0.49	0.17	0.24	0.18	0.10
Nonane, 2-methyl-	**0.50**	**0.48**	0.48	0.42	0.37	0.46	0.48	**0.51**	0.48	-0.03	0.32	0.49	**0.53**	0.13	0.35	0.13	0.01
***n*-Undecane**	**0.71**	**0.74**	**0.65**	**0.61**	0.22	**0.68**	**0.74**	**0.74**	**0.67**	-0.04	0.45	**0.69**	**0.75**	0.19	0.34	0.19	0.08
***n*-Dodecane**	**0.69**	**0.67**	**0.63**	**0.58**	**0.59**	**0.69**	**0.66**	**0.67**	**0.68**	-0.03	0.47	**0.69**	**0.71**	0.16	0.32	0.19	0.12

Table A.14: Summer correlations of saturated aliphatic and aromatic species, values in bold indicate correlations greater than 0.50. Two of the aromatic species were below the detection limit of the GC×GC instrument, isopropyl-benzene and indan, and as such have not been included.

	Benzene	Toluene	Benzene, ethyl-	*m*- and *p*-Xylene	*o*-Xylene	Benzene, propyl-	Toluene, 3-ethyl-	Toluene, 4-ethyl-	Benzene, 1,3,5-trimethyl-	Toluene, 2-ethyl-	Benzene, 1,2,4-trimethyl-	Toluene, 4-*iso*-propyl-	Benzene, 1,2,3-trimethyl-	Benzene, *tert*-butyl-	Benzene, 1,3-diethyl-	Benzene, 1,4-diethyl-	Napthalene
Methane	**0.64**	**0.72**	**0.66**	**0.68**	**0.64**	0.28	0.33	0.26	0.49	0.30	0.27	-0.04	0.44	0.00	0.32	**0.60**	0.33
Ethane	**0.70**	**0.79**	**0.73**	**0.76**	**0.72**	0.29	0.37	0.24	**0.50**	0.29	0.29	0.02	0.45	0.02	0.33	**0.66**	0.36
Propane	**0.87**	**0.90**	**0.88**	**0.88**	**0.87**	0.40	0.44	0.40	**0.58**	0.35	0.38	0.07	**0.55**	0.11	0.37	**0.69**	0.46
***n*-Butane**	**0.79**	**0.80**	**0.80**	**0.79**	**0.79**	0.40	0.39	0.43	**0.52**	0.34	0.38	0.08	0.49	0.10	0.35	**0.61**	0.45
***iso*-Butane**	**0.80**	**0.82**	**0.82**	**0.82**	**0.81**	0.38	0.38	0.42	**0.51**	0.33	0.36	0.10	0.48	0.08	0.34	**0.60**	0.47
***n*-Pentane**	**0.90**	**0.89**	**0.89**	**0.86**	**0.86**	0.44	0.42	0.45	**0.56**	0.40	0.36	0.19	**0.55**	0.09	0.39	**0.66**	**0.52**
***iso*-Pentane**	**0.89**	**0.89**	**0.90**	**0.87**	**0.86**	0.48	0.43	0.47	**0.58**	0.41	0.36	0.20	**0.55**	0.06	0.40	**0.69**	**0.52**
Cyclopentane	**0.67**	**0.74**	**0.73**	**0.75**	**0.69**	0.37	0.26	0.42	**0.51**	0.26	0.15	0.06	0.47	0.03	0.31	**0.53**	0.35
***n*-Hexane**	**0.77**	**0.75**	**0.75**	**0.72**	**0.73**	0.37	0.36	0.44	**0.50**	0.37	0.30	0.14	**0.52**	0.10	0.36	**0.55**	0.42
Pentane, 2+3-methyl-	**0.93**	**0.93**	**0.92**	**0.90**	**0.90**	0.47	0.46	**0.50**	**0.62**	0.46	0.35	0.16	**0.61**	0.09	0.43	**0.73**	**0.54**
***n*-Heptane**	**0.82**	**0.85**	**0.86**	**0.85**	**0.84**	0.42	0.41	0.44	0.57	0.37	0.38	0.10	**0.53**	0.09	0.36	**0.66**	0.47
Butane, 2,2,3-trimethyl-	**0.76**	**0.78**	**0.76**	**0.75**	**0.75**	**0.60**	**0.61**	**0.58**	**0.66**	**0.50**	**0.54**	0.19	**0.61**	0.11	**0.52**	**0.83**	**0.62**
***n*-Octane**	**0.80**	**0.79**	**0.81**	**0.79**	**0.85**	0.38	0.40	0.40	0.49	0.32	0.36	0.13	0.48	0.23	0.31	**0.51**	0.44
Pentane, 2,2,4-trimethyl-	**0.87**	**0.87**	**0.86**	**0.86**	**0.84**	0.43	0.41	0.42	**0.55**	0.38	0.35	0.19	0.49	0.12	0.35	**0.60**	**0.50**
***n*-Nonane**	**0.66**	**0.68**	**0.65**	**0.63**	**0.63**	**0.63**	**0.68**	**0.61**	**0.67**	**0.64**	**0.53**	0.15	**0.65**	0.01	**0.56**	**0.96**	**0.51**
***n*-Decane**	**0.51**	**0.50**	0.49	0.47	0.47	0.47	0.40	0.43	0.46	0.39	0.24	0.34	0.39	-0.08	0.41	**0.69**	**0.57**
Nonane, 2-methyl-	**0.53**	**0.54**	**0.53**	**0.52**	**0.52**	0.35	0.34	0.30	0.40	0.31	0.34	0.50	0.35	0.13	0.35	0.46	**0.72**
***n*-Undecane**	**0.77**	**0.79**	**0.78**	**0.76**	**0.77**	**0.68**	**0.65**	**0.64**	**0.70**	**0.60**	**0.55**	0.11	**0.70**	0.14	**0.56**	**0.88**	**0.55**
***n*-Dodecane**	**0.71**	**0.74**	**0.71**	**0.70**	**0.67**	**0.68**	**0.67**	**0.64**	**0.72**	**0.66**	**0.52**	0.15	**0.72**	-0.01	**0.61**	**0.98**	**0.51**

Table A.15: Summer correlations of saturated aliphatic and grouped species, values in bold indicate correlations greater than 0.50.

	C_6 aliphatics	C_7 aliphatics	C_8 aliphatics	C_9 aliphatics	C_{10} aliphatics	C_{11} aliphatics	C_{12} aliphatics	C_{13} aliphatics	C_4 substituted monoaromatics	C_{10} monoterpenes
Methane	0.28	0.45	0.38	0.36	**0.53**	0.42	0.39	0.18	0.21	-0.15
Ethane	0.33	0.44	0.42	0.37	0.45	0.38	0.41	0.19	0.25	-0.05
Propane	**0.53**	**0.61**	**0.61**	**0.55**	**0.59**	0.48	0.46	0.45	0.46	-0.05
***n*-Butane**	**0.54**	**0.59**	**0.61**	**0.52**	0.49	0.40	0.39	0.43	0.46	-0.02
***iso*-Butane**	**0.52**	**0.58**	**0.59**	**0.51**	0.47	0.39	0.39	0.41	0.44	-0.03
***n*-Pentane**	**0.61**	**0.66**	**0.66**	**0.60**	**0.51**	0.43	0.44	0.48	**0.51**	0.06
***iso*-Pentane**	**0.64**	**0.67**	**0.69**	**0.60**	0.49	0.43	0.45	0.46	**0.50**	0.09
Cyclopentane	0.41	**0.54**	**0.57**	0.47	0.34	0.32	0.36	0.29	0.39	0.06
***n*-Hexane**	0.49	**0.59**	**0.56**	**0.54**	0.42	0.34	0.34	0.42	0.44	0.03
Pentane, 2+3-methyl-	**0.64**	**0.71**	**0.72**	**0.65**	**0.63**	**0.50**	**0.52**	0.49	**0.58**	0.05
***n*-Heptane**	**0.56**	**0.64**	**0.64**	**0.59**	**0.50**	0.45	0.47	0.43	0.45	-0.01
Butane, 2,2,3-trimethyl-	**0.66**	**0.78**	**0.76**	**0.66**	**0.50**	**0.53**	**0.51**	0.42	**0.52**	0.03
***n*-Octane**	**0.52**	**0.56**	**0.55**	**0.56**	**0.64**	**0.55**	0.47	**0.59**	0.47	0.01
Pentane, 2,2,4-trimethyl-	**0.59**	**0.58**	**0.63**	**0.55**	0.49	0.41	0.44	**0.50**	**0.50**	0.07
***n*-Nonane**	**0.52**	**0.78**	**0.69**	**0.64**	0.42	**0.50**	**0.51**	0.24	0.38	0.04
***n*-Decane**	0.37	**0.56**	0.45	0.44	0.27	0.31	0.35	0.10	0.23	0.09
Nonane, 2-methyl-	0.43	0.48	0.47	0.48	0.41	0.41	0.39	0.29	0.30	0.01
***n*-Undecane**	**0.70**	**0.82**	**0.79**	**0.71**	**0.54**	**0.55**	**0.58**	0.48	**0.58**	0.06
***n*-Dodecane**	**0.57**	**0.81**	**0.72**	**0.67**	0.44	**0.52**	**0.60**	0.23	0.43	0.11

Table A.16: Summer correlation of unsaturated aliphatic species, values in bold indicate correlations greater than 0.50.

	Ethene	Acetylene	Propene	Propadiene	Propyne	Butene, *trans*-2-	1-Butene	*iso*-Butene	Butene, *cis*-2-	1,2-Butadiene	1,3-Butadiene	Pentene, *trans*-2-	1-Pentene	Isoprene	Styrene	α-Pinene
Acetylene	**0.87**															
Propene	**0.94**	**0.83**														
Propadiene	**0.84**	**0.82**	**0.82**													
Propyne	**0.79**	**0.52**	**0.65**	0.45												
Butene, *trans*-2-	**0.77**	**0.78**	**0.78**	**0.75**	0.24											
1-Butene	**0.84**	**0.84**	**0.86**	**0.73**	0.41	**0.83**										
***iso*-Butene**	**0.86**	**0.88**	**0.84**	**0.84**	0.39	**0.92**	**0.87**									
Butene, *cis*-2-	**0.78**	**0.79**	**0.79**	**0.78**	0.16	**0.98**	**0.83**	**0.93**								
1,2-Butadiene	-0.01	-0.03	-0.01	-0.08	n/a	0.02	0.01	-0.03	0.00							
1,3-Butadiene	**0.71**	**0.72**	**0.68**	**0.85**	0.34	**0.83**	**0.69**	**0.82**	**0.85**	0.41						
Pentene, *trans*-2-	**0.74**	**0.76**	**0.74**	**0.74**	0.24	**0.97**	**0.79**	**0.91**	**0.97**	-0.03	**0.82**					
1-Pentene	**0.81**	**0.82**	**0.79**	**0.77**	0.37	**0.92**	**0.89**	**0.94**	**0.93**	-0.01	**0.79**	**0.94**				
Isoprene	0.19	0.21	0.23	0.12	0.17	0.35	0.44	0.30	0.32	0.00	0.16	0.26	0.34			
Styrene	0.25	0.24	0.25	0.18	-0.16	0.23	0.29	0.24	0.23	0.06	0.09	0.21	0.24	0.30		
α-Pinene	0.23	0.23	0.26	0.17	**0.52**	0.35	0.40	0.31	0.32	0.00	0.25	0.29	0.35	**0.72**	0.23	
Limonene	0.05	0.07	0.08	0.09	0.41	0.15	0.16	0.12	0.13	-0.08	0.22	0.13	0.16	0.28	-0.06	0.37

Table A.17: Summer correlations of unsaturated aliphatic and aromatic species, values in bold indicate correlations greater than 0.50. Two of the aromatic species were below the detection limit of the GC×GC instrument, iso-propylbenzene and indan, and as such are not included.

	Benzene	Toluene	Benzene, ethyl-	*m*- and *p*-Xylene	*o*-Xylene	Benzene, propyl-	Toluene, 3-ethyl-	Toluene, 4-ethyl-	Benzene, 1,3,5-trimethyl-	Toluene, 2-ethyl-	Benzene, 1,2,4-trimethyl-	Toluene, 4-*iso*-propyl-	Benzene, 1,2,3-trimethyl-	Benzene, *tert*-butyl-	Benzene, 1,3-diethyl-	Benzene, 1,4-diethyl-	Napthalene
Ethene	**0.91**	**0.85**	**0.83**	**0.80**	**0.80**	0.43	0.41	0.47	**0.56**	0.40	0.36	0.23	**0.56**	0.06	0.41	**0.66**	**0.54**
Acetylene	**0.90**	**0.85**	**0.83**	**0.81**	**0.81**	0.46	0.47	0.45	**0.53**	0.40	0.40	0.21	**0.60**	0.06	0.43	**0.66**	**0.51**
Propene	**0.87**	**0.81**	**0.80**	**0.77**	**0.77**	0.41	0.39	0.47	**0.53**	0.38	0.34	0.24	**0.56**	0.06	0.40	**0.61**	**0.51**
Propadiene	**0.84**	**0.80**	**0.78**	**0.79**	**0.77**	0.39	0.39	0.43	0.49	0.36	0.27	0.20	0.47	0.09	0.39	**0.57**	0.45
Propyne	**0.78**	**0.72**	**0.75**	**0.74**	**0.74**	0.32	-0.65	**0.66**	**0.81**	-0.19	0.11	0.04	**0.67**	0.67	-0.68	**0.63**	**0.56**
Butene, *trans*-2-	**0.84**	**0.86**	**0.84**	**0.83**	**0.77**	0.47	0.42	0.44	**0.55**	0.42	0.31	0.23	**0.56**	-0.01	0.40	**0.68**	0.47
1-Butene	**0.83**	**0.80**	**0.80**	**0.76**	**0.76**	0.47	0.45	0.46	**0.54**	0.42	0.38	0.23	**0.61**	0.03	0.41	**0.65**	0.49
***iso*-Butene**	**0.94**	**0.93**	**0.90**	**0.90**	**0.87**	0.43	0.44	0.44	**0.55**	0.41	0.34	0.22	**0.54**	0.08	0.39	**0.65**	**0.52**
Butene, *cis*-2-	**0.86**	**0.87**	**0.84**	**0.84**	**0.78**	0.44	0.41	0.42	**0.54**	0.42	0.30	0.22	**0.54**	0.02	0.40	**0.67**	0.47
1,2-Butadiene	-0.04	-0.04	-0.04	-0.03	-0.04	-0.02	-0.02	-0.04	-0.02	0.30	-0.02	-0.07	0.00	0.32	0.00	-0.04	-0.03
1,3-Butadiene	**0.78**	**0.73**	**0.68**	**0.69**	**0.60**	0.31	0.22	0.34	0.41	0.33	0.08	0.33	0.41	-0.15	0.32	0.47	0.36
Pentene, *trans*-2-	**0.85**	**0.89**	**0.85**	**0.86**	**0.80**	0.44	0.44	0.40	**0.57**	0.42	0.30	0.20	**0.55**	0.02	0.40	**0.69**	0.46
1-Pentene	**0.90**	**0.91**	**0.89**	**0.88**	**0.85**	0.44	0.45	0.41	**0.58**	0.42	0.32	0.23	**0.55**	0.05	0.41	**0.71**	**0.51**
Isoprene	0.17	0.13	0.20	0.14	0.14	0.13	0.08	0.16	0.09	0.07	0.12	0.22	0.12	-0.10	0.10	0.16	0.18
Styrene	0.23	0.25	0.28	0.25	0.25	0.19	0.20	0.21	0.27	0.19	0.29	0.22	0.31	-0.01	0.29	0.29	0.37
α-Pinene	0.23	0.20	0.24	0.20	0.20	0.16	0.17	0.20	0.10	0.11	0.14	0.24	0.12	0.03	0.14	0.19	0.17
Limonene	0.06	0.03	0.06	0.04	0.04	0.14	0.14	0.12	0.00	0.10	0.05	**0.58**	0.05	-0.03	0.10	0.13	0.01

Table A.18: Summer correlation of unsaturated aliphatic and grouped species, values in bold indicate correlations greater than 0.50.

	C_6 aliphatics	C_7 aliphatics	C_8 aliphatics	C_9 aliphatics	C_{10} aliphatics	C_{11} aliphatics	C_{12} aliphatics	C_{13} aliphatics	C_4 substituted monoaromatics	C_{10} monoterpenes
Ethene	**0.53**	**0.65**	**0.62**	**0.55**	0.42	0.37	0.39	0.35	0.43	0.05
Acetylene	**0.54**	**0.62**	**0.61**	**0.53**	0.43	0.35	0.39	0.41	0.44	0.06
Propene	0.49	**0.61**	**0.57**	**0.51**	0.37	0.33	0.34	0.33	0.38	0.07
Propadiene	0.46	**0.55**	**0.55**	0.46	0.39	0.35	0.37	0.31	0.37	0.08
Propyne	**0.67**	**0.68**	**0.67**	**0.65**	**0.67**	**0.68**	**0.68**	**0.59**	0.31	0.41
Butene, *trans*-2-	**0.52**	**0.61**	**0.62**	**0.51**	0.34	0.30	0.39	0.26	0.35	0.13
1-Butene	**0.57**	**0.65**	**0.63**	**0.56**	0.44	0.38	0.40	0.44	0.44	0.13
***iso*-Butene**	**0.59**	**0.64**	**0.66**	**0.55**	0.45	0.38	0.41	0.42	0.47	0.09
Butene, *cis*-2-	**0.53**	**0.60**	**0.62**	**0.51**	0.35	0.30	0.38	0.27	0.38	0.10
1,2-Butadiene	-0.04	0.00	-0.04	0.02	-0.03	0.00	-0.01	-0.04	-0.02	-0.08
1,3-Butadiene	0.34	0.36	0.41	0.30	0.11	0.06	0.18	0.09	0.23	0.23
Pentene, *trans*-2-	**0.52**	**0.60**	**0.62**	**0.53**	0.37	0.32	0.42	0.27	0.38	0.10
1-Pentene	**0.57**	**0.63**	**0.65**	**0.56**	0.45	0.41	0.45	0.39	0.44	0.12
Isoprene	0.25	0.20	0.22	0.17	0.10	0.12	0.14	0.16	0.04	0.28
Styrene	0.20	0.25	0.23	0.24	0.25	0.24	0.21	0.15	0.21	-0.06
α-Pinene	0.25	0.22	0.24	0.20	0.08	0.15	0.18	0.09	0.03	0.36
Limonene	0.16	0.16	0.14	0.10	0.01	0.07	0.12	0.04	0.03	**0.99**

Table A.19: Summer correlations of aromatic species, values in bold indicate correlations greater than 0.50. Two of the aromatic species were below the detection limit of the GC×GC instrument, iso-propyl-benzene and inda, and as such have not been included.

	Benzene	Toluene	Benzene, ethyl-	*m*- and *p*-Xylene	*o*-Xylene	Benzene, propyl-	Toluene, 3-ethyl-	Toluene, 4-ethyl-	Benzene, 1,3,5-trimethyl-	Toluene, 2-ethyl-	Benzene, 1,2,4-trimethyl-	Toluene, 4-*iso*-propyl-	Benzene, 1,2,3-trimethyl-	Benzene, *tert*-butyl-	Benzene, 1,3-diethyl-	Benzene, 1,4-diethyl-
Toluene	**0.94**															
Benzene, ethyl-	**0.92**	**0.96**														
***m*- and *p*-Xylene**	**0.91**	**0.97**	**0.98**													
***o*-Xylene**	**0.89**	**0.94**	**0.97**	**0.97**												
Benzene, propyl-	0.45	0.46	0.47	0.45	0.46											
Toluene, 3-ethyl-	0.44	0.47	0.44	0.43	0.45	**0.65**										
Toluene, 4-ethyl-	0.46	0.47	0.46	0.45	0.46	**0.60**	**0.55**									
Benzene, 1,3,5-trimethyl-	**0.59**	**0.62**	**0.60**	**0.59**	**0.58**	**0.62**	**0.57**	**0.58**								
Toluene, 2-ethyl-	0.42	0.44	0.40	0.39	0.39	**0.62**	**0.59**	**0.58**	**0.70**							
Benzene, 1,2,4-trimethyl-	0.36	0.39	0.38	0.37	0.40	**0.55**	**0.58**	0.37	**0.54**	0.46						
Toluene, 4-*iso*-propyl-	0.17	0.16	0.21	0.18	0.17	0.10	0.07	0.04	0.03	0.07	0.01					
Benzene, 1,2,3-trimethyl-	**0.59**	**0.60**	**0.57**	**0.56**	**0.56**	**0.59**	**0.54**	**0.57**	**0.68**	**0.65**	**0.51**	-0.02				
Benzene, *tert*-butyl-	0.09	0.08	0.10	0.10	0.13	0.05	0.07	0.07	0.02	0.00	0.02	-0.07	0.03			
Benzene, 1,3-diethyl-	0.41	0.42	0.40	0.40	0.39	0.48	0.48	**0.53**	**0.66**	0.49	0.40	0.08	0.48	0.04		
Benzene, 1,4-diethyl-	**0.70**	**0.73**	**0.70**	**0.69**	**0.66**	**0.69**	**0.68**	**0.65**	**0.73**	**0.67**	**0.53**	0.07	**0.72**	-0.01	**0.61**	
Napthalene	**0.52**	**0.52**	**0.54**	**0.53**	**0.53**	0.32	0.33	0.39	0.38	0.26	0.28	**0.55**	0.34	0.06	0.36	0.44

Table A.20: Summer correlations of aromatic and grouped species, values in bold indicate correlations greater than 0.50. Two of the aromatic species were below the detection limit of the GC×GC instrumemt, iso-propyl-benzene and indan, and as such were not included.

	C_6 aliphatics	C_7 aliphatics	C_8 aliphatics	C_9 aliphatics	C_{10} aliphatics	C_{11} aliphatics	C_{12} aliphatics	C_{13} aliphatics	C_4 substituted monoaromatics	C_{10} monoterpenes
Benzene	**0.60**	**0.67**	**0.67**	**0.59**	**0.51**	0.44	0.45	0.45	0.49	0.04
Toluene	**0.58**	**0.67**	**0.68**	**0.59**	**0.55**	0.47	0.48	0.41	0.48	0.02
Benzene, ethyl-	**0.59**	**0.67**	**0.68**	**0.60**	**0.54**	0.48	0.49	0.44	0.49	0.05
***m*- and *p*-Xylene**	**0.56**	**0.66**	**0.66**	**0.58**	**0.54**	0.46	0.47	0.41	0.48	0.03
***o*-Xylene**	**0.57**	**0.65**	**0.66**	**0.60**	**0.60**	**0.51**	0.48	0.49	**0.51**	0.02
Benzene, propyl-	**0.53**	**0.63**	**0.56**	**0.50**	0.33	0.37	0.43	0.27	0.36	0.12
Toluene, 3-ethyl-	0.38	**0.55**	0.47	**0.51**	0.38	0.41	0.46	0.31	0.34	0.10
Toluene, 4-ethyl-	0.46	**0.63**	**0.58**	**0.56**	0.30	0.40	0.43	0.29	0.42	0.11
Benzene, 1,3,5-trimethyl-	**0.53**	**0.67**	**0.69**	**0.64**	0.41	0.46	0.49	0.29	0.46	0.00
Toluene, 2-ethyl-	0.48	**0.58**	**0.59**	**0.57**	0.30	0.39	0.44	0.22	0.40	0.09
Benzene, 1,2,4-trimethyl-	0.44	**0.54**	**0.52**	0.48	0.38	0.39	0.43	0.29	0.34	0.01
Toluene, 4-*iso*-propyl-	0.10	0.10	0.07	0.10	0.08	0.07	0.08	0.01	0.02	**0.59**
Benzene, 1,2,3-trimethyl-	0.49	**0.70**	**0.64**	**0.57**	0.40	0.39	0.46	0.32	0.40	0.01
Benzene, *tert*-butyl-	0.16	0.07	0.10	0.13	0.11	0.09	0.07	0.27	0.22	-0.05
Benzene, 1,3-diethyl-	0.34	**0.53**	0.48	0.45	0.26	0.33	0.40	0.14	0.27	0.09
Benzene, 1,4-diethyl-	**0.59**	**0.82**	**0.74**	**0.67**	0.44	**0.52**	**0.60**	0.23	0.43	0.12
Napthalene	0.38	0.44	0.41	0.36	0.25	0.26	0.27	0.21	0.24	0.01

Table A.21: Summer correlations of grouped species, values in bold indicate correlations greater than 0.50.

	C_6 aliphatics	C_7 aliphatics	C_8 aliphatics	C_9 aliphatics	C_{10} aliphatics	C_{11} aliphatics	C_{12} aliphatics	C_{13} aliphatics	C_4 substituted monoaromatics
C_7 aliphatics	**0.71**								
C_8 aliphatics	**0.77**	**0.89**							
C_9 aliphatics	**0.64**	**0.83**	**0.81**						
C_{10} aliphatics	0.43	0.49	0.47	**0.59**					
C_{11} aliphatics	0.43	**0.59**	**0.54**	**0.71**	**0.79**				
C_{12} aliphatics	0.45	**0.65**	**0.58**	**0.78**	**0.62**	**0.88**			
C_{13} aliphatics	**0.54**	0.42	0.45	**0.54**	**0.66**	0.46	0.34		
C_4 substituted monoaromatics	**0.62**	**0.65**	**0.68**	**0.75**	0.44	0.39	0.41	**0.72**	
C_{10} monoterpenes	0.13	0.14	0.12	0.08	-0.02	0.06	0.11	-0.01	-0.02

Table A.22: Summer correlations of the two halogenated species with the other species measured, values in bold indicate correlations of greater than 0.50. Two of the aromatic species, iso-propyl-benzene and indan, were below the detection limit of the GC×GC instrument during the summer campaign and as such have not been included.

	Methane, dichloro	**Ethylene, trichloro**		**Methane, dichloro**	**Ethylene, trichloro**		**Methane, dichloro**	**Ethylene, trichloro**		**Methane, dichloro**	**Ethylene, trichloro**
Methane	0.46	**0.55**	**Ethene**	**0.60**	**0.69**	**Benzene**	**0.67**	**0.76**	**C_6 aliphatics**	**0.63**	**0.73**
Ethane	**0.51**	**0.60**	**Acetylene**	**0.63**	**0.72**	**Toluene**	**0.65**	**0.77**	**C_7 aliphatics**	**0.73**	**0.85**
Propane	**0.65**	**0.75**	**Propene**	**0.55**	**0.62**	**Benzene, ethyl-**	**0.65**	**0.77**	**C_8 aliphatics**	**0.72**	**0.82**
***n*-Butane**	**0.62**	**0.70**	**Propadiene**	**0.52**	**0.60**	***m*- and *p*-Xylene**	**0.63**	**0.75**	**C_9 aliphatics**	**0.69**	**0.76**
***iso*-Butane**	**0.60**	**0.68**	**Propyne**	0.45	**0.63**	***o*-Xylene**	**0.64**	**0.75**	**C_{10} aliphatics**	**0.58**	**0.58**
***n*-Pentane**	**0.64**	**0.73**	***Trans*-2-Butene**	**0.55**	**0.66**	**Benzene, propyl-**	**0.55**	**0.69**	**C_{11} aliphatics**	**0.60**	**0.61**
***iso*-Pentane**	**0.65**	**0.77**	**1-Butene**	**0.61**	**0.71**	**Toluene, 3-ethyl-**	**0.53**	**0.67**	**C_{12} aliphatics**	**0.60**	**0.65**
Cyclopentane	0.41	**0.58**	***iso*-Butene**	**0.64**	**0.72**	**Toluene, 4-ethyl-**	**0.51**	**0.64**	**C_{13} aliphatics**	**0.50**	**0.52**
									C_4 substituted monoaromatics	**0.55**	**0.62**
***n*-Heptane**	**0.51**	**0.60**	***cis*-2-Butene**	**0.56**	**0.66**	**Benzene, 1,3,5-trimethyl-**	**0.60**	**0.71**			
Pentane, 2+3-methyl-	**0.68**	**0.78**	**1,2-Butadiene**	-0.03	-0.04	**Toluene, 2-ethyl-**	**0.52**	**0.61**	**C_{10} monoterpenes**	0.06	0.10
***n*-Heptane**	**0.63**	**0.73**	**1,3-Butadiene**	0.32	0.41	**Benzene, 1,2,4-trimethyl-**	**0.50**	**0.60**			
Butane, 2,2,3-trimethyl-	**0.82**	**0.93**	***trans*-2-Pentene**	**0.55**	**0.67**	**Toluene, 4-*iso*-propyl-**	0.28	0.05			
***n*-Octane**	**0.58**	**0.66**	**1-Pentene**	**0.63**	**0.73**	**Benzene, 1,2,3-trimethyl-**	**0.60**	**0.72**			
Pentane, 2,2,4-trimethyl-	**0.63**	**0.72**	**Isoprene**	0.19	0.21	**Benzene, *tert*-butyl-**	0.13	0.15			
***n*-Nonane**	**0.74**	**0.85**	**Styrene**	0.37	0.31	**Benzene, 1,3-diethyl-**	**0.52**	**0.58**			
***n*-Decane**	**0.60**	**0.56**	**α-Pinene**	0.20	0.21	**Benzene,, 1,4-diethyl-**	**0.75**	**0.89**			
Nonane, 2-methyl-	**0.68**	**0.51**	**Limonene**	0.07	0.11	**Napthalene**	**0.62**	0.49			
***n*-Undecane**	**0.85**	**0.99**									
***n*-Dodecane**	**0.78**	**0.88**									

A.3 Correlations with oxygenated volatile organic compounds

Table A.23: Winter correlation of OVOC species, values in bold indicate correlations greater than 0.50. There were several OVOC species that were below the detection limit of the GC×GC instrument and as such have not been included in this table.

	Acetaldehyde	Butanal	Hexanal	Benzaldehyde	Methanol	Ethanol	Propanol	Butanol	Acetone	Butanone	Pentanone, 4-methyl-2-
Butanal	0.28										
Hexanal	**0.66**	0.25									
Benzaldehyde	**0.51**	0.14	0.39								
Methanol	0.26	0.06	0.21	0.20							
Ethanol	**0.78**	0.24	**0.76**	0.48	0.43						
Propanol	0.28	0.12	0.21	0.18	0.13	0.30					
Butanol	0.35	0.10	0.24	0.14	0.07	0.24	0.23				
Acetone	**0.76**	0.28	**0.62**	0.37	0.18	**0.65**	0.28	0.32			
Butanone	**0.68**	0.13	**0.50**	0.46	0.20	**0.66**	0.29	0.28	**0.57**		
Pentanone, 4-methyl-2-	**0.56**	0.15	**0.59**	0.34	0.10	0.49	0.19	0.22	0.46	0.49	
Acetate, ethyl	-0.21	-0.08	-0.33	-0.18	-0.12	-0.23	0.04	0.08	-0.16	-0.17	-0.21

Table A.24: Winter correlations of saturated aliphatic compounds with OVOCs, values in bold indicate correlations greater than 0.50. Several of the OVOC species were below the detection limit of the GC×GC instrument during the winter campaign and as such they have not been included in this table.

	Methane	Ethane	Propane	*iso*-Butane	*n*-Butane	*n*-Pentane	*iso*-Pentane	Cyclopentane	*n*-Hexane	Pentane, 2/3-methyl	*n*-Heptane	Butane, 2,2,3-trimethyl-	*n*-Octane	Pentane, 2,2,4-trimethyl-	*n*-Nonane	*n*-Decane	Nonane, 2-methyl-	*n*-Undecane	*n*-Dodecane
Acetaldehyde	**0.76**	**0.74**	**0.80**	**0.82**	**0.77**	**0.88**	**0.90**	**0.74**	**0.83**	**0.90**	**0.73**	**0.77**	**0.91**	**0.76**	**0.86**	**0.83**	**0.77**	**0.86**	**0.82**
Butanal	0.24	0.23	0.25	0.25	0.22	0.27	0.26	0.23	0.26	0.28	0.22	0.23	0.30	0.22	0.26	0.24	0.23	0.26	0.26
Hexanal	**0.68**	**0.65**	**0.67**	**0.66**	**0.61**	**0.71**	**0.68**	**0.50**	**0.69**	**0.67**	**0.51**	**0.58**	**0.70**	**0.58**	**0.68**	**0.70**	**0.58**	**0.68**	**0.71**
Benzaldehyde	0.44	0.39	0.43	0.44	0.41	**0.51**	**0.50**	0.34	**0.50**	**0.52**	0.39	**0.59**	**0.50**	0.45	**0.53**	**0.54**	**0.59**	**0.53**	**0.55**
Methanol	0.25	0.24	0.26	0.26	0.24	0.28	0.27	0.17	0.27	0.26	0.20	0.22	0.29	0.24	0.25	0.27	0.22	0.25	0.26
Ethanol	**0.78**	**0.74**	**0.79**	**0.79**	**0.73**	**0.83**	**0.80**	**0.58**	**0.82**	**0.80**	**0.64**	**0.68**	**0.81**	**0.64**	**0.77**	**0.78**	**0.68**	**0.77**	**0.77**
Propanol	0.23	0.22	0.27	0.30	0.29	0.30	0.31	0.19	0.32	0.32	0.28	0.29	0.31	0.27	0.33	0.31	0.29	0.33	0.30
Butanol	0.15	0.13	0.25	0.32	0.31	0.34	0.37	0.13	0.34	0.42	0.36	0.36	0.33	0.34	0.41	0.33	0.36	0.41	0.34
Acetone	**0.64**	**0.64**	**0.67**	**0.66**	**0.61**	**0.71**	**0.72**	**0.57**	**0.68**	**0.72**	**0.57**	**0.61**	**0.73**	**0.56**	**0.69**	**0.66**	**0.61**	**0.69**	**0.67**
Butanone	**0.60**	**0.55**	**0.59**	**0.59**	**0.55**	**0.66**	**0.64**	0.42	**0.65**	**0.68**	**0.54**	**0.70**	**0.67**	**0.58**	**0.75**	**0.74**	**0.70**	**0.75**	**0.74**
Pentanone, 4-methyl-2-	0.46	0.42	0.44	0.43	0.39	0.49	0.49	**0.52**	0.45	**0.51**	0.39	0.49	**0.50**	0.41	**0.58**	**0.55**	0.49	**0.58**	**0.55**
Acetate, ethyl-	-0.31	-0.22	-0.21	-0.19	-0.17	-0.23	-0.20	-0.15	-0.21	-0.20	-0.13	-0.19	-0.18	-0.20	-0.22	-0.24	-0.19	-0.22	-0.30

Table A.25: Winter correlations of unsaturated aliphatic compounds with OVOCs, values in bold indicate correlations greater than 0.50. Two unsaturated aliphatic species, Propyne and 1,2-Butadiene were not measured during the winter campaign and as such are not included in this table. Several OVOC species were below the detection limit of the GC×GC instrument and have also not been included.

	Ethene	**Acetylene**	**Propene**	**Propadiene**	**Butene, *trans*-2-**	**1-Butene**	***iso*-Butene**	**Butene, *cis*-2-**	**1,3-Butadiene**	**Pentene, *trans*-2-**	**1-Pentene**	**Isoprene**	**Styrene**	**α-Pinene**	**Limonene**
Acetaldehyde	**0.83**	**0.80**	**0.81**	**0.87**	**0.89**	**0.87**	**0.91**	**0.89**	**0.84**	**0.86**	**0.86**	**0.87**	**0.75**	-0.15	**0.75**
Butanal	0.29	0.26	0.27	0.24	0.27	0.28	0.27	0.26	0.27	0.24	0.25	0.24	0.32	-0.08	0.23
Hexanal	**0.66**	**0.62**	**0.66**	**0.63**	**0.64**	**0.72**	**0.68**	**0.64**	**0.65**	**0.60**	**0.58**	**0.74**	**0.54**	-0.13	**0.76**
Benzaldehyde	**0.50**	0.47	0.49	**0.52**	0.49	**0.51**	**0.50**	**0.51**	0.46	0.42	0.44	0.49	0.41	-0.04	0.38
Methanol	0.29	0.33	0.25	0.29	0.26	0.27	0.27	0.26	0.28	0.28	**0.57**	0.26	0.17	0.09	0.24
Ethanol	**0.77**	**0.81**	**0.75**	**0.77**	**0.77**	**0.82**	**0.81**	**0.77**	**0.78**	**0.72**	**0.71**	**0.80**	**0.64**	-0.14	**0.81**
Propanol	0.29	0.30	0.30	0.29	0.31	0.32	0.32	0.32	0.26	0.28	0.29	0.27	0.24	-0.06	0.29
Butanol	0.29	0.28	0.32	0.36	0.41	0.34	0.39	0.42	0.28	0.39	0.42	0.33	0.27	-0.09	0.31
Acetone	**0.68**	**0.62**	**0.66**	**0.65**	**0.72**	**0.71**	**0.72**	**0.72**	**0.67**	**0.65**	**0.63**	**0.67**	**0.64**	-0.17	**0.70**
Butanone	**0.68**	**0.67**	**0.65**	**0.71**	**0.64**	**0.68**	**0.67**	**0.65**	**0.62**	**0.57**	**0.55**	**0.59**	**0.61**	-0.15	**0.57**
Pentanone, 4-methyl-2-	0.40	0.32	0.43	0.40	0.46	0.47	0.47	0.46	0.39	0.44	0.42	**0.51**	**0.56**	-0.13	**0.57**
Acetate, ethyl-	-0.28	-0.22	-0.24	-0.26	-0.18	-0.25	-0.21	-0.19	-0.21	-0.15	-0.11	-0.22	-0.19	0.03	-0.24

Table A.26: Winter correlations of aromatic compounds with OVOCs, values in bold indicate correlations greater than 0.50. There were several OVOC species below the detection limit of the GC×GC instrument during the winter campaign and as such have not been included in this table.

	Benzene	Toluene	Benzene, ethyl-	*m-* and *p*-Xylene	*o*-Xylene	Benzene, *iso*-propyl-	Benzene, propyl-	Toluene, 3-ethyl-	Toluene, 4-ethyl-	Benzene, 1,3,5-trimethyl-	Toluene, 2-ethyl-	Benzene, 1,2,4-trimethyl-	Toluene, 4-*iso*-propyl-	Benzene, 1,2,3-trimethyl-	Indan	Benzene, *tert*-butyl-	Benzene, 1,3-diethyl-	Benzene, 1,4-diethyl-	Naphthalene
Acetaldehyde	**0.84**	**0.92**	**0.87**	**0.92**	**0.90**	**0.72**	**0.68**	**0.72**	**0.68**	**0.80**	**0.64**	**0.65**	0.42	**0.83**	**0.77**	0.05	**0.82**	**0.86**	**0.77**
Butanal	0.25	0.27	0.24	0.29	0.29	0.24	0.20	0.16	0.25	0.21	0.21	0.21	0.35	0.26	0.25	0.08	0.22	0.24	0.23
Hexanal	**0.59**	**0.66**	**0.59**	**0.66**	**0.61**	0.44	**0.62**	**0.65**	**0.53**	**0.60**	**0.54**	**0.53**	0.37	**0.67**	**0.63**	0.04	**0.72**	**0.74**	**0.58**
Benzaldehyde	**0.51**	**0.50**	0.44	0.49	0.45	0.34	0.43	0.47	0.40	0.40	0.35	0.39	0.36	**0.50**	**0.53**	0.14	**0.52**	**0.52**	**0.59**
Methanol	0.30	0.27	0.23	0.31	0.27	0.16	0.19	0.19	0.17	0.22	0.17	0.18	0.14	0.26	**0.65**	0.04	0.22	0.22	0.22
Ethanol	**0.76**	**0.79**	**0.72**	**0.78**	**0.75**	**0.50**	**0.70**	**0.72**	**0.60**	**0.68**	**0.60**	**0.62**	0.40	**0.77**	**0.71**	0.08	**0.75**	**0.75**	**0.68**
Propanol	0.27	0.32	0.29	0.33	0.29	0.10	0.21	0.21	0.24	0.24	0.23	0.19	0.11	0.32	**0.55**	0.02	0.30	0.29	0.29
Butanol	0.33	0.41	0.37	0.43	0.34	0.29	0.29	0.31	0.38	0.35	0.37	0.22	0.07	0.38	0.33	0.05	0.35	0.37	0.36
Acetone	**0.61**	**0.73**	**0.72**	**0.75**	**0.70**	**0.53**	**0.54**	**0.52**	**0.58**	**0.64**	**0.60**	0.44	0.36	**0.68**	**0.65**	0.10	**0.66**	**0.71**	**0.61**
Butanone	**0.70**	**0.69**	**0.65**	**0.69**	**0.65**	**0.61**	**0.59**	**0.61**	**0.57**	**0.65**	**0.58**	**0.52**	0.43	**0.72**	**0.59**	-0.01	**0.71**	**0.67**	**0.70**
Pentanone, 4-methyl-2-	0.37	**0.50**	0.49	**0.55**	0.46	**0.50**	0.46	0.49	0.48	**0.57**	**0.50**	0.37	0.25	**0.53**	0.48	0.02	**0.64**	**0.63**	0.49
Acetate, ethyl-	-0.27	-0.21	-0.18	-0.18	-0.13	-0.09	-0.16	-0.21	-0.20	-0.25	-0.22	-0.22	-0.25	-0.19	0.02	0.01	-0.25	-0.23	-0.19

Table A.27: Winter correlations of grouped species with OVOCs, values in bold indicate correlations greater than 0.50. There were several OVOC species below the detection limit of the GC×GC instrument during the winter campaign and as such have not been included in this table.

	C_6 aliphatics	C_7 aliphatics	C_8 aliphatics	C_9 aliphatics	C_{10} aliphatics	C_{11} aliphatics	C_{12} aliphatics	C_{13} aliphatics	C_4 substituted monoaromatics	C_{10} monoterpenes
Acetaldehyde	**0.73**	**0.82**	**0.85**	**0.81**	0.47	**0.85**	**0.84**	**0.87**	**0.85**	**0.86**
Butanal	0.20	0.25	0.26	0.22	0.10	0.27	0.25	0.27	0.26	0.26
Hexanal	0.49	**0.67**	**0.69**	**0.66**	0.36	**0.67**	**0.62**	**0.67**	**0.66**	**0.67**
Benzaldehyde	0.44	0.47	**0.52**	0.46	0.33	**0.53**	0.49	**0.53**	**0.53**	**0.53**
Methanol	0.22	0.23	0.25	0.24	0.18	0.25	0.23	0.25	0.24	0.25
Ethanol	**0.62**	**0.73**	**0.76**	**0.73**	**0.50**	**0.76**	**0.72**	**0.77**	**0.74**	**0.76**
Propanol	0.28	0.31	0.32	0.31	0.19	0.33	0.32	0.33	0.31	0.32
Butanol	0.41	0.38	0.35	0.40	0.16	0.38	0.41	0.41	0.39	0.40
Acetone	**0.57**	**0.68**	**0.70**	**0.67**	0.35	**0.69**	**0.67**	**0.70**	**0.68**	**0.69**
Butanone	**0.69**	**0.67**	**0.71**	**0.66**	0.43	**0.72**	**0.70**	**0.75**	**0.71**	**0.72**
Pentanone, 4-methyl-2-	0.42	**0.57**	**0.59**	**0.56**	0.21	**0.54**	**0.52**	**0.55**	**0.55**	**0.57**
Acetate, ethyl-	-0.20	-0.18	-0.22	-0.17	-0.14	-0.19	-0.17	-0.22	-0.19	-0.21

Table A.28: Summer correlation of OVOC species, values in bold indicate correlations of greater than 0.50

	Acetaldehyde	Propanal, 2-methyl-	Butanal	Butanal, 3-methyl-	Butanal, 2-methyl-	Methacrolein	Pentanal	Hexanal	Benzaldehyde	Methanol	Ethanol	Propanol	Butanol	Acetone	Butanone	Ketone, methyl-vinyl-	Pentanone, 2-	Pentanone, 4-methyl-2-	Hexanone, 2-	Cyclohexanone
Propanal, 2-methyl-	0.05																			
Butanal	0.06	**0.98**																		
Butanal, 3-methyl-	0.09	**0.89**	**0.93**																	
Butanal, 2-methyl-	0.06	**0.98**	**0.98**	**0.91**																
Methacrolein	0.06	**0.98**	**0.98**	**0.91**	**0.98**															
Pentanal	0.06	**0.98**	**0.97**	**0.92**	**0.98**	**0.98**														
Hexanal	0.08	**0.98**	**0.96**	**0.91**	**0.98**	**0.97**	**0.98**													
Benzaldehyde	**0.58**	0.04	0.05	0.04	0.05	0.04	0.06	0.06												
Methanol	**0.67**	0.06	0.05	0.08	0.08	0.07	0.05	0.05	0.49											
Ethanol	**0.82**	0.02	0.04	0.03	0.03	0.03	0.04	0.06	**0.52**	**0.66**										
Propanol	**0.80**	0.04	0.05	0.09	0.05	0.04	0.05	0.07	**0.56**	**0.65**	**0.72**									
Butanol	0.38	-0.05	-0.07	-0.03	-0.04	-0.06	-0.07	-0.05	0.33	0.37	0.38	0.40								
Acetone	**0.68**	0.17	0.16	0.20	0.19	0.18	0.15	0.15	0.45	**0.69**	**0.56**	**0.71**	0.39							
Butanone	0.07	**0.98**	**0.98**	**0.76**	**0.99**	**0.90**	**0.99**	**0.99**	0.08	0.10	0.09	0.06	-0.02	0.19						
Ketone, methyl-vinyl-	0.12	**0.65**	**0.67**	**0.70**	**0.65**	**0.66**	**0.67**	**0.64**	0.10	0.10	0.04	0.10	-0.05	0.19	**0.54**					
Pentanone, 2-	0.09	**0.89**	**0.91**	**0.98**	**0.93**	**0.93**	**0.92**	**0.91**	0.03	0.09	0.02	0.08	-0.03	0.21	**0.77**	**0.69**				
Pentanone, 4-methyl-2-	0.12	**0.90**	**0.94**	**0.98**	**0.92**	**0.92**	**0.94**	**0.93**	0.05	0.08	0.05	0.09	-0.05	0.18	**0.77**	**0.72**	**0.96**			
Hexanone, 2-	0.12	**0.84**	**0.88**	**0.94**	**0.86**	**0.86**	**0.87**	**0.86**	0.00	0.06	0.03	0.06	-0.04	0.16	**0.72**	**0.66**	**0.93**	**0.93**		
Cyclohexanone	0.05	**0.98**	**0.97**	**0.92**	**0.98**	**0.98**	**0.98**	**0.98**	0.05	0.05	0.03	0.02	-0.07	0.13	**0.98**	**0.66**	**0.92**	**0.94**	**0.87**	
Acetate, ethyl	0.13	**0.90**	**0.95**	**0.95**	**0.92**	**0.93**	**0.94**	**0.94**	0.05	0.09	0.05	0.09	-0.06	0.18	**0.77**	**0.74**	**0.93**	**0.99**	**0.90**	**0.94**

Table A.29: Summer correlations of saturated aliphatic compounds with OVOCs, values in bold indicate correlations that are greater than 0.50.

	Methane	**Ethane**	**Propane**	***iso*-Butane**	***n*-Butane**	***n*-Pentane**	***iso*-Pentane**	**Cyclopentane**	***n*-Hexane**	**Pentane, 2/3-methyl**	***n*-Heptane**	**Butane, 2,2,3-trimethyl-**	***n*-Octane**	**Pentane, 2,2,4-trimethyl-**	***n*-Nonane**	***n*-Decane**	**Nonane, 2-methyl-**	***n*-Undecane**	***n*-Dodecane**
Acetaldehyde	**0.63**	**0.71**	**0.87**	**0.78**	**0.81**	**0.89**	**0.89**	**0.73**	**0.73**	**0.93**	**0.84**	**0.75**	**0.88**	**0.86**	**0.59**	0.41	**0.52**	**0.77**	**0.65**
Propanal, 2-methyl-	-0.16	-0.07	-0.05	-0.02	-0.03	0.06	0.10	0.05	0.03	0.05	-0.01	0.04	0.01	0.07	0.03	0.10	0.01	0.06	0.10
Butanal	-0.15	-0.04	-0.03	-0.01	-0.02	0.07	0.10	0.06	0.04	0.07	0.00	0.04	0.02	0.07	0.05	0.10	0.02	0.07	0.12
Butanal, 3-methyl-	-0.11	-0.02	0.00	0.02	0.01	0.10	0.14	0.05	0.05	0.07	0.03	0.09	0.05	0.12	0.07	0.14	0.19	0.11	0.13
Butanal, 2-methyl-	-0.15	-0.04	-0.03	-0.01	-0.02	0.07	0.11	0.06	0.05	0.07	0.00	0.04	0.03	0.08	0.05	0.10	0.01	0.07	0.12
Methacrolein	-0.16	-0.05	-0.05	-0.02	-0.03	0.06	0.10	0.05	0.03	0.05	-0.01	0.03	0.01	0.07	0.03	0.08	0.01	0.06	0.10
Pentanal	-0.15	-0.05	-0.04	-0.02	-0.03	0.07	0.10	0.06	0.03	0.06	0.00	0.04	0.02	0.08	0.04	0.09	0.02	0.07	0.12
Hexanal	-0.11	-0.03	-0.02	0.01	0.00	0.09	0.12	0.08	0.07	0.09	0.03	0.06	0.05	0.11	0.08	0.12	0.03	0.09	0.15
Benzaldehyde	0.46	0.44	**0.60**	**0.52**	**0.50**	**0.57**	**0.55**	0.31	**0.52**	**0.57**	**0.53**	**0.62**	**0.59**	**0.52**	**0.50**	0.30	0.38	**0.68**	**0.50**
Methanol	0.36	0.39	**0.60**	**0.58**	**0.55**	**0.62**	**0.62**	0.40	0.49	**0.60**	**0.59**	**0.57**	**0.64**	**0.60**	0.42	0.27	0.35	**0.59**	0.42
Ethanol	**0.56**	**0.66**	**0.79**	**0.72**	**0.70**	**0.77**	**0.76**	**0.67**	**0.62**	**0.78**	**0.71**	**0.72**	**0.72**	**0.76**	**0.59**	0.42	0.44	**0.74**	**0.63**
Propanol	0.47	**0.53**	**0.71**	**0.67**	**0.65**	**0.77**	**0.80**	**0.61**	**0.63**	**0.79**	**0.73**	**0.69**	**0.70**	**0.73**	**0.58**	0.39	0.43	**0.73**	**0.64**
Butnal	0.24	0.31	0.35	0.30	0.29	0.36	0.39	0.32	0.27	0.47	0.34	0.38	0.32	0.39	0.31	0.12	0.25	0.41	0.35
Acetone	0.26	0.36	**0.53**	**0.51**	0.49	**0.64**	**0.69**	0.44	0.47	**0.59**	**0.55**	**0.58**	**0.58**	**0.60**	0.42	0.29	0.35	**0.60**	0.43
Butanone	-0.16	-0.04	-0.03	-0.01	-0.01	0.07	0.11	0.05	0.05	0.07	0.00	0.12	0.03	0.09	0.10	0.17	0.04	0.11	0.15
Ketone, methyl-vinyl-	-0.10	-0.05	0.04	0.08	0.06	0.11	0.15	0.05	0.07	0.07	0.04	0.06	0.12	0.15	-0.01	-0.01	0.12	0.08	0.02
Pentanone, 2-	-0.12	-0.02	-0.01	0.01	0.01	0.09	0.14	0.04	0.04	0.07	0.02	0.08	0.05	0.12	0.06	0.14	0.18	0.10	0.12
Pentanone, 4-methyl-2-	-0.12	-0.03	0.01	0.04	0.03	0.11	0.14	0.07	0.06	0.08	0.04	0.07	0.08	0.13	0.06	0.10	0.17	0.10	0.11
Hexanone, 2-	-0.07	0.02	0.02	0.03	0.04	0.12	0.14	0.06	0.09	0.10	0.06	0.11	0.07	0.14	0.07	0.19	0.26	0.07	0.12
Cyclohexanone	-0.14	-0.03	-0.03	-0.01	-0.02	0.07	0.09	0.07	0.05	0.07	-0.01	0.05	0.01	0.06	0.07	0.12	0.02	0.07	0.13
Acetate, ethyl-	-0.13	-0.04	0.01	0.04	0.04	0.10	0.14	0.08	0.06	0.07	0.04	0.06	0.09	0.12	0.06	0.06	0.14	0.09	0.10

Table A.30: Summer correlations of unsaturated aliphatic compounds with OVOCs, values in bold indicate correlations of greater than 0.50.

	Ethene	Acetylene	Propene	Propadiene	Propyne	Butene, *trans*-2-	1-Butene	*iso*-Butene	Butene, *cis*-2-	1,2-Butadiene	1,3-Butadiene	Pentene, *trans*-2-	1-Pentene	Isoprene	Styrene	α-Pinene	Limonene
Acetaldehyde	**0.78**	**0.80**	**0.76**	**0.73**	**0.71**	**0.78**	**0.80**	**0.88**	**0.78**	-0.03	**0.57**	**0.80**	**0.89**	0.22	0.26	0.27	0.07
Propanal, 2-methyl-	0.04	0.06	0.07	0.06	0.45	0.13	0.14	0.09	0.10	-0.09	0.19	0.10	0.12	0.30	-0.05	0.37	**0.98**
Butanal	0.06	0.07	0.09	0.08	0.41	0.14	0.15	0.10	0.11	-0.08	0.24	0.11	0.13	0.28	-0.05	0.36	**0.98**
Butanal, 3-methyl-	0.07	0.09	0.09	0.07	**0.55**	0.15	0.18	0.13	0.13	-0.08	0.25	0.13	0.16	0.30	0.06	0.36	**0.82**
Butanal, 2-methyl-	0.06	0.08	0.09	0.07	0.41	0.14	0.17	0.11	0.11	-0.08	0.24	0.11	0.14	0.30	-0.06	0.36	**0.75**
Methacrolein	0.04	0.07	0.07	0.06	0.41	0.14	0.15	0.10	0.11	-0.08	0.23	0.11	0.14	0.31	-0.06	0.37	**0.94**
Pentanal	0.05	0.06	0.07	0.08	0.41	0.13	0.13	0.10	0.11	-0.08	0.23	0.11	0.13	0.28	-0.05	0.37	**0.91**
Hexanal	0.10	0.10	0.12	0.10	0.41	0.15	0.15	0.12	0.14	-0.05	0.24	0.13	0.14	0.28	-0.04	0.37	**0.94**
Benzaldehyde	0.45	0.42	0.40	0.36	0.16	0.39	0.45	0.49	0.40	-0.02	0.13	0.42	0.49	0.09	0.21	0.14	0.06
Methanol	**0.53**	**0.55**	0.46	0.43	0.27	0.45	**0.56**	**0.59**	0.45	-0.02	0.12	0.45	**0.58**	0.24	0.16	0.23	0.09
Ethanol	**0.73**	**0.74**	**0.66**	**0.65**	**0.62**	**0.67**	**0.67**	**0.78**	**0.68**	-0.03	**0.57**	**0.69**	**0.77**	0.01	0.17	0.13	0.07
Propanol	**0.67**	**0.68**	**0.63**	**0.58**	**0.93**	**0.67**	**0.75**	**0.73**	**0.66**	0.14	**0.53**	**0.67**	**0.77**	0.33	0.28	0.35	0.06
Butnaol	0.30	0.32	0.28	0.28	-0.07	0.32	0.34	0.36	0.36	0.12	0.41	0.36	0.41	0.00	0.12	-0.03	-0.03
Acetone	0.48	**0.53**	0.47	0.38	**0.60**	0.48	**0.68**	**0.58**	0.47	0.02	0.21	0.46	**0.66**	0.49	0.25	0.43	0.19
Butanone	0.05	0.08	0.08	0.08	0.41	0.15	0.16	0.12	0.12	-0.07	0.21	0.13	0.15	0.27	-0.05	0.36	**0.77**
Ketone, methyl-vinyl-	0.07	0.08	0.10	0.06	0.41	0.15	0.16	0.15	0.13	-0.08	0.11	0.12	0.14	0.35	0.26	0.33	**0.59**
Pentanone, 2-	0.06	0.09	0.09	0.06	0.41	0.15	0.19	0.13	0.13	-0.08	0.24	0.13	0.16	0.33	0.06	0.37	**0.83**
Pentanone, 4-methyl-2-	0.09	0.10	0.11	0.10	**0.57**	0.15	0.18	0.14	0.13	-0.08	0.24	0.13	0.16	0.29	0.04	0.36	**0.83**
Hexanone, 2-	0.13	0.14	0.16	0.13	0.30	0.17	0.20	0.16	0.15	-0.08	0.28	0.14	0.17	0.28	0.09	0.34	**0.77**
Cyclohexanone	0.05	0.06	0.07	0.07	0.31	0.12	0.13	0.09	0.10	-0.12	0.22	0.10	0.12	0.24	-0.07	0.32	**1.00**
Acetate, ethyl-	0.08	0.10	0.10	0.10	**0.57**	0.14	0.17	0.14	0.13	-0.08	0.22	0.12	0.16	0.28	0.01	0.35	**0.83**

Table A.31: Summer correlations of aromatic compounds with OVOCs, values in bold indicate correlations that are greater than 0.50. Two aromatic species, *iso*-propyl-benzene and Indan, were below the detection limit of the GC×GC instrument during the summer campaign and as such are not included in this table.

	Benzene	Toluene	Benzene, ethyl-	*m*- and *p*- xylene	*o*- xylene	Benzene, propyl-	Toluene, 3-ethyl-	Toluene, 4-ethyl-	Benzene, 1,3,5-trimethyl-	Toluene, 2-ethyl-	Benzene, 1,2,4-trimethyl-	Toluene, 4-*iso*-propyl-	Benzene, 1,2,3-trimethyl-	Benzene, *tert*-butyl-	Benzene, 1,3-diethyl-	Benzene, 1,4-diethyl-	Napthalene
Acetaldehyde	**0.90**	**0.93**	**0.95**	**0.94**	**0.95**	0.43	0.41	0.41	**0.57**	0.37	0.37	0.16	**0.53**	0.16	0.36	**0.63**	**0.51**
Propanal, 2-methyl-	0.04	0.01	0.03	0.02	0.01	0.12	0.10	0.11	-0.01	0.08	0.01	**0.59**	0.00	-0.04	0.09	0.11	0.02
Butanal	0.05	0.03	0.06	0.04	0.03	0.12	0.11	0.11	0.00	0.09	0.01	**0.57**	0.02	-0.05	0.09	0.12	0.03
Butanal, 3-methyl-	0.08	0.05	0.07	0.05	0.05	0.13	0.08	0.10	0.05	0.09	0.02	**0.70**	0.03	-0.04	0.09	0.11	0.19
Butanal, 2-methyl-	0.05	0.02	0.05	0.03	0.02	0.12	0.11	0.11	0.00	0.09	0.02	**0.58**	0.02	-0.05	0.08	0.13	0.02
Methacrolein	0.04	0.01	0.04	0.02	0.01	0.12	0.10	0.10	-0.01	0.08	0.01	**0.58**	0.01	-0.05	0.08	0.11	0.01
Pentanal	0.05	0.02	0.05	0.04	0.03	0.13	0.11	0.10	0.00	0.09	0.01	**0.58**	0.01	-0.05	0.09	0.12	0.02
Hexanal	0.08	0.06	0.09	0.07	0.07	0.13	0.11	0.12	0.03	0.12	0.01	**0.57**	0.04	-0.05	0.11	0.15	0.04
Benzaldehyde	**0.51**	**0.53**	**0.55**	**0.53**	**0.57**	0.47	**0.51**	0.43	0.49	0.42	0.40	0.04	0.49	0.22	0.28	**0.51**	0.30
Methanol	**0.63**	**0.57**	**0.60**	**0.55**	**0.60**	0.34	0.33	0.29	0.33	0.28	0.32	0.08	0.36	0.11	0.22	0.42	0.35
Ethanol	**0.83**	**0.82**	**0.80**	**0.81**	**0.81**	0.45	0.46	0.43	**0.53**	0.40	0.36	0.10	**0.52**	0.17	0.37	**0.63**	0.44
Propanol	**0.76**	**0.73**	**0.76**	**0.72**	**0.73**	0.42	0.42	0.45	**0.58**	0.41	0.37	0.04	**0.56**	0.12	0.37	**0.64**	0.41
Butanol	0.36	0.38	0.37	0.36	0.36	0.22	0.26	0.22	0.35	0.28	0.21	0.01	0.28	0.04	0.19	0.36	0.24
Acetone	**0.57**	**0.53**	**0.59**	**0.53**	**0.57**	0.31	0.31	0.30	0.37	0.26	0.30	0.14	0.35	0.12	0.24	0.44	0.38
Butanone	0.06	0.03	0.05	0.04	0.04	0.18	0.20	0.17	0.02	0.11	0.08	**0.58**	0.08	-0.04	0.13	0.16	0.03
Ketone, methyl-vinyl-	0.08	0.06	0.09	0.08	0.08	0.03	0.06	0.04	-0.02	0.04	0.02	**0.55**	0.01	0.01	0.05	0.01	0.13
Pentanone, 2-	0.07	0.03	0.06	0.04	0.03	0.12	0.07	0.10	0.04	0.09	0.02	**0.71**	0.02	-0.05	0.08	0.10	0.17
Pentanone, 4-methyl-2-	0.09	0.06	0.09	0.07	0.08	0.10	0.07	0.10	0.03	0.08	0.01	**0.69**	0.01	-0.01	0.08	0.09	0.16
Hexanone, 2-	0.12	0.09	0.13	0.11	0.11	0.06	0.08	0.08	0.04	0.06	0.02	**0.76**	0.04	-0.08	0.10	0.08	0.27
Cyclohexanone	0.04	0.03	0.05	0.04	0.03	0.12	0.11	0.11	0.00	0.08	0.01	**0.60**	0.01	-0.05	0.08	0.14	0.03
Acetate, ethyl-	0.09	0.06	0.09	0.08	0.09	0.10	0.08	0.09	0.01	0.08	0.00	**0.65**	0.02	0.01	0.07	0.09	0.12

Table A.32: Summer correlations of grouped species with OVOCs, values in bold indicate correlations greater than 0.50.

	C_6 aliphatics	C_7 aliphatics	C_8 aliphatics	C_9 aliphatics	C_{10} aliphatics	C_{11} aliphatics	C_{12} aliphatics	C_{13} aliphatics	C_4 substituted monoaromatics	C_{10} monoterpenes
Acetaldehyde	**0.60**	**0.63**	**0.65**	**0.59**	**0.61**	**0.54**	**0.50**	**0.53**	**0.50**	0.05
Propanal, 2-methyl-	0.15	0.15	0.13	0.09	0.00	0.07	0.12	0.02	0.00	**0.98**
Butanal	0.14	0.15	0.12	0.08	-0.01	0.06	0.10	0.00	-0.01	**0.74**
Butanal, 3-methyl-	0.16	0.13	0.14	0.11	0.04	0.11	0.13	0.04	0.00	**0.93**
Butanal, 2-methyl-	0.14	0.15	0.11	0.08	-0.01	0.06	0.10	0.00	-0.02	**0.79**
Methacrolein	0.14	0.14	0.11	0.07	-0.02	0.06	0.10	0.01	-0.02	**0.76**
Pentanal	0.13	0.15	0.12	0.08	-0.01	0.07	0.11	-0.01	-0.02	**0.72**
Hexanal	0.12	0.17	0.14	0.10	0.00	0.08	0.12	-0.02	-0.01	**0.75**
Benzaldehyde	**0.56**	**0.59**	**0.53**	**0.58**	**0.53**	**0.51**	0.47	**0.55**	**0.54**	0.05
Methanol	**0.52**	0.43	0.44	0.44	0.47	0.45	0.38	**0.56**	0.41	0.04
Ethanol	**0.55**	**0.60**	**0.61**	**0.54**	0.49	0.42	0.42	0.49	**0.52**	0.03
Propanol	**0.62**	**0.64**	**0.67**	**0.64**	**0.52**	**0.50**	**0.50**	**0.56**	**0.55**	0.04
Butanol	0.37	0.33	0.34	0.35	0.26	0.21	0.21	0.40	0.46	-0.08
Acetone	**0.52**	0.43	0.46	0.43	0.42	0.42	0.38	**0.53**	0.39	0.14
Butanone	0.17	0.19	0.15	0.13	0.03	0.08	0.14	0.05	0.05	**0.74**
Ketone, methyl-vinyl-	0.12	0.07	0.08	0.07	0.13	0.14	0.13	0.10	0.04	**0.68**
Pentanone, 2-	0.16	0.12	0.12	0.09	0.04	0.10	0.13	0.04	-0.01	**0.92**
Pentanone, 4-methyl-2-	0.15	0.13	0.13	0.11	0.07	0.13	0.13	0.06	0.03	**0.94**
Hexanone, 2-	0.10	0.10	0.09	0.06	0.01	0.08	0.09	-0.02	-0.06	**0.88**
Cyclohexanone	0.13	0.17	0.12	0.09	-0.02	0.05	0.10	-0.01	0.01	**0.81**
Acetate, ethyl-	0.15	0.14	0.13	0.11	0.08	0.14	0.13	0.07	0.04	**0.95**

Table A.33: Winter and summer correlations of halogenated compounds with OVOCs, values in bold indicate correlations that are greater than 0.50. Trichloroethylene was below the detection limit of the GC×GC instrument during the winter campaign. There were also several OVOC species that were below the limit of detection in winter, indicated by - in the winter dichloromethane column.

	Winter	**Summer**	
	Methane, dichloro	**Methane, dichloro**	**Trichloroethylene**
Acetaldehyde	**0.73**	**0.65**	**0.75**
Propanal, 2-methyl-	-	0.08	0.10
Butanal	0.18	0.07	0.11
Butanal, 3-methyl-	-	0.22	0.11
Butanal, 2-methyl-	-	0.07	0.11
Methacrolein	-	0.06	0.10
Pentanal	-	0.07	0.10
Hexanal	**0.63**	0.08	0.12
Benzaldehyde	0.43	**0.55**	**0.68**
Methanol	0.20	**0.56**	**0.59**
Ethanol	**0.72**	**0.61**	**0.72**
Propanol	0.36	**0.63**	**0.75**
Butanol	0.39	0.38	0.40
Acetone	**0.62**	**0.52**	**0.59**
Butanone	**0.66**	0.10	0.13
Ketone, methyl-vinyl-	-	0.15	0.09
Pentanone, 2-	-	0.21	0.10
Pentanone, 4-methyl-2-	**0.55**	0.19	0.10
Hexanone, 2-	-	0.21	0.06
Cyclohexanone	-	0.08	0.11
Acetate, ethyl-	-0.16	0.17	0.11

Abbreviations

ATSDR	Agency for Toxic Substances and Disease Registry
AURN	Automatic Urban and Rural Network
b:135tmb	benzene to 1,3,5-trimethyl benzene ratio
b:t	benzene to toluene ratio
BVOCs	Biogenic Volatile Organic Compounds
C*	saturation concentration
CALNEX	California research at the nexus of air quality and climate change
CCN	Cloud Condensation Nuclei
ClearfLo	Clean Air for London
CPC	Condensation Particle Counter
DC–GC	Dual Channel–Gas Chromatography
DCM	dichloromethane
DS	Deans Switch
E5	5% ethanol blended gasoline
E10	10% ethanol blended gasoline
E85	85% ethanol blended gasoline
EKMA	Empirical Kinetic Modelling Approach

ELVOC	Extremely Low Volatile Organic Compounds
EPA	Environment Protection Agency
EU	European Union
f/a	formaldehyde to acetaldehyde ratio
FAMEs	Fatty Acid Methyl Esters
FFV	Flexible Fuel Vehicles
FGAM	Facility for Ground based Atmospheric Measurements
FID	Flame Ionisation Detector
GAW	Global Atmospheric Watch monitoring stations
GC	Gas Chromatography
GC×GC	Comprehensive Two–Dimensional Gas Chromatography
GC-GC	Heart-cut GC
GC–GC×GC	Heart–cut combined with Comprehensive Two–Dimensional Gas Chromatography
IOF	International Operating Fund
IOPs	Intensive Operating Periods
IPCC	Intergovernmental Panel on Climate Change
IVOC	Intermediate Volatile Organic Compounds
LIF	Laser Induced Fluoresence
LOD	Limit of Detection
LVOC	Low Volatile Organic Compounds
MCM	Master Chemical Mechanism
MDGC	Multidimensional Gas Chromatography
MIR	Maximum Incremental Reactivity

MR	Marylebone Road, ClearfLo measurement site
MS	Mass Spectrometer
NAEI	National Atmospheric Emissions Inventory
NAME	Numerical Atmospheric dispersion Modelling Environment
NCAS	National Centre for Atmospheric Science
NERC	National Environment Research Council
NK	North Kensington, ClearfLo Site
NMHCs	Non-Methane Hydrocarbons
NMVOCs	Non-Methane Volatile Organic Compounds
NPL	National Physical Laboratories
OA	Organic Aerosol
OFP	Ozone Formation Potential
OVOCs	Oxygenated Volatile Organic Compounds
PAN	Peroxyacyl nitrates
PLOT	Porous Layer Open Tubular
PM	Particulate Matter
PM_{10}	Particulate matter with diameters of 10 μm or less
$PM_{2.5}$	Particulate matter with diameters of 2.5 μm or less
POA	Primary Organic Aerosol
POCPs	Photochemical Ozone Creation Potentials
PTR-MS	Proton Transfer Reaction-Mass Spectrometer
REVIHAAP	Review of Evidence on Health Aspects of Air Pollution report
RF	Response Factor
RTFO	Road Transport Fuel Obligation

SIA	Secondary Inorganic Aerosol
SOA	Secondary Organic Aerosol
SVOC	Semi Volatile Organic Compounds
TD	Thermal Desorption
t/b	toluene to benzene ratio
TCE	trichloroethylene
UCM	Unresolved Complex Mixture
UN	United Nations
VOCs	Volatile Organic Compounds
WAS	Whole Air Samples
WHO	World Health Organisation

References

[1] J.S. Gaffney and N.A. Marley. The impacts of combustion emissions on air quality and climate - From coal to biofuels and beyond. *Atmospheric Environment*, 43(1):23–36, 2009.

[2] A.J. Haagen-Smit and M.M. Fox. Photochemical ozone formation with hydrocarbons and automobile exhaust. *Air Repair*, 4(3):105–136, 1954.

[3] European Environment Agency. Air Quality in Europe. 2014.

[4] H. Walton, D. Dajnak, S. Beevers, M. Williams, P. Watkiss, and A. Hunt. Understanding the health impacts of air pollution in London. Technical report, King's College London, Transport for London and the Greater London Authority, 2015.

[5] United Nations, Department for Economic, and Social Affairs. World Urbanization Propects, the 2014 revision, 2014.

[6] J. Fenger. Urban air quality. *Atmospheric Environment*, 33(29):4877 – 4900, 1999.

[7] G.R. McMeeking, M. Bart, P. Chazette, J.M. Haywood, and J.R. Hopkins *et al.* Airborne measurements of trace gases and aerosols over the London metropolitan region. *Atmospheric Chemistry and Physics*, 12(11):5163–5187, 2012.

[8] D.D. Parrish, W.C. Kuster, M. Shao, Y. Yokouchi, and Y. Kondo *et al.* Comparison of air pollutant emissions among mega-cities. *Atmospheric Environment*, 43(40):6435–6441, 2009.

[9] X. Han and L.P. Naeher. A review of traffic-related air pollution exposure assesssment studies in the developing world. *Environment International*, 32(1):106–120, 2006.

[10] World Health Organisation. Review of evidence on health aspects of air pollution – REVIHAAP project. Technical report, World Health Organisation, Regional Office for Europe, Copenhagen, Denmark, 2013.

[11] M. Kampa and E. Castanas. Human health effects of air pollution. *Environmental Pollution*, 151(2):362 – 367, 2008.

[12] European Environment Agency. Air Quality in Europe. 2013.

[13] European Environment Agency. Every breath we take. Improving air quality in Europe. Technical report, European Environment Agency,, 2013.

[14] J.E.C. Lerner, T. Kohajda, M.E. Aguilar, L.A. Massolo, and E.Y. Sánchez *et al.* Improvement of health risk factors after reduction of VOC concentrations in industrial and urban areas. *Environmental Science and Pollution Research*, 21(16):9676–9688, 2014.

[15] *Directive of the European Union 2000/69/EC*, 2000.

[16] H. Guo, S.C. Lee, L.Y. Chan, and W.M. Li. Risk assessment of exposure to volatile organic compounds in different indoor environments. *Environmental Research*, 94(1):57 – 66, 2004.

[17] O. Herbarth and S. Matysik. Decreasing concentrations of volatile organic compounds (VOC) emitted following home renovations. *Indoor Air*, 20(2):141–146, 2010.

[18] J.T. Spickett, H.L. Brown, and K. Rumchev. Climate Change and Air Quality: The potential impact on health. *Asia-Pacific Journal of Public Health*, 23(2):37S–45S, 2011.

[19] E. von Schneidemesser, P.S. Monks, J.D. Allan, L. Bruhwiler, and P. Forster *et al.* Chemistry and the linkages between air quality and climate change. *Chemical Reviews*, 115(10):3856–3897, 2015.

[20] M.L. Bell, R. Goldberg, C. Hogrefe, P.L. Kinney, and K. Knowlton *et al.* Climate change, ambient ozone, and health in 50 US cities. *Climatic Change*, 82(1-2):61–76, 2007.

[21] S.S. Lim, T. Vos, A.D. Flaxman, G. Danaei, and K. Shibuya *et al.* A comparative risk assessment of burden of disease and injury attributable to 67 risk factors and

risk factor clusters in 21 regions, 1990-2010: a systematic analysis for the Global Burden of Disease Study 2010. *The Lancet*, 380(9859):2224 – 2260, 2013.

[22] R.A. Silva, J.J. West, Y. Zhang, S.C. Anenberg, and J.-F. Lamarque *et al.* Global premature mortality due to anthropogenic outdoor air pollution and the contribution of past climate change. *Environmental Research Letters*, 8(3):034005, 2013.

[23] M.R. Heal, P. Kumar, and R.M. Harrison. Particles, air quality, policy and health. *Chemical Society Reviews*, 41:6606–6630, 2012.

[24] D.W. Dockery and C.A. Pope. Acute respiratory effects of particulate air pollution. *Annual Review of Public Health*, 15(1):107–132, 1994.

[25] C. Pope III, R.T. Burnett, M.J. Thun, E.E. Calle, D. Krewski, K. Ito, and G.D. Thurston. Lung cancer, cardiopulmonary mortality, and long-term exposure to fine particulate air pollution. *Journal of the American Medical Association*, 287(9):1132–1141, 2002.

[26] B. Alföldy, B. Giechaskiel, W. Hofmann, and Y. Drossinos. Size-distribution dependent lung deposition of diesel exhaust particles. *Journal of Aerosol Science*, 40(8):652 – 663, 2009.

[27] IPCC. Summary for Policymakers. Climate change 2013: The physical science basis. Technical report, Contribution of Working Group I to the Fifth Assessment Report of the Intergovernmental Panel on Climate Change, Cambridge, UK and New York, NY, 2013.

[28] T. F. Stocker, D. Qin, G.-K. Plattner, L. V. Alexander, and S. K. Allen *et al.* Climate change 2013: The physical science basis. Technical report, Contribution of Working Group I to the Fifth Assessment Report of the Intergovernmental Panel on Climate Change, Cambridge, UK and New York, NY, 2013.

[29] D.S. Stevenson, P.J. Young, V. Naik, J.-F. Lamarque, and D.T. Shindell *et al.* Tropospheric ozone changes, radiative forcing and attribution to emissions in the Atmospheric Chemistry and Climate Model Intercomparison Project (ACCMIP). *Atmospheric Chemistry and Physics*, 13(6):3063–3085, 2013.

[30] D. Hofmann, J. Butler, E. Dlugokencky, J. Elkings, K. Masarie, S. Montzka, and

P. Tans. The role of carbon dioxide in climate forcing from 1979 to 2004: introduction of the Annual Greenhouse Gas Index. *Tellus B*, 58(5), 2006.

[31] G. Myhre, D. Shindell, F.-M. Bréon, W. Collins, and J. Fuglestvedt *et al.* Anthropogenic and Natural Radiative Forcing. In Climate Change 2013: The Physical Science Basis. Technical report, Contribution of Working Group I to the Fifth Assessment Report of the Intergovernmental Panel on Climate Change, Cambridge, UK and New York, NY, 2013.

[32] M.J. Prather, C.D. Holmes, and J. Hsu. Reactive greenhouse gas scenarios: Systematic exploration of uncertainties and the role of atmospheric chemistry. *Geophysical Research Letters*, 39(9):L09803, 2012.

[33] C.D. Holmes, M.J. Prather, O.A. Søvde, and G. Myhre. Future methane, hydroxyl, and their uncertainties: key climate and emission parameters for future predictions. *Atmospheric Chemistry and Physics*, 13(1):285–302, 2013.

[34] A.M. Fiore, D.J. Jacob, B.D. Field, D.G. Streets, S.D. Fernandes, and C. Jang. Linking ozone pollution and climate change: The case for controlling methane. *Geophysical Research Letters*, 29(19):25–1–25–4, 2002. 1919.

[35] W.J. Collins, R.G. Derwent, C.E. Johnson, and D.S. Stevenson. The oxidation of organic compounds in the troposphere and their global warming potentials. *Climatic Change*, 52(4):453–479, 2002.

[36] T. Berntsen, J. Fuglestvedt, M. Joshi, K. Shine, and N. Stuber *et al.* Response of climate to regional emissions of ozone precursors: sensitivities and warming potentials. *Tellus B*, 57(4), 2011.

[37] V. Naik, D. Mauzerall, L. Horowitz, M.D. Schwarzkopf, V. Ramaswamy, and M. Oppenheimer. Net radiative forcing due to changes in regional emissions of tropospheric ozone precursors. *Journal of Geophysical Research: Atmospheres*, 110(D24):306, 2005.

[38] D.T. Shindell, G. Faluvegi, D.M. Koch, G.A. Schmidt, N. Unger, and S.E. Bauer. Improved attribution of climate forcing to emissions. *Science*, 326(5953):716–718, 2009.

[39] J.H. Seinfeld and S.N. Pandis. *Atmospheric Chemistry and Physics: From air pollution to climate change*. J Wiley and Sons, INC, 2nd edition, 2006.

[40] R. Atkinson and J. Arey. Gas-phase tropospheric chemistry of biogenic volatile organic compounds: a review. *Atmospheric Environment*, 37(2):S197–S219, 2003.

[41] N. Poisson, M. Kanakidou, and P.J. Crutzen. Impact of non-methane hydrocarbons on tropospheric chemistry and the oxidizing power of the global troposphere: 3-dimensional modelling results. *Journal of Atmospheric Chemistry*, 36(2):157–230, 2000.

[42] G.A. Folberth, D.A. Hauglustaine, J. Lathière, and F. Brocheton. Interactive chemistry in the Laboratoire de Meteorologie Dynamique general circulation model: model description and impact analysis of biogenic hydrocarbons on tropospheric chemistry. *Atmospheric Chemistry and Physics*, 6(8):2273–2319, 2006.

[43] R. Atkinson. Atmospheric chemistry of VOCs and NO_x. *Atmospheric Environment*, 34(12-14):2063–2101, 2000.

[44] J. Haywood and O. Boucher. Estimates of the direct and indirect radiative forcing due to tropospheric aerosols: A review. *Reviews of Geophysics*, 38(4):513–543, 2000.

[45] K.S. Carslaw, O. Boucher, D.V. Spracklen, G.W. Mann, J.G.L. Rae, S. Woodward, and M. Kulmala. A review of natural aerosol interactions and feedbacks within the Earth system. *Atmospheric Chemistry and Physics*, 10(4):1701–1737, 2010.

[46] B.A. Albrecht. Aerosols, cloud microphysics, and fractional cloudiness. *Science*, 245(4923):1227–1230, 1989.

[47] P.S. Monks, C. Granier, S. Fuzzi, A. Stohl, and M.L. Williams *et al.* Atmospheric composition change - global and regional air quality. *Atmospheric Environment*, 43(33):5268 – 5350, 2009.

[48] M. Williams. Tackling climate change: what is the impact on air pollution? *Carbon Management*, 3(5):511–519, 2012.

[49] E. von Schneidemesser and P.S. Monks. Air quality and climate - synergies and trade-offs. *Environmental Science: Processes and Impacts*, 15:1315–1325, 2013.

[50] J.R. Hopkins, A.C. Lewis, and P.W. Seakins. Analysis and applications of measurements of source dominated hydrocarbon concentrations from the PUMA campaigns in June/July 1999 and January/February 2000 at an urban background site in Birmingham, UK. *Atmospheric Environment*, 39(3):535–548, 2005.

[51] W.L. Chameides, F. Fehsenfeld, M.O. Rodgers, C. Cardelino, and J. Martinez *et al.* Ozone precursor relationships in the ambient atmosphere. *Journal of Geophysical Research-Atmosphere*, 97(D5):6037–6055, 1992.

[52] N.M. Donahue, A.L. Robinson, C.O. Stanier, and S.N. Pandis. Coupled partitioning, dilution, and chemical aging of semivolatile organics. *Environmental Science & Technology*, 40(8):2635–2643, 2006.

[53] N.M. Donahue, J.H. Kroll, S.N. Pandis, and A.L. Robinson. A two-dimensional volatility basis set-part 2: Diagnostics of organic-aerosol evolution. *Atmospheric Chemistry and Physics*, 12(2):615–634, 2012.

[54] N.M. Donahue, I.K. Ortega, W. Chuang, I. Riipinen, and F. Riccobono *et al.* How do organic vapors contribute to new-particle formation? *Faraday Discuss.*, 165:91–104, 2013.

[55] S. Reimann and A.C. Lewis. *Volatile organic compounds in the atmosphere, Chapter 2: Anthropogenic VOCs*, pages 33–81. Blackwell Publishing Ltd, 2007.

[56] J. Kesselmeier and M. Staudt. Biogenic volatile organic compounds (VOC): An overview on emission, physiology and ecology. *Journal of Atmospheric Chemistry*, 33(1):23–88, 1999.

[57] A.H. Steiner and A.L. Goldstein. *Volatile organic compounds in the atmosphere, Chapter 3: Biogenic VOCs*, pages 82–128. Blackwell Publishing Ltd, 2007.

[58] J.-F. Müller. Geographical distribution and seasonal variation of surface emissions and deposition velocities of atmospheric trace gases. *Journal of Geophysical Research: Atmospheres*, 97(D4):3787–3804, 1992.

[59] J. Williams and R. Koppmann. *Volatile organic compounds in the atmosphere, Chapter 1: Volatile organic compounds in the atmosphere: an overview*, pages 1–32. Blackwell Publishing Ltd, 2007.

[60] A. Guenther. The contribution of reactive carbon emissions from vegetation to the carbon balance of terrestrial ecosystems. *Chemosphere*, 49(8):837 – 844, 2002.

[61] S.M. Saunders, M.E. Jenkin, R.G. Derwent, and M.J. Pilling. Protocol for the development of the Master Chemical Mechanism, MCM v3 (Part A): tropospheric degradation of non-aromatic volatile organic compounds. *Atmospheric Chemistry and Physics*, 3(1):161–180, 2003.

[62] M.E. Jenkin, S.M. Saunders, V. Wagner, and M.J. Pilling. Protocol for the development of the Master Chemical Mechanism, MCM v3 (Part B): tropospheric degradation of aromatic volatile organic compounds. *Atmospheric Chemistry and Physics*, 3(1):181–193, 2003.

[63] P.V. Doskey, V.R. Kotamarthi, Y. Fukui, D.R. Cook, F.W. Breitbeil, and M.L. Wesely. Air-surface exchange of peroxyacetyl nitrate at a grassland site. *Journal of Geophysical Research: Atmospheres*, 109(D10):310, 2004.

[64] R.J. Kieber, B. Peake, J.D. Willey, and G. Brooks Avery. Dissolved organic carbon and organic acids in coastal New Zealand rainwater. *Atmospheric Environment*, 36(21):3557 – 3563, 2002.

[65] A. Fornaro and I.G.R. Gutz. Wet deposition and related atmospheric chemistry in the São Paulo metropolis, Brazil: Part 2-contribution of formic and acetic acids. *Atmospheric Environment*, 37(1):117 – 128, 2003.

[66] I.T. Cousins, , and D. Mackay. Gas-particle partitioning of organic compounds and its interpretation using relative solubilities. *Environmental Science & Technology*, 35(4):643–647, 2001.

[67] Z. Klimont, D.G. Streets, S. Gupta, J. Cofala, F. Lixin, and Y. Ichikawa. Anthropogenic emissions of non-methane volatile organic compounds in China. *Atmospheric Environment*, 36(8):1309 – 1322, 2002.

[68] A. Borbon, H. Fontaine, N. Locoge, M. Veillerot, and J.C. Galloo. Developing receptor-oriented methods for non-methane hydrocarbon characterisation in urban air. Part II: source apportionment. *Atmospheric Environment*, 37(29):4065 – 4076, 2003.

[69] J.D. Fuentes, L. Gu, M. Lerdau, R. Atkinson, and D. Baldocchi *et al.* Biogenic hydrocarbons in the atmospheric boundary layer: a review. *Bulletin of the American Meteorological Society*, 81(7):1537–1575, 2000.

[70] A.B. Guenther, X. Jiang, C.L. Heald, T. Sakulyanontvittaya, T. Duhl, L.K. Emmons, and X. Wang. The Model of Emissions of Gases and Aerosols from Nature version 2.1 (MEGAN2.1): an extended and updated framework for modeling biogenic emissions. *Geoscientific Model Development*, 5(6):1471–1492, 2012.

[71] MCMv3.2 Website. First accessed 12/12/2011.

[72] S.R. Utembe, M.E. Jenkin, R.G. Derwent, A.C. Lewis, J.R. Hopkins, and J.F. Hamilton. Modelling the ambient distribution of organic compounds during the August 2003 ozone episode in the southern UK. *Faraday Discussions*, 130:311–326, 2005.

[73] P.S. Monks. Gas-phase radical chemistry in the troposphere. *Chemical Society Reviews*, 34(5):376–395, 2005.

[74] B.J. Finlayson-Pitts and J.N. Pitts Jr. *Chemistry of the Upper and Lower Atmosphere.* Academic Press, London, 1999.

[75] S. Li, J. Matthews, and A. Sinha. Atmospheric hydroxyl radical production from electronically excited NO_x and H_2O. *Science*, 319(5870):1657–1660, 2008.

[76] X. Ren, D. van Duin, M. Cazorla, S. Chen, and J. Mao *et al.* Atmospheric oxidation chemistry and ozone production: Results from SHARP 2009 in Houston, Texas. *Journal of Geophysical Research: Atmospheres*, 118(11):5770–5780, 2013.

[77] A.P. Altshuller. Nonmethane organic-compound to nitrogen-oxide ratios and organic composition in cities and rural-areas. *JAPCA-The Journal of the Air and Waste Management Association*, 39(7):936–943, 1989.

[78] J.D. Lee, J.C. Young, K.A. Read, J.F. Hamilton, and J.R. Hopkins *et al.* Measurement and calculation of OH reactivity at a United Kingdom coastal site. *Journal of Atmospheric Chemistry*, 64(1):53–76, 2009.

[79] K.M. Emmerson, N. Carslaw, D.C. Carslaw, J.D. Lee, and G. McFiggans *et al.* Free radical modelling studies during the UK TORCH Campaign in Summer 2003. *Atmospheric Chemistry and Physics*, 7:167–181, 2007.

[80] P.V. Hobbs. *Introduction to Atmospheric Chemistry*. Cambridge Unversity Press, 2000.

[81] R. Atkinson. Gas-phase tropospheric chemistry of volatile organic compounds .1. Alkanes and alkenes. *Journal of Physical and Chemical Reference Data*, 26(2):215–290, 1997.

[82] R. Atkinson and J. Arey. Atmospheric degradation of volatile organic compounds. *Chemical Reviews*, 103(12):4605–4638, 2003.

[83] R.F. Hansen, S.M. Griffith, S. Dusanter, P.S. Rickly, and P.S. Stevens *et al.* Measurements of total hydroxyl radical reactivity during CABINEX 2009 – Part 1: field measurements. *Atmospheric Chemistry and Physics*, 14(6):2923–2937, 2014.

[84] A.C. Lewis, N. Carslaw, P.J. Marriott, R.M. Kinghorn, and P. Morrison *et al.* A larger pool of ozone-forming carbon compounds in urban atmospheres. *Nature*, 405(6788):778–781, 2000.

[85] R.M. Harrison, M. Dall'Osto, D.C.S. Beddows, A.J. Thorpe, and W.J. Bloss *et al.* Atmospheric chemistry and physics in the atmosphere of a developed megacity (London): an overview of the REPARTEE experiment and its conclusions. *Atmospheric Chemistry and Physics*, 12(6):3065–3114, 2012.

[86] F. Ludwig, E. Reiter, E. Shelar, and W.B. Johnson. The relation of oxidant levels to precursor emissions and meterological features., Vol. 1. Analysis and Findings. Technical Report EPA-50/3-77-022a, Environmental Protection Agency, Office of Air Quality Standards and Planning,, Research Triangle Park, N.C., 1977.

[87] M.D. Zeldin and W. Meisel. Use of meteorological data in air quality trend analysis. Technical report, Technology Service Corporation,, 1978.

[88] G.T. Wolff and P.J. Lioy. Empirical model for forecasting maximum daily ozone levels in northeastern United States. *Journal of the Air Pollution Control Association*, 28(10):1034–1038, 1978.

[89] D.J. Wackter and P.V. Bayly. *The effectiveness of emission controls on reducing ozone levels in Connecticut from 1976 through 1987*. Air and Waste Management Association,, 1988.

[90] A.K. Pollack. Application of a simple meteorological index of ambient ozone potential to ten cities. Technical report, Paper 86-19.5 in Proceedings of the 79th Annual Meeting and Exhibition of the Air Pollition Control Association,, Minneapolis, Minn., 1986.

[91] G. Kuntasal and T.Y. Chang. Trends and relationships of O_3, NO_x and HC in the south coast air basin of California. *JAPCA-The International Journal of Air Pollution Control and Hazardous Waste Management*, 37(10):1158–1163, 1987.

[92] M.A. Atwater. Influence of meteorolgy on high ozone concentrations. Technical report, Air Pollution Control Association Internation Specialty Conference on Evaluation of the Scientific Basis for Ozone/Oxidants Standard, Houston, Texas, November 27-30 1984.

[93] RTI (Research Triangle Institute). Investigation of rural oxidant levels as related to urban hydrocarbon control strategies. Technical report, U.S. Environmental Protection Agency,, Research Triangle Park, N.C. 359 pp., 1975.

[94] C.E. Decker, L.A. Ripperton, J.J.B. Worth, F.M. Vukovich, and W.D. Bach *et al.* Formation and transport of oxidants along the Gulf Coast and in Northern U.S. Technical Report EPA-450/3-76-003, U.S. Environmental Protection Agency,, Research Triangle Park, N.C.,, 1976.

[95] L.I. Kleinman. Low and high NO_x tropospheric photochemistry. *Journal of Geophysical Research-Atmospheres*, 99(D8):16831–16838, 1994.

[96] M.C. Dodge. *Combined use of modeling techniques and smog chamber data to derive ozone precursor relationships. Pp. 881-889 in International Conference on Photochemical Oxidant Pollution and its Control: Proceedings, Vol. II.,*. EPA/600/3-77-001b. U.S. Environmental Protection Agency, Environmental Sciences Research Laboratory, Research Triangle Park, N.C., 1977.

[97] European Environment Agency. Air Quality in Europe. 2012.

[98] Environmental Protection Agency. Our nation's air – Status and trends through 2008. Technical report, United States Environmental Protection Agency,, 2010.

[99] M. Hallquist, J. C. Wenger, U. Baltensperger, Y. Rudich, and D. Simpson *et al.*

The formation, properties and impact of secondary organic aerosol: current and emerging issues. *Atmospheric Chemistry and Physics*, 9(14):5155–5236, 2009.

[100] H.B. Singh. Guidance for the collection and use of ambient hydrocarbon species data in development of Ozone control strategies. *U.S. Environmental Protection Agency,*, EPA 450/4-80-008, 1980.

[101] R.G. Ackman. Flame Ionization Detector - Further comments on molecular breakdown and fundamental group responses. *Journal of Gas Chromatography*, 6(10):497, 1968.

[102] J. Cochran. Evaluation of comprehensive two-dimensional gas chromatography - time-of-flight mass spectrometry for the determination of pesticides in tobacco. *Journal of Chromatography A*, 1186(1-2):202–210, 2008.

[103] A.H. Goldstein and I.E. Galbally. Known and unexplored organic constituents in the Earth's atmosphere. *Environmental Science & Technology*, 41(5):1514–1521, 2007.

[104] J.F. Hamilton. Using comprehensive two-dimensional gas chromatography to study the atmosphere. *Journal of Chromatographic Science*, 48(4):274–282, 2010.

[105] J.F. Hamilton and A.C. Lewis. Monoaromatic complexity in urban air and gasoline assessed using comprehensive GC and fast GC-TOF/MS. *Atmospheric Environment*, 37(5):589–602, 2003.

[106] J.C. Giddings. Concepts and comparisons in multidimensional separation. *Journal of High Resolution Chromatography*, 10(5):319–323, 1987.

[107] M. Edwards, A. Mostafa, and T. Gorecki. Modulation in comprehensive two-dimensional gas chromatography: 20 years of innovation. *Analytical and Bioanalytical Chemistry*, 401(8):2335–2349, 2011.

[108] Z.Y. Liu and J.B. Phillips. Comprehensive two-dimensional gas-chromatography using an on-column thermal modulator interface. *Journal of Chromatographic Science*, 29(6):227–231, 1991.

[109] M. Kallio, M. Jussila, T. Rissanen, P. Anttila, and K. Hartonen *et al.* Comprehensive two-dimensional gas chromatography coupled to time-of-flight mass spectrometry in the identification of organic compounds in atmospheric aerosols from coniferous forest. *Journal of Chromatography A*, 1125(2):234–243, 2006.

[110] O. Amador-Munoz and P.J. Marriott. Quantification in comprehensive two-dimensional gas chromatography and a model of quantification based on selected summed modulated peaks. *Journal of Chromatography A*, 1184(1-2):323–340, 2008.

[111] R.E. Murphy, M.R. Schure, and J.P. Foley. Effect of sampling rate on resolution in comprehensive two-dimensional liquid chromatography. *Analytical Chemistry*, 70(8):1585–1594, 1998.

[112] J.C. Giddings. Maximum number of components resolvable by gel filtration and other elution chchromatograph methods. *Analytical Chemistry*, 39(8):1027–1028, 1967.

[113] Z.Y. Liu, D.G. Patterson, and M.L. Lee. Geometric approach to factor-analysis for the estimation of orthogonality and practical peak-capacity in comprehensive two-dimensional separations. *Analytical Chemistry*, 67(21):3840–3845, 1995.

[114] J.F. Hamilton and A.C. Lewis. *Volatile organic compounds in the atmosphere, Chapter 11: Comprehensive two-dimensional gas chromatography*, pages 467–488. Blackwell Publishing Ltd, 2007.

[115] J. Dalluge, L.L.P. van Stee, X.B. Xu, J. Williams, J. Beens, R.J.J. Vreuls, and U.A.T. Brinkman. Unravelling the composition of very complex samples by comprehensive gas chromatography coupled to time-of-flight mass spectrometry - Cigarette smoke. *Journal of Chromatography A*, 974(1-2):169–184, 2002.

[116] J. Dalluge, J. Beens, and U.A.T. Brinkman. Comprehensive two-dimensional gas chromatography: a powerful and versatile analytical tool. *Journal of Chromatography A*, 1000(1-2):69–108, 2003.

[117] J.A. Murray. Qualitative and quantitative approaches in comprehensive two-dimensional gas chromatography. *Journal of Chromatography A*, 1261:58 – 68, 2012.

[118] C. Meinert and U.J. Meierhenrich. A new dimension in separation science: Comprehensive two-dimensional gas chromatography. *Angewandte Chemie International Edition*, 51(42):10460–10470, 2012.

[119] J.B. Phillips and J. Beens. Comprehensive two-dimensional gas chromatography: a hyphenated method with strong coupling between the two dimensions. *Journal of Chromatography A*, 856(1-2):331–347, 1999.

[120] C.J. Venkatramani and J.B. Phillips. Comprehensivetwo-dimensional gas-chromatography applied to the analysis of complex-mixtures. *Journal of Microcolumn Separations*, 5(6):511–516, 1993.

[121] Z. Liu and J.B. Phillips. Sensitivity and detection limit enhancement of gas chromatographic detection by thermal modulation. *Journal of Microcolumn Separations*, 6(3):229–235, 1994.

[122] Z. Liu, S.R. Sirimanne, D.G. Patterson Jr., L.L. Needham, and J.B. Phillips. Comprehensive two-dimensional gas chromatography for the fast separation and determination of pesticides extracted from human serum. *Analytical Chemistry*, 66(19):3086–3092, 1994.

[123] J.B. Phillips and J.Z. Xu. Comprehensive multidimensional Gas-Chromatography. *Journal of Chromatography A*, 703(1-2):327–334, 1995.

[124] J. Beens, R. Tijssen, and J. Blomberg. Prediction of comprehensive two-dimensional gas chromatographic separations: A theoretical and practical exercise. *Journal of Chromatography A*, 822(2):233 – 251, 1998.

[125] R.B. Gaines, , G.S. Frysinger, M.S. Hendrick-Smith, and J.D. Stuart. Oil spill source identification by comprehensive two-dimensional gas chromatography. *Environmental Science & Technology*, 33(12):2106–2112, 1999.

[126] J.B. Phillips and E.B. Ledford. Thermal modulation: A chemical instrumentation component of potential value in improving portability. *Field Analytical Chemistry & Technology*, 1(1):23–29, 1996.

[127] J.B. Phillips, R.B. Gaines, J. Blomberg, F.W.M. van der Wielen, and J.M. Dimandja *et al.* A robust thermal modulator for comprehensive two-dimensional gas chromatography. *HRC-Journal of High Resolution Chromatography*, 22(1):3–10, 1999.

[128] J. Beens, H. Boelens, R. Tijssen, and J. Blomberg. Quantitative aspects of comprehensive two-dimensional gas chromatography (GC×GC). *HRC-Journal of High Resolution Chromatography*, 21(1):47–54, 1998.

[129] G.S. Frysinger, R.B. Gaines, and E.B. Ledford. Quantitative determination of BTEX and total aromatic compounds in gasoline by comprehensive two-dimensional

gas chromatography (GC×GC). *HRC-Journal of High Resolution Chromatography*, 22(4):195–200, 1999.

[130] P.J. Marriott and R.M. Kinghorn. Longitudinally Modulated Cryogenic System. A generally applicable approach to solute trapping and mobilization in gas chromatography. *Analytical Chemistry*, 69(13):2582–2588, 1997.

[131] R.T. Lidster, J.F. Hamilton, and A.C. Lewis. The application of two total transfer valve modulators for comprehensive two-dimensional gas chromatography of volatile organic compounds. *Journal of Separation Science*, 34(7):812–821, 2011.

[132] M. Pursch, K. Sun, B. Winniford, H. Cortes, A. Weber, T. McCabe, and J. Luong. Modulation techniques and applications in comprehensive two-dimensional gas chromatography (GC×GC). *Analytcal and Bioanalytical Chemistry*, 373(6):356–367, 2002.

[133] J.F. Hamilton, A.C. Lewis, and K.D. Bartle. Peak amplitude and resolution in comprehensive gas chromatography using valve modulation. *Journal of Separation Science*, 26(6-7):578–584, 2003.

[134] C.A. Bruckner, B.J. Prazen, and R.E. Synovec. Comprehensive two dimensional high-speed gas chromatography with chemometric analysis. *Analytical Chemistry*, 70(14):2796–2804, 1998.

[135] J.V. Seeley, F. Kramp, and C.J. Hicks. Comprehensive two-dimensional gas chromatography via differential flow modulation. *Analytical Chemistry*, 72(18):4346–4352, 2000.

[136] P.A. Bueno and J.V. Seeley. Flow-switching device for comprehensive two-dimensional gas chromatography. *Journal of Chromatography A*, 1027(1-2):3–10, 2004.

[137] R.E. Mohler, B.J. Prazen, and R.E. Synovec. Total-transfer, valve-based comprehensive two-dimensional gas chromatography. *Analytica Chimica Acta*, 555(1):68–74, 2006.

[138] House of Commons, Environmental Audit Committee. Air Quality: A follow-up report, Ninth Report. Technical report, House of Commons, London, The Stationary Office Ltd., 2012.

[139] A.L. Robinson, N.M. Donahue, M.K. Shrivastava, E.A. Weitkamp, and A.M. Sage *et al.* Rethinking organic aerosols: Semivolatile emissions and photochemical aging. *Science*, 315(5816):1259–1262, 2007.

[140] J.R. Odum, T.P.W. Jungkamp, R.J. Griffin, H.J.L. Forstner, R.C. Flagan, and J.H. Seinfeld. Aromatics, reformulated gasoline, and atmospheric organic aerosol formation. *Environmental Science & Technology*, 31(7):1890–1897, 1997.

[141] E. von Schneidemesser, P.S. Monks, and C. Plass-Duelmer. Global comparison of VOC and CO observations in urban areas. *Atmospheric Environment*, 44(39):5053–5064, 2010.

[142] C. Warneke, J.A. de Gouw, J.S. Holloway, J. Peischl, and T.B. Ryerson *et al.* Multiyear trends in volatile organic compounds in Los Angeles, California: Five decades of decreasing emissions. *Journal of Geophysical Research: Atmospheres*, 117(D21), 2012.

[143] M. Cames and E. Helmers. Critical evaluation of the European diesel car boom - global comparison, environmental effects and various national strategies. *Environmental Sciences Europe*, 25(15), 2013.

[144] N.R Passant. Speciation of UK emissions of non-methane volatile organic compounds. Technical report, AEA Technology Report ENV-05452002, Culham, Abingdon, United Kingdom, 2002.

[145] Exxon Mobil. The Outlook for Energy: A view to 2040. Technical report, Exxon Mobil Corporation,, Texas, 2014.

[146] V. Gros, J. Sciare, and T. Yu. Air-quality measurements in megacities: Focus on gaseous organic and particulate pollutants and comparison between two contrasted cities, Paris and Beijing. *Comptes Rendus Geoscience*, 339(11-12):764–774, 2007.

[147] J.L. Jimenez, M.R. Canagaratna, N.M. Donahue, A.S.H. Prevot, and Q. Zhang *et al.* Evolution of organic aerosols in the atmosphere. *Science*, 326(5959):1525–1529, 2009.

[148] D.R. Gentner, G. Isaacman, D.R. Worton, A.W.H. Chan, and T.R. Dallmann *et al.* Elucidating secondary organic aerosol from diesel and gasoline vehicles through

detailed characterization of organic carbon emissions. *Proceedings of the National Academy of Sciences of the United States of America*, 109(45):18318–23, 2012.

[149] R. Bahreini, A.M. Middlebrook, J.A. de Gouw, C. Warneke, and M. Trainer *et al.* Gasoline emissions dominate over diesel in formation of secondary organic aerosol mass. *Geophysical Research Letters*, 39(6), 2012.

[150] T.D. Gordon, D.S. Tkacik, A.A. Presto, M. Zhang, and S.H. Jathar *et al.* Primary gas- and particle-phase emissions and secondary organic aerosol production from gasoline and diesel off-road engines. *Environmental Science & Technology*, 47(24):14137–14146, 2013.

[151] S.M. Platt, I. El Haddad, A.A. Zardini, M. Clairotte, and C. Astorga *et al.* Secondary organic aerosol formation from gasoline vehicle emissions in a new mobile environmental reaction chamber. *Atmospheric Chemistry and Physics*, 13(18):9141–9158, 2013.

[152] T.D. Gordon, A.A. Presto, A.A. May, N.T. Nguyen, and E.M. Lipsky *et al.* Secondary organic aerosol formation exceeds primary particulate matter emissions for light-duty gasoline vehicles. *Atmospheric Chemistry and Physics*, 14(9):4661–4678, 2014.

[153] T.D. Gordon, A.A. Presto, N.T. Nguyen, W.H. Robertson, and K. Na *et al.* Secondary organic aerosol production from diesel vehicle exhaust: impact of after treatment, fuel chemistry and driving cycle. *Atmospheric Chemistry and Physics*, 14(9):4643–4659, 2014.

[154] S.H. Jathar, T.D. Gordon, C.J. Hennigan, H.O.T. Pye, and G. Pouliot *et al.* Unspeciated organic emissions from combustion sources and their influence on the secondary organic aerosol budget in the United States. *Proceedings of the National Academy of Sciences*, 111(29):10473–10478, 2014.

[155] J.J. Ensberg, P.L. Hayes, J.L. Jimenez, J.B. Gilman, and W.C. Kuster *et al.* Emission factor ratios, SOA mass yields, and the impact of vehicular emissions on SOA formation. *Atmospheric Chemistry and Physics*, 14(5):2383–2397, 2014.

[156] H.E. Stewart, C.N. Hewitt, R.G.H. Bunce, R. Steinbrecher, G. Smiatek, and T. Schoenemeyer. A highly spatially and temporally resolved inventory for bio-

genic isoprene and monoterpene emissions: Model description and application to Great Britain. *Journal of Geophysical Research: Atmospheres*, 108(D20), 2003.

[157] M.Z. Jacobson. *Atmospheric Pollution: History, Science and Regulation.* Cambridge Unversity Press, 2002.

[158] D.C. Carslaw, S.D. Beevers, J.E. Tate, E.J. Westmoreland, and M.L. Williams. Recent evidence concerning higher NO_x emissions from passenger cars and light duty vehicles. *Atmospheric Environment*, 45(39):7053 – 7063, 2011.

[159] S.I. Bohnenstengel, S.E. Belcher, A. Aiken, J.D. Allan, and G. Allen *et al.* Meteorology, air quality, and health in London: The ClearfLo project. *Bulletin of the American Meteorological Society*, 2014.

[160] A. Bigi and R.M. Harrison. Analysis of the air pollution climate at a central urban background site. *Atmospheric Environment*, 44(16):2004–2012, 2010.

[161] J.R. Hopkins, A.C. Lewis, and K.A. Read. A two-column method for long-term monitoring of non-methane hydrocarbons (NMHCs) and oxygenated volatile organic compounds (OVOCs). *Journal of Environmental Monitoring*, 5:8–13, 2003.

[162] J.R. Hopkins, C.E. Jones, and A.C. Lewis. A dual channel gas chromatograph for atmospheric analysis of volatile organic compounds including oxygenated and monoterpene compounds. *Journal of Environmental Monitoring*, 13(8):2268–2276, 2011.

[163] M. de Blas, M. Navazo, L. Alonso, N. Durana, and J. Iza. Automatic on-line monitoring of atmospheric volatile organic compounds: Gas chromatography-mass spectrometry and gas chromatography-flame ionization detection as complementary systems. *Science of the Total Environment*, 409(24):5459–5469, 2011.

[164] J. Slemr, F. Slemr, H. D'Souza, and R. Partridge. Study of the relative response factors of various gas chromatograph-flame ionisation detector systems for measurement of C_2-C_9 hydrocarbons in air. *Journal of Chromatography A*, 1061(1):75 – 84, 2004.

[165] J.D. Lee, S.J. Moller, K.A. Read, A.C. Lewis, L. Mendes, and L.J. Carpenter. Year-round measurements of nitrogen oxides and ozone in the tropical North Atlantic marine boundary layer. *Journal of Geophysical Research-Atmospheres*, 114, 2009.

[166] D.C. Carslaw and K. Ropkins. openair – An R package for air quality data analysis. *Environemtal Modelling & Software*, 27-28:52–61, 2012.

[167] D.C. Carslaw and K. Ropkins. Openair: Open-source tools for the analysis of air pollution data. *R package version 0.6-2.*, 2012.

[168] R Development Core Team. *R: A Language and Environment for Statistical Computing*. R Foundation for Statistical Computing, Vienna, Austria, 2012.

[169] J.F. Barlow, C.H. Halios, S.E. Lane, and C.R. Wood. Observations of urban boundary layer structure during a strong urban heat island event. *Environmental Fluid Mechanics*, 15(2):373–398, 2015.

[170] Y. Nannoolal, J. Rarey, D. Ramjugernath, and W. Cordes. Estimation of pure component properties: Part 1. Estimation of the normal boiling point of non-electrolyte organic compounds via group contributions and group interactions. *Fluid Phase Equilibria*, 226:45 – 63, 2004.

[171] Y. Nannoolal, J. Rarey, and D. Ramjugernath. Estimation of pure component properties: Part 3. Estimation of the vapor pressure of non-electrolyte organic compounds via group contributions and group interactions. *Fluid Phase Equilibria*, 269:117 – 133, 2008.

[172] D.R. Gentner, D.R. Worton, G. Isaacman, L.C. Davis, and T.R Dallmann *et al.* Chemical composition of gas-phase organic carbon emissions from motor vehicles and implications for ozone production. *Environmental Science & Technology*, 47(20):11837–11848, 2013.

[173] Y. Zhao, C.J. Hennigan, A.A. May, D.S. Tkacik, and J.A. de Gouw *et al.* Intermediate-volatility organic compounds: A large source of secondary organic aerosol. *Environmental Science & Technology*, 48(23):13743–13750, 2014.

[174] A. Borbon, H. Fontaine, M. Veillerot, N. Locoge, J.C. Galloo, and R. Guillermo. An investigation into the traffic-related fraction of isoprene at an urban location. *Atmospheric Environment*, 35(22):3749–3760, 2001.

[175] P. Gaffron. Urban transport, environmental justice and human daily activity patterns. *Transport Policy*, 20(SI):116–129, 2012.

[176] J.A. de Gouw, A.M. Middlebrook, C. Warneke, P.D. Goldan, and W.C. Kuster *et al.* Budget of organic carbon in a polluted atmosphere: Results from the New England Air Quality Study in 2002. *Journal of Geophysical Research-Atmospheres*, 110(D16), 2005.

[177] T.B. Ryerson, A.E. Andrews, W.M. Angevine, T.S. Bates, and C.A. Brock *et al.* The 2010 California research at the nexus of air quality and climate change (CalNex) field study. *Journal of Geophysical Research: Atmospheres*, 118(11):5830–5866, 2013.

[178] Department of Energy & Climate Change. Road transport energy consumption at regional and local authority level, 2014. www.gov.uk/government/statistical-data-sets/road-transport-energy-consumption-at-regional-and-local-authority-level.

[179] P.J. Ziemann and R. Atkinson. Kinetics, products, and mechanisms of secondary organic aerosol formation. *Chemical Society Reviews*, 41:6582–6605, 2012.

[180] R. Atkinson. Kinetics of the gas-phase reactions of OH radicals with alkanes and cycloalkanes. *Atmospheric Chemistry and Physics*, 3(6):2233–2307, 2003.

[181] E.S.C. Kwok and R. Atkinson. Estimation of hydroxyl radical reaction-rate constants for gas-phase organic-compounds using a struture-reactivity relathionship - an update. *Atmospheric Environment*, 29(14):1685–1695, 1995.

[182] S.M. Aschmann and R. Atkinson. Rate constants for the gas-phase reactions of OH radicals with *E*-7-tetradecene, 2-methyl-1-tridecene and the C_7-C_{14} 1-alkenes at 295 ± 1 K. *Physical Chemistry Chemical Physics*, 10:4159–4164, 2008.

[183] Q. Zhang, J.L. Jimenez, M.R. Canagaratna, I.M. Ulbrich, N.L. Ng, D.R. Worsnop, and Y. Sun. Understanding atmospheric organic aerosols via factor analysis of aerosol mass spectrometry: a review. *Analytical and Bioanalytical Chemistry*, 401(10):3045–3067, 2011.

[184] D.E. Young, J.D. Allan, P.I. Williams, D.C. Green, and M.J. Flynn *et al.* Investigating the annual behaviour of submicron secondary inorganic and organic aerosols in London. *Atmospheric Chemistry and Physics*, 15:6351–6366, 2015.

[185] A. Yoshino, Y. Sadanaga, K. Watanabe, S. Kato, Y. Miyakawa, J. Matsumoto, and Y. Kajii. Measurement of total OH reactivity by laser-induced pump and probe tech-

nique - comprehensive observations in the urban atmosphere of Tokyo. *Atmospheric Environment*, 40(40):7869 – 7881, 2006.

[186] A. Yoshino, Y. Nakashima, K. Miyazaki, S. Kato, and J. Suthawaree *et al.* Air quality diagnosis from comprehensive observations of total OH reactivity and reactive trace species in urban central Tokyo. *Atmospheric Environment*, 49(0):51 – 59, 2012.

[187] C. Dolgorouky, V. Gros, R. Sarda-Esteve, V. Sinha, and J. Williams *et al.* Total OH reactivity measurements in Paris during the 2010 MEGAPOLI winter campaign. *Atmospheric Chemistry and Physics*, 12(20):9593–9612, 2012.

[188] V. Michoud, A. Kukui, M. Camredon, A. Colomb, and A. Borbon *et al.* Radical budget analysis in a suburban European site during the MEGAPOLI summer field campaign. *Atmospheric Chemistry and Physics*, 12(24):11951–11974, 2012.

[189] Y. Nakashima, S. Kato, J. Greenberg, P. Harley, and T. Karl *et al.* Total OH reactivity measurements in ambient air in a southern Rocky mountain ponderosa pine forest during BEACHON-SRM08 summer campaign. *Atmospheric Environment*, 85:1 – 8, 2014.

[190] B. Langford, E. Nemitz, E. House, G.J. Phillips, and D. Famulari *et al.* Fluxes and concentrations of volatile organic compounds above central London, UK. *Atmospheric Chemistry and Physics*, 10(2):627–645, 2010.

[191] R.G. Derwent, M.E. Jenkin, S.M. Saunders, and M.J. Pilling. Photochemical ozone creation potentials for organic compounds in northwest Europe calculated with a master chemical mechanism. *Atmospheric Environment*, 32(14-15):2429–2441, 1998.

[192] J.G. Calvert, R.G. Derwent, J.J. Orlando, G.S. Tyndall, and T.J. Wallington. *Mechanisms of atmospheric oxidation of the alkenes*. Oxford University Press, New York,, 2008.

[193] W.P.L. Carter. SAPRC-07 Atmospheric Chemistry Mechanisms and VOC Reactivity Scales, 2010.

[194] R.G. Derwent, M.E. Jenkin, M.J. Pilling, W.P.L. Carter, and A. Kaduwela. Reactivity scales as comparative tools for chemical mechanisms. *Journal of the Air & Waste Management Association*, 60(8):914–924, 2010.

[195] X. Zhang, C.D. Cappa, S.H. Jathar, R.C. McVay, J.J. Ensberg, M.J. Kleeman, and J.H. Seinfeld. Influence of vapor wall loss in laboratory chambers on yields of secondary organic aerosol. *Proceedings of the National Academy of Sciences*, 111(16):5802–5807, 2014.

[196] A.A. Presto, M.A. Miracolo, N.M. Donahue, and A.L. Robinson. Secondary organic aerosol formation from high-NO_x photo-oxidation of low volatility precursors: *n*-alkanes. *Environmental Science & Technology*, 44(6):2029–2034, 2010.

[197] C. Knote, A. Hodzic, J.L. Jimenez, R. Volkamer, and J.J. Orlando *et al.* Simulation of semi-explicit mechanisms of SOA formation from glyoxal in aerosol in a 3-D model. *Atmospheric Chemistry and Physics*, 14(12):6213–6239, 2014.

[198] D.C. Carslaw and G. Rhys-Tyler. New insights from comprehensive on-road measurements of NO_x, NO_2 and NH_3 from vehicle emission remote sensing in London, UK. *Atmospheric Environment*, 81(0):339 – 347, 2013.

[199] European Commission. EU Transport in Figures, 2012. available at http://ec.europa.eu/transport/facts-fundings/statistics/doc/2012/pocketbook2012.pdf.

[200] U.S. Energy Information Administration. Petroleum and Other Liquids, 2014.

[201] E. von Schneidemesser, P.S. Monks, V. Gros, J. Gauduin, and O. Sanchez. How important is biogenic isoprene in an urban environment? A study in London and Paris. *Geophysical Research Letters*, 38, 2011.

[202] D.A. Sarigiannis, S.P. Karakitsios, A. Gotti, I.L. Liakos, and A. Katsoyiannis. Exposure to major volatile organic compounds and carbonyls in European indoor environments and associated health risk. *Environment International*, 37(4):743 – 765, 2011.

[203] J.-H. Park, A.H. Goldstein, J. Timkovsky, S. Fares, R. Weber, J. Karlik, and R. Holzinger. Eddy covariance emission and deposition flux measurements using proton transfer reaction - time of flight - mass spectrometry (PTR-TOF-MS): comparison with PTR-MS measured vertical gradients and fluxes. *Atmospheric Chemistry and Physics*, 13(3):1439–1456, 2013.

[204] D.R. Gentner, R.A. Harley, A.M. Miller, and A.H. Goldstein. Diurnal and seasonal variability of gasoline-related volatile organic compound emissions in riverside, california. *Environmental Science & Technology*, 43(12):4247–4252, 2009. PMID: 19603630.

[205] Z.L. Fleming, P.S. Monks, and A.J. Manning. Review: Untangling the influence of air-mass history in interpreting observed atmospheric composition. *Atmospheric Research*, 104:1–39, 2012.

[206] J.D. Lee, A.C. Lewis, P.S. Monks, M. Jacob, and J.F. Hamilton *et al.* Ozone photochemistry and elevated isoprene during the UK heatwave of August 2003. *Atmospheric Environment*, 40(39):7598–7613, 2006.

[207] R.R. Hoque, P.S. Khillare, T. Agarwal, V. Shridhar, and S. Balachandran. Spatial and temporal variation of BTEX in the urban atmosphere of Delhi, India. *Science of The Total Environment*, 392(1):30 – 40, 2008.

[208] J. Liu, Y. Mu, Y. Zhang, Z. Zhang, X. Wang, Y. Liu, and Z. Sun. Atmospheric levels of BTEX compounds during the 2008 Olympic Games in the urban area of Beijing. *Science of The Total Environment*, 408(1):109 – 116, 2009.

[209] R. Perry and I.L. Gee. Vehicle emissions in relation to fuel composition. *Science of The Total Environment*, 169(13):149 – 156, 1995. Transport and Air Pollution.

[210] D. Brocco, R. Fratarcangeli, L. Lepore, M. Petricca, and I. Ventrone. Determination of aromatic hydrocarbons in urban air of Rome. *Atmospheric Environment*, 31(4):557 – 566, 1997.

[211] N.V. Heeb, A.M. Forss, C. Bach, S. Reimann, A. Herzog, and H.W. Jäckle. A comparison of benzene, toluene and C_2-benzenes mixing ratios in automotive exhaust and in the suburban atmosphere during the introduction of catalytic converter technology to the Swiss Car Fleet. *Atmospheric Environment*, 34(19):3103 – 3116, 2000.

[212] A. Monod, B.C. Sive, P. Avino, T. Chen, D. R Blake, and F S. Rowland. Monoaromatic compounds in ambient air of various cities: a focus on correlations between the xylenes and ethylbenzene. *Atmospheric Environment* , 35(1):135 – 149, 2001.

[213] C.Y Chan, L.Y Chan, X.M Wang, Y.M Liu, and S.C Lee *et al.* Volatile organic

compounds in roadside microenvironments of metropolitan Hong Kong. *Atmospheric Environment*, 36(12):2039 – 2047, 2002.

[214] V.T.Q. Truc and N.T.K. Oanh. Roadside BTEX and other gaseous air pollutants in relation to emission sources. *Atmospheric Environment*, 41(36):7685 – 7697, 2007.

[215] M.A. Alghamdi, M. Khoder, A.S. Abdelmaksoud, R.M. Harrison, and T. Hussein *et al.* Seasonal and diurnal variations of BTEX and their potential for ozone formation in the urban background atmosphere of the coastal city Jeddah, Saudi Arabia. *Air Quality, Atmosphere & Health*, 7(4):467–480, 2014.

[216] A. Muezzinoglu, M. Odabasi, and L. Onat. Volatile organic compounds in the air of Izmir, Turkey. *Atmospheric Environment*, 35(4):753 – 760, 2001.

[217] M. Caselli, G. de Gennaro, A. Marzocca, L. Trizio, and M. Tutino. Assessment of the impact of the vehicular traffic on BTEX concentration in ring roads in urban areas of Bari (Italy). *Chemosphere*, 81(3):306 – 311, 2010.

[218] P.F. Nelson and S.M. Quigley. Nonmethane hydrocarbons in the atmosphere of Sydney, Australia. *Environmental Science & Technology*, 16(10):650–655, 1982.

[219] A.J. Buczynska, A. Krata, M. Stranger, A.F.L. Godoi, and V. Kontozova-Deutsch *et al.* Atmospheric BTEX-concentrations in an area with intensive street traffic. *Atmospheric Environment*, 43(2):311 – 318, 2009.

[220] L. Miller, L.D. Lemke, X. Xu, S.M. Molaroni, and H. You *et al.* Intra-urban correlation and spatial variability of air toxics across an international airshed in Detroit, Michigan (USA) and Windsor, Ontario (Canada). *Atmospheric Environment*, 44(9):1162 – 1174, 2010.

[221] L. Tong, X. Liao, J. Chen, H. Xiao, L. Xu, F. Zhang, Z. Niu, and J. Yu. Pollution characteristics of ambient volatile organic compounds (VOCs) in the southeast coastal cities of China. *Environmental Science and Pollution Research*, 20(4):2603–2615, 2013.

[222] S. Yurdakul, M. Civan, and G. Tuncel. Volatile organic compounds in suburban Ankara atmosphere, Turkey: Sources and variability. *Atmospheric Research*, 120 - 121:298 – 311, 2013.

[223] S.C. Lee, M.Y. Chiu, K.F. Ho, S.C. Zou, and X. Wang. Volatile organic compounds (VOCs) in urban atmosphere of Hong Kong. *Chemosphere*, 48(3):375 – 382, 2002.

[224] S.M Owen, P Harley, A Guenther, and C.N Hewitt. Light dependency of VOC emissions from selected Mediterranean plant species. *Atmospheric Environment*, 36(19):3147 – 3159, 2002.

[225] S. Kim, T. Karl, A. Guenther, G. Tyndall, J. Orlando, P. Harley, R. Rasmussen, and E. Apel. Emissions and ambient distributions of Biogenic Volatile Organic Compounds (BVOC) in a ponderosa pine ecosystem: interpretation of PTR-MS mass spectra. *Atmospheric Chemistry and Physics*, 10(4):1759–1771, 2010.

[226] P.K. Misztal, C.N. Hewitt, J. Wildt, J.D. Blande, and A.S.D. Eller *et al.* Atmospheric benzenoid emissions from plants rival those from fossil fuels. *Scientific Reports*, 5:12064, 2015.

[227] C. E. Jones, J. R. Hopkins, and A. C. Lewis. In situ measurements of isoprene and monoterpenes within a south-east Asian tropical rainforest. *Atmospheric Chemistry and Physics*, 11(14):6971–6984, 2011.

[228] T. Ingham, A. Goddard, L.K. Whalley, K.L. Furneaux, and P.M. Edwards *et al.* A flow-tube based laser-induced fluorescence instrument to measure OH reactivity in the troposphere. *Atmospheric Measurement Techniques*, 2(2):465–477, 2009.

[229] X. Ren, H. Harder, M. Martinez, R.L. Lesher, and A. Oliger *et al.* HO_x concentrations and OH reactivity observations in New York City during PMTACS-NY2001. *Atmospheric Environment*, 37(26):3627 – 3637, 2003.

[230] J. Mao, X. Ren, S. Chen, W.H. Brune, and Z. Chen *et al.* Atmospheric oxidation capacity in the summer of Houston 2006: Comparison with summer measurements in other metropolitan studies. *Atmospheric Environment*, 44(33):4107 – 4115, 2010.

[231] S. Chatani, N. Shimo, S. Matsunaga, Y. Kajii, and S. Kato *et al.* Sensitivity analyses of OH missing sinks over Tokyo metropolitan area in the summer of 2007. *Atmospheric Chemistry and Physics*, 9(22):8975–8986, 2009.

[232] T.A. Kovacs, W.H. Brune, H. Harder, M. Martinez, and J.B. Simpas *et al.* Direct measurements of urban OH reactivity during Nashville SOS in summer 1999. *J. Environ. Monit.*, 5:68–74, 2003.

[233] Y. Sadanaga, A. Yoshino, S. Kato, A. Yoshioka, and K. Watanabe *et al.* The importance of NO_2 and volatile organic compounds in the urban air from the viewpoint of the OH reactivity. *Geophysical Research Letters*, 31(L08):102, 2004.

[234] T.R. Shirley, W.H. Brune, X. Ren, J. Mao, and R. Lesher *et al.* Atmospheric oxidation in the Mexico City Metropolitan Area (MCMA) during April 2003. *Atmospheric Chemistry and Physics*, 6(9):2753–2765, 2006.

[235] X. Ren, W.H. Brune, J. Mao, M.J. Mitchell, and R.L. Lesher *et al.* Behavior of OH and HO_2 in the winter atmosphere in New York City. *Atmospheric Environment*, 40, Supplement 2:252 – 263, 2006. Particulate Matter Supersites Program and Related Studies.

[236] V. Sinha, J. Williams, J.N. Crowley, and J. Lelieveld. The Comparative Reactivity Method - a new tool to measure total OH Reactivity in ambient air. *Atmospheric Chemistry and Physics*, 8(8):2213–2227, 2008.

[237] S. Lou, F. Holland, F. Rohrer, K. Lu, and B. Bohn *et al.* Atmospheric OH reactivities in the Pearl River Delta - China in summer 2006: measurement and model results. *Atmospheric Chemistry and Physics*, 10(22):11243–11260, 2010.

[238] Jessica B. Gilman, William C. Kuster, Paul D. Goldan, Scott C. Herndon, Mark S. Zahniser, Sara C. Tucker, W. Alan Brewer, Brian M. Lerner, Eric J. Williams, Robert A. Harley, Fred C. Fehsenfeld, Carsten Warneke, and Joost A. de Gouw. Measurements of volatile organic compounds during the 2006 texaqs/gomaccs campaign: Industrial influences, regional characteristics, and diurnal dependencies of the oh reactivity. *Journal of Geophysical Research: Atmospheres*, 114(D7):n/a–n/a, 2009.

[239] E.C. Apel, L.K. Emmons, T. Karl, F. Flocke, A.J. Hills, S. Madronich, J. Lee-Taylor, A. Fried, P. Weibring, J. Walega, D. Richter, X. Tie, L. Mauldin, T. Campos, A. Weinheimer, D. Knapp, B. Sive, L. Kleinman, S. Springston, R. Zaveri, J. Ortega, P. Voss, D. Blake, A. Baker, C. Warneke, D. Welsh-Bon, J. de Gouw, J. Zheng, R. Zhang, J. Rudolph, W. Junkermann, and D.D. Riemer. Chemical evolution of volatile organic compounds in the outflow of the mexico city metropolitan area. *Atmospheric Chemistry and Physics*, 10(5):2353–2375, 2010.

[240] H. Singh, Y. Chen, A. Tabazadeh, Y. Fukui, I. Bey, R. Yantosca, D. Jacob, F. Arnold, K. Wohlfrom, E. Atlas, F. Flocke, D. Blake, N. Blake, B. Heikes, J. Snow, R. Talbot, G. Gregory, G. Sachse, S. Vay, and Y. Kondo. Distribution and fate of selected oxygenated organic species in the troposphere and lower stratosphere over the atlantic. *Journal of Geophysical Research: Atmospheres*, 105(D3):3795–3805, 2000.

[241] H.B. Singh, L.J. Salas, R.B. Chatfield, E. Czech, A. Fried, J. Walega, M.J. Evans, B.D. Field, D.J. Jacob, D. Blake, B. Heikes, R. Talbot, G. Sachse, J.H. Crawford, M.A. Avery, S. Sandholm, and H. Fuelberg. Analysis of the atmospheric distribution, sources, and sinks of oxygenated volatile organic chemicals based on measurements over the Pacific during TRACE-P. *Journal of Geophysical Research: Atmospheres*, 109(D15), 2004. D15S07.

[242] R. Sommariva, J. A. de Gouw, M. Trainer, E. Atlas, P. D. Goldan, W. C. Kuster, C. Warneke, and F. C. Fehsenfeld. Emissions and photochemistry of oxygenated VOCs in urban plumes in the Northeastern United States. *Atmospheric Chemistry and Physics*, 11(14):7081–7096, 2011.

[243] Y. Liu, B. Yuan, X. Li, M. Shao, S. Lu, Y. Li, C.C. Chang, Z. Wang, W. Hu, X. Huang, L. He, L. Zeng, M. Hu, and T. Zhu. Impact of pollution controls in Beijing on atmospheric oxygenated volatile organic compounds (OVOCs) during the 2008 Olympic Games: observation and modeling implications. *Atmospheric Chemistry and Physics*, 15(6):3045–3062, 2015.

[244] D.J. Jacob, B.D. Field, E.M. Jin, I. Bey, Q. Li, J.A. Logan, R.M. Yantosca, and H.B. Singh. Atmospheric budget of acetone. *Journal of Geophysical Research: Atmospheres*, 107(D10):ACH 5–1–ACH 5–17, 2002.

[245] A.C. Valach, B. Langford, E. Nemitz, A.R. MacKenzie, and C.N. Hewitt. Concentrations of selected volatile organic compounds at kerbside and background sites in central London. *Atmospheric Environment*, 95(0):456 – 467, 2014.

[246] R.G. Derwent and M.E. Jenkin. Hydrocarbons and the long-range transport of ozone and PAN across Europe. *Atmospheric Environment*, 25A(8):1661–1678, 1991.

[247] D. Grosjean, E. Grosjean, , and A.W. Gertler. On-road emissions of carbonyls from light-duty and heavy-duty vehicles. *Environmental Science & Technology*, 35(1):45–53, 2001.

[248] P. Ciccioli and M. Mannozzi. *Volatile organic compounds in the atmosphere, Chapter 8: High-molecular-weight carbonyls and carboxylic acids*, pages 292–341. Blackwell Publishing Ltd, 2007.

[249] J.J. Schauer, M.J. Kleeman, G.R. Cass, and B.R.T. Simoneit. Measurement of emissions from air pollution sources. 5: C_1-C_{32} organic compounds from gasoline-powered motor vehicles. *Environmental Science & Technology*, 36(6):1169–1180, 2002.

[250] J.J. Schauer, M.J. Kleeman, G.R. Cass, and B.R.T. Simoneit. Measurement of emissions from air pollution sources. 2: C_1 through C_{30} organic compounds from medium duty diesel trucks. *Environmental Science & Technology*, 33(10):1578–1587, 1999.

[251] T. Murrells and Y. Li. Road transport emissions from biofuel consumption in the UK. Technical report, AEA Energy & Environment,, AEA Technology plc,, 2008.

[252] S. López-Aparicio and C. Hak. Evaluation of the use of bioethanol fuelled buses based on ambient air pollution screening and on-road measurements. *Science of the Total Environment*, 452–453:40–49, 2013.

[253] S. Manzetti and O. Andersen. A review of emission products from bioethanol and its blends with gasoline. Background for new guidelines for emission control. *Fuel*, 140:293 – 301, 2015.

[254] J.A. de Gouw, J.B. Gilman, A. Borbon, C. Warneke, and W.C. Kuster *et al.* Increasing atmospheric burden of ethanol in the United States. *Geophysical Research Letters*, 39(15), 2012.

[255] H. Zhai, H.C. Frey, N.M. Rouphail, G.A. Goncalves, and T.L. Farias. Comparison of flexible fuel vehicle and life-cycle fuel consumption and emissions of selected pollutants and greenhouse gases for ethanol 85 versus gasoline. *Journal of the Air & Waste Management Association*, 59(8):912–924, 2009.

[256] W.D. Hsieh, R.H. Chen, T.L. Wu, and T.H. Lin. Engine performance and pollutant emission of an SI engine using ethanol-gasoline blended fuels. *Atmospheric Environment*, 36(3):403 – 410, 2002.

[257] S.H. Yoon and C.S. Lee. Lean combustion and emission characteristics of bioethanol and its blends in a Spark Ignition (SI) engine. *Energy & Fuels*, 25(8):3484–3492, 2011.

[258] X. Pang, Y. Mu, J. Yuan, and H. He. Carbonyls emission from ethanol-blended gasoline and biodiesel-ethanol-diesel used in engines. *Atmospheric Environment*, 42(6):1349 – 1358, 2008.

[259] M.A. Costagliola, L. De Simio, S. Iannaccone, and M.V. Prati. Combustion efficiency and engine out emissions of a S.I. engine fueled with alcohol/gasoline blends. *Applied Energy*, 111:1162 – 1171, 2013.

[260] P.J. Brooks and J.A. Theruvathu. DNA adducts from acetaldehyde: implications for alcohol-related carcinogenesis. *Alcohol*, 35(3):187 – 193, 2005.

[261] S. Myou, M. Fujimura, K. Nishi, T. Ohka, and T. Matsuda. Aerosolized acetaldhyde induces histamine-mediated bronchoconstriction in asthmatics. *American Review of Respiratory Disease*, 148(4):940–943, 1993.

[262] W.M. Kluwe, C.A. Montgomery, H.D. Giles, and J.D. Prejean. Encephalopathy in rats and nephropathy in rats and mice after subchronic oral exposure to benzaldehyde. *Food and Chemical Toxicology*, 21(3):245 – 250, 1983.

[263] Air Quality Expert Group. Ozone in the United Kingdom. Technical report, 2009.

[264] P.C. Vasconcellos, L.R.F. Carvalho, and C.S. Pool. Volatile organic compounds inside urban tunnels of São Paulo City, Brazil. *Journal of the Brazilian Chemical Society*, 16:1210–1216, 2005.

[265] D. Grosjean, A.H. Miguel, and T.M. Tavares. Urban air pollution in Brazil: Acetaldehyde and other carbonyls. *Atmospheric Environment. Part B. Urban Atmosphere*, 24(1):101 – 106, 1990.

[266] J.B. de Andrade, H.L.C. Pinheiro, and M.V. Andrade. The formaldehyde and acetaldehyde content of atmospheric aerosol. *Journal of the Brazilian Chemical Society*, 6(3):287–290, 1995.

[267] J.D. Lee, L.K. Whalley, D.E. Heard, D. Stone, R.E. Dunmore, J.F. Hamilton, D.E. Young, J.D. Allan, S. Laufs, and J. Kleffmann. Detailed budget analysis of HONO

in central London reveals a missing daytime source. *Atmospheric Chemistry and Physics Discussions*, 2015.

[268] R.E. Dunmore, J.R. Hopkins, R.T. Lidster, J.D. Lee, and M.J. Evans *et al.* Diesel-related hydrocarbons can dominate gas phase reactive carbon in megacities. *Atmospheric Chemistry and Physics*, 15(17):9983–9996, 2015.

[269] R.E. Dunmore, L.K. Whalley, T. Sherwen, M.J. Evans, D.E. Heard, J.R. Hopkins, J. Lee, A.C. Lewis, R.T. Lidster, A.R. Rickard, and J.F. Hamilton. Atmospheric ethanol in london and the potential impacts of future fuel formulations. *Faraday Discuss.*, 2015.

[270] R. Atkinson, D. L. Baulch, R. A. Cox, J. N. Crowley, R. F. Hampson, R. G. Hynes, M. E. Jenkin, M. J. Rossi, J. Troe, and IUPAC Subcommittee. Evaluated kinetic and photochemical data for atmospheric chemistry: Volume ii – gas phase reactions of organic species. *Atmospheric Chemistry and Physics*, 6(11):3625–4055, 2006.

[271] E. Grosjean, D. Grosjean, R. Gunawardena, and R.A. Rasmussen. Ambient concentrations of ethanol and methyltert-butyl ether in Porto Alegre, Brazil, March 1996–April 1997. *Environmental Science & Technology*, 32(6):736–742, 1998.

[272] C.N. Hewitt, J.D. Lee, A.R. MacKenzie, M.P. Barkley, and N. Carslaw *et al.* Overview: oxidant and particle photochemical processes above a south-east Asian tropical rainforest (the OP3 project): introduction, rationale, location characteristics and tools. *Atmospheric Chemistry and Physics*, 10(1):169–199, 2010.

[273] P.J. Marriott, G.T. Eyres, and J.P. Dufour. Emerging opportunities for flavor analysis through hyphenated gas chromatography. *Journal of Agricultural and Food Chemistry*, 57(21):9962–9971, 2009.

[274] B. Maikhunthod, P.D. Morrison, D.M. Small, and P.J. Marriott. Development of a switchable multidimensional/comprehensive two-dimensional gas chromatographic analytical system. *Journal of Chromatography A*, 1217(9):1522 – 1529, 2010.

[275] J.M. Davis and J.C. Giddings. Statistical method for estimation of number of components from single complex chromatograms: application to experimental chromatograms. *Analytical Chemistry*, 57(12):2178–2182, 1985.

[276] C.M. Delahunty, G. Eyres, and J.P. Dufour. Gas chromatography-olfactometry. *Journal of Separation Science*, 29(14):2107–2125, 2006.

[277] M. Parker, A.P. Pollnitz, D. Cozzolino, I.L. Francis, and M.J. Herderich. Identification and quantification of a marker compound for 'pepper' aroma and flavor in Shiraz grape berries by combination of chemometrics and gas chromatography-mass spectrometry. *Journal of Agricultural and Food Chemistry*, 55(15):5948–5955, 2007.

[278] Y.F. Wong, C. Hartmann, and P.J. Marriott. Multidimensional gas chromatography methods for bioanalytical research. *Bioanalysis*, 6(18):2461 – 2479, 2014.

[279] B. Mitrevski and P.J. Marriott. Novel hybrid comprehensive two-dimensional – multidimensional gas chromatography for precise, high-resolution characterization of multicomponent samples. *Analytical Chemistry*, 84(11):4837–4843, 2012.

[280] S.T. Chin, G.T. Eyres, and P.J. Marriott. System design for integrated comprehensive and multidimensional gas chromatography with mass spectrometry and olfactometry. *Analytical Chemistry*, 84(21):9154–9162, 2012.

[281] T. Gorecki, J. Harynuk, and O. Panic. The evolution of comprehensive two-dimensional gas chromatography (GC×GC). *Journal of Separation Science*, 27(5-6):359–379, 2004.

[282] P.Q. Tranchida, D. Sciarrone, P. Dugo, and L. Mondello. Heart-cutting multidimensional gas chromatography: A review of recent evolution, applications, and future prospects. *Analytica Chimica Acta*, 716:66 – 75, 2012.

[283] M. Adahchour, J. Beens, and U.A.T. Brinkman. Recent developments in the application of comprehensive two-dimensional gas chromatography. *Journal of Chromatography A*, 1186(1-2):67–108, 2008.

[284] P.J. Marriott, S.T. Chin, B. Maikhunthod, H.G. Schmarr, and S. Bieri. Multidimensional gas chromatography. *TrAC Trends in Analytical Chemistry*, 34:1 – 21, 2012.

[285] P. Dussort, N. Deprêtre, E. Bou-Maroun, C. Fant, and E. Guichard *et al.* An original approach for gas chromatography-olfactometry detection frequency analysis: Application to gin. *Food Research International*, 49(1):253 – 262, 2012.

[286] M. Capobiango, R.B. Mastello, S.-T. Chin, E. de Souza Oliveira, Z. de Lourdes Cardeal, and P.J. Marriott. Identification of aroma-active volatiles in banana Terra spirit using multidimensional gas chromatography with simultaneous mass spectrometry and olfactometry detection. *Journal of Chromatography A*, 1388:227 – 235, 2015.

[287] G. Eyres, P.J. Marriott, and J.-P. Dufour. The combination of gas chromatography-olfactometry and multidimensional gas chromatography for the characterisation of essential oils. *Journal of Chromatography A*, 1150(1-2):70 – 77, 2007.

[288] C. Cordero, J. Kiefl, P. Schieberle, S.E. Reichenbach, and C. Bicchi. Comprehensive two-dimensional gas chromatography and food sensory properties: potential and challenges. *Analytical and Bioanalytical Chemistry*, 407(1):169–191, 2015.

[289] L.J. Carpenter, Z.L. Fleming, K.A. Read, J.D. Lee, and S.J. Moller *et al.* Seasonal characteristics of tropical marine boundary layer air measured at the Cape Verde Atmospheric Observatory. *Journal of Atmospheric Chemistry*, 67(2-3):87–140, 2010.

[290] W.T. Sturges and C.E. Reeves. Atmospheric chemistry in the tropics: marine, biosphere and climate connections. *International Global Atmospheric Chemistry Newsletter*, 42, December 2009.

[291] K.A. Read, A.S. Mahajan, L.J. Carpenter, M.J. Evans, and B.V.E. Faria *et al.* Extensive halogen-mediated ozone destruction over the tropical Atlantic Ocean. *Nature*, 453(7199):1232–1235, 2008.

[292] K.H. Kim, M.H. Lee, and J.E. Szulejko. Simulation of the breakthrough behavior of volatile organic compounds against sorbent tube sampler as a function of concentration level and sampling volume. *Analytica Chimica Acta*, 835:46 – 55, 2014.

[293] A.C. Valach, B. Langford, E. Nemitz, A.R. MacKenzie, and C.N. Hewitt. Seasonal trends in concentrations and fluxes of volatile organic compounds above central london. *Atmospheric Chemistry and Physics Discussions*, 15(5):6601–6644, 2015.